Condition Monitoring and Fault Diagnosis of Fluid Machines in Process Industries

Robin Appadoo

A thesis submitted to the University of Huddersfield in partial fulfilment of the requirements for the degree of Doctor of Philosophy

School of Computing and Engineering

Centre for Efficiency and Performance Engineering

March 2021

Abstract

Condition Monitoring (CM) of fluid machines plays a critical role in maintaining efficient productivity in many processing industries. Conventional vibration techniques generally provide more localised information with the need for many sensors, associated data acquiring and processing efforts, which are difficult for system deployment and are reluctantly accepted by those industries, for example paper mills and food production lines making marginal profits.

To find adequate CM techniques for such industries this research investigates a new cost-effective scheme of implementing CM, which combines the high diagnostic capability of using Surface Vibration (SV) with the global detection capability of using the Instantaneous Angular Speed (IAS) measurements and Airborne Sound (AS). To address specific techniques involved in the scheme, this research is arranged in three consecutive Phases: Phase I is the technical evaluation; Phase II is the field implementation practices and Phase III is the application of AS through Convolution Neural Networks (CNN).

In Phase I, widely used reciprocating compressor is investigated numerically and experimentally, which clarifies the performances of SV, IAS, AS, pressure and motor current in a quantitative way for differentiating common faults such as leakages happening in valves and intercoolers, faulty motor drives and mechanical transmission systems. It paves the foundations for the field implementation in Phase II.

In Phase II, this novel scheme is realised on three sets of vacuum pumps in a paper mill. Based on an analytic study of dynamic responses to common faults on these pumps, a field test was conducted to verify the feasibility of the scheme and the preliminary study shows that airborne sound can show the relative spectral components for each machine to a good degree of accuracy.

Knowledge gained from the preceding phases of study is now applied to Phase III. New techniques based on airborne signal differences through CNN have been demonstrated to give a good indication of the sound propagation and location of noise sources under all operating discharge pressure conditions at 100% validation accuracy, proving that the state of the art deep leaning approaches can be used to deal with complicated acoustic data.

Dedication

This thesis is dedicated to my mother and father who first taught me the ability to understand the concept of life and the value of education as a progressive lifetime pursuit.

My gratitude also goes to my dear wife, daughter, sons and the rest of my beloved family back in Mauritius for their patience, love and support during my journey.

Table of Contents

List of Figures

List of Tables

List of Abbreviations

AB (GB)	Airborne Sound Gear Box
AB (P)	Airborne Sound Pump
ADC	Analogue Digital Converter
AE	Acoustic Emission
AG1	Acoustic Gearbox
AI	Artificial Intelligence
Amp	Ampere
ANN	Artificial Neural Networks
AP	Acoustic Pump
AR	Autoregressive
AS	Airborne Acoustic
ASPR	Advanced Supervised Pattern Recognition
BDC	Bottom Dead Centre
BHP	Brake Horsepower
BL	Baseline
BNC	Bayonet-Neil-Concelman-Connector
BNN	Bayesian Neural Network
BNN	Biological Neural Networks
BPIR	Ball Pass Frequency Inner Race
BPOR	Ball Pass Frequency Outer Race
BSF	Ball Spin Frequency
°C	Degree Celsius
CA-YD-185	Type of Piezoelectric Accelerometer
CED	Cambridge Electronic Design
CEPE	Centre for Efficiency and Performance Engineering
CFD	Computational Fluid Dynamic
CHZ-211	Type of microphone
CM	Condition Monitoring
CMMS	Computerized Maintenance Management System
CNN	Convolution Neural Networks
CUFT	Cubic Feet

CVA	Canonical Variate Analysis
DAC	Data Acquisition
dB	Decibel
DE	Drive End
DNN	Deep Neural Network
DTTI	Digital Infrared Thermal Imaging
DTW	Dynamic Time Warping
DV	Discharge Valve Leakages
DVC	Discharge Valve Close
DVO	Discharge Valve Open
FEA	Finite Element Analysis
FFT	Fast Fourier Transform
FLZ	Fuzzy Logic System
FTF	Fundamental Train Frequency
GA	Genetic Algorithm
GBI	Gearbox Input
GBO	Gearbox Output
GPM	Gallons Per Minute
GPU	Graphics Processing Unit
HgV	Inches of Mercury (Gauge)
HMC	Hybrid Monte Carlo
HP	High-Pressure
HP	Horse Power
Hz	Hertz
IAS	Instantaneous Angular Speed
IC	Intercooler Leakages
IP	Ingress Protection
IRF	Impulsion Response Functions
IRT	Infrared Thermal
IV	Inlet Valve
IVC	Inlet Valve Closing
Kg	Kilogram
KHz	Kilo Hertz

kW	Kilowatt
KX-C184	Type of Motor
LCD	Liquid Crystal Display
LRVP	Liquid Ring Vacuum Pump
MCMC	Markov Chain Monte Carlo
MCSA	Motor Current Signature Analysis
MHCT	Mounting Hall Effect Current Transformer
ML (NDE)	Motor Left Non-Drive End
MPa	Megapascal
MR (DE)	Motor Right Drive End
ms^{-2}	Meter per second squared
MSSP	Mechanical System and Signal Processing
mv	Milli Volt
mv/ms^{-2}	Milli volt per meter per second squared
mV/Pa	Millivolts/Pascal
MΩ	Megohm
NDE	Non-Drive End
NDT	Non-Destructive Testing
NN	Neural Network
OEE	Overall Equipment Effectiveness
PC	Personal Computer
PCA	Principal Component Analysis
PCP	Printed Circuit Board
PL (DE)	Pump Left Drive End
PNN	Probabilistic Neural Network
PR (NDE)	Pump Right Non-Drive End
psi	Pounds per square inch
PV	Pressure Volume
RC	Reciprocating Compressor
RCA	Root Cause Analysis
RMS	Root Mean Square
RPM	Revolution Per Minute
RS	High service components distributor across the UK.

SAP	System Application and Products
SNR	Signal to Noise Ratio
Sp.Gr	Specific Gravity
SPL	Sound Pressure Level
SPR	Supervised Pattern Recognition
SPWVD	Smoothed-Pseudo-Wigner Ville Distribution
STFT	Short Time Fourier Transform
SUE	System Usage Event
SV	Surface Vibration
SVC	Suction Valve Close
SVM	Support Vector Machines
SVO	Suction Valve Open
TDC	Top Dead Centre
TDH	Total Dynamic Head
TPM	Total Productive Maintenance
UCM	Ultrasonic Condition Monitoring
USB	Universal Serial Bus
V	Volt
Vdc	Direct current voltage
VG1L	Vibration Gearbox 1 left
VG1R	Vibration Gearbox 1 Right
VM1L	Vibration Motor 1 Left
VM1R	Vibration Motor 1 Right
VP1L	Vibration Pump 1 Left
VP1R	Vibration Pump 1 Right
YE 623	Type of Data Acquisition

List of Nomenclature

°C	Degree Celsius
ω	IAS of the crankshaft (rad/sec)
θ	Crank angle
V	Voltage
I_1	Current
n_s	Synchronous speed
n	Rotor speed
f	Supply frequency
p	Pole
s	Motor slip
P_{in}	Electrical power
P_{sci}	Partial Electrical power dissipated due to stator copper loss
P_{il}	Dissipated heat in the stator core due to iron losses
P_{ag}	Remaining electrical power carried to air gap
P_{rci}	Partial electrical power dissipated due to rotor copper loss
P_m	Residual electrical power in mechanical power
T_m	Motor torque
n_r	Equal number of turns
θ_r	Rotor separating the three-phase winding
$(V_{r\ Phase1}\ V_{r\ Phase2}\ V_{r\ Phase3})$	Three phase Rotor's Voltages
$(V_{s\ Phase1}\ V_{s\ Phase2}\ V_{s\ Phase3})$	Three phase Stator's Voltages
$(i_{r\ Phase1}\ i_{r\ Phase2}\ i_{r\ Phase3})$	Three Phase rotor current
$(i_{s\ Phase1}\ i_{s\ Phase2}\ i_{s\ Phase3})$	Three phase stator current
ψ_r	Rotor's fluxes (Weber)
ψ_s	Stator's fluxes (Weber)
R_r	Rotor's winding (ohm)
R_s	Stator's winding (ohm)
L_{sr}	Mutual-inductances (Henry)
L_{ss}	Stator's self-inductances (Henry)

L_{rr}	Rotor's self-inductances (Henry)
T_e	Electromagnetic Torque
J	Moment of inertia (kgs^2)
$T_e\,(t)$	Induction motor torque
$T_{fLH}\,(t)$	Frictional torque of entire system
$T_{pmr\,LH}\,(t)$	Cylinder pressure resultant torque
x_p	Piston displacement (mm)
f_{ptf}	Force produced tangentially by the internal cylinder pressure
f_{mtf}	Force produced tangentially by the inertia of the reciprocating mass
r_1	Crank shaft radius
l_1	Connecting rod
P_{cp}	In-cylinder pressure
S_{cs}	Cross-sectional area of the cylinder
d	Bore diameter of the cylinder
m_{rm}	Reciprocating mass of first and second stages
m_{pi}	Piston mass
m_{crm}	Reciprocating mass of the connecting rod
x_{ocd}	Clearance distance between cylinder head at TDC
$\ddot{x}_p$	Vertical piston acceleration ($m\ s^{-2}$)
$P_{cyL,H}$	Cylinder pressures Low and High Pressure
$\dot{P}_{cyL,H}$	In-cylinder pressure derivatives for L and H stages
$V_{cyL,H}$	Cylinder volume for Low and High Stages
$V_{cyoL,H}$	Clearance volume for Low and High Stages
$\dot{V}_{cyL,H}$	Rate of change in the cylinder volume Low and High
$\dot{m}_{viL,H}$	Mass flow rate through inlet valve Low and High
$\dot{m}_{voL,H}$	Mass flow rate through outlet valve Low and High
$\dot{m}_{viL}$	Mass flow rates for the first stage inlet valves
$\dot{m}_{viH}$	Mass flow rates for the second stage inlet valves
$\dot{m}_{voL}$	Mass flow rates for the first stage outlet valves
$\dot{m}_{voH}$	Mass flow rates for the second stage outlet valves

$C_{y\,iL,H}^2$	Square speed of sound in the inlet plenum Low and High
$C_{y\,cyL,H}^2$	Square speed of sound in the cylinder Low and High
$\gamma RT_{iL,H}$	Square speed of sound in the inlet plenum Low and High
$\gamma RT_{cyL,H}$	Square speed of sound in the cylinder Low and High
R	Gas constant of air
$D_{cyL,H}$	Cylinder diameter Low and High
$T_{iL,H}$	Average absolute temperature of inlet air at atmospheric temp of ℃ $+ 273K$ Low and High
β_{iLH}	Flow direction parameter
p_{iLH}	Pressure in the suction plenum
C_{diLH}	Variable inlet/suction coefficient
A_{fiLH}	Maximum flow area of the suction valve
X_{pvsLH}	Valve plate displacement
$\dot{X}_{pvsLH}$	Valve plate velocity
$\ddot{X}_{pvsLH}$	Valve plate acceleration
$C_{dsLH,}$	Damping coefficient
$M_{pvsLH,}$	Equivalent mass of the inlet valve plate
K_{csLH}	Contact stiffness between the seat valve for both suction and discharge process
K_{nvsLH}	Non-linear spring stiffness when the valve is in motion between the valve seats
C_{cdsLH}	Contact damping coefficient is represented
Σf_{rvsLH}	Resultant force acting on the valve plate
f_{svoLH}	Pre-set spring force
W_{rsvLH}	Valve weight
$C_{fc}\ S_{rsvLH}$	Force due to the pressure difference between each side of the valve
P_{iLH}	Pressure in the inlet plenum
P_{cyLH}	Cylinder pressure
C_{fc}	Coefficient changing with the valve's lift magnitudes

S_{rsvLH}	Slot area for a single channel due to pressure difference between each side of the valve
Σf_{rvsLH}	Resultant force acting on the valve plate
C_{dsLH}	Calculated damping coefficient
$2\xi\sqrt{K_{nvsLH}}M_{pvsLH}$	Calculated damping coefficient
q_{th}	Theoretical suction capacity
μ	Effects of blades thickness coefficient
α	Relative immersion blades depth
v	Ratio of hub radius:impeller radius
λ	Flow coefficient
P_d	Discharge pressure
P_s	Suction pressure
q_d	Volumetric discharge capacity
P_a	Atmospheric pressure
b	Impeller width, m
P_V	Saturated vapor pressure
Au	Coefficient of circumferential speed of impeller
R	Inner radius of casing M
φ	Circumferential angle in degree
ρ	Length, m density in kg/m³
e	Expansion
g	Gas
A	Coefficient
ε	Coefficient
R	Inner radius of casing

Appendix

Declaration

No portion of the work referred to in this thesis has been submitted in support of an application for another degree or qualification of this or any other university or other institute of learning.

Copyright

i. The author of this thesis (including any appendices and/or schedules to this thesis) owns any copyright in it (the "Copyright") and he has given The University of Huddersfield the right to use such Copyright for any administrative, promotional, educational and/or teaching purposes.

ii. Copies of this thesis, either in full or in extracts, may be made only in accordance with the regulations of the University Library. Details of these regulations may be obtained from the Librarian. This page must form part of any such copies made.

iii. The ownership of any patents, designs, trademarks and any other intellectual property rights except for the Copyright (the "Intellectual Property Rights") and any reproductions of copyright works, for example, graphs and tables ("Reproductions"), which may be described in this thesis, may not be owned by the author and may be owned by third parties. Such Intellectual Property Rights and Reproductions cannot and must not be made available for use without permission of the owner(s) of the relevant Intellectual Property Rights and/or Reproductions.

Acknowledgement

My sincere thanks go to my academic supervisors, Prof Andrew David Ball and Prof Fengshou Gu, for supporting me during these past years. Andrew is someone that has always been there for me and is a person that you will never forget once you meet him. He has been an inspiring role model to me for his consistent guidance, support and valuable exchange of academic ideas. I am also deeply indebted to Prof Fengshou Gu who has been very supportive and given me the freedom to pursue various projects without objection. He has also provided me with insightful discussions, is my main resource for getting my scientific questions answered and was instrumental in assisting me to complete this PhD as a part-time researcher. His patience, continuous support, honesty and critical advice is unique and incomparable.

I would like to also extend thanks to my lovely family: my wife Priyanka, my daughter Rumi and my sons Robinson and Aaron for their patience and support throughout my research and for helping by harmonising themselves to my world.

My parents: my mother Padmini and my father Balnarain who are the prime reasons for my success today as they never abandoned me at any time in their thoughts and prayers. I would also like to thank all my relatives and friends back home for their patience during my studies.

I would also like to extend my thanks to my previous and present employers and colleagues during the time of my studies. My gratitude also goes to my colleagues at the University during my academic time: Mr Chris Daykins, Dr Peter Mather, Dr Mahmed Ahmed, Dr Tian Xiange, Dr Ugo Muo, Dr Ussama Habba, Dr Khalid Rabeyee, Mr Miashou Li, Mr Rongfeng Deng, Mrs Sam Ascroft, Mrs Audrey Dobson, Beverley Murphy, the staff of the Research Office of Computing and Engineering at the University of Huddersfield, all my fellow lab mates for the good times we spent together and to my Bahai friends from the UK and back home in Mauritius. Finally, I express my sincere appreciation to everybody who has directly or indirectly made this amazing journey both enjoyable and unforgettable.

The Author

Robin Appadoo is an Electrical/Reliability Engineer and is originally from Mauritius. Robin's career as an engineer encompasses Marine Engineering, teaching in Mauritius and leading a team of engineers in a Five Star Hotel in Seychelles. His work in the UK comprises of working as an Electrical Engineer/Engineering Manager/TPM leader/Reliability Engineer. His experience varies from working in the train detection signalling system, bottling, paper and food industries.

Robin works full time whilst he has been doing his PhD part-time. His interest lies in Modern World Class Maintenance and he has contributed to several professional publications.

Chapter 1. **Introduction**

This chapter embarks on a broad description of the area of the research, with an explanation of the reasons for undertaking this specific project, research motivation, aims and objectives, work plan and a report structure. Compressors and vacuum pumps play an important role in maintaining efficient productivity in many industries. If proper maintenance is not followed the machines can cause irreparable damage to themselves and the processes which could, in turn, lead to a large deficit to the company. Some of the disadvantages are as follows:

- *A decrease of Overall Equipment Effectiveness (OEE)*
- *Increase of downtime to the business*
- *Make employees life harder which will lead to frustration*
- *Produce more waste instead of a good quality product*
- *The risk of losing customers if the product is not delivered on time and not of good quality.*

Nowadays in this modern highly automated industry, there has always been an increasing demand concerning the safety, quality, reliability, productivity and performance of machinery. To improve the productivity of the plant, CM has been implemented in many sectors of industries and has brought many benefits including:

- *Advanced warning of potential plant problems, minimising unscheduled downtime*
- *Reduction of maintenance costs by improving the predictability of productivity levels*
- *Improving machine service time by minimising unscheduled and planned maintenance*
- *Maintaining the high standard quality through CM*
- *Reducing potential risks of machine failures improving OEE*
- *Improving morale within production and engineering*
- *Employees and Employers satisfaction and hence more confidence in the market.*

1.1 Background

This research is based on the development of a robust and innovative approach to the monitoring of key machines such as compressors and pumps as these machines are critical in process industries. This research will be investigated in three consecutive phases.

Phase I is the technical evaluation and improvement, in which various techniques relating to SV and IAS have been examined and refined based on a two-stage Reciprocating Compressor (RC) which shares many physical processes such as pressured flows, electrical powers and mechanical rotors.

Phase II is the field implementation on the vacuum pumps which has been carried out in a paper mill facility. The main vacuum pumps at this facility are being monitored daily and a report is produced monthly where recommendations are being made for the engineers to take necessary actions before a failure occurs. The condition monitoring techniques used on that site are the vibration and frequency analysis. In April 2014, one of the vacuum pumps of that facility; "Pump M243" the "Dewatering Box Vac pump 1" failed and the plant was down for weeks. The reason for that impeller being cracked was due to the build-up of limescale. The shaft Non-Drive End (NDE) bearing was spinning on the shaft. The CM System on site did detect an initial failure but as the readings were only being taken monthly, the engineers were unable to react responsively and the failure had already occurred before the report was generated on the 09/04/14 as shown from Figure 6-7.

According to the Root Cause Analysis (RCA) exercise of why the bearing was loaded and heated up was due to a lack of lubrication and scale build-up, this pump could have run for a longer period but due to its environment, it is recorded as failing every five years. In 2014, that was the second time it had failed. It was predicted that this pump would fail again in 2019, therefore the decision was taken to replace that pump in 2018 with a refurbished pump at the cost of £30,000. That company has also bought an additional pump already at the price of £149,000 which is kept as a replacement. To prevent any major incident in the future the frequency of the data collection by the CM team on site has been increased from monthly to weekly and the lubrication programme has also been increased.

Phase III is designed to study the airborne sound acoustic learned from the industrial monitoring machine from Phase II and to locate the ideal position to capture the acoustic signal from the compressor through various analysis. Phase III also studies and applies the Convolutional Neural Networks (CNN) in determining and localising an optimal position away

from the compressor, for the collection of data and to show which signal proves to be a good indication of sound propagation which can easily locate noise sources under the four operating discharge pressure conditions at the highest validation accuracy.

1.2 Research Motivation

There are lots of new research methods in Condition Monitoring however they are not being used wisely in industries. Applying some of the new methods will make machines more reliable and cost-effective and this has inspired the author to execute his ideas and experience in developing a new approach on how to diagnose different parameters of this system:

- Instantaneous Angular Speed and Power Consumption
- Instantaneous Multi-Current Signature
- Process Parameters
- Angular Velocity
- Convolutional Neural Networks

These parameters will give the machine a better life expectancy and will enable us to prolong its longevity and predict its failure.

1.3 Research Aims and Objectives

1.3.1 Aims

This research aims to develop a cost-effective scheme of implementing CM for fluid machines, which combines the high diagnostic capability of using Surface Vibration (SV) with the global detection capability of using the Instantaneous Angular Speed (IAS) measurements, Non-Destructive Testing (NDT) via Airborne Acoustic (AS) and Convolutional Neural Networks (CNN). The project will be fulfilled in three consecutive phases:

Phase I - Technique validation, in which various monitoring techniques including SV and IAS are examined and refined based on a two-stage reciprocating compressor to identify their potential advantages and disadvantages for large scale field applications. The performances of fault detection, diagnosis and condition prognosis are evaluated along with the feasibility of deployment, operation and installation investment. As a result, it will suggest an integral scheme that can be deployed easily to multiple sets of fluid machines such as vacuum pumps.

Phase II - Field implementation, in which the proposed approaches will be evaluated and refined further by applying it to three sets of vacuum pumps referred to as the target machine. Both the hardware and software will be developed based on the field machines and then the monitoring performances will be evaluated based on on-site measured data and corresponding maintenance records. The sensing data storage and processing techniques will be ensured in the aspects of suitability, not only for the convenience of deployment and cost-effectiveness but also for monitoring the likely faults during long term operation.

Phase III – Skills from preceding phases of the study are applied to a reciprocating compressor. An innovative movable system set up with an array of four microphones that can be moved at different horizontal and vertical distances away from the compressor is being implemented. New techniques based on Non-Destructive Testing (NDT) is being applied such as airborne acoustic techniques which have proven to be a good indication of the sound propagation and for the locating of noise sources under all operating discharge pressure conditions. The Convolutional Neural Network (CNN) has been implemented to identify an ideal position of sound localisation at the highest validation accuracy.

1.3.2 Objectives

The main objectives are detailed as follows:

Phase I

Objective 1: Understand the current CM technology and find the gap in its application by reviewing the existing systems in the market and research community through intensive literature review.

Objective 2: To design a mathematical model and numerical analysis for the investigation of the behaviour of the dynamic responses of the Reciprocating Compressor (RC).

Objective 3: To design and build a comprehensive reciprocating compressor test facility in the lab to simulate faults and obtain experimental data. Sample data will assist in analysing the effectiveness of the system with different monitoring strategies.

Objective 4: To familiarise and study the practical and theoretical aspects of all components of the compressor and study the function of the data acquisition so that samples of the raw data signal from the machine can be captured, analysed and a report produced. Also to understand the signal processing methods and techniques used for analysis which is the Frequency and

Time Domain, Root Mean Square (RMS), Instantaneous Angular Speed (IAS) spectrum and Current Waveform Spectrum.

Objective 5: To seed-specific quantified faults into the machine so that experimental data can be gained on the subsequent system behaviour and its effect on the compressor performance so that data can be compared and analysed.

Objective 6: To implement various techniques relating to SV and IAS into the system to analyse the effect and evaluate the possibility for field implementation in phase II. Examine the detection and diagnosis performances of the developed CM systems in line with potential issues for field implementation.

Phase II

Objective 1: To study and evaluate the current CM technology which offers the most potential to the paper industry by exploring existing systems in the market and research community. Develop a scheme based on the typical paper industry and built on actual demand, addressing the gap in technology and develop a mathematical model based on the system.

Objective 2: To assess the capability of the target system through its working history and planned maintenance schedule for comparison in discussion and evaluation by examining the suitability and performance during the full course of the CM process, which includes the measurement system specification, data acquisition definition and implementation, data analysis method selection and evaluation, detection and diagnosis performance confirmation.

Objective 3: To conduct and look at the feasibility of the scheme in terms of sensor installations and performances, data acquisition methods, system specification and fault diagnosis admissibility so that sample data could easily be taken and analysed.

Objective 4: To conduct a quantitative study and fault mode analysis of these pumps by examining the detection and diagnosis performances of the vacuum pumps by using the (vibration data statistic, airborne sound statistic, frequency spectra for vibration and envelope spectra) techniques to prove its effectiveness and IAS approaches.

Phase III

Objective 1: To apply airborne sound acoustic learned from the industrial monitoring machine from Phase II into the Broomwade compressor used in phase I.

Objective 2: To develop a movable rig for the collection of 16-point data collection away from the reciprocating compressor.

Objective 3: To study, identify, quantify and qualify the best location to capture the acoustic signal from the compressor.

Objective 4: To study the RMS of frequency range according to the sound localisation.

Objective 5: To Study and apply the Convolutional Neural Networks (CNN) in determining and localising an optimal position away from the compressor for the collection of signals to find which signal proves to be a good indication of sound propagation and locating noise sources under the four operating discharge pressure conditions.

1.3.3 Work Plan

The planning of this research has been done in a methodological manner and three separate Phases. The work in Phase I is mainly the study and monitoring of the compressor with various monitoring techniques and fault simulation where the results and knowledge gained will assist in enabling the field implementation plan in Phase II in an industrial setting. Phase II emphasises on the introduction, application and cost benefits on the Industrial machine. Phase III is set to be applied back into a laboratory setting to study the application of acoustics to laboratory machinery and the study of data mining techniques based on Convolutional Neural Networks.

1.4 Thesis Structure

Chapter One

Introduction

Chapter one gives a brief overview of the area of research with an explanation of why this specific project is being undertaken. The Liquid Ring Vacuum Pump (LRVP) is identified as a crucial machine in the paper industry. To improve its reliability and get a better overview of the actual system performance a new approach is sought to be implemented. A brief introduction is given on the social and cost benefits of condition monitoring followed by the background, research motivation, aims, objectives and work plan followed by a structured report.

Chapter Two

Literature Review of Condition Monitoring Techniques

Chapter two provides a structured outline of the current Condition Monitoring techniques used in industry and new research advances. This starts with a review of standard current CM

techniques, the industrial CM in four main parts: the vibration, lubrication, thermal and process parameters. It is then followed by the new research methods: motor signature current analysis, ultrasound, airborne acoustic, instantaneous angular speed and new vibration methodology. It also explains the study of acoustics monitoring, a review of all techniques neural and conventional neural networks, artificial intelligence, application of convolutional neural networks, deep learning and condition monitoring techniques applied to fluid Machines.

Phase I Chapter Three

Mathematical Modelling and Numerical Analysis of Dynamics Responses of a Two Stage Reciprocating Compressor with Different Faults

This chapter examines the behaviour of the dynamic response of a reciprocating compressor by mathematical modelling and numerical analysis. The model comprises an electrical motor model, in-cylinder pressure model, mass flow models crankshaft IAS model, valve motion model. This is then accompanied by a numerical analysis which will focus on the evaluation of monitoring information that is included in each dynamic response followed by key findings and results.

Chapter Four

Evaluation of Waveform Analysis Based on Intrusive and Non-Intrusive In-cylinder Pressure Measurements

This chapter describes the establishment of the Test Rig and then summarises the achievement in Phase I, which addresses the implementation of the updated techniques, reviewed in chapter two, upon a laboratory compressor bench. This section also outlines the test faults cases of the compressor pressure trace, test procedure and performance characteristic and also introduces the experimental work undertaken on the test rig to evaluate common CM techniques including time domain and frequency domain methods applied to vibration, Motor Current Signature Analysis (MCSA), IAS and RMS.

Phase II Chapter Five

Analytic Modelling of a Liquid Ring Vacuum Pump

This chapter depicts an analytical analysis of a Liquid Ring Vacuum Pump (LRVP). It gives a thorough understanding of the dynamic behaviour and operation of the LRVP to assist in the monitoring and accurate diagnosis of the machine in Phase II. This chapter starts with an introduction of the LRVP followed by an overview of the model. A good understanding of gas

flow and pressure pulsations is also described based on an analytic theoretical model of the operating principle of LRVP at various parameters followed by key findings.

Chapter Six

A Preliminary Implementation of Vibration and Acoustics Monitoring to an Industrial Environment

Chapter Six introduces the "Industrial Machine" the Liquid Ring Vacuum Pump (LRVP), with an abstract of its functionality and categories. A brief overview of the liquid vacuum pump construction, operation and its effectiveness through its reliability followed with the current advanced techniques on the vacuum pump and the actual CM used on the site.

Chapter six also introduces the preliminary experimental work carried out in Phase II from the existing facility by applying the technical knowledge gained from Phase I. This is followed by an explanation of the characteristics of the vacuum pump instrumentation, measurement, data acquisition and the vacuum pump experiment plan. It also describes the data collection process for all three systems with a brief description of the work carried out on the test facility to investigate the statistical data analysis of the motor, pumps, gearboxes vibration and airborne sound data. More experimental work has also been carried out on the data analysis of the measured vibration signal of the three systems in the time domain, airborne sound data, spectra of vibration, envelope spectra vibration followed by a discussion.

Phase III Chapter Seven

Acoustic Monitoring of the Laboratory Compressor based on Conventional Analysis

Chapter Seven gives an understanding of sound generation mechanisms from a compressor and the deficiency in loss of performance and capacity with potential knocking effect. A brief overview of 'noise sources' and their dynamic characteristics is explained together with a summary of the type of faults and wear in a compressor. A review of acoustics monitoring study using Conventional Analysis Techniques has been undertaken. Airborne acoustic monitoring has proven to be a possibility for replacing the need for several vibration sensors that need mounting at various locations on the machine with the potential of being detached from the machine's surface. This chapter also explains the general system set up and how this investigation has proceeded. A spiral array has been used to locate sources of airborne sound at a higher frequency. This section stipulates the difference from the time domain RMS Analysis and the distance of the microphones in contrast with the compressor.

Chapter Eight

Acoustic Monitoring of the Laboratory Compressor with State-of-the-Art Convolutional Neural Networks

Chapter Eight is based on Convolutional Neural Networks (CNN) which will be used to extract the data from RC acoustics for the detection of the machine airborne signal differences between the data collection of sixteen points from a reciprocating compressor. Different fault scenarios will be assessed to gauge CNN capability and to try to localise an optimal position away from the compressor for the collection of signals. This section also explains the methodologies, general system set up, preferred classification, data preparation, a brief example of data processing and training results.

Chapter Nine

Conclusion and Further Works

Chapter Nine reviews the research objectives and achievements. The foundation of this thesis is based on the conclusions from all three Phases followed by the contribution to knowledge and lastly discusses possible areas of future works which the author considers would further improve this study and make a useful contribution to the advance monitoring of rotating and fluids machines

Chapter 2. **Literature Review of Condition Monitoring Techniques**

This chapter briefly describes different types of Condition Monitoring (CM) techniques available and provides a structured outline of the current CM used in the industry together with its application to fluid machines. It starts with a review of the standard current CM techniques and is then followed by the new research methods, namely: motor current signature analysis; ultrasound; airborne acoustic; instantaneous angular speed and new vibration methodology. This chapter also gives an overview of acoustics monitoring and a review of Artificial Neural Networks (ANN) techniques such as Neural and Conventional Neural Networks (CNN), Application of convolutional neural networks, deep learning and condition monitoring techniques applied to fluid machines.

2.1 Review of Conventional Condition Monitoring Techniques

With the development of modern technologies, especially in electronic, communication and engineering, many CM techniques are available for the industry at a reduced cost. Many industries are interested in applying CM through its impressive and powerful condition-based monitoring techniques, machine failures have a detrimental effect on productivity and maintenance costs therefore a high level of interest in condition monitoring is vital. This method enables the company to monitor each piece of equipment and has its own holistic and personalised condition management programme. This technology has flourished and has shown an increase in data accuracy. The algorithms that are used are precise and reliable in assessing equipment condition and predicting an accurate diagnosis of equipment failure [1-4].

Many other predictive maintenance techniques can be used to monitor machine condition. Machine operators are the most powerful diagnostic tool in a plant and they can use their senses (sight, smell, sound and touch). It has been proven that if manufacturing team members are encouraged to use these correctly they can detect 75% of all equipment related problems at an early stage [5].

CM performs the continuous analysis of machinery and the early detection of problems by means of several different measurement and data processing techniques. Based on measurement techniques, CM can be generalised in three general-purpose monitoring parameters

- Vibration
- Lubrication
- Thermal
- Power
- Process

To gain an understanding of each of the techniques, a brief overview is explained in this chapter. The characteristics of each technique will be explained in the aspect of its operating principles and application conditions.

2.1.1 Vibration

Any machine that has moving parts can generate vibration and has the possibility for vibration monitoring. Some of the common machine parts monitored are gears, bearings, shafts, machine

frame and more. Vibration can be sensed by an accelerometer which is distorted or changed when vibration occurs. It may sense the displacement, velocity or acceleration however it is not only accelerometers that can be used for measuring vibration. All rotating and reciprocating machines such as electric motors generate a wide range of vibration frequencies. The total spectrum of frequencies is called a machine signature [4, 6, 7]. Even two identical machines will have different signature due to the small dimensional and assembly differences [4]. Each peak on the spectrum has its fundamental reason and if there are lots of machine faults the shape of the peak levels in the signatures will change drastically.

An example is a rotor which develops basic frequencies that originate in a motor. The amplitude of the signal at these frequencies will normally increase if the machine develops a fault [4]. Another example is an imbalanced shaft which if constantly exciting the assembly, will develop a forced damped vibration due to the driving force. The amplitude of the forced vibration is highly determined by the magnitude of the driving force. If the forcing frequency coincides with a natural frequency of the system, the resulting amplification leads to an extremely high and destructive level of vibration and this is called ‘resonance’. If a fault produces a signal at a known frequency, then the magnitude of that signal is expected to rise as the faults develop [4]. The vacuum pump consists mainly of rotating parts therefore if the correct sensor is used and at the correct place on the machine this would give a good indication of the health of the machine and according to Alhussein Salim Albarbar to implement a successful CM based monitoring system care should be given to the sensor selection, feature extraction and comparison and lastly the decision process determination [8].

2.1.2 Lubrication

To reduce the cost of machine energy consumption and reduce unnecessary breakdown, it is vital to improve the reliability and availability of those machines as they depend largely on the protective properties of the lubrication. Transmission such as gearboxes will require the oil to be properly applied and free from any degradation for a good run. The purpose of lubrication oil condition monitoring, degradation and detection is to determine whether oils have deteriorated to a point where they no longer satisfy their requirement [9]. Lubrication oil is an important information source for early machine failure detection just like the human blood sample testing to detect the sign of any disease. In recent years, the health of condition monitoring and prognostic of lubrication oil has become very popular among academics and industries. A lot of work and effort has been put into the oil diagnostic and prognostic system development and research. Lubrication oil monitoring provides approximately ten times earlier

warnings for machine malfunction and failure in comparison with the vibration-based machine health monitoring techniques [10].

Many researchers have stated that the main function of lubrication oil is to provide a continuous layer of film between surfaces in relative motion to reduce friction and prevent the process of wear and hence prevent the seizure of mating parts. The secondary function is to cool the working parts, protect metal surfaces against corrosion, flush away the ingress of contaminants and keep the mating component reasonably free of deposits. In a lubricating system, variation in the physical, chemical, electrical (magnetic) and optical properties change the character of the lubrication conditions and lead to the degradation of its protective properties [11].

2.1.3 Thermal

Any human being, machine, process or system constantly releases thermal energy to the environment in the form of invisible radiant energy. When a component or body heats up it radiates more energy from its surface [12]. Medical Thermography is also being used clinically for the research of early pre-clinical diagnosis and control during the treatment of homeostatic imbalances. It's a non-contact tool that uses the heat from the body to help in diagnosing a health condition.

In its application, the Digital Infrared Thermal Imaging (DITI) is used extensively, mainly in the fields of Rheumatology, Neurology, Physiotherapy, Sports medicine and Oncology [13]. Thermography is the science of obtaining images of the heat distribution of a system. With thermal imaging, the inspection can be done while the machine is in full operation and there is no need for any planned maintenance nor any loss of production.

The advantage of thermal imaging is huge:

- It can pinpoint a failure at a very early stage and remedial work can be planned and conducted before a sporadic failure occurs which could then cause a longer delay in production.
- It has a great accuracy that can aid to quickly scan and measure the temperature distribution of the entire surfaces of the machine and electrical equipment that are under normal load.
- Thermal imaging is a non-destructive testing process which involves no physical contact and consequently there is no potential for damage to the system or machine under investigation.

- Increases safety and reduces the risk of fire [14].

2.1.4 Power Parameters

Many plants do not consider the monitoring of power parameters in their electrical system and this technology is emerging rapidly nowadays. This can include the monitoring of electrical parameters including resistance, current and voltages. Any rise in current from a motor will indicate an increase in resistance. In turn, this shows an indication of anomaly happening to the system. This indicates the possibility from a misalignment, jam, blocked filters or damaged bearings. The list is long and can include the monitoring of Instantaneous Angular Speed (IAS) and Motor Current Signature Analysis (MCSA) which is discussed later in this chapter [15] [16] [17].

2.1.5 Process Parameters

Process parameters are other types of elements that can be measured from a system. Many businesses are not running within the operating range of their equipment. Process parameters are a feature that can be unrecognized and should be part of the predictive maintenance programme. If the process of parameter monitoring is included alongside other monitoring programmes, the prediction of the machine failure will be more accurate hence improving the reliability of the machine. The lack of awareness of the technology means that machines could be running at 50% efficiency and the loss is hidden and unknown which is a form of waste.

Process inefficiency nowadays is a serious problem in the plant and the losses in productivity and profitability are sometimes greater than the total cost of the maintenance operation. If the process parameters programme includes the monitoring of the suction, discharge pressures and the current load of compressors and vacuum pumps it would have saved companies a lot of money [18].

The integration and maintenance of components such as; flow meter, ammeter, voltage detector, pressure gauge and much more would be very beneficial and would help the machine to stay healthier and more reliable. However, even though some of the systems are equipped with gauges, thermometers and other instruments, many of the gauges are broken or no longer functioning through lack of planned maintenance. Machines that can be also monitored through the process parameters are boilers, heat exchangers, pumps and much more critical systems in a plant [18].

2.1.6 Application of Conventional Condition Monitoring to Fluid Machine

Not many CM techniques have been applied to the monitoring of fluid machinery. A brief overview of the following few techniques used, such as the vibration sound, IAS, temperature, motor currents applied to fluid machines is explained below.

Based on current CM techniques it has been proven that Surface Vibration (SV) of a cylinder head, dynamic cylinder pressure and crankshaft Instantaneous Angular Speed (IAS) is achievable for the detection and diagnosis of valve faults on a two-stage reciprocating compressor [19]. Accelerometers are preferred to microphones as they can withstand high temperature and are cheaper. The time-domain analysis of the vibration signal provides good information about the location and severity of the valve faults whereas the frequency spectrum of the valve impact can assist for fault detection [19]. According to Elahi, IAS provides useful information on a compressor that can be used for fault detection and fault diagnoses and the signal is very much less likely to be distorted during sampling in an industrial environment compared with vibration or airborne acoustic signal [19].

Mona Jawad Al-Qattan's [16] study was based on Industrial Application of Speed and Power for fault Detection and diagnosis of a large compressor. Her findings in the definition of the effect on IAS and power consumption is that by varying the volumetric clearance pressure this consequently changes the re-expansion and compression strokes of a healthy single stage single cylinder double acting compressor and the IAS undergoes a remarkable change [16]. In her work, the power consumption trends are directly related to the area under the Pressure-Volume (PV) curve which indicates that any factor that affects the PV curve would automatically be reflected in the power consumption plot. According to Mona, her research on the CM system of the hydrogen make-up compressor shows that when the cylinder pressure increases, the load on the compressor increases which leads to a decrease in the speed. In addition to that, the excess volumetric clearance reduced the load on the compressor which in turn increased the IAS [16].

2.2 Review of Latest Condition Monitoring Ideas

Condition monitoring provides thorough information about the status and health of the machine, warning engineers to replace a component in a system before deterioration occurs. This will also help with the pre-planning of potential breakdowns thus avoiding any expensive urgent repairs.

Nowadays the level of quality and precision in condition monitoring is improving.

The advantage of such a highly advanced predictive maintenance tool is that it can be used to not only spot developing faults within a system but also to identify factors in a machine that can cause these faults to develop in the first place. The following sub-chapter gives an overview of some of those new technologies.

2.2.1 Motor Current Signature Analysis

Motor Current Signature Analysis (MCSA) is a relatively new technique and is quickly gaining access in the industry [20]. This technology is an online analysis of current, detecting faults and analysing the trend in a three-phase motor drive whilst the machine is running [17].

This technique was first used in 1980 [21]. It is an inexpensive system which can help in the reliability base maintenance programme and provides savings in the power consumption by providing the most efficient motors [22].

The Motor Current Signature Analysis can identify faults such as:

- shorted turns in low voltage windings
- broken rotor bars abnormality
- air gap eccentricity and certain mechanical failures [17].

MCSA is the monitoring of stator current, more specifically the supply current to the motor. The single stator current monitoring system is the most commonly used in the monitoring of only one phase of the motor supply current. The motor stator windings are used as a transducer in MCSA and pick the induced current signals from the rotor and at the same time reveal information about the health and state of the stator [23].

2.2.2 Ultrasound

The monitoring of ultrasound uses the same principles as the vibration analysis. Both systems monitor the noise that is being generated by the machines to determine the actual monitoring condition. Ultrasonic monitors the higher frequencies, unlike the vibration monitoring which can measure a signal from <1 to 20000 Hertz (Hz) [18]. The frequency range for the ultrasonic signal is 20000 to 100000 Hertz and are beyond the range of a human being [24]. The instrument electronically decodes the ultrasound frequencies through a process called “heterodyning”, down into the audible range where they are heard through headphones and observed as intensity and or dB levels on a display panel. Sound can be received in two ways, i.e through the air and solid surfaces [24].

The main application for ultrasonic monitoring is in leak detection [18] which assists in determining effective leak (mechanical and electrical) and followed-up by action to resolve the issue.

2.2.3 Ultrasonic Condition Monitoring

Ultrasonic Condition Monitoring (UCM) is a technique that uses airborne (non-contact) and structure-borne (contact) instruments to receive high-frequency emissions produced by any operating equipment [24].

There are two types of ultrasound monitoring techniques, active and passive.

The active technique is an approach where a precisely guided beam of ultrasound is transmitted to a physical structure to analyse both surfaces and sub-surfaces discontinuities like disbands, delamination, cracks and porosity at early stages.

The guided wave interacts with the structural discontinuity that reflects from a depth in material or scattering of guided waves in all directions which results in a transmission loss [25].

The passive ultrasound is used mainly for the contact methods of monitoring bearing faults, gear failures, pump cavitation, lubrication and non-contact methods of a leak in a boiler, condensers and heat exchangers monitoring [26], corona in high voltage equipment and electrical discharge [27].

Airborne ultrasound detects high-frequency sound produced by mechanical equipment, electrical discharges and most leakages which are highly shortwave making them very directional and localised, making it easy for them to be separated from background plant noises to enable detection of their exact location [24].

2.2.4 Instantaneous Angular Speed

The analysis of the Instantaneous Angular Speed (IAS) is another form of CM monitoring technique that can be used in any rotating machine, reciprocating engines [28-30] gear transmission [30, 31] roller bearings [32] by the aid of an encoder.

The encoder is attached to the drive end shaft of the rotating machine and the measured IAS is the value of the angular speed at any instant. It is measured in radian per second or Revolution Per Minute (RPM) [33].

The IAS is key information which assists in understanding the machine operation and identifying any potential faults. The IAS is the averaged data between two increments on the

encoder. The rotation of the shaft is the result of the global operation of the machine which contains valuable information about all the mechanical processes contributing to the constant rotation. Any failure has a theoretical effect on the instantaneous speed [28-30].

When a crankshaft rotates during an angle $d\Theta$ in time dt, the average angular speed over the interval dt is given by $\omega(t) = d\Theta/dt$.

The smaller time interval dt means that $\omega(t)$ will be closer to the IAS. These methods can be applied to diagnose faults such as leaking valves within the compressor.

The IAS of any compressor will vary over the working cycle as stated by Yuhua et al from the Mechanical System and Signal Processing (MSSP) [34, 35].,

During the compression stroke, the IAS will be less than during the expansion stroke. The main disadvantage of this technique is that it requires more work and is complicated to implement. However this technique is good for confirming the identification of faults detected by other methods [36].

2.2.5 Application of Latest Condition Monitoring Ideas to Fluid Machine

Liang et al [37] developed a procedure for valve fault diagnosis utilising the vibration responses both analytically and experimentally. The procedure used Smoothed-Pseudo-Wigner Ville Distribution (SPWVD) to interpret monitored impact vibration responses. The impact between the valve plate and seat operation shows a characteristic pattern in the time-frequency. A higher frequency vibration is observed at the closed position as opposed to when open coinciding with a higher pressure in the cylinder during the compression stroke causing the valve to move faster and resulting in a higher impact on the valve seat. This study shows that a discharge valve takes more time to open than close due to the difference in spring stiffness.

Besides, Elhaj et al [38] also conducted a study on the early detection of leakage in reciprocating compressor valves using vibration and acoustic wavelet features. Their main finding was that valve leakage is the primary issue that causes failure and this can have a major effect on the operation and performance [19].

They found that there are two main sources of vibration and acoustics, the valve impact and the non-stationary flow induction. Their work shows that the conventional analysis in the time-frequency domain could not detect information from the acoustic signal due to noise interference [38]. This assumption is in line with Mohamed Ali Elhaj's statement at the beginning of the literature review [19].

However, according to Elhaj et al [38] the joint time-frequency domain analysis of the Continuous Wavelet Transform (CWT) was capable of extracting fault detection successfully however the acoustic monitoring needed more signal processing than vibration monitoring but this can be implemented remotely as stated by the authors [38].

Manepatil et al [39] developed a mathematical model to simulate the effect of piston ring leakage and valve faults on a compressor cycle. Manepatil's work was to simulate the effects of faults so that the cylinder pressure could be determined in the time domain and to predict the machine performance of CM. His study proved that suction valves leakage resulted in a steeper re-expansion stroke, followed by a decrease in the discharge pressure peak, an increase in the volumetric efficiency, flow rate and a decrease in the performance ratio. The discharge valve leakage resulted in a flatter re-expansion stroke which causes the compression stroke to move.

The Discharge valve leakage indicated a decrease in the volume flow rate, an increase in volumetric efficiency and the cylinder pressure. Besides, the piston ring leakage ends up with a decrease in volumetric efficiency and cylinder pressure [39].

2.3 Review of Acoustics Monitoring

Direct sound listening on moving machinery is intuitively used by experienced engineers through the holding of a screwdriver against a bearing housing however this method provides an intuitive evaluation which is more of an art rather than science [40].

Several diagnostic techniques using sound signatures and data processing have been designed but they have not been used widely which causes great difficulty in the interpretation of sound signals. The instrumentation technique is like the vibration analysis but the problem lies in the fundamental between the transmissions [40]. Sound is vibration transmitted through liquid, solid or gas. It is made up of frequencies that are easily detected by ears. Acoustics is the study of sound over the entire range of different sources types, propagation modes and receiving conditions [40]

2.3.1 Airborne Acoustics

Sound monitoring is the fluid-borne pressure wave phenomena which are also known as airborne. Generally, this is simply airborne and may not be either melodious or harmonic in the tonal sense [41]. Sound is a scalar quantity with no directional parameter and the positioning of the sensor makes no difference, this a big problem in the diagnostic monitoring

of airborne sound [41]. Airborne acoustic can be used for the measurement and detection of defects in the rolling element bearings [42], gearbox system [43] and much more. Airborne acoustic monitoring has different advantages and disadvantages.

It has the possibilities of replacing the need for several vibration sensors that need mounting at various locations on the machine and the potential of being detached from the machine surface. The airborne acoustic by nature is a non-contact system and is good in high frequency and short wavelengths [43].

2.3.2 Acoustic

Acoustics is the science of sound which deals with the origin of the sound and its propagation, either in free space, pipes and channels or in closed spaces [44]. It can also be defined as the study of sound over the entire range of different source types, propagation modes and receiving conditions [45]. Infrasound is below the sound of hearing which is less than 20 Hz known as the audible range [46]. Infrasound can cause health damage in an extreme situation, it has an unpleasant effect on human beings, a side effect being nausea [44]. Any sound with a frequency above the audible range of hearing, that is above 20 000 Hz (20 kHz), is known as an ultrasound [46]. Acoustic monitoring is the fluid-borne pressure wave phenomena which are also known as airborne. Generally, this is simply airborne and may not be either melodious or harmonic in the tonal sense [41]. Acoustic can be defined as a time-varying disturbance of the density of a fluid from its equilibrium value, which is accompanied by a proportional disturbance of sound pressure and is associated with small oscillatory movements of fluid particles [47]. Acoustic monitoring of machines has been around for many years and this technique focuses on the analysis of noise or acoustic signals. When machines operate they create both vibration and noise. The reason why acoustics is preferred for the monitoring of fluid machines is that it is non-destructive.

2.3.3 Microphones

Microphones are used to pick up acoustic signals instead of vibrational sensors. Microphones are sensitive, easy to mount and possess wide frequency response ranges that can generate appropriate and valuable information. It can be used in many applications where sensors cannot be added such as gearbox, bearing, engine and pumps [48], [49], [50] Microphones are electroacoustic transducers and can convert the acoustic signal into an electrical current which can be processed and displayed. They are known to be small in size, reliable, high in sensitivity and low in cost [51].

2.3.4 Acoustic Compared to Vibration

Vibration signal, measured on machines, generates a wide range of vibration frequencies with valuable information, however when implementing the vibration technology many sensors are required and need to be mounted on the machine, whilst with airborne sound measurement it can be placed away from the machine eradicating any high-temperature vibration sensors, mounting elements and reducing any associated risk. Some of the common machine parts monitored are gears, bearings, shafts, machines frame and many other mechanisms. If the correct sensor is used and at the correct place on a machine this would clearly give a good indication of the health of the machine but controversially this technique is limited to its application and machine availability as some plant run constantly and the sensors can't be connected to the machine. The advantages of using airborne acoustic monitoring are that it has the capability of replacing the need for several vibration sensors that need mounting at various locations on the machine and the potential of being detached from the machine surface. The airborne acoustic, by nature, is a non-contact system and is good in both high frequency and short wavelengths [43].

2.3.5 Application to Acoustic Monitoring

G Ramroop et al investigated a comparison of conventional vibration and acoustic monitoring in a multi-stage gearbox system. They proved that acoustic condition monitoring offers more advantages over the conventional surface vibration methods [43]. However, the use of the correct techniques is dependent on its application whereas Saruhan et al in their work of vibration analysis of rolling element bearings defects, state that the best techniques to use for the rolling element bearings condition monitoring is the vibration spectrum analysis [52]. Conversely, Abdullah et al describes that acoustic emission offers earlier fault detection and improved identification capabilities than the vibration analysis in rolling element bearings [53].

2.4 Review of Artificial Neural Networks

There are various types of neural networks but they are all application dependent. In this research, CNN will be based on obtaining the data from Reciprocating Compressor (RC) acoustics for the detection of an ideal position away from the RC for collection of data. A good literature review is required on the topic hence below is a brief understanding of neural networks. The concept of "Artificial Intelligence" (AI) was first established in the mid 19th Century at Dartmouth College in the US by four professors: H.Simon et al at Carnegie Mellon University, Professor J.McCarthy at Stanford University and Professor L.Minsky at

Massachusetts Institute of Technology. Their vision on AI is that machines will have the capability to comprehend and react similarly to the human mind, opening the opportunity of using computers to simulate human intelligence [54]. According to Stefan Holtel in his article on "Artificial intelligence creates a wicked problem for the enterprise" he postulates that at the beginning of the 21st Century there is a possibility that artificial intelligence will be available on a larger scale and will outperform the human brainpower [55].

According to Yunhe Pan and his work on "Heading toward Artificial Intelligence 2.0," he stipulates that AI is making a rapid transformation. Media and politics are showing strong interest and big firms such as Google, Microsoft, Twitter, Apple and Intel are investing a huge amount of money in the research and development of AI [54].

The requirement for AI is needed in areas where it is not easy to prove analytical knowledge. With the aid of AI, new knowledge is created from the existing idea and input data form a set of monitored variables. AI can be used in CM vibration data sets and contains a lot of valuable information that can result in a large set of features. Nevertheless, Mahmud Ahmed believes that AI is an ideal method compared to the conventional methods such as frequency domain, time domain and envelope analysis, allowing great savings and efficiency. AI is more user-friendly and economical compared to the conventional methods as it does not require a lot of human resources with a wealth of experience, nor an enormous amount of time which can be very significant in price [56].

2.4.1 Brief Development of Neural Network

The first digital computer-based artificial neural network was developed in the early 1950s. Since then many researchers, mathematicians, scientists and engineers have done an enormous amount of work with Artificial Neural Networks (ANN) [57]. Neural networks are an excellent tool made up of a set of algorithms that assist us to learn lots of different types of patterns. It has been modelled very similarly to the human brain which is also designed to recognize patterns [58]. Our brain contains neurons which resemble a kind of organic switches. Depending on the strength of their chemical or electrical input these switches can alter their output state. The neural network in a human brain is an immense interconnected network of neurons [59].

If we repetitively learn an art, that means we are hard-wiring our brain to the network and repeatedly activating certain neural connections.

The outcome would be fruitful which is tailored to the specified input [59]. The Biological Neural Networks (BNN) contain biological neurons or nerve cells and there are about 200 billion neurons, 32 trillion connections. The neuron size is 10 to 6 cm, 6 to 10 joules per second of energy consumption with learning capability [60]. Artificial Neural Network merely tries to imitate the behavioural state of the brain [59]. A neural network is generally distributed into two sections of research. The first application is the neuronal modelling, which stresses on the biological plausibility of artificial neural network and the second approach is the exploration of the artificial neural networks as a parallel computing architecture application [61]. In this thesis, the second approach will be used. The following section gives some basic concepts of artificial neural networks.

Neural Network (NN) transmits sensory data via a type of machine perception, labelling or clustering raw input. They recognize numerical patterns, contained in vectors, where there is all real-world data whether it be sound, images, text, time series, electrical or mechanical signals [58].

2.4.2 Basic Concepts

As explained briefly above an ANN is made up of neurons, a connection topology and a learning algorithm [61]. ANN is fast but inferior to BNN with 102 to 104 nodes depending on the type of application and design network. The learning capability is very precise, well-structured and formatted data is needed to tolerate ambiguity. It has a robust performance but has the potential to be tolerant to a fault and has a continuous memory [60]. Artificial Neural Networks can be considered as weighted directed graphs where neurons are nodes and directed edges with weights are connections between neuron outputs and neuron inputs. Weights are defined as the information used by the neural network to solve an issue.

The ANN collects information externally in the form of pattern and image in vector form. These inputs are designated by the notation x(n) for number of inputs in a mathematical form. Each input is multiplied by its corresponding weights.

Normally weight is the strength of the interconnection between neurons inside the neural network. Inside the computing unit, the weighted inputs are added. If the weighted sum is zero, bias is then added to increase the output to higher than zero or to scale up the system response. There are both linear and non-linear activation functions where the activation function is set to the transfer function to get the desired output. The most commonly used activation function is binary and sigmoidal hyperbolic [62].

2.4.3 Artificial Neural Network Architecture

Figure 2-1 below shows an ANN Model. In ANN, there are a huge number of artificial neurons called units which are organized in a series of layers. An ANN usually comprises of different layers as shown in Figure 2-2 below.

Input Layer

The Input layer contains Artificial Neurons which are specific units that are input from the outside world where the network will learn to recognize patterns or processes [60].

Output Layer

Output Layer comprises of units that respond to information about how it learned any task [60].

Hidden Layer

Hidden Layer is units that are between the input and output layers. The hidden layer changes the input so that the output unit can be utilized [60]. NN are generally fully linked where each hidden neuron is fully connected to every neuron in its previous input layer and the following output layer [60].

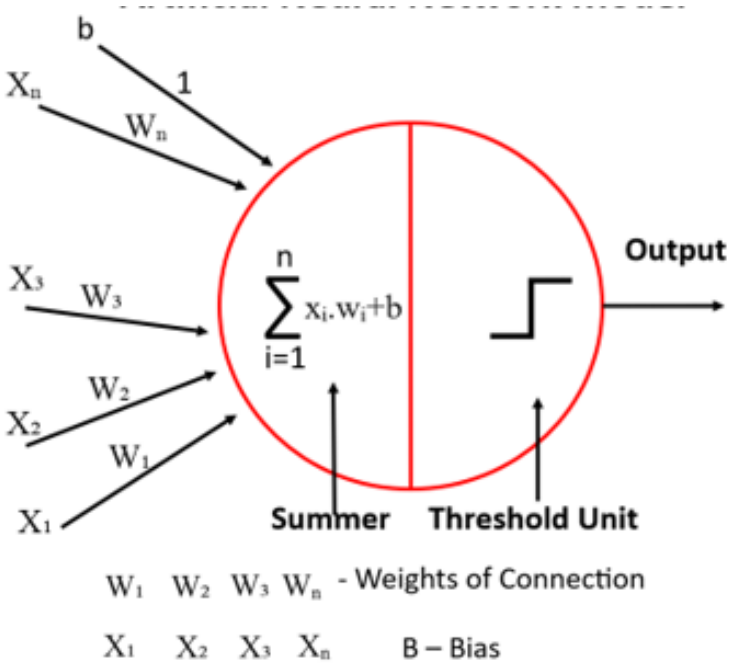

Figure 2-1 An Artificial Neural Network Model [62]

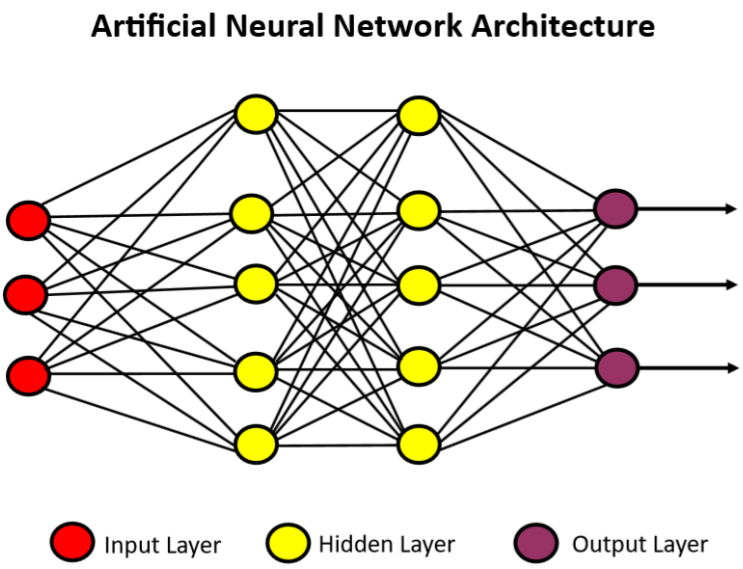

Figure 2-2 Artificial Neural Network [60]

2.4.4 Convolutional Neural Networks

Convolutional Neural Networks (CNN) is a combination of artificial neural networks and recent deep learning methods. Due to its distinct correlation in data mining, CNN's can decrease the number of trained parameters in networks to improve the back-propagation algorithm deficit of a forward propagation network [63]. CNN pre-processing is much lower in comparison to other classification algorithms. In the olden days, the filter methods were hand-engineered whereas nowadays with adequate training, CNN can learn these filters and their characteristics. The CNN architecture is like the connectivity pattern of neurons in the human brain and was enthused by the organization of the visual cortex where each neuron responds to stimuli only in a restricted region on the visual field known as the receptive field [64].

Xiaofeng, et al postulated that CNN's attain optimal results in the application of recognizing handwritten numerals and that CNN's can be used in more various recognition tasks. The training speed and final training effect can be immensely influenced by the number of filters in each layer of CNN's structure. The training time can be shortened and certain recognition rates retained if the suitable number of filters are selected appropriately in each layer. If there are not enough samples an excessive number of filters can make the network training fail to converge and prevent attaining an effective recognition. They strongly believe that if it is possible to increase the training speed of the network and improve the performance and the versatility of the models, great improvement of the technical level of convolutional neural networks in image recognition can be achieved and applied in various fields [63].

As previously seen under the supervised learning chapter, a neural network is a strong tool where classification tasks are dependent on various labelled datasets [58]. Simard et al postulated that it is essential to get a larger training set, expand it by adding a new form of distorted data and that convolutional neural networks are appropriate for many visual document problems. However, they confirmed that CNN also exploits the facts that the inputs are dependent elements with the knowledge of input topology but arise from a spatial structure. According to their research, the convolutional neural network does not require complex methods, the results give better analysis and allow simple debugging [65].

2.4.5 Deep Learning

Deep learning will be explained further in Chapter 8. Deep learning is a segment of machine learning that teaches computers to mimic human logical behaviour, in another sense to learn from experience [66] as explained previously.

Machine learning algorithms employ computational methods to learn and project information directly from data without the need to depend on a predetermined equation as a model. This technique of deep learning is suitable for image recognition, facial recognition, the possibility of autonomous driving, lane detection, autonomous parking, pedestrian detection and motion detection. Deep learning takes advantage of the neural networks to learn important representations of features directly from data.

Inspired by the biological nervous systems, neural networks combine multiple nonlinear processing layers, using simple elements operating in parallel. State-of-the-art accuracy in object classification, sometimes exceeding human capability, can be attained through the deep learning models [66].

Models are trained using a large set of labelled data and neural network architectures that consist of numerous layers, sometimes including some convolutional layers. Training these models can be intensive in computing and sometimes training can be accelerated by using a high-performance Graphics Processing Unit (GPU). Lots of deep learning systems use an image file, sometimes they are immense, for ease of accessibility, MATLAB gives access to the image datastore function to read batches of images automatically for faster machine learning processes and computer vision applications. If the memory is too large it imports data from the image collection and depending on the folder names it will label the image data automatically [66].

2.4.6 Transfer Learning

Deep learning applications are usually employed in transfer learning. A new pre-trained network can be used as an initial point to learn a new task. Fine-tuning a network with transfer learning is much easier and faster than training a new network. The network can be made to learn a new task quicker by utilising a smaller number of training images. The advantage is that the pre-trained network would have already learned a large set of features that can be applied to a wider array of other small tasks. It can fine-tune a pre-trained network with smaller data sets more efficiently than the original trained data. For a larger dataset, transfer learning may not be as fast as training a new network [66].

The advantages of transfer learning are:

1. Faster and easier than training a new network
2. Reduce dataset size and training time
3. Transfer a pre-trained network learning features to a new problem
4. Deep learning can be achieved without the need for learning how to create an entire network [66].

2.4.7 Supervised and Unsupervised Learning

Classification tasks depend on the labelled datasets where humans transfer their knowledge to the datasets so that the neural network learns the correlation between label and data which is known as supervised learning. This can identify a person in images, recognize facial expressions, detect faces, identify objects in images, recognize gesture in the video, identify speakers, transcribe speech to text voice recognition, classify text as spam (in emails), fraudulent claims and more [58].

The detection of similarities is made through grouping or clustering. Unsupervised learning is learning without labels. The world is made of a majority of unlabelled data.

2.5 Application of Artificial Neural Networks and Deep Learning Applied to Condition Monitoring

A brief overview of the ANN technique applied to fluid Machine is explained below, such as the work of Ahmed Mahmud [56] who works on the use of advance soft computing for machinery CM. He believes that the investigation of vibration signal under different operating conditions has shown that the signal is complex and there is a huge amount of information

associated with the signal waveform and that this approach is difficult, however, his result demonstrates that the vibration analysis is a reliable technique to identify the health of reciprocating compressors by the valve motions. He also states that the time domain analysis and frequency domains are more sensitive to fault detection [56].

Nowadays ANN can automatically detect and diagnose machine condition. Probabilistic Neural Network (PNN) also exists which has improved in recent times as it provides sound statistical confidence levels [56]. It is possible to model higher-order interaction and predict multiple topics using shared hidden features through the Neural Networks according to Erik Wiener in his work on "A Neutral Network Approach to Topic Spotting". His work was based on a data-driven approach to topic spotting that applies nonlinear networks to estimate topic probabilities [67].

Tiwari et al developed an innovative technique based on the Bayesian Neural Network (BNN) to model the temperature variation record from the Western Himalayas. The BNN is trained with the Hybrid Monte Carlo (HMC) and Markov Chain Monte Carlo (MCMC) simulation algorithm.

The result of the new algorithm was tested on destructive first-order Autoregressive (AR) and random models. It was then applied to model the temperature variation record decoded from widths of trees of the Western Himalayas for the period spanning over 1226 to 2000 AD. The best network parameters were chosen to model the actual tree ring temperature data. It was found that the BNN prediction model, when compared to ANN and AR models, makes a better prediction. This new BNN modelling technique is a feasible means for the study of climate and may be used for modelling other kinds of environmental data [68]. Patel et al used artificial intelligence techniques to predict and analyse bearing faults. They trained the backpropagation multilayer neural network and used it to test 369 pre-treated normalised features. They argue that support-vector machine techniques can give better results over ANN [69]. In M. Ahmed et al work, regarding the use of Genetic Algorithms (GAs) and neural networks (NNs) to select an effective diagnostic feature of a reciprocating compressor, a huge number of common features are computed from the time and frequency domains and envelope analysis. They found that the envelope analysis was the most capable of differentiating their application of GAs and NNs from three common faults, namely valve and intercooler leakage and loose drive belt. At the same time, the spread parameter of the probabilistic NN was optimised. They established that their technique, with the trained NN, possesses the general characteristics for fault detection and diagnosis [70]. Many researchers have effectively investigated machine failures

using ANN. Samanta et al compared the performance of bearing fault detection using two different classifiers: Artificial Neural Networks (ANN) and Support Vector Machines (SVM). Their findings demonstrate the effectiveness of the features and the classifiers in the detection of machine condition [71]. Samanta also used GAs to improve the features vector for fault gear detection using experimental vibration data from a gearbox. It was found that SVM is better than ANN, without GA. With GA the progress of both classifiers is comparable in most situations. The training time of SVMs is considerably less compared to ANNs [72].

Artificial intelligence (AI), if widely used in the field of condition monitoring and fault diagnosis of machines, will assist a lot of companies to save a large amount of money as 40% of company expenses go into maintenance. Maintenance cost is like an iceberg where most of the ice is underneath the water. The subsection of this chapter will explain some of the previous research and developments in the field of signal analysis through the aid of artificial intelligence. As previously explained above in Section 2.4 Review and Application Intelligent Systems, such as Artificial Intelligence, Artificial Neural Network (ANN), Genetic Algorithm (GA), Support Vector Machine (SVM) and Fuzzy Logic System (FLS), Deep Neural Network (DNN), Probabilistic Neural Network PNN, Bayesian Neural Network (BNN), Autoregressive (AR), Neural Networks (NNs) and Convolutional Neural Network (CNN) can be a great tool if it has the capability of automatically detecting and diagnosing machine condition.

Scholars from Boston University and Cambridge University studied the interactions amongst earthquakes, precursor quakes and seeded fault quakes to create a new technique to predict a real earthquake. Those researchers have created an AI system to analyse and predict the acoustic signal coming from the faults.

They have used steel blocks to simulate the physical forces at work in a real earthquake and record samples of the seismic signals and sounds that are emitted. Machine learning was then used to find the relationship between the acoustic signal coming from the faulty block then analyse and predict the failure. They successfully found that the machine learning algorithm was able to determine a specific pattern in the sound which was thought to be mere noise that normally happened long before an earthquake. This characteristic of the sound pattern can give an exact estimation of the stress on the fault and estimate the remaining time before it fails. This is a breakthrough in science as this is the first time that machine learning has been used to analyse acoustic data to predict when an earthquake will occur, without any warning, long before it happens. As the datasets are too large to handle manually, machine learning analyses the data and then gives an unbiased warning to people before an earthquake occurs [73].

Past research has proven that the use of AI in ANN is capable and efficient in predicting faults in the machine [74]. More work has been done in the machine diagnosing of bearing, rotating machine and mechanical gear with more vibration signal compared to acoustic. There is a big demand for more Acoustic Emission (AE) analysing tools for a different source of AE data. Due to this demand new advances have been made in flexible pattern recognition software, combining traditional graphical AE analysis and Advanced Supervised Pattern Recognition (ASPR) and Supervised Pattern Recognition (SPR). Various test cases on the application of ASPR techniques on AE data has explained the damage evolution and the possibility of noise discrimination [75].

Balusahi et al have recommended a system to diagnose the faults of gears by wavelet transformation and ANN for AE signal processing. Features were being taken from the wavelet transformation and used as an input to an ANN-based on analysing method [76]. The AE vibration signal was utilised as an input signal in the fault prognosis systems. In addition to that ANN was used as a prognosis system in detecting failures in rotating machine [77]. Previous study in the use of AE for early detection of helicopter rotor head dynamic component faults has been done using the wavelet method to analyse stress wave of a flight test data by assessing the background noise in comparison to machine failure results. To determine the correct flight regime the feed-forward neural network was utilised as a classifier [78].

The utilisation of neural networks in a grinding test with an aluminium-oxide-grinding wheel was tried to reach the classification on burn degrees on the surface of the grinding machine by Aguiar et al. The inputs of the neural networks used for the statistics from the digital signal processing were the AE and power signal together [74].

Goebel et al designed a hybrid architecture, containing fuzzy logic and neural network to withstand the feeble point of the common methods for monitoring and diagnosing an unattended milling machine. Acoustic emission and force spindle current were utilised as inputs to the neural network after undergoing some signal processing in the calculation of the membership functions of the fuzzy relations. The problem of tool wear and chattering was also approached by fuzzy logic principles [79].

Artificial intelligence has many advantages in comparison to traditional mathematical modelling and statistical analysis [80].

It has been found that ANN is the most popular method in condition monitoring with Acoustic emission signal. More work has been carried-out on ANN in comparison to the use of fuzzy,

SVM and GA [80] and CNN [81]. ANN-based on AE has been successfully applied to several applications.

However, the application of AE, advance signal processing combined with AI in the conditioning of machine is limited. There is still a gap in the world of AI to CM where lots of new advancement in this technology can be achieved. This allows for more opportunities in the development of new intelligent signal processing techniques, sensor and data acquisition in the field of condition monitoring, hence the reason why CNN will be used to mine data from RC acoustics for the detection of best location for data collection in this study as this is a novel approach and is a contribution to knowledge. Furthermore, this CNN based scheme will allows high diagnostic accuracy, as well as the determination of the most suitable microphone localisation.

2.6 Research Gap Identified

A lot of developments have been made in the field of CM by many scholars in the last half century however as our world is becoming increasingly competitive, demand from industries is becoming the norm. However further demand shows a surge in superior precision and high quality. Technology is moving so fast that the computational of data and cost of system implementation is becoming unfeasible.

Numerable amounts of research is studied in various types of CM used in the industry together with its application to fluid machines. Whilst there are many new research methodologies namely: MCSA; ultrasound; airborne acoustic; instantaneous angular speed and new vibration methodology, ANN techniques such as Neural and CNN however there is little evidence new techniques based on airborne signal differences through CNN combined with acoustic. Although it is evident that those previously discussed techniques are already making an industry change their limited process capability and the reduced relationship and integration to CNN is evident.

However, the application of AE, advance signal processing combined with AI in the conditioning of machine is limited. There is still a gap in the world of AI to CM where lots of new advancement in this technology can be achieved. This opens more opportunities in the development of new intelligent signal processing techniques, sensor and data acquisition in the field of condition monitoring.

Therefore, CNN techniques in conjunction with acoustical signal have been used to determine the characteristics and difference in accuracy in finding the most suitable signal acquisition

position from a two-stage reciprocating compressor with various discharge pressure with and without faults.

Phase I

Evaluating Condition Monitoring Techniques based on a Laboratory Compressor

Chapter 3

Mathematical Modelling and Numerical Analysis of Dynamic Responses of a Two-Stage Reciprocating Compressor with Different Faults

Chapter 4

Evaluating Condition Monitoring Techniques based on Intrusive and Non-intrusive In-Cylinder Pressure Measurements

Chapter 3. **Mathematical Modelling and Numerical Analysis of Dynamics Responses of a Two-Stage Reciprocating Compressor with Different Faults**

This chapter investigates the dynamic responses behaviour of a two-stage reciprocating compressor by modelling and numerical analysis. The dynamic responses of interests include Instantaneous Angular Speed (IAS)/torsional vibration, motor current, structural vibration and airborne acoustics that can be perceived by non-intrusive or even remote ways. The model developed consists of a motor model, in-cylinder pressure model, mass flow models, crankshaft IAS model, valve motion model that takes into account common faults on valves, intercoolers, motor and mechanical transmission. The numeral analysis focuses on the evaluation of monitoring information that is included in each dynamic response. Specifically, the numerical solutions of different models are obtained for both baseline and faulty cases; the solutions due to faults is subtracted from the baseline one, which results in pure changes or signatures caused by faults for a straightforward and yet accurate comparison made in the angular domain. Based on these changes quantitative evaluations can be made for each dynamic response upon its suitability for implementing system-level and/or component level diagnostics. Besides, critical comments are also made on the complexity of data acquisition and process of the responses.

3.1 Introduction

The use of external measurements signals such as current, pressures, IAS, vibration and acoustics for motoring compressors, a good knowledge of the various internal processes variables such as pressure oscillations, air flows, valve, piston and crankshaft movements are all essential. The investigation of reciprocating processes using mathematical modelling can be an effective tool which enables to link the external measurements with internal variables consequently gaining an understanding of characteristics of measurements towards revealing the changes inside the compressor. In general, the world around us operates through the description of our beliefs and those beliefs are translated into the language of Mathematics [82].

In this chapter multiple models are derived and overviewed for the conversion of electrical energy from an induction motor into the compressive energy of a Reciprocating Compressor (RC). To examine external measurements of interest the model includes a power flow electrical model, three-phase induction motor model, dynamic of a crankshaft and piston-driven mechanism model, torque performance model of the induction motor to the crankshaft, kinematics of a crankshaft piston mechanism model, in-cylinder pressure model, mass flow model of suction and discharge valve dynamic model.

The derivation process will allow the various physical processes in compressor operation to be understood analytically through sub-process, which helps to gain a general trend of different influence factors on compressor operation and paves the way for subsequent numerical analysis. The numerical analysis then allows for a more accurate understanding of the complex compressor system that is integrated by several models with different physical principles. In particular, the changes of interested measurements can be quantified for subsequent data acquisition and analytics in accurate and efficient methods.

The effect of various physical parameters has been considered for mathematical analysis and appropriate thermodynamic equation has been utilised for the models. Many advantages can be emancipated from models such as:

- Assisting in getting a good knowledge of the machine and the relationships of its component predicting fault signatures in RC. Machine reliability can also be improved through the modelling of the reciprocating compressor and fault simulation [83].
- Can help formulate ideas and identify underlying assumptions [82].

- Can assist Matlab to perform numerical calculations.

Specifically the model development mainly follows the work [84] that has been validated experimentally. However, new understandings of modelling Vibro-acoustics have been included to more accurately describe the vibroacoustic formulation and behavioural changes with operating conditions and fault variations.

3.2 Overview of Reciprocating Compressor Models

The focus of this study is on a two-stage, single-acting reciprocating compressor, with 'V' form cylinders, which are employed widely in industry. The compressor delivers compressed air to a horizontal air receiver. The crankshaft is driven by a 'V' type transmission belt which is powered by an electric motor where the electrical energy is converted through a connecting rod from mechanical rotational to linear motion as shown in Figure 3-4.

At the start of the compressor, the motor starts driving the pulleys through the V-belt which then in turn force the crankshaft to rotate causing the first cylinder (low pressure) piston to move downwards from Top Dead Centre (TDC) to the Bottom Dead Centre (BDC) and this causes the suction valve to open through the pressure difference across the valve head. In the compression cycle, the (BDC) returns to (TDC), once the in-cylinder pressure is higher than the plenum pressure this causes the valve to be forced open moving the pressure to the next stage of the second cylinder (high pressure) through the intercooler which cools the air by removing the heat that is created after the first stage compression. After the second stage air starts to build in the storage tank to a set value, when that is reached a diaphragm pressure switch cuts off the electrical circuit and stops the motor. The processes of the model are based primarily on the electrical, mechanical and fluid transmission and motion which will be discussed further below.

3.2.1 Mathematical Modelling Objectives

The objectives of the mechanistic model are to evaluate the dynamic response and effect of the different operating conditions of the existing reciprocating compressor model. The model will also investigate the working principles of how gas in a reciprocating compressor is created. Initiating from the motor induction, crankshaft motion, in pressure volumes of both first and second stage, intercooler pipe gas transmission to air distribution. This can provide important signatures that can't be studied and simulated in a real-time scenario [84], developed scientific understanding, tests the effect of changes in the system and help the decision making [82]. The

language of mathematics is very precise and this will describe the behaviour of the reciprocating compressor and assist in formulating ideas and identify underlying assumptions [82]. Solving engineering problems through computational approaches are vital due to their application and effectiveness. As briefly explained above, the language of mathematics is very precise as it is a concise language with well-defined rules where the numerical calculations can only be achieved by computers [82].

3.2.2 An overview of Reciprocating Compressor Modelling

Some relatively simple mathematical models have been developed since 1950 which explains the compressor, its working mechanism and fluid. The early model was developed by Costagliola [85]. His study was mainly based on the analysis of valve dynamics, most models are now based to some degree on his pioneering work.

In 1967, Wambsganss et al [86] developed a similar model based on the performance of a sealed hermetic refrigeration compressor fitted with reed type valves and using air or R12 refrigerant. Their correlation could be judged as being good when allowances are made due to the size of the small compressor and its valve. MacLaren et al carried out a similar exercise and concluded that an analytical model could provide qualitative results much more cost-effectively. The assumption has been made that the valve had only a single degree of freedom and this was not sufficient to represent the valve dynamic in a high-speed compressor [87]. Borisoglebski et al [88] combined the simultaneous flow and dynamic equations into a single non-linear differential equation, the same as Costagliola. In 1970, Traversari et al designed a model based on the theory of Costagliola with few modifications compared to MacLaren et al. Traversari concluded that there were differences between analytical and experimental results [89].

There are a variety of approaches on how to simulate the cycle of a compressor and the first type of model is the polytropic or isentropic principle inside the cylinder according to Li [90] and Posch et al [91]. They are used to predict mass flow rate, electrical power and discharge temperature. Posch [91] concluded that there is no obvious model that can satisfy the accuracy demands. Singh postulates that the modelling for a reciprocating compressor can be improved by accounting for the suction and discharge line oscillation which would bind a stronger internal relationship within its mechanism [92]. Manepatil et al [39] developed a mathematical model to simulate the effect of piston ring leakage and valve faults on a compressor cycle. His model proved that the in-cylinder pressure can predict compressor performance [39]. Besides,

Liang et al [37] developed a procedure for valve fault diagnosis utilising the vibration responses of the cylinder head. Elhaj et al model on numerical simulation shows how valve leakage influences the load with various operating condition. His experimental model demonstrates the use of in-cylinder pressure and speed fluctuations of the crankshaft to detect and diagnose various faults [84] [93]. Dutra et al model on the hermetic RC for prediction of compressor performance proposed a single-phase motor model for the calculation of motor slip and estimation speed of the compressor at the different operating condition. His work was also based on the relationship of motor efficiency and compressor power. The predicted model was in good agreement with his experimental model [94].

The brief review above demonstrates the existence of some RC models in determining the simulation of the behaviour affecting its performance. However, not many researchers have modelled an RC with the objectives of investigating the dynamic responses behaviour and numerical analysis.

3.3 Motor Current Model

3.3.1 Fundamentals of Induction Motors

The principles of a three-phase motor are briefly discussed in the following for dynamic modelling. Induction motor consists of two main components: the stator and rotor both of which have three identical and symmetrical windings positioned 120° apart. A small air gap separates the rotor from the stator as shown in Figure 3-1 and the legend is indicated in Table 3-1 [95].

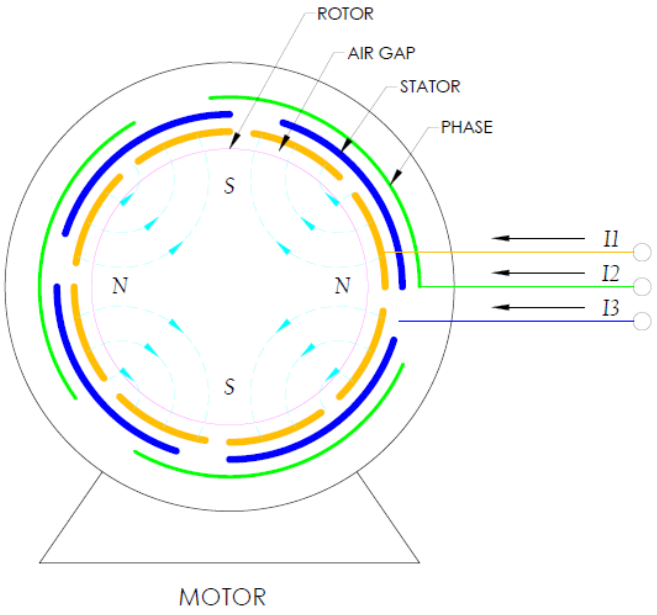

Figure 3-1 Three Phase Induction Motor [95]Error! Reference source not found.

Table 3-1 Three Phase Four Pole Induction Motor

Three Phase Four Pole Induction Motor	
1	Phase 1
2	Phase 3
3	Phase 2
4	Rotor
5	Air gap
6	Stator

Three sets of voltages (V_1, V_2, V_3) are applied to the stator causing three sets of current (I_1, I_2, I_3) to flow. A rotating magnetic field which is also known as the synchronous speed n_s and rotor speed n is produced with alternate N-S poles.

$$n_s = \frac{120f}{p} \tag{3.1}$$

where f is electric supply frequency of the stator in hertz; p is the number of pole pairs.

The definition of slip is the difference between the synchronous speed n_s and rotor speed n which is calculated by [95]:

$$s = \frac{n_s - n}{n_s} \tag{3.2}$$

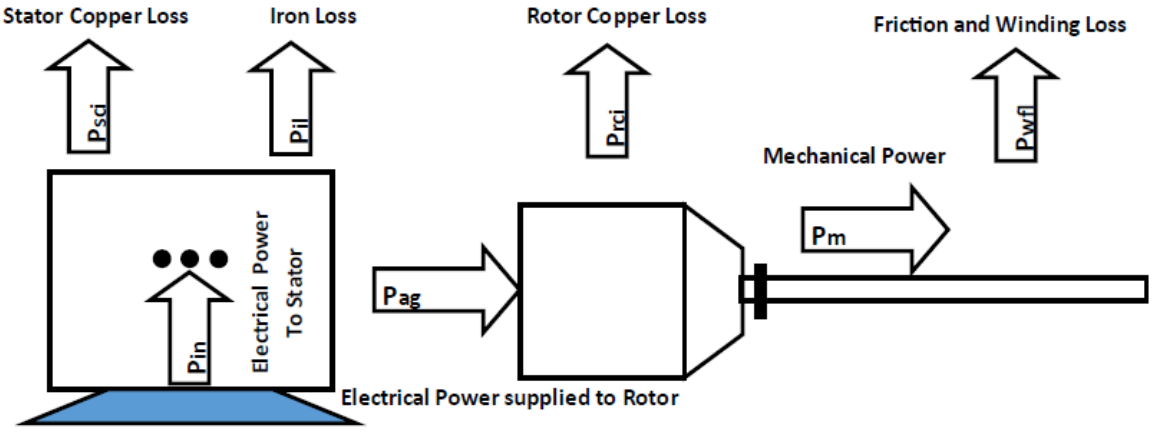

Figure 3-2 Power Flow Electrical Model of an Induction Motor [95]

Figure 3-2 describes the conversion of electrical energy into mechanical energy in an induction motor. Initially the electrical power P_{in} flows into the stator. A partial of the electrical power P_{sci} is dissipated heat in the windings due to the stator copper losses whereas the remaining electrical power P_{il} is dissipated heat in the stator core due to iron losses. Consequently, the remaining electrical power P_{ag} is transported across the air gap and transferred to the rotor through electromagnetic induction. P_{rci} which is another percentage of electrical power is dissipated as heat due to the rotor copper losses. Lastly P_m which is the residual electrical power is available in the form of mechanical power [95].

In practice mechanical power to drive the load $< P_m$ due to P_{wfl} where $P_{rci} = P_{ag}$, therefore mechanical power can be expressed as:

$$P_{m} = P_{ag} - P_{rci} \ (1-s)P_{ag} \tag{3.3}$$

Motor torque T_m can be calculated by the mechanical power by combining Equations (2) and (4) as described by [95].

$$T_m = \frac{P_m}{\left(2\pi\frac{n}{60}\right)} = \frac{60}{2\pi}\frac{(1-s)P_{ag}}{(1-s)n_s} = 9.55\frac{P_{ag}}{n_s} \tag{3.4}$$

3.3.2 Three Phase Symmetrical Induction Motor Model

To understand the induction motor principle it is essential to understand the three-phase symmetrical winding in the stator function and the relationship of how the voltage equation of the stator and rotor equation is normally developed in respect to its mutual and self-inductance due to the phase angle between the stator and the rotor symmetrical winding. The winding is

displaced by 120º with equivalent N_s turns whilst the three phases of the rotor winding are also displaced by 120º with n_r equal number of turns. The rotor θ_r separates the three-phase winding of the rotor as shown in Figure 3-3 and this phase angle causes the electromagnetic forces to rotate the rotor [96] [97].

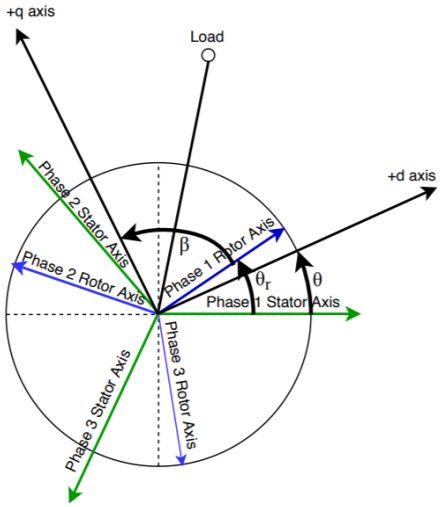

Figure 3-3 Three Phase Symmetrical Induction Motor Model [96]

The voltage equations of an induction motor can be formulated for the rotor and stator respectively as [96] [98].

$$V_r = R_r I_r + p\psi_r \tag{3.5}$$

$$V_s = R_s I_s + p\psi_s \tag{3.6}$$

And the voltage, current and flux linkage vectors:

$$V_r = (V_{r\ Phase1}\ V_{r\ Phase2}\ V_{r\ Phase3})^{\mathrm{T}} \tag{3.7}$$

$$V_s = (V_{s\ Phase1}\ V_{s\ Phase2}\ V_{s\ Phase3})^{\mathrm{T}} \tag{3.8}$$

$$i_r = (i_{r\ Phase1}\ i_{r\ Phase2}\ i_{r\ Phase3})^{\mathrm{T}} \tag{3.9}$$

$$i_s = (i_{s\ Phase1}\ i_{s\ Phase2}\ i_{s\ Phase3})^{\mathrm{T}} \tag{3.10}$$

$$\psi_r = (\psi_{r\ Phase1}\ \psi_{r\ Phase2}\ \psi_{r\ Phase3})^{\mathrm{T}} \tag{3.11}$$

$$\psi_s = (\psi_{s\ Phase1}\ \psi_{s\ Phase2}\ \psi_{s\ Phase3})^{\mathrm{T}} \tag{3.12}$$

$$R_r = diag(R_r R_r R_r) \tag{3.13}$$

$$R_s = diag(R_s R_s R_s) \tag{3.14}$$

The flux linkage is described by currents and inductances as:

$$\begin{bmatrix}\psi_r \\ \psi_s\end{bmatrix} = \begin{bmatrix}\mathrm{L_{rs}}\ \mathrm{L_{rr}} \\ \mathrm{L_{ss}}\ \mathrm{L_{sr}}\end{bmatrix} \cdot \begin{bmatrix}i_r \\ i_s\end{bmatrix} \tag{3.15}$$

Where the rotor inductance matrix:

$$L_{rr} = \begin{bmatrix} L_{rr} & M_r & M_r \\ M_r & L_{rr} & M_r \\ M_r & M_r & L_{rr} \end{bmatrix} \tag{3.16}$$

stator inductance matrix

$$L_{ss} = \begin{bmatrix} L_{ss} & M_s & M_s \\ M_s & L_{ss} & M_s \\ M_s & M_s & L_{ss} \end{bmatrix} \tag{3.17}$$

and mutual inductance

$$L_{sr} = \begin{bmatrix} M_{sr}cos\theta_r & M_{sr}cos\theta_{r1} & M_{sr}cos\theta_{r2} \\ M_{sr}cos\theta_{r2} & M_{sr}cos\theta_r & M_{sr}cos\theta_{r1} \\ M_{sr}cos\theta_{r1} & M_{sr}cos\theta_{r2} & M_{sr}cos\theta_r \end{bmatrix} \tag{3.18}$$

$$L_{rs} = L_{sr}^T \tag{3.19}$$

The final model is represented below as:

$$\begin{bmatrix} V_r \\ V_s \end{bmatrix} = \begin{bmatrix} Z_{rs} & Z_{rr} \\ Z_{ss} & Z_{sr} \end{bmatrix} \cdot \begin{bmatrix} i_r \\ i_s \end{bmatrix} \tag{3.20}$$

With impedance matrices defined as follows:

$$\mathrm{Zrr} = \begin{bmatrix} R_\mathrm{r} + \mathrm{pL_{rr}} & pM_\mathrm{r} & pM_\mathrm{r} \\ pM_\mathrm{r} & M_\mathrm{sr}\cos\theta_\mathrm{r} & pM_\mathrm{r} \\ pM_\mathrm{r} & pM_\mathrm{r} & R_\mathrm{r} + \mathrm{pL_{rr}} \end{bmatrix} \tag{3.21}$$

$$Z_{rs} = Z_{sr}^T \tag{3.22}$$

$$Z_{ss} = \begin{bmatrix} R_s + pL_{rr} & pM_s & pM_S \\ pM_s & R_s + pL_{ss} & pM_s \\ pM_s & pM_s & R_s + pL_{ss} \end{bmatrix} \tag{3.23}$$

$$Z_{sr} = \begin{bmatrix} pM_{sr}\,cos\theta_r & pM_{sr}\,cos\theta_{r_1} & pM_{sr}\,cos\theta_{r_2} \\ pM_{sr}\,cos\theta_{r_2} & pM_{sr}\,cos\theta_r & pM_{sr}\,cos\theta_{r_1} \\ pM_{sr}\,cos\theta_{r_1} & pM_{sr}\,cos\theta_{r_2} & pM_{sr}\,cos\theta_r \end{bmatrix} \tag{3.24}$$

With current components calculated, electromagnetic torque T_e can be obtained by:

$$\begin{aligned} T_e = PM_{sr}[&i_{s\,Phase1}\,(i_{r\,Phase1}\,sin\theta_r + i_{r\,Phase2}\,sin\theta_{r1} + i_{r\,Phase3}\,sin\theta_{r2}) + \\ &i_{s\,Phase1}\,(i_{r\,Phase1}\,sin\theta_{r2} + i_{r\,Phase2}\,sin\theta_r + i_{r\,Phase3}\,sin\theta_{r1}) + \\ &i_{s\,Phase3}\,(i_{r\,Phase1}\,sin\theta_{r1} + i_{r\,Phase2}\,sin\theta_{r2} + i_{r\,Phase3}\,sin\theta_r)\,] \end{aligned} \tag{3.25}$$

3.4 IAS of Crankshaft – Low-Frequency Vibrations

The following compressor model Figure 3-4 illustrates a crankshaft and piston in motion accompanied by the legend Table 3-2. A brief overview of the general operation of the air generation and its mechanism is briefly explained above. The crankshaft is driven by an induction motor which in turn operates in a rotational motion together with the connecting rod. The connecting rod transmits the compressive and tensile forces from the crankshaft and its piston and rotates both ends causing the up and down movement in a reciprocation motion. This reciprocation movement helps the piston to moves in a linear motion inside the cylinder. The model is based as a function of the crankshaft angle represented as θ. The compressor cyclic process comprises of the suction and discharge processes where the cycle commences with the Top Dead Center (TDC) $\theta = 0°$ in the low pressure cylinder and finishes at the same place after one full revolution when $\theta = 360^{\circ}$. As the high-pressure cylinder leads the low-pressure cylinder by $\frac{\pi}{2}$ therefore this phase difference is taken into account when applying the equation to the high-pressure cylinder.

Crankshaft and Piston Driven Mechanism model

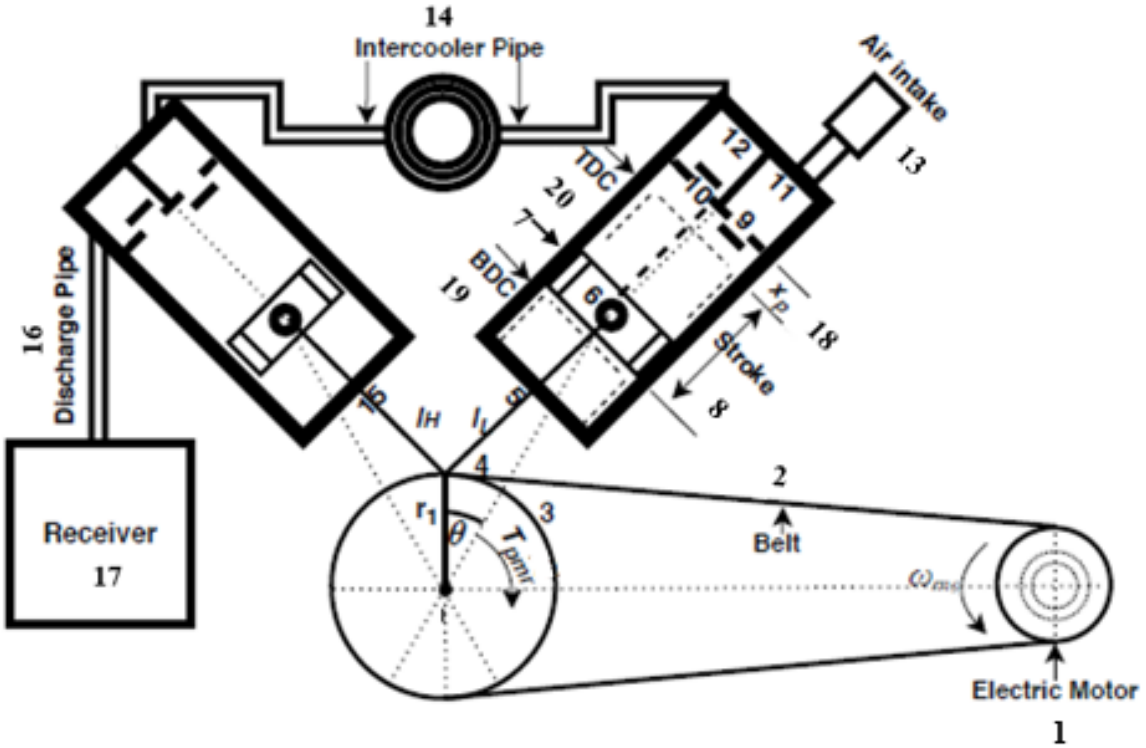

Figure 3-4 Compressor Model [84]

Table 3-2 Legend

Key components	
1	Electric Motor
2	Belt
3	Crankshaft
4	Connecting Rod
5	First Stage Cylinder
6	Piston
7	Cylinder
8	Stroke
9	Suction Valve
10	Discharge Valve
11	Suction Plenum
12	Discharge Plenum
13	Air Filter
14	Intercooler Pipe
15	Second Stage Cylinder
16	Discharge Pipe
17	Receiver
18	Clearance Volume
19	BDC
20	TDC

In a simplistic form, the torque balance of the crankshaft is also influenced by the air inside the cylinder, vertical unbalanced inertia forces and the load of the motor and as per Newton's second law is:

$$J\,\dot{\omega}_c(t) = T_e\,(t) - T_{pmr\,L,H}\,(t)\; - T_{flh}\,(t) \tag{3.26}$$

Where J is the overall moment of inertia for the mechanical and electrical movement of the reciprocation and rotational elements of the compressor, and ω_c is Instantaneous Angular Speed (IAS) of the crankshaft. Besides the subscripts $_{i,\,d,\,c,\,L,\,H,\,LH}$ stand for the inlet, discharge, cylinder, low-pressure first stage, high-pressure second stage, both low and high pressure first and second stage. $T_e\,(t)$ is to induction motor torque; $T_{pmr\,LH}\,(t)$ is the cylinder pressure resultant torque, the connecting rods for both suction and discharge stages and the reciprocating inertia force of the pistons [84].

$$T_{pmr\,LH}(t) = -T_{pmrL} + T_{pmrH} \tag{3.27}$$

and $T_{fLH}\,(t)$ is the frictional torque of the entire system.

3.4.1 Pressure Torque

The methodology proposed herein is the model which consists of the crankshaft piston mechanism, valves motion in both stages and in-cylinder pressure. A description of the reciprocating operation and design is previously described above. The displacement of the compressor piston from TDC is indicated as x_p for a crank angle of θ rotation as shown in Figure 3-5 assuming that the crankshaft rotates steadily at ω, angular speed [84] [93]. The piston C travels in a straight line causing the crank to rotate the connecting rod l_1 and the red dotted circle is the loci of the crank mechanism.

The resultant torque due to internal pressures for both the first and second stage compressions, the force of inertia of the piston and the connecting rod is described as:

$$T_{pmr\,LH} = \left(f_{ptf} + f_{mtf}\right)r \tag{3.28}$$

Where f_{ptf} is the force produced tangentially by the internal cylinder pressure, the inertia of the reciprocating mass produces the tangential force f_{mtf} and crankshaft radius is r_1. The internal pressure in a cylinder can be attained by the tangential force

$$f_{ptf} = P_{cp}S_{cs}\left(cos\theta + \sin\theta\ \frac{\left({}^{r_1}/_{l_1}\right)sin\theta}{\sqrt{1-\left({}^{r}/_{l_1}\right)^2 sin^2\,\theta}}\right) \tag{3.29}$$

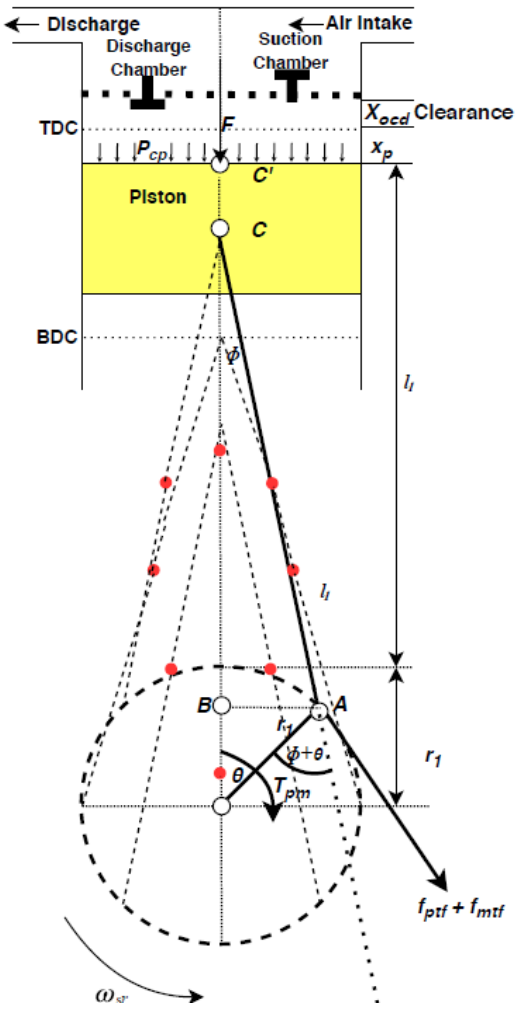

Figure 3-5 Crankshaft Piston Model

where P_{cp}, S_{cs} and d stand for in-cylinder pressure, cross sectional area of the cylinder and bore diameter of the cylinder respectively.

3.4.2 Inertia Torque

The inertia of the reciprocating mass produces torque applied to the crankshaft, which can be calculated by:

$$f_{mtf} = M_{rm}\ddot{x}_p \left(\sin\theta + \cos\theta \frac{\left({}^{r_1}/_{l_1}\right) sin\theta}{\sqrt{1 - \left({}^{r}/_{l_1}\right)^2 sin^2\,\theta}} \right) \tag{3.30}$$

where $m_{rm}, m_{pi}, and\ m_{crm}$ are the reciprocating mass of first and second stages, piston mass and reciprocating mass of the connecting rod and:

$$m_{rm} = m_{pi} + 0.5m_{crm} \tag{3.31}$$

by taking the TDC of the low-pressure stage as the reference point, the displacement of piston is

$$f\_mtf = m\_rm\ x\ddot{}\_p\ (sin\theta + cos\theta\ ((r\_1\ /\ l\_1\ )\ \ sin\theta)/\sqrt{(1 - (r \quad / \ l\_1\ )\hat{}2\ sin^2\theta))} \tag{3.32}$$

$$x_p\ = x_{ocd}\ + r_1\ (1 - r_1 cos\theta) + \ l_1 \left[1 - \sqrt{1 - \left({}^{r_1}/_{l_1}\right)^2 sin^2\theta}\right] \tag{3.33}$$

where *the term* x_{ocd} means the clearance distance between the cylinder head at TDC and the piston. The piston's velocity and acceleration can be acquired by differentiating it with respect to time:

$$\dot{x} = \omega_{r1}\ sin\theta \frac{\left(1+{}^{r_1}/_{l_1}\right)cos\theta}{\sqrt{1-\left({}^{r_1}/_{l_1}\right)^2 sin^2\theta}} \tag{3.34}$$

Acceleration can be simplified as

$$\ddot{x}_p = \omega^2 r_1 \left(cos\theta + {}^{r_1}/_{l_1}\ cos2\theta\right) \tag{3.35}$$

due to the square term $\left({}^{r_1}/_{l_1}\right)\ sin^2\theta < 1$

3.5 Pressure Oscillations – the Root of Vibroacoustic

3.5.1 In-cylinder pressures

The operation of the RC is briefly explained in Section 3.2. The reciprocating compressor increases air pressure in an oscillating way due to periodic reciprocating motions of the piston. These reciprocating motions are primary causes of vibrations in terms that they create dynamic loads to the structures enclosing the pressure chamber and crankshaft system. Besides, the volumetric change inside the cylinder is the direct source of sound waves. Therefore, modelling and understanding pressure behaviour is vital to understand the dynamics of secondary parameters such as motor current, IAS, vibration and acoustics of valve operation. Especially, these external measurements are extensively investigated in engines for in-cylinder pressure reconstructions [99].

Following the application of the fundamental gas laws and ignoring the slow effect of heat transfer to surroundings, the cylinder pressures $P_{cyL,H}$ in either the Low Pressure (LP) stage or High-Pressure stage (HP) can be obtained according to the first law of thermodynamics [100]:

$$\dot{P}_{cyLH} = \frac{1}{V_{cyLH}} \left(C^2_{yiL,H}\dot{m}_{yiL,H} - C^2_{yoL,H}\dot{m}_{yoL,H} - \gamma P_{cyL,H}\dot{V}_{cyL,H}\right) \quad (3.36)$$

$\dot{P}_{cyL,H}$ denotes in-cylinder pressure derivatives for L and H stages respectively; $P_{cyL,H}$ is the equation of volume cylinder pressure; and the cylinder volume $V_{cyL,H}$ is determined by the piston motion and clearance volume $V_{cyoL,H}$:

$$V_{cyL,H} = S_{cyL,H}X_{PiL,H} + V_{cyoL,H} \quad (3.37)$$

The rate of change in the cylinder volume $V_{cyL,H}$ can be determined using the velocity of the piston and geometric parameters of cylinder:

$$\dot{V}_{cyL,H} = \dot{X}_{PiL,H}\dot{S}_{cyL,H} \quad (3.38)$$

The mass flow rate through the inlet and outlet valves are $\dot{m}_{viL,H}$ and $\dot{m}_{voL,H}$ which consists of $\dot{m}_{viL}, \dot{m}_{viH}, \dot{m}_{voL}$ and $\dot{m}_{voH}$ representing the mass flow rates for the first stage inlet and discharge/outlet valves and second stage respectively as shown in Figure 3-6 below.

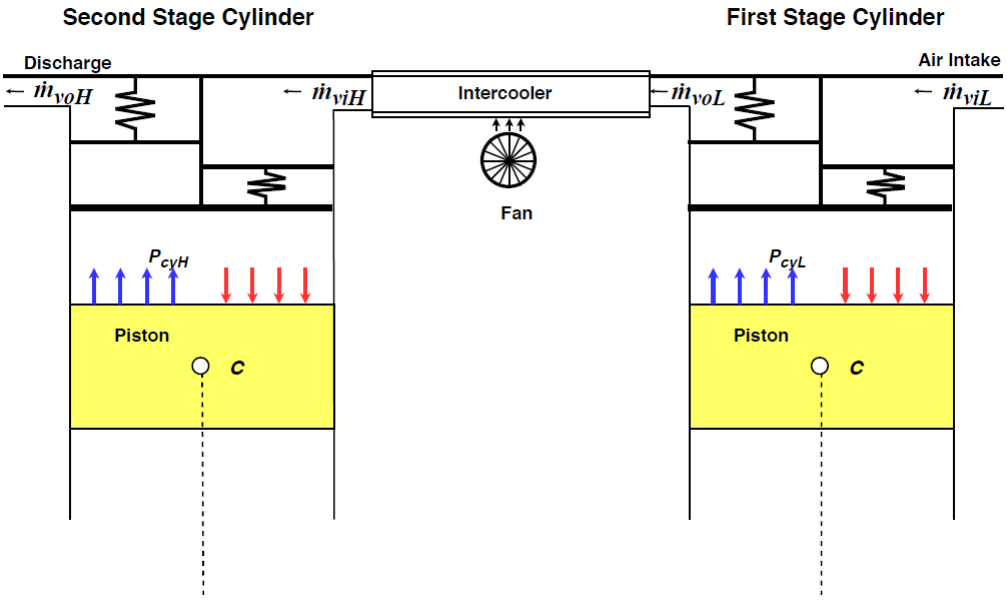

Figure 3-6 Mass Flow Rate of First and Second Stage Valves [93]

The square speed of sound in the inlet plenum is $C^2_{y\,iL,H} = \gamma RT_{iL,H}$ and the square speed of sound in the cylinder is $C^2_{y\,cyL,H} = \gamma RT_{cyL,H}$. The gas constant for air is R and $D_{cyL,H}$ stands for the cylinder diameter. Assuming if the gas goes through an isentropic process there will be no heat transfer in the vicinity, which is acceptable as fast dynamic behaviours such as in-cylinder pressure are examined in this study. This will result in a varied temperature at different stages of the compression process and can be determined as:

$$T_{cyL,H} = T_{iL,H}\left(P_{cyL,H}/P_{iL,H}\right)^{(\gamma-1)\times\gamma} \tag{3.39}$$

where $P_{cyL,H}$ is the cylinder pressure, $T_{iL,H}$ is the average absolute temperature of the inlet air at atmospheric temperature calculated according to $℃ + 273K$.

According to Equation (3.40), to calculate in-cylinder pressures, piston motions and flow rates through valves should be calculated. Equations giving piston motions are derived in Section 3.4.1. Next is to develop the formulas to calculate mass flows.

3.5.2 Mass Flows through Valves

The mass flow model through the suction and discharge valve can be obtained by mass flow rates $\dot{m}_{viLH}, \dot{m}_{voLH}$ at the cylinder pressure $\dot{P}_{cyLH}$ and the mass flow rate is illustrated into the inlet/suction and outlet/discharge flow rates as described in Figure 3-7. As the dynamic of the valve plates and pin-cylinder pressures changes it is these flow rates that induce airborne sounds in suction and discharge plenums according to the model developed in [101] [102]. However, the constant passages are not considered as their acoustic impedances remain the same for the fixed geometric dimensions for the compressor underline.

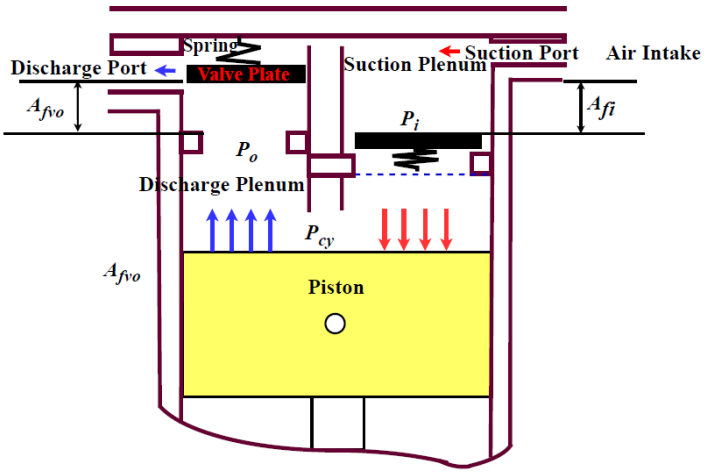

Figure 3-7 Mass Flow Model of Suction and Discharge Valves [103]

The suction and discharge valve and its dynamic behavioural equation and mass flow rate of $\dot{m}_{viLH}$ (kg/s) is modelled below as an incompressible flow through and an orifice port (valve):

$$\dot{m}_{viL,H} = \beta_{iL,H}\, C_{diL,H}\, A_{fiL,H}\sqrt{\left(2\rho_{cyLH}\,|p_{iL,H} - p_{cyL,H}|\right)} \tag{3.40}$$

Where the flow direction parameter is $\beta_{iLH} = sign\left(p_{iL,H} - p_{cyL,H}\right)$

p_{iLH} represent the pressure in the suction plenum, C_{diLH} is the variable inlet/suction coefficient which is to reduce the flow area which is a product of the divided flow and changes in the valve lift, A_{fiLH} is the maximum flow area of the suction valve according to G.R Price et al [104] and:

$$\rho_{cyL,H} = \rho_{ref}\left(p_{cyL,H}/p_{cyL,H}\right)^{1/\gamma} \tag{3.41}$$

is derived from the isentropic flow which is the density of the air inside the cylinder.

The same approach is applied to get the mass flow rate of the discharge valve which is represented as:

$$\dot{m}_{voL,H} = \beta_{voL,H}\, C_{dvoL,H}\, A_{fvoL,H}\sqrt{\left(2\rho_{cyL,H}|p_{iL,H} - p_{cyL,H}|\right)} \tag{3.42}$$

As mass flows are coupled with cylinder pressures in a nonlinear way, it is hard to find a closed-form analytic solution for the pressure differential equations. Therefore, the requirements of the numerical method are needed to analyse pressure behaviours.

3.6 Valve Dynamics - High-Frequency Vibrations

The performance of a compressor is highly dependent on the valve operation. Valves can be manually or automatically operated through the difference in pressure, flow or temperature and are vital; they can be physically designed and positioned inside the cylinder to allow a flow of gas either inside or outside of the cylinder with at the least one suction valve and one discharge valve in each compression chamber [105] [106]. Compressor valves contain some basic parts such as valve seat, sealing elements, lift constraint (guard) and spring(s). The vital part of a compressor valve is the sealing element which is normally spring-loaded and can move between two stops. The valve moves linearly [107] [38] and is closed when it rests against the valve seat and fully opened when resting against the valve guard. The sealing element can then travel between these distances which are called the valve lift. The sealing element does not move mechanically, it is moved by the action of the air force and a spring force. Whilst the valve is opened, the flowing gas will apply a dynamic gas pulling force on the valve plate which is of the order of magnitude of the pressure drop of the gas flow across the valve and is multiplied by the valve plate area. When the valve is closed it has to be able to hold the full static pressure discrepancy between suction and discharge pressures which can be very high [106]. Figure 3-8, shows the model of a non-linear vibration impact system [84] [93].

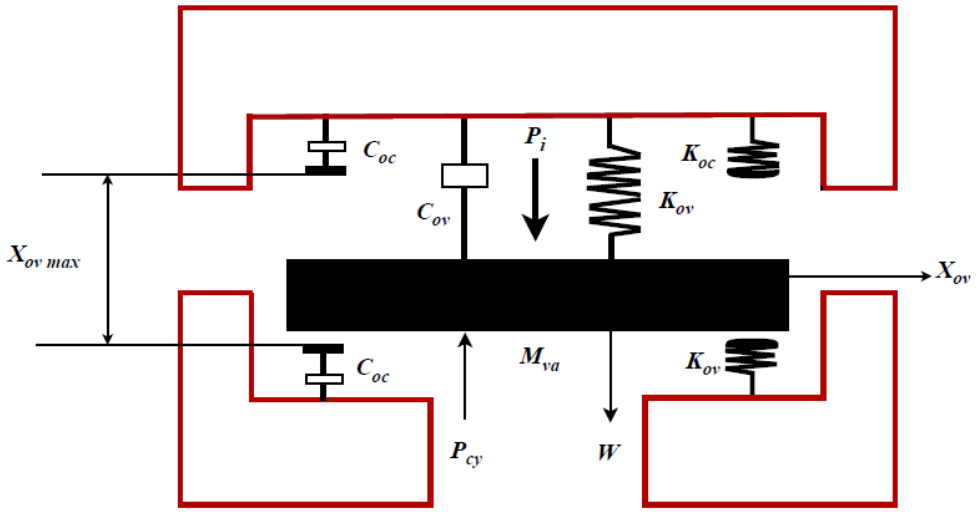

Figure 3-8 Valve Model of a Non- Linear Vibration Impact System [93]

The action of opening and closing of the inlet/suction valve derived the equation of motion for the inlet/suction valve when $0 \leq X_{pvs} \geq X_{pvs\ max}$ is:

$$M_{pvsL,H}\ddot{X}_{pvsL,H+}C_{dsL,H}\dot{X}_{pvsL,H} + K_{pvsL,H}X_{pvsL,H=}\Sigma f_{pvsL,H} \tag{3.43}$$

When the valve is completely open or closed and the valve plate is in contact with the valve seats the impacts $0 \leq X_{ovL,H}\ or\ X_{ovL,H} \geq X_{pvs\ max}$ is:

$$M_{pvsLH}\ddot{X}_{pvsLH} + C_{dsLH}\dot{X}_{pvsLH} + K_{pvsLH}X_{pvsLH} + C_{dsLH}\dot{X}_{pvsLH+}K_{dsLH}X_{pvsLH} = \Sigma f_{pvsLH} \tag{3.44}$$

The valve plate displacement, velocity and acceleration are represented by: $X_{pvsLH}\ \dot{X}_{pvsLH}\ and\ \ddot{X}_{pvsLH}$. The damping coefficient is expressed by $C_{dsLH,}$ The equivalent mass of the inlet valve plate is $M_{pvsLH,}$; The contact stiffness between the seat valve for both suction and discharge process is denoted by K_{csLH}; The non-linear spring stiffness when the valve is in motion between the valve seats is K_{nvsLH} whilst the contact damping coefficient is represented by C_{cdsLH}. The resultant force acting on the valve plate is represented by Σf_{rvsLH} which is a combination of three forces: the pre-set spring force, the valve weight and the force due to the pressure difference between each side of the valve which is represented by f_{svoLH}, W_{rsvLH} and $C_{fc}\ S_{rsvLH}(P_{iLH} - P_{cyLH})$ respectively, where P_{iLH} is the pressure in the inlet plenum, P_{cyLH} is the cylinder pressure, C_{fc} is a coefficient changing with the valve's lift magnitudes and S_{rsvLH} is the slot area for a single channel due to pressure difference between each side of the valve.

Following in a similar way, the equation of motion of discharge valves can be obtained in the same forms as Equations (3.43) and (3.44).

The required equivalent inlet valve plate mass is a third of the valve spring-mass added with the valve plate mass and represented as:

$$M_{pvsLH=1/3}M_{spring} + M_{plate} \tag{3.45}$$

where the calculated damping coefficient is:

$$C_{dsLH} = 2\xi\sqrt{K_{nvsLH}}M_{pvsLH} \tag{3.46}$$

In which the damping ratio ξ due to fluid viscous effect and spring stiffness K_{nvsLH}.

The resultant force acting on the valve plate represented by Σf_{rvsLH}.is

$$\Sigma f_{rvsLH} = f_{psvoLH} + W_{rsvLH} \tag{3.47}$$

3.7 Implementation of Numerical Analysis

3.7.1 Numerical Calculation Flowchart

To understand the characteristics of the interesting parameters, a couple of differential equations need to be solved numerically. A popular explicit Runge-Kutta solver is available in MATLAB, which allows differential equations to be solved with a great degree of accuracy by its adaptive time steps, being suitable for solving equations with different physical parameters in this study.

Based on the interconnections between various equations, the solver is programmed according to the flowchart shown in Figure 3-9. In this way, two sets of differential equations corresponding to the AC motor subsystem and RC subsystem are solved iteratively with respect to time increment.

Through several times of trial and error in balancing the accuracy and computational efficiency, it has been found that the time step and internal errors settings used can result in solutions for motor currents and cylinder pressures being agreeable with experiments, as was validated in reference [84] [93].

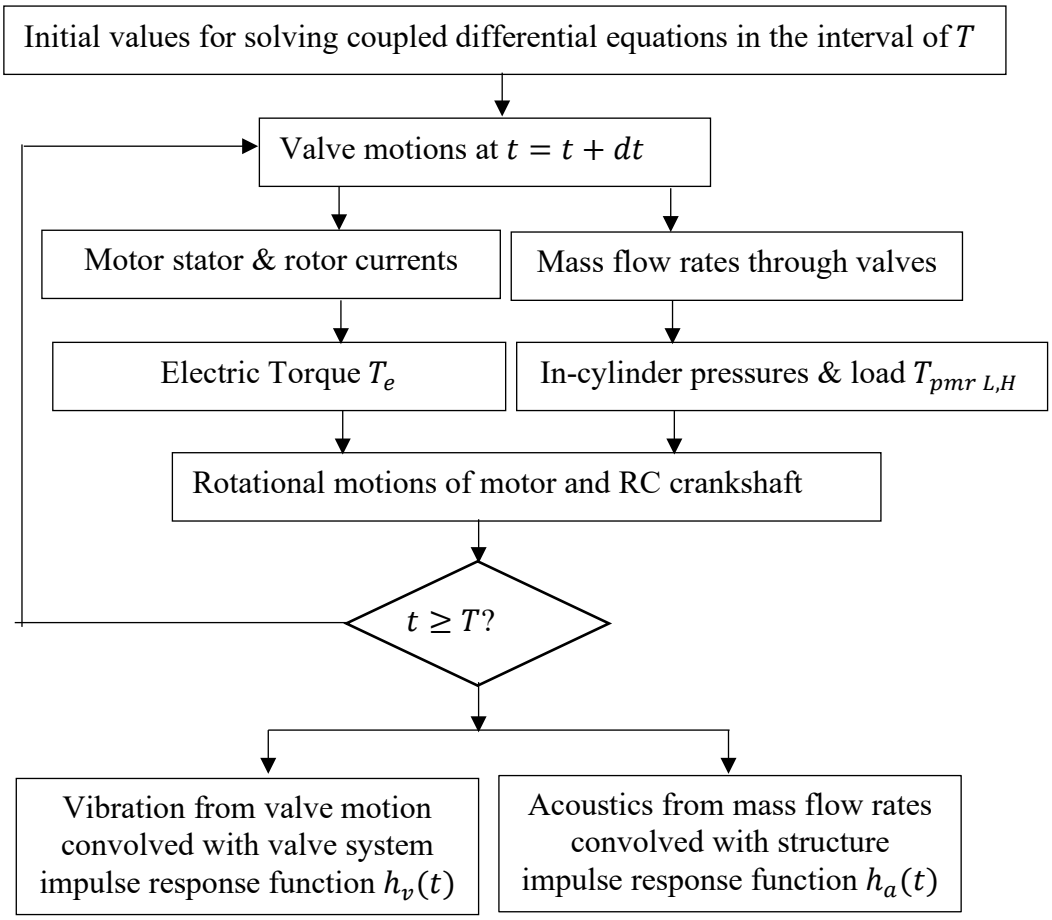

Figure 3-9 Basic Flowchart of Numerical Analysis

Moreover, the vibroacoustic due to valve motions and mass flow rates are obtained by a post convolution, which will be detailed in the foregoing analysis. In this way, it avoids the high demands for computational complexity in solving partial differential equations relating to sound waves in the valve plenums and the structural dynamics using finite element analysis.

Thereafter, the solution process was carried out for Baseline (BL) conditions under three successive discharge pressures: 60 psi, 90 psi and 120 psi (or 0.41 MPa, 0.62 MPa, and 0.83MPa) respectively. These pressures correspond the lowest, medium and the highest operating pressures that are specified with the RC. The same solution procedure is then used for different faults cases including Inlet Valve Leakage (IV-Leak), Discharge Valve Leakages (DV-Leak) in HP stage and Intercooler Leakages (IC-Leak), which are set in airflow passages, also transmission Belt Looseness (BL-Loose) and Motor Broken Bars (Motor-BRB) which are on system level.

To gain an in-depth understanding of behaviours for the interested variables including in-cylinder pressures, motor current, crankshaft IAS, vibrations and acoustics, their results are

presented in the angular domain that corresponds to the rotation of the crankshaft. This allows each variable to be easily correlated with key dynamic events: intake, compression, discharge and expansion sub-processes involved in an RC. Furthermore, these results are also compared with the baseline case under different discharge pressures so that it is possible to identify the key differences of various faults from baseline and between different ones, which overlays the basis for analysing experimental data which are usually contaminated with strong noise and unexpected interferences.

3.7.2 Fault Simulation Models

Leakages are a common fault in fluid machines. In this study, air leakages are simulated in three main parts: HP discharge valve, HP inlet valve and of HP stage, intercooler between LP and HP which are exposed to high dynamic load and thermal impact. An additional mass flow rate is induced to each part by increasing the equivalent flow area by 0.2%, 2% and 0.2% respectively, which can result in similar amplitude changes in-cylinder pressures. These leaking flows are calculated by using Equation (3.40), (3.42) and then included in Equation (3.36) for calculating in-pressures. These three fault cases are denoted by DV2-Leak, IV2-Leak and IC-Leak for the convenience of the preceding analysis.

Transmission belt is inevitably subject to wear and fatigue, consequently leading to a loosened belt transmission or more slippages between belt and pulleys. To simulate this effect, a higher slip coefficient of 0.02 is used, which is doubled compared with the baseline value of 0.01 that is induced by considering the effect of elasticity in a longitudinal direction of the belt. For ease of foregoing discussion, this fault is shortened as BL-loose.

AC motors are rugged machines but can also be faulty mechanically and electrically due to high dynamic load operations of RC machines. Broken Rotor Bars (BRB) are a common fault and can be simulated by reducing the resistance values by 5% in one of the three rotor phases.

3.8 In-cylinder Pressure Characteristics with Compressor Faults

3.8.1 In-cylinder Pressure under Different Discharge Pressures

As a direct indicator in-cylinder pressure is one of the most important measures of RC performance. Meanwhile, it is also the root of vibro-acoustics. Therefore an in-depth understanding of the behaviours of in-cylinder pressure will lay fundamental comprehension of the changes in other indirect parameters such as motor current signal, IAS and vibroacoustic. Consequently it helps to develop effective methods to monitor the condition of RCs.

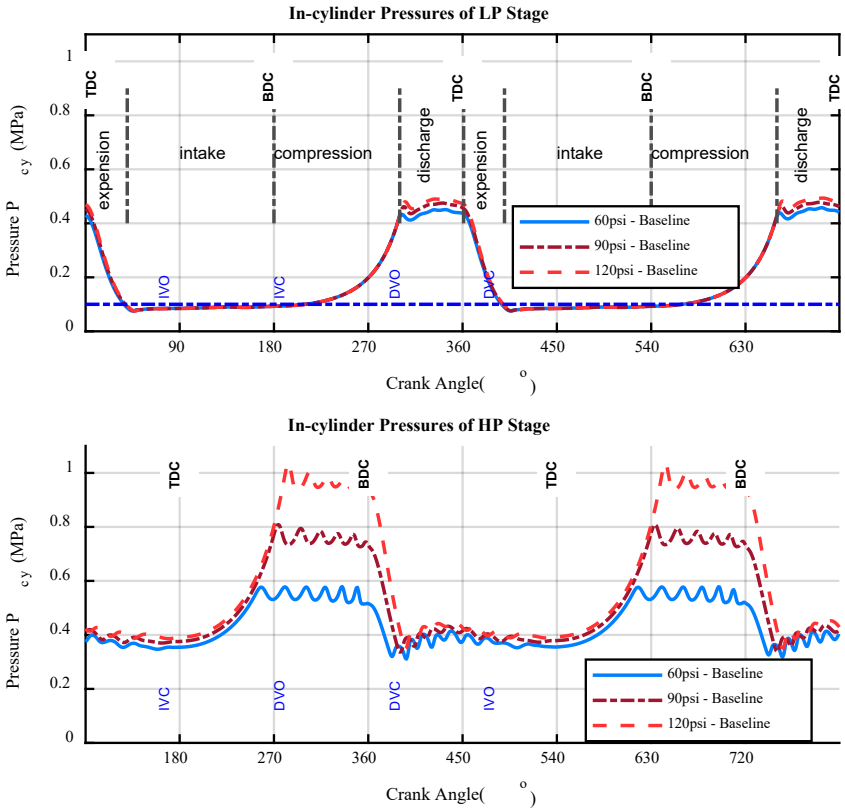

Figure 3-10 In-Cylinder Pressures under Different Discharge Pressures

Figure 3-10 presents the in-cylinder pressures of both LP and HP stages against crankshaft angles for two operating cycles (2 × 360°=720°). Presenting the pressures this way can easily identify the dynamic events including the TDC's and BDC's of piston motions and Inlet Valve Opening (IVO), Inlet Valve Closing (IVC), Discharge Valve Opening (DVO) and Discharge Valve Closing (DVC). Besides, the key sub-process of RC working cycles can be seen easily, which are expansion, intake, compression and discharge, as illustrated in the plot for the LP stage. For HP stage, the cylinder has a 90° delay. Similarly, all dynamic events can be easily found in the graph. Based on these dynamic activities, vibroacoustic including IAS, can be easily understood which will be examined in foregoing sections.

Moreover, the profiles of in-cylinders are agreeable with the theoretical prediction. Especially the pressure amplitudes during the discharge stage which significantly increases with the RC loads i.e. the static discharge pressure, whereas only a small variation is shown in other sub-processes. These confirm not only the accuracy of numerical calculation but also gives quantitative measures for the pressure change in amplitudes and positions, which provide sufficient knowledge for setting up data acquisition systems and analysis tools.

3.8.2 Pressure Changes by Different Faults

To see the change in pressure due to different faults, pressure differences Δ are calculated by subtracting the baseline pressure from corresponding pressures as presented in Figure 3-11. These two graphs show the changes when RC is under a lower discharge pressure and a higher discharge pressure respectively.

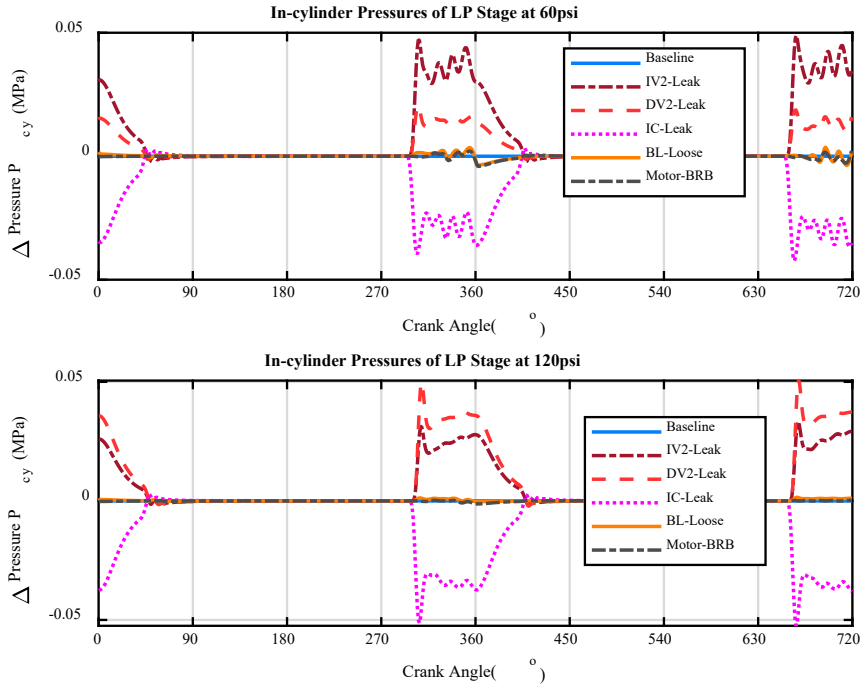

Figure 3-11 Changes in in-Cylinder Pressures at the LP Stage due to Faults

It can be seen that for the LP stage a significant change is exhibited in the discharge phase for different leakages including IV2-leak, DV2-leak and IC-leak. Although these leaks occur in HP stages, they transfer to the LP stage because of air leakages through the intercooler passage. It means that by observing pressure of either cylinder such leakages can be detected. Besides, IC-leak can be differentiated from other leaks by referring to its negative values. However, faults not occurring on the air passages such as BL-loose and Motor-BRB cannot be resolved sufficiently, although tiny oscillations can be seen they are hard to be measured in practice.

Pressure changes at HP stage are shown in Figure 3-12. Note that the crank angle is aligned to that of the LP, which is different to the present HP pressure by Figure 3-10, to find a consistent change that can be easily achievable in a real situation and avoids any confusions in forgoing discussion. It can be seen in the figure, pressure changes spread over entire angular ranges even though the discharge phase shows higher oscillations. This provides more information for detecting and diagnosing the three leak cases directly occurring in air passages. Similar to LP

pressure changes in Figure 3-11, it is still hard to see the change induced by BL-loose and Motor-BRB by HP pressures, further confirming it is not easy to detect such faults by pressure analysis alone.

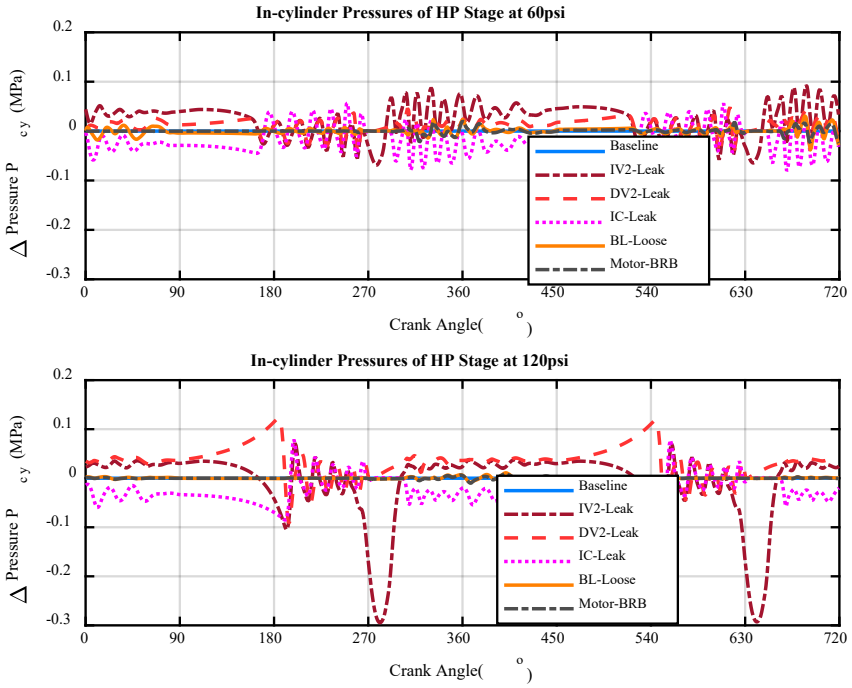

Figure 3-12 Changes in in-Cylinder Pressures at HP Stage due to Faults

3.9 IAS – Torsional Vibration Characteristics with Compressor Faults

Because of the easiness of measurements and robust signatures, IAS or torsional vibration of RC's crankshaft is an indirect parameter for indicating the operating condition of RCs. As shown in the aforementioned modelling sections IAS or ω_c in Equation (3.26) it results from a combined effect of motor torque, air and inertial torques. Changes in pressures due to faults will greatly affect IAS signatures.

3.9.1 IAS under Different Discharge Pressures

The top plot of Figure 3-13 presents IAS signatures varying with the load or discharge pressures. Clear differences can be seen in both the peaks and troughs of IAS profiles.

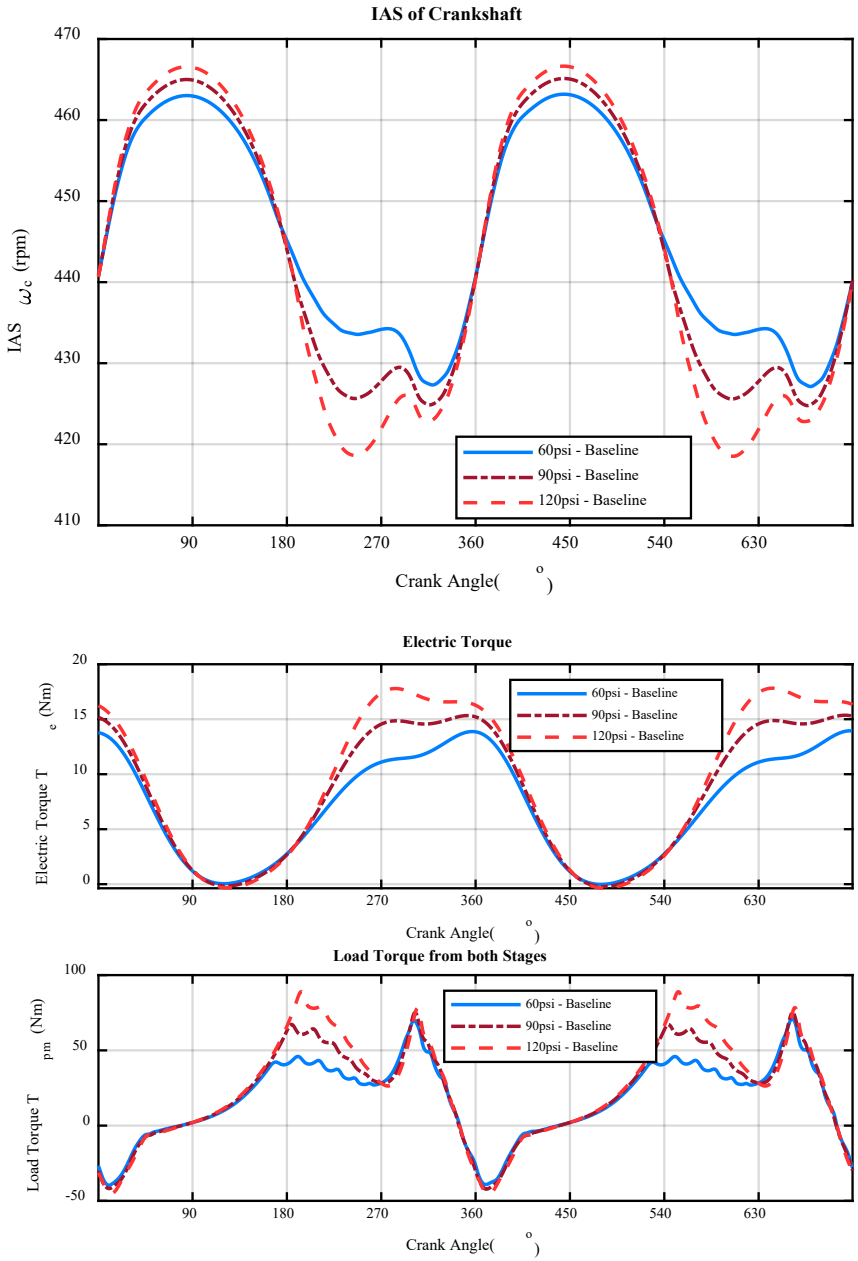

Figure 3-13 Crankshaft IAS under Different Discharge Pressures

In particular, the peak-peak amplitudes increases with discharge pressures, effectively indicating the pressure changes of in-cylinders with interactions between motor torques and load torques shown by the model and bottom graphs in Figure 3-13. Interestingly, the changes in load torques happen in a limited angular range from 180° to 270° where the HP cylinder is in the compression cycle, whereas the electric torque shows a change in a wider range and higher amplitudes. Because of the effect of these wider and higher amplitude changes, the IAS display the corresponding changes. In other words, the coupling effect between RC torque and electrical torque by the dynamics of a rotational system governed by Equation (3.26) magnifies

the changes in mechanical torques and consequently makes it possible to detect and diagnose faults in RC systems. However, IAS is probably less informative for component-level diagnosis i.e. unable to pinpoint which stages may have faults.

3.9.2 IAS Changes due to Faults

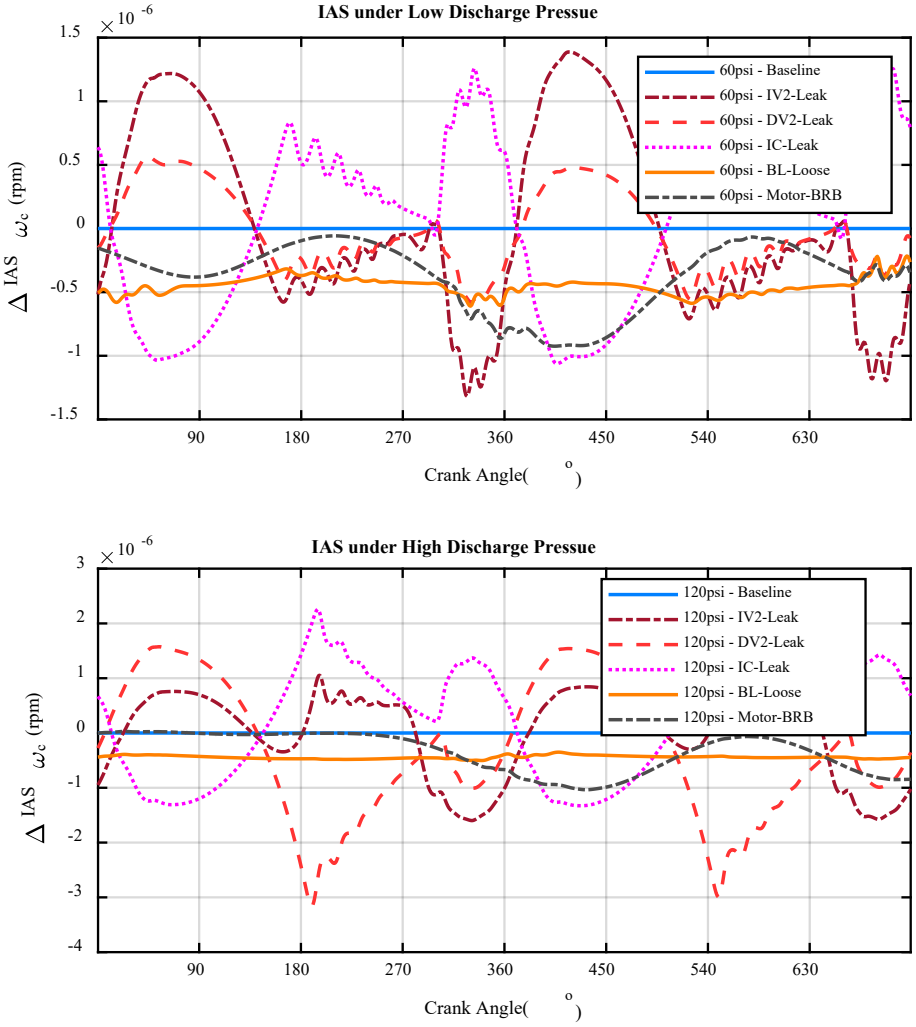

Figure 3-14 Changes in IAS for lower and higher-pressure operations

To see the changes caused by various faults, the difference between faulted IAS and the baseline is calculated and presented in Figure 3-14. Similar to pressure changes, IAS allows leak related faults to be diagnosed with great confidence by the high changing amplitudes and distinctive patterns. Moreover, it also allows other two faults; BL-loose and Motor-BRB to be diagnosed effectively as the change of patterns along with amplitude variations are significantly different between these two and from the other three faults. Particularly, loosened

belt transmissions are less responding to dynamic fluctuations of crankshaft motions and result in a biased but relatively level change. For the motor faults, additionally slow oscillatory components at twice slip frequency arise in the motor current, the change mainly follows the slow oscillation due to BRB effects. This shows that IAS provides good detail of monitoring information and for system-level diagnostics.

3.10 Motor Current Characteristics with Compressor Faults

3.10.1 Current Signals under Different Discharge Pressures

To balance the torque oscillations as shown in Figure 3-13, AC motor current will also adjust adaptively to overcome RC load for steady operations. This adjustment results in an Amplitude Modulation (AM) to the supply components at 50 Hz. As shown by the top graph of Figure 3-15, there is a clear change in current signal amplitudes, being time/angle-varying in accordance with the torque graphs. Besides, the spectrum of motor current signals shown by the bottom graph of Figure 3-15 exhibits clear sidebands around supply frequency. Especially the amplitudes of sidebands shows an increase with the discharge pressures. This demonstrates that the sidebands can be an effective indicator to show the changes in the RC system.

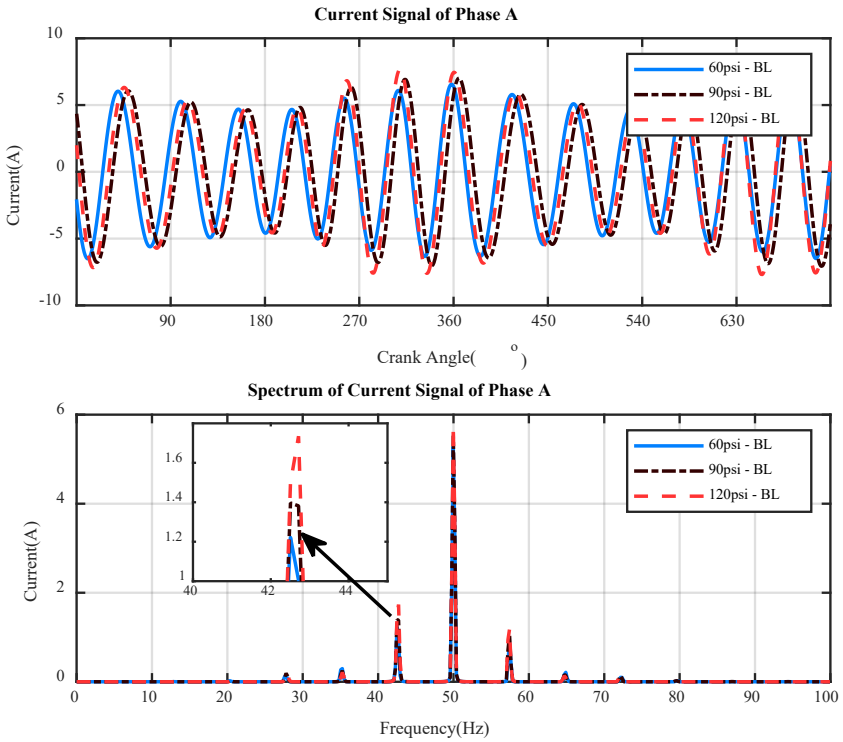

Figure 3-15 Motor Currents under Different Discharge Pressures

3.10.2 Current Signal Change due to Faults

By taking away the baseline effect from the motor current signals due to faults, Figure 3-16 highlights the changes in current signal due to various faults simulated. It can be seen that significant changes are exhibited in the motor current. It allows all different faults to be detected and diagnosed for both the lower and higher-pressure operations. This shows that motor current signals can provide comprehensive information for condition monitoring.

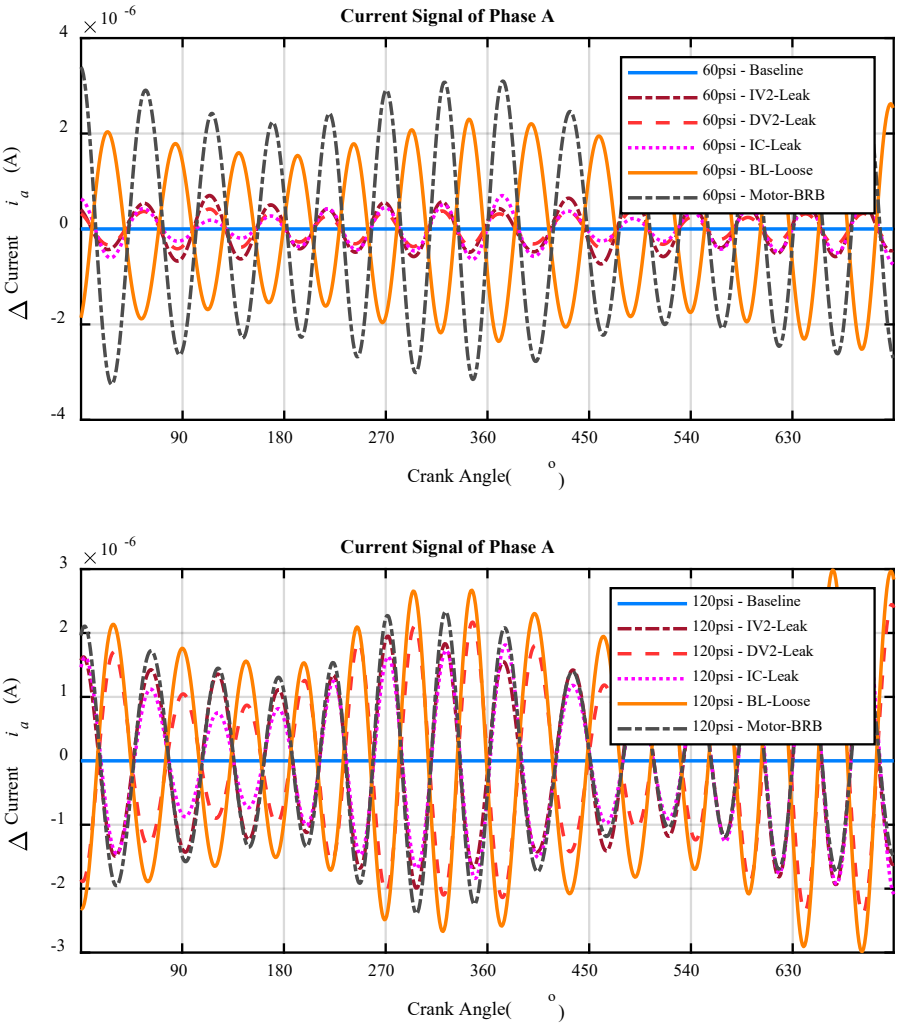

Figure 3-16 Changes in Motor Currents due to Faults under Different Discharge Pressures

However, the amplitudes of current signals are probably not very consistent with discharge pressures. In particular, Motor-BRB under higher pressure does not show a clear increase compared with that of lower pressure but a clear phase shift can be observed between the two modulation profiles. It means that it can be difficult to make the differentiation between faults

by amplitude changes alone. Therefore, a dedicated signal processing is needed to combine both the phase and amplitude changes for a joint diagnostic feature. In general, motor current signals can also provide sufficient information for system-level diagnostics.

3.11 Acoustic Characteristics with Compressor Faults

In-cylinder pressure can be taken as direct acoustics as they have the feature of pressure oscillations. As seen in Figure 3-10 of Section 3.8, in-cylinder waves generally exhibit slower fluctuation and thus are regarded as low-frequency acoustic waves. Because these acoustic waves are enclosed inside cylinders an intrusive measurement is needed to measure it and is probably costly and inconvenient to be used for condition monitoring. Nevertheless, in-cylinder pressure is unable to diagnose faults from other sub-systems such as electric motor and loose belt as discussed in Section 3.8.

However, the rapid suction and discharge effects driven by in-cylinder pressures will lead to a time-varying mass flows, which consequently radiates more sound waves into the inlet and discharge passages. These passages often have typical distinctive acoustic outlines. Their distinctive resonance modes can be excited by the fast changes in flow rates and produce sound waves. Especially, the sound waves leaking from the suction side can be perceived remotely by a microphone which is potentially useful for indicating the changes in RC conditions. Therefore, this section focuses on investigating these mass flows and characterising the general behaviours of the sounds including main frequency bands and potentials for differentiating the faults of interests.

3.11.1 Acoustic Responses under Different Discharge Pressures

Figure 3-17 presents mass flow rates through four valves, which are denoted as IV1, DV1, IV2 and DV2 respectively, when RC is operating at three discharge pressures. Typically, these flow rates exhibit localised pulses with short durations. LP stage ones show much fewer fluctuations than that of HPs. This agrees to the dynamics of in-cylinder pressures as the pressure changes of LP is lower and less oscillatory, which was explored according to Figure 3-10 in Section 3.8. Besides, with the changes in discharge pressures, these flow rate pulses can be observed to have certain variations in amplitudes and time shifts. This indicates that they can be used for detection and diagnostics. However, as these small changes are localised within a narrow time/angular range, they exhibit as highly nonstationary and it is probably difficult to perceive and process such signals for achieving accurate detections. Besides, it will be more expensive

to measure flows with such small changes as it needs a high specification measurement system in terms of sensitivity, dynamic range and temperature resistance. Besides, it needs time-frequency methods such as wavelet decomposition and Short-Time Fourier transform (STFT) to resolve the changes of every nonstationary flow rate signals shown in Figure 3-17. These methods not only require high computational power but also always suffer from numerical error, therefore inefficient to resolve small changes.

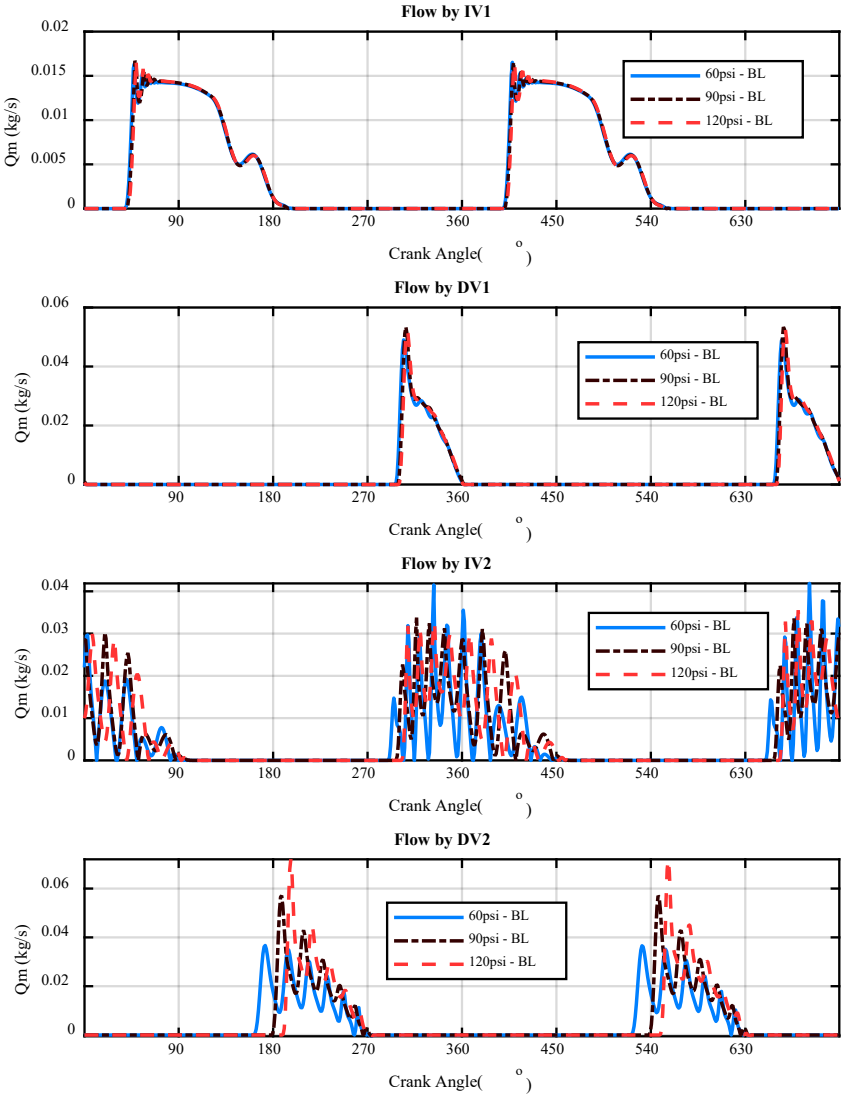

Figure 3-17 Mass Flow Rates through Four Valves under Different Discharge Pressures

From an acoustic point of view, these time-varying flow rates will induce acoustic waves inflow passages which can be obtained by convoluting these pulses with appreciate acoustic Impulsion Response Functions (IRF). Based on the geometries of flow passages it can be

modelled as an acoustic duct system with several acoustic modes corresponding to the mass enclosed in the chambers of valve plenum, pipeline and inlet silencer. These acoustic modes can be easily determined based on the geometrical dimensions of each chamber along with experimental calibrations [102]. The top graph of Figure 3-18 shows such modes by IRFs estimated based on the dimension of flow passages and spectral profile of measured acoustic signals. With IRFs available, a convolution was performed in the time domain to obtain acoustic responses, which are shown by the middle and bottom plots of Figure 3-18 for the waveforms and spectrum respectively. This time approach, rather than the frequency approach [108] allows waveforms to be obtained for a more direct and accurate comparison with less computing effort.

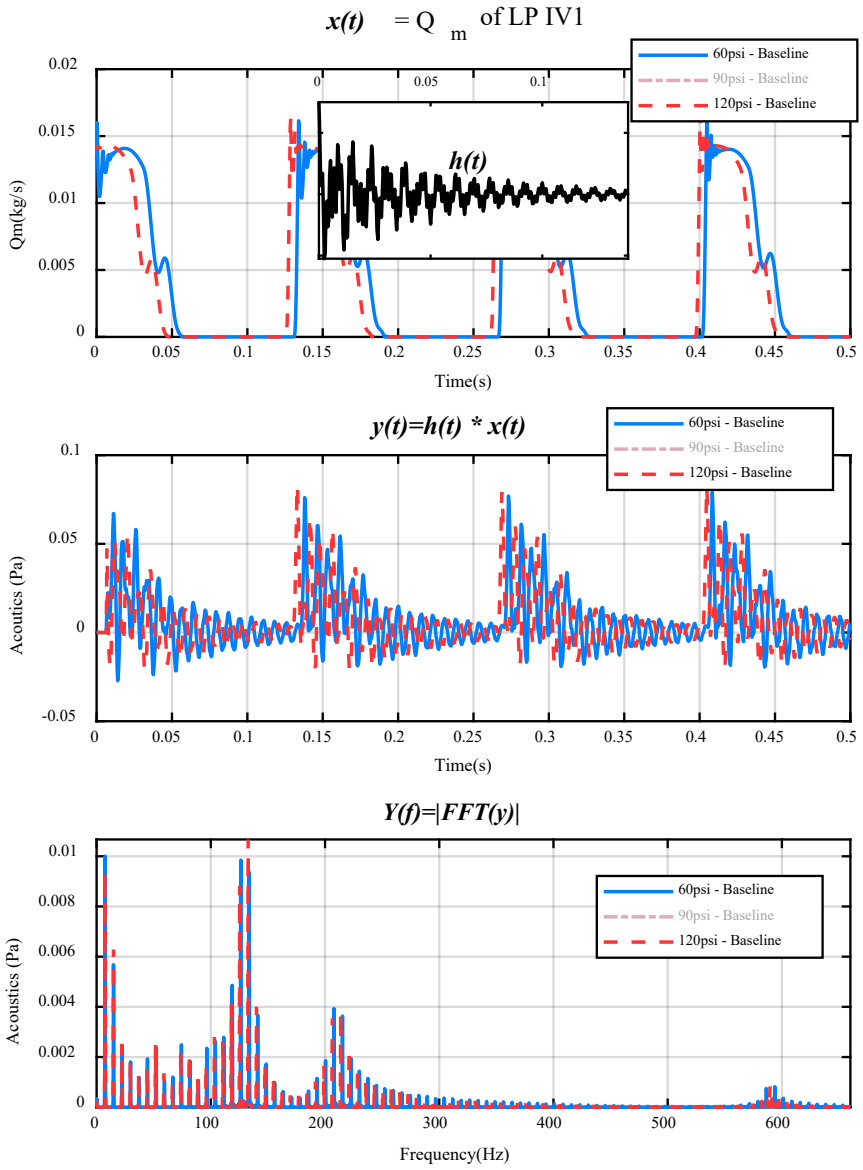

Figure 3-18 Acoustic Waves from Different Flow Rates under Different Discharge Pressures

Moreover, acoustic waveforms in the middle graph of Figure 3-18 shows more observable changes as their oscillations spread over the entire time range, thanks to the magnification of acoustic modes. As a result, the changes can be easily sensed and identified under a high Signal to Noise Ratio (SNR). Specifically, the time-shifts shown in the mass flow rate shown by the top plots of the figure can be clearly seen in the middle plots. Besides, the waveform becomes more stationary and can be more accurately characterised by a simple Fourier transform-based spectrum analysis, which results in the bottom graph of Figure 3-18. From the spectrum, the changes between the two discharge pressures are well presented by the spectral amplitudes in

the frequency range from 120Hz to 600Hz in which the 3rd acoustic mode at 580Hz is related to the acoustic chamber of valve plenum.

In general, because of the magnification and smoothing of acoustic modes inflow passages, acoustic signals exhibit to be more stationary and carry better resolvable information regarding pressure changes. Additionally, acoustic signals can mainly be observed in a low-frequency band below 600Hz, Therefore, acoustic signals provide information for both components and system-level diagnostics.

3.11.2 Acoustic Response Changes with Faults

To verify the performance of using acoustics for fault diagnosis further, typical changes in acoustic signals for different fault cases were obtained by subtracting the baseline signal. Figure 3-19 presents the change for the acoustics of inlet valve at LP state, where acoustic waves can run to open-air through RC silencer, compared with other valves where their acoustic waves are enclosed by mechanical structures which can have higher attenuation to wave transmissions.

It can be seen in the figure the acoustic changes from the baseline and between different cases for both the lower and higher pressures. Not only these changes significantly enhance the faults occurring inflow passages, IV2-Leak, DV2-Leak and IC-Leak, but also faults in other components such as Motor-BRB and BL-Loose become more detectable, as highlighted by the plots inside the blue box, even though they cannot be detected using in-cylinder pressures. This shows acoustic monitoring can also have the capability for whole system monitoring, being as powerful as using IAS and motor current signals.

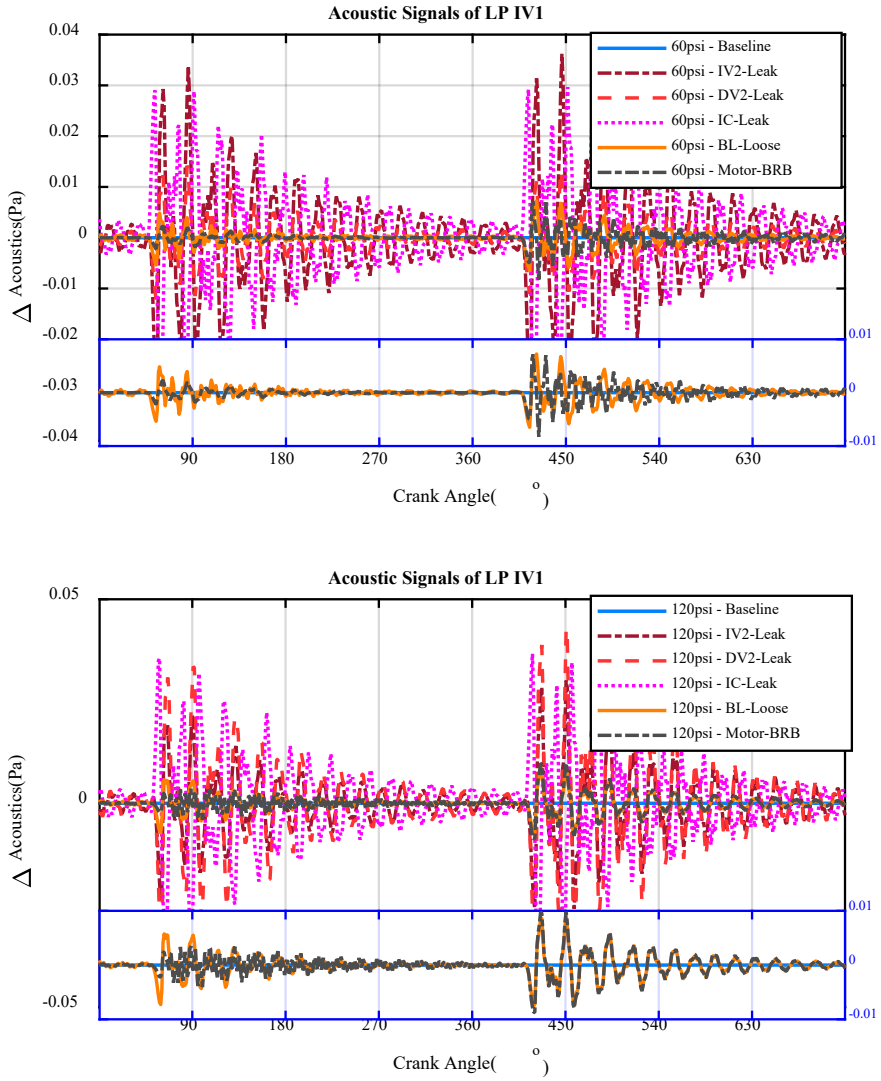

Figure 3-19 Changes in Acoustics Waves due to Various Faults under Different Discharge Pressures

3.12 Valve Vibration Translational Vibration Characteristics with Compressor Faults

As the low-frequency vibration, IAS of crankshaft shows good detection capability for different faults. However, it can provide limited information regarding fault locations. To compensate for this deficiency high-frequency vibration responses may need to be used to achieve more detailed diagnostics. Previous studies [84] [93] [38] have found experimentally that valve activities are usually the main sources of high-frequency vibrations. Therefore, this section focuses on examining the vibration characteristics due to valve motions under different fault conditions.

3.12.1 Valve Vibration with Discharge Pressures

Vibrations due to valve are mainly created by valve dynamic movement. Figure 3-20 shows the valve plate displacement for under different operating pressure, which is obtained according to Equation (3.43) and (3.44) for inlet and discharge valves respectively. It is evident from the figure that the suction valves motion across a wider angular range with high amplitudes because of their lower stiffness of valve spring. In this way it allows the cylinder to be fully charged. Moreover, the valve plate often reaches its maximum (1.5 mm), creating impacts on valve plates. Besides, as the HP stage has a higher-pressure fluctuation, its inlet valve undergoes more oscillations and creates more impacts on its seat. Moreover, the impact looks stronger and shifts later when RC operates under higher pressures, as illustrated by the HP IV2 displacement graph on the third row of the figure.

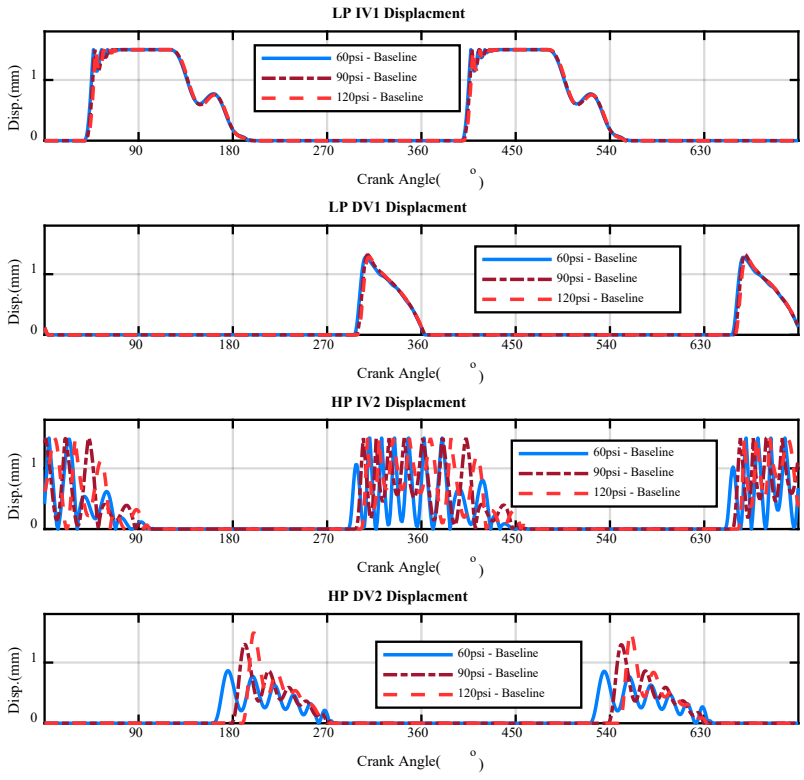

Figure 3-20 Valve Plate Displacements under Different Discharge Pressures

To have more detail of the impact to valve seats and stops, impact forces are calculated based on Equation (3.43) and (3.44) and presented in Figure 3-21. It can be observed that the inlet valve (IV) opening produces higher impact forces and lasts longer for the suction valves. Besides, visible IVC and DVC impacts for all valves can also be seen during valve closing

even though its amplitude is smaller. This probably shows that the valve close landing is soft due to the gradual reduction of in-cylinder pressure during the expansion process. Similar to valve displacement, HP valves exhibit higher oscillatory forces but its peak value is only slightly higher than LP valves, besides, each valve has different angular positions for opening and closing events. For example, the HP DV2 exhibit later opening and earlier closing as discharge becomes higher, which is steadier than amplitude changes and can be easily characterised for valve diagnosis. This insightful information is very helpful to explain the vibration measurements, but impact forces are limited in a short angular range, like displacement, which is difficult to be measured for on-line monitoring.

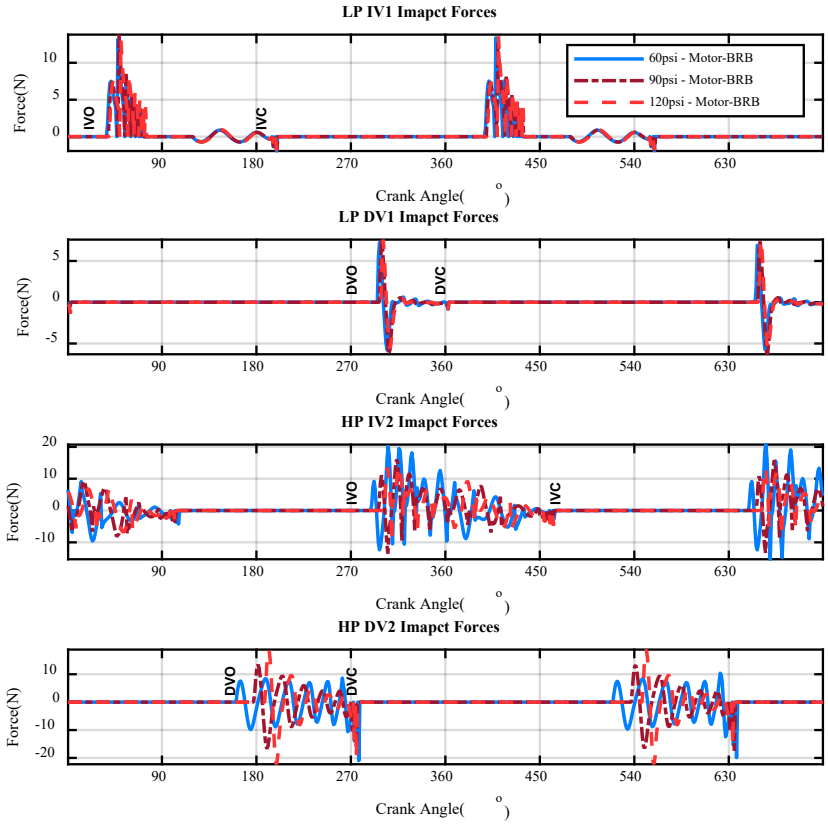

Figure 3-21 Valve Impact Forces Applied to Surrounding under Different Discharge Pressures

By taking a convolution operation between the impact forces and structure IRFs of the cylinder head, estimated by a hammer test, acceleration vibrations can be obtained. Figure 3-22 shows such vibrations of the four valves. Like acoustic signals, vibration response can exhibit in a much wider angular range which enlarges the impact effect and allows the differences to be observed easily. LP valves show a lower amplitude of vibration, compared with HP valves.

Especially, HP valve shows a higher vibration for the low discharge pressure of 60psi than other two high-pressure cases. Also, all vibration signals become more complicated in terms of oscillatory patterns, showing that it needs more advanced signal analysis tools such as time-frequency methods to directly process these signals to resolve the steady behaviour of valve opening and closing events, which is more promising to indicate changes in in-cylinder pressures.

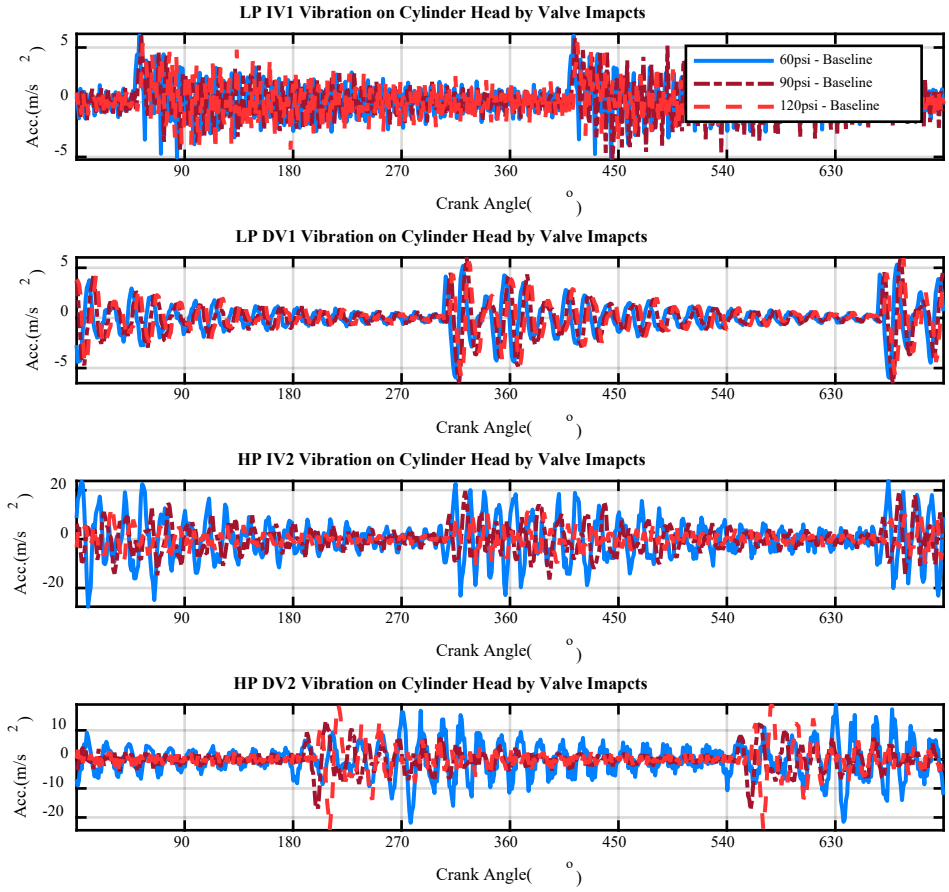

Figure 3-22 Vibration Responses of Structures from Valve Impact Force under Different Discharge Pressures

3.12.2 Valve Vibration Changes due to Faults

To show that the vibration responses can have more information for diagnostics, their differences from baseline cases are presented in Figure 3-23 for two typical operating discharge pressures. The changes are significantly higher from the baseline and across fault cases in both amplitudes and angular ranges. Especially, two faults outside flow passages: Motor-BRB and BL-loose also exhibit clear differences. This shows that vibration responses certainly provide

rich information about valve motions to indicate in-cylinder pressures and valve motion behaviours for system and components level diagnostics.

It is worth noting that as these differences are found in the angular domain, IAS and its torsional incremental phases need to be accurately obtained to achieve this analysis which has to use a high-resolution encoder for high accuracy measurement IAS. It means that valve vibrations should be measured along with IAS measurement to have an accurate diagnostics.

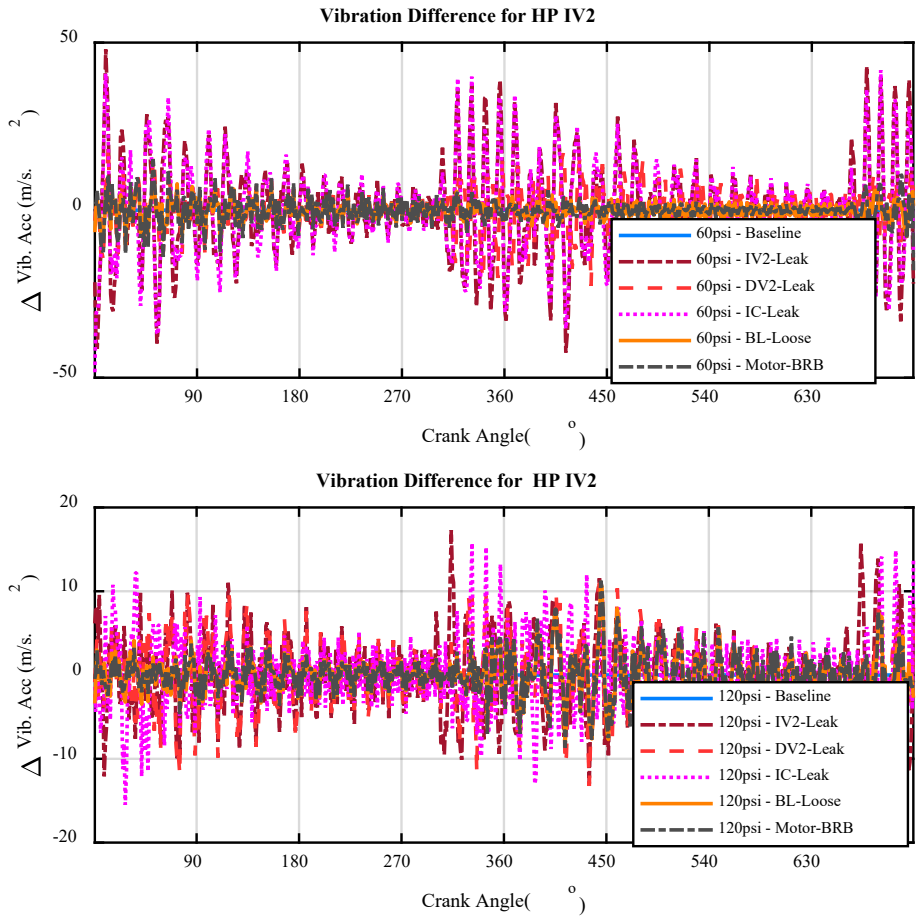

Figure 3-23 Changes in Vibration Responses due to Faults under Different Discharge Pressures

3.13 Key Findings by Modelling and Numerical Analysis

Based on the modelling numerical analysis aforementioned, novel understandings achieved on each dynamic response and associated method adopted are summarised as follows.

3.13.1 Modelling and Numerical Simulation

The direct numerical comparison between the signatures with baseline removed provides an easy and feasible approach to quantitatively evaluate different dynamic responses. As a result, for the first time, accurate and reliable head to head comparisons are obtained numerically for these four popular dynamic responses, ordinary these are hard to be achieved by experimental studies as there are many uncertain errors in data acquisition and data processing

Modelling Vibroacoustic responses as multi-modal systems allows quantitative analysis of structural vibration and airborne acoustics from valve motions, gaining a detailed understanding of vibroacoustic and provide sufficient knowledge for data acquisition and processing. In this way this numerical study is efficiently completed, demonstrating the capability to perform the large volume of analysis tasks over different fault cases under a wide range of discharge pressures. It would take too long by other modelling schemes such as Finite Element Analysis (FEA) and boundary element analysis.

3.13.2 Numerical Results

By comparing numerical results under different cases, it has been found that:

a) In-cylinder pressure show good details of RC operations and can be used for diagnosing faults occurring in flow passages such as various air leakages happening in valves and intercoolers. However, it cannot indicate faults from motor drives and mechanical transmission systems for a system-level diagnosis.

b) IAS show significant changes between different fault cases, providing sufficient detail to diagnose fault location largely and thus can be used for system-level diagnostics but not the component-level diagnostics.

c) Motor current signal also shows significant changes between different fault cases providing sufficient detail to diagnose fault location largely for system-level diagnostics but not for the component-level diagnostics.

d) Acoustics from both flow passages and structural vibration provides more resolvable information regarding different faults. It is understood that acoustic modes are the critical effect that turns the impulsive valve flow events into more stationary responses so that the perceived signals have higher SNR compared with direct measurements of such events, besides flow-induced acoustics mainly below 700Hz being lower than that of structural vibrations.

Moreover, acoustics have rich information for both the system-level and the component-level diagnostics however advanced signal processing methods must be accompanied. Nevertheless, its remote data acquisition proves much more convenient for field applications compared with the contacting measurements of using structural vibrations.

e) Valve vibration response shows a wide band response and contains detailed and comprehensive information for implementing not only component diagnostics but also system-level monitoring. However, similar to acoustic signals, this high-frequency signature is very complicated and needs high-resolution data acquisitions and advanced signal processing tools to resolve different valve events that have small differences.

Chapter 4. **Evaluation of Waveform Analysis Based on Intrusive and Non-Intrusive In-cylinder Pressure Measurements**

Chapter four addresses the implementation of the key updated techniques, reviewed in chapter 2, upon a laboratory Reciprocating Compressor (RC) test bench, which is planned as Phase I of the research.

The testing compressor is then equipped with four potential monitoring systems:

- *Surface Vibration (SV) Condition Monitoring (CM) using two accelerometers mounted on the surface of the two cylinders;*
- *Instantaneous Angular Speed (IAS) CM using one shaft encoder mounted on the end of the crankshaft;*
- *Pressure CM using two pressure transducers installed intrusively into the two cylinders;*
- *Motor current CM using one current sensor mounted on the electrical power supply line.*

This chapter focusses on the vibration-based Condition Monitoring (CM) for four common fault cases: Discharge Valve Leakage (DVL), Suction Valve Leakage (SVL), Intercooler Leakage (IL) and Loose Transmission Belt (LB). It also studies the compressor crankshaft Instantaneous Angular Speed (IAS), Current waveform, Root Mean Square (RMS) Envelope, Current Spectrum analysis in comparison with the above four seeded parameters. Through this study, the behaviours of pressure, vibration and current differences of these faults can be identified as the basis for fault detection and diagnosis. To show the effects of each fault on the compressor, in-cylinder pressures are presented together with the vibration and electrical signals. Because compressors operate under different discharge pressures, the investigation is made of three typical operating pressures: (40 psi) 2.8 bar, (80 psi) 5.5 bar and (120psi) 8.3 bar respectively under each fault to explore the changes and monitoring performance.

The work in Phase I will then prepare the author to apply the techniques to Phase II in the field implementation plant at an industrial level. Phase II is explained further in chapter five and six.

4.1 Introduction

As previously described in Section 2.1.1 any machine that has moving parts can produce vibration and has the potential for vibration monitoring and which would consequently produce noise. All rotating and reciprocating machines generate a wide range of vibration frequencies, the total spectrum of frequencies is called a machine signature [4, 6, 7]. Even two identical machines will have different signatures due to the small dimensional and assembly differences [4]. Each peak on the spectrum has its fundamental reason and if there are lots of machine faults the shape of the peak levels in the signatures will change drastically.

These signal signatures can be processed and analysed through a range of techniques such as the Time and frequency domain. Any variation in those signatures would detect any incipient failures before any catastrophic failure occurs.

The monitoring of reciprocating compressors and fault diagnosis is a vital procedure in the good running of these machines. Signal analysis is another important technique in the monitoring of machines. The generated signal contains useful information about the actual machine status and has the possibility of data extraction for fault diagnostic. Fast Fourier Transform (FFT) is another common mathematical technique used for signal processing in the conversion of time domain to frequency domain. Frequency domain has the capability of identifying and isolating certain specific frequency components. Time-Frequency analysis is a powerful technique used for the condition monitoring of machinery. The time-frequency analysis is more advantageous compared to the FFT due to its two-dimensional representations of frequency versus scale and time.

4.2 Compressor Experimental Data Analysis

4.2.1 Time Domain Signal and Analysis

This part of the thesis is based on the measurement techniques for the detection of specific faults in reciprocating compressors. Several sensors have been mounted on the body of the compressors. The data processing techniques used to analyse these signals were of the conventional methods created in the application of time domain, frequency domain, time-frequency domain and adaptive approaches.

The time-domain signal represents the time history of the energy contained in the signal and is dominated by the most energetic or noisiest elements. Time-domain measurement is often

considered the simplest of the measurement techniques and requires relatively inexpensive and unsophisticated instrumentation. In the time domain, a defect condition is often detected and evaluated using statistic descriptors of the vibration signal, such as the peak value, Root Mean Square (RMS), Crest factor or Kurtosis [109].

To achieve a good performance of machine fault diagnosis, the type of features extraction and selection process is paramount as per Ahmed Mahmud [56]. He also stated that Vibration monitoring techniques can be used to detect faults in a compressor, vacuum pumps body and different components in their early stages. This information can then be used to prolong the life of the compressor and protect the system from any catastrophic failure. The vibration signal measurement on the cylinder head of a compressor is mainly a combination of the response to two main types of vibration excitation; a) flow-induced vibration when the airflow interacts with valves or other associated components which cause periodic oscillation in the flow and b) vibration due to the abrupt opening and closing of the valve plate when hitting the seat [56].

A. Mahmud also stated that the time domain analysis leads to popular statistical feature parameters such as RMS, peak factor, skewness and kurtosis whereas the frequency domain analysis, which is the (Standard Fourier Transform) analysis, produces features including amplitudes at frequencies.

His study explores the features derived from the time domain, frequency domain and envelope analysis, which are the most commonly used in Condition Monitoring (CM) [56].

Similarly, Kim et al [110] state that the time domain analysis of the vibration signals waveform is a raw unprocessed signal obtained from the vibration transducer and it is a graph amplitude of the vibration signal as a function of time. The time-domain signal is complex because it is the sum of all the individual frequency components that are present and is also a visual representation of the instantaneous value of motion. When executing a fault diagnosis using the time domain vibration signal, statistical methods are invariably applied and the most common statistical parameters are the (RMS), Crest Factor (CF), peak value (PK), skewness (SK) and kurtosis [110].

Even according to G.Dalpiaz et al [111] in their work on the effectiveness and sensitivity of vibration processing techniques for local fault detection in gears, they state clearly that the time domain analysis is based on the time series by plotting its amplitude against time and their characteristic features of signals are very much similar as mentioned by A. Mamud [70] such as the mean, peak to peak interval, standard deviation, crest factor, RMS, skewness and kurtosis

are calculated and used to describe the statistics of signals. These features are generally called time-domain features of statistical parameters.

Shreve stated that the main purpose of vibration signals is to determine the magnitude of the vibration generated and the source of the vibration. To achieve a good vibration analysis this will depend largely on the data acquisition system and processes used to measure the amplitude and frequency of the individual components, relative phases of the vibration signal and trend of the overall vibration level [112].

4.2.2 Frequency Domain Analysis of Vibration Signal

Rao states that the spectrum of the frequency-domain signal is a plot of the amplitude of the vibration signal as a function of frequency. The vibration signal of a machine is generated both by the individual components and by their assembly and installation and that each component in a working machine will generate specific identifiable frequencies, thus a given frequency spectrum can be attributed directly to corresponding machine components [113].

Spectral analysis, also called the frequency domain, gives the spectral information and is sometimes used for data analysis. The frequency-domain transforms the signals from the time-domain into the frequency-domain through the Fast Fourier transform (FFT). The spectrum analysis is the most widely used conventional analysis through the (FFT) [114].

The main principle of spectral analysis is to look at the spectrum in its entirety at certain frequency components of interest and then extract features from the signal. The power spectrum is one of the most commonly used tools in the spectrum analysis. There are other useful tools for spectrum analysis such as the graphical presentation of the spectrum, frequency filters, envelope analysis and sideband structure analysis [115].

Equally, Ali Kahirdey states that the time domain, the frequency domain analysis, is also one of the popular methods used in the ball bearing analysis. He states that in the frequency domain analysis, both low and high-frequency range of the signal is analysed using the (FFT) analysers.

Due to the complexities in the vibration behaviour of the ball bearings and the interaction between the defects and the rolling elements, this causes shock pulses that excites the natural frequency of the whole system which results in an increase of the vibrational energy at these excited frequencies [116].

Even Heng et al state that there is a limitation with the time domain compared to the frequency domain as each component of the gear has its characteristic frequency as does any faults associated with that component. These frequency signatures, or signal spectral content, are a good key to check the bearing condition. These signatures will also not be lost in the overall signal as they appear at distinct frequencies. The (FFT) of the vibration signal is the most common way for converting the time domain to the frequency domain. Trending of the frequency components is a common approach [117].

4.3 Establishment of the Laboratory Test Rig

This chapter provides a full demonstration of the model to give readers a broad idea of the test rig facilities design, construction and how faults will be seeded into the compressor to gain the required experimental data for comparison intended for future projects. The measurement system, signal analysis and data management will be then analysed based upon this compressor.

4.3.1 Test Rig Description

The test rig consists of a Broomwade TS-9 compressor as shown in Figure 4-1. This specific compressor has been used previously by researchers from the Centre for Efficiency and Performance Engineering (CEPE) group and is the property of the School of Computing and Engineering at the University of Huddersfield. A risk assessment has been carried out before using the device and regular checks are being carried out by the relevant authority. The compressor comprises of three main components, the induction motor, two cylindrical compression unit of which is composed of a low and high pressure cylinder and an air receiver. The compressor delivers compressed air at 0.8 MPa (8bar)/120 psi to the horizontal air receiver tank with a maximum working pressure of about 1.35MPa (13.5bar)/200 psi. It's a two-stage, single-acting reciprocating compressor and the cylinders are in the "V" form. The crankshaft is driven by a 'V' type transmission belt and the electric motor is a foot mounted, squirrel cage, air-cooled, type KX-C184. A 2.5kW motor rated speed of 1420 rpm, drive a multi-belt pulley system at ratio transmission of 3:2:1. The speed of the flywheel is rated at 440 rpm.

The following Table 4-1 shows the Compressor Specification and Figure 4-1 shows the Broomwade TS-9 Compressor Layout

Table 4-1 Compressor Specification

Broom Wade TS9 Compressor	
Max working pressure	200 psi=1.38 MPa
Number of cylinders	2 cylinders at 90° opposed
Piston stroke	76.2 mm
Compressor Speed	420 rpm at 7.2 Hz
Motor Power	2.5Kw
Motor Speed	1420 rpm
Voltage	380/420V
Current	4.1/4.8 A
Low Pressure First Stage Cylinder/Piston Diameter	93.6 mm
High Pressure Second Stage Cylinder/Piston Diameter	55.6 mm

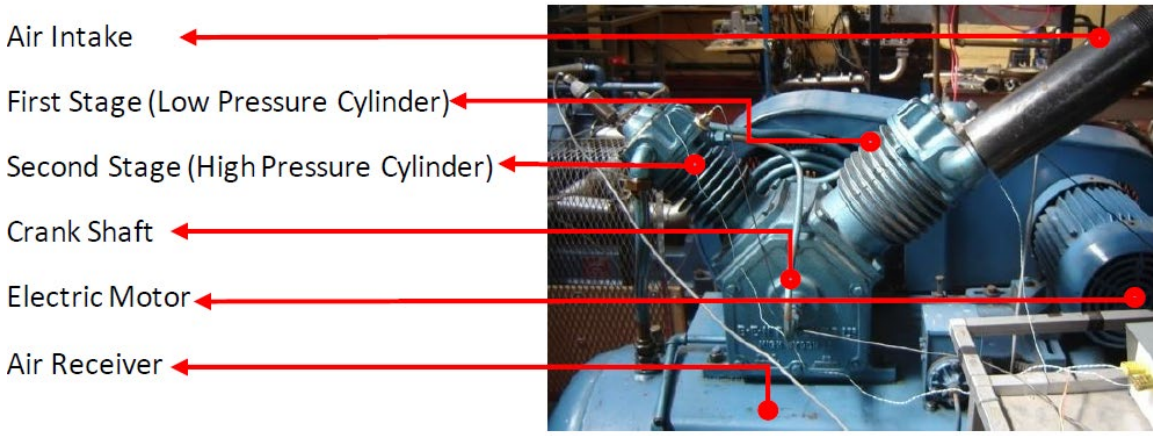

Figure 4-1 Broomwade TS-9 Compressor Layout

Brief Operation

On the start-up of the compressor, the motor drives the pulleys through the v belt which then, in turn, forces the crankshaft to rotate causing the first cylinder (low pressure) to compress and then steps to the next stage to the second cylinder (high pressure), through the intercooler which cools the air by removing the heat that is created after having been compressed through the first stage. That heat helps the air to develop and demands an increase of horsepower for further air compression. Cooling is then vital as it assists in limiting the temperature discharge and reduces the power demand.

The air passing through the intercooler is supplied by the crankcase breather which allows air to flow in and out of the crankcase through the displacement of the pistons [75]. Air now starts to build in the storage tank to a set value of about 8 bars. As soon as that value is reached a diaphragm pressure switch cuts off the electrical circuit to the motor and stops the motor from turning. Whenever air from the receiver is used, the air pressure drops and the motor starts again filling up the tank to the required amount and that cyclic event carries on.

On top of the receiver, there is a pressure relief valve which acts also as a safety valve. It is set to 200 psi approximately 13.8 bars. In the case of an excessive volume of air and if the diaphragm pressure switch failed the tank is protected by that pressure relief valve. In the case of a disaster or for the comfort of data sampling an extra emergency push button is added to the device. The compressor motor is supplied by a three-phase direct online starter. Tyco anti-vibration pad is utilised on the compressor feet to reduce the noise and vibration level. A manual valve has been fitted to release any trapped condensation. Figure 4-2 General System Set up.

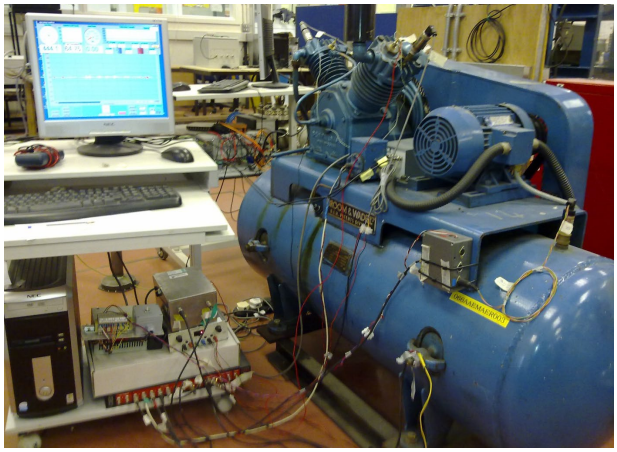

Figure 4-2 General System Set up

4.3.2 Introducing different Common Compressor Fault

The vibration and motor current signals have been studied to be able to conduct a thorough evaluation of the Reciprocating Compressor (RC) performance. Five working condition data sets were being collected sequentially one at time. Before instigating any fault to the compressor, it is essential to have a baseline sample, this is when the compressor is operating under normal condition free from any failure.

After that process, the common faults were separately seeded into the system. They are the discharge valve leakage, suction valve leakage, intercooler leakage and loose transmission belt. The experimental test sequence was as shown in Table 4-2 and the baseline signal deviations were measured

Table 4-2 Sequential Experimental Test Conditions

Experimental Test Conditions	
Test Cases	Description
BL	Healthy Compressor/Baseline
DVL	Discharge Valve Leakage at 2nd Stage
SVL	Suction Valve leakage at First Stage
IL	Intercooler Leakage
LB	Loose Transmission Belt

4.3.2.1 Simulation of Valve Leakage

Discharge Valve

Compressor valves work in a harsh environment and are exposed to a huge number of impacts per second during their lifetime. This makes valves the most susceptible part of the compressor. During the compressing cycle, non-uniformity wear is inevitable and this can lead to a faulty valve which in turn reduces the reliability of the compressor. In this research, the test rig valve is fitted with a faulty plate valve as shown in Figure 4-3.

As explained briefly above, the compressed gas is transferred from the first stage suction valve (low-pressure) cylinder to the second stage discharge valve (high pressure) cylinder through the intercooler pipe.

Efficient operation of the discharge valve is important to the functioning of the compressor, if not it can affect the performance of the machine enormously. A leaky valve is also the most common fault in RC. Any leakage in the valve is an extra reduction flow of air which will decrease the compressor performance. A leaking valve causes high-temperature air to be forced across the valve surface by differential pressure which accelerates the deterioration of the valve plate, including the valve spring, and weakens the compressor performance considerably [121].

The discharge leak valve occurs more often due to the high impact velocity and temperatures in the chamber. The flow of gas to and from the leaking valve travelled around the enclosure in an erratic flow pattern, through cylinder openings and cavities under and above the valve. The uneven distribution of gas flow can affect and cause other plate valves to wobble during the opening and closing motion creating an abnormal mechanical action [121].

Discharge valve leakage is more critical than the leakage in the inlet valve as the pressure is greater than upstream of the inlet valve and it reduces the compressor capacity.

The introduced faulty valve to simulate the leak is a 2mm diameter drilled hole which is 2% of the cross-sectional airflow. Figure 4-5 (a) shows the faulty discharge valve and Figure 4-5 shows the test rig compressor schematic.

Figure 4-3 Second Stage-Discharge Valve Components

4.3.2.2 Simulation of Intercooler Leakage

The pressure is carried from the first stage to the second stage through pipes and here leakage is very common in the intercooler joints. In this case, a loose intercooler fault is seeded into the system. To simulate this fault the intercooler pipe joint was loosened slightly by one revolution to model a minor leak as illustrated in Figure 4-5 (b). However, it was not practical to measure the leakage as a percentage of the airflow cross-sectional area.

The function of the intercooler is to chill the 2nd stage air by removing the heat that is created after having been compressed through the first stage. Cooling assists in limiting the temperature discharge and reduces the power demand, if improper cooling is carried out this will affect the performance of the machine and more work will be required to keep the machine running at the desired pressure.

Suction Valve

The suction valve is the initial phase of the first cylinder (low pressure) compressing the air in the first stage chamber and then passing it to the next stage, the second stage cylinder (high pressure). Therefore, this cylinder pressure is a direct parameter in measuring the operating performance of a reciprocating compressor. It expresses all the functions and working processes in all the subsystems components, such as valve movement in each stage, air-flow dynamics and motor speed-load signature etc. A faulty valve spring is seeded into the RC as shown in Figure 4-5 (c).

4.3.2.3 Simulation of Loose Transmission Belt

The loose transmission belt is also another common fault in the compressors. It never reaches its designed speeds as the belt will slip on the drive pulleys causing faults, e.g. excessive noise and vibration. The compressor also never reaches its designed outlet pressure and most failures

in industries are also usually caused by a loose transmission belt. The compressor transmission belt undertakes a great variable load when driven and the load amplitude will be more than three times higher during the transient start-up process. The amplitude during acceleration will surpass the amplitude of the friction force between the wheel and the belt resulting in slippage during this time. The slip will gradually wear the belt and deteriorate the inside structure which will lead to a loose belt [56] [122].

To simulate this fault, the belt was loosened in the system by reducing the distance of the two drive pulleys from 169mm to 174mm by an adjusting clamp and with the aid of a Dial Test Indicator also known as a (DTI). This will show the accuracy and determine whether any corresponding changes could be detected in the cylinder pressures. Figure 4-4 gives an overview of the test procedure.

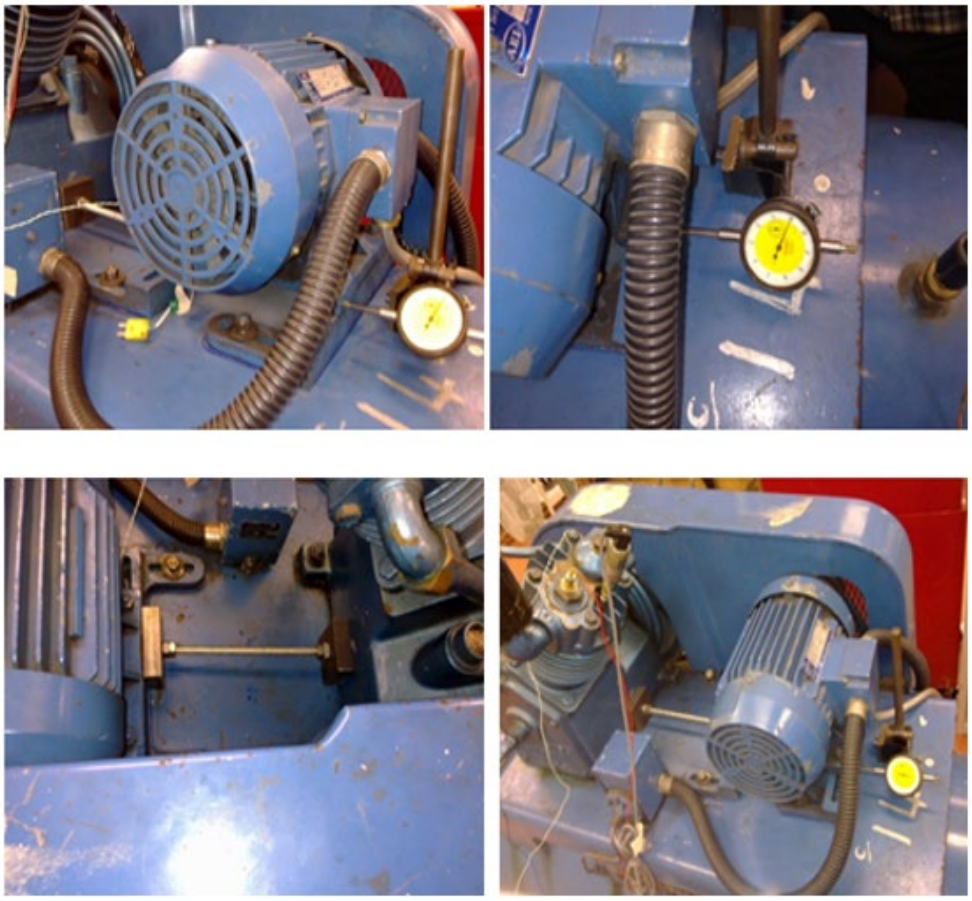

Figure 4-4 Loose Transmission Belt Procedure

(a) Faulty Discharge Valve
(b) Loose Intercooler Joint
(c) Faulty Suction Valve
(d) Loose Belt

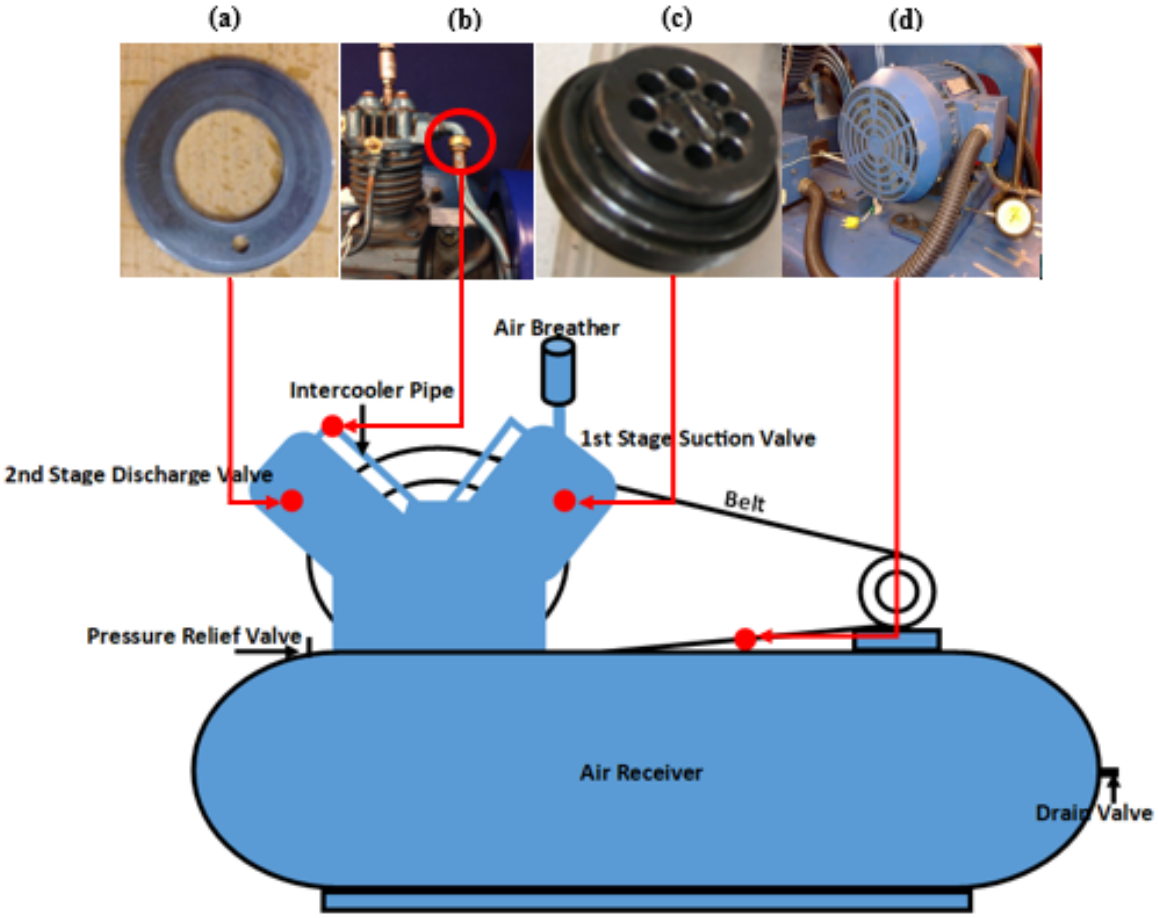

Figure 4-5 Test Rig Schematic Diagram and Fault Simulation

4.4 Instrumentation and Measurement

Several studies have previously been used for the machine condition monitoring by the same test rig. However, a variety of sensors were mounted on the test rig such as dynamic and static pressure transducers, accelerometers, thermocouple, shaft encoder and current transducers. Sample data was collected from those transducers and projected to the Data Acquisition System (DAC) and Coaxial BNC cables were utilised for noise signal reduction.

4.4.1 Accelerometer

Two accelerometers are situated on the first and second stage pressure cylinder to measure the vibration level. They are of type YD-3 with a frequency range from 0.4 to 10 kHz, at a sensitivity of 74mv/ms^{-2}, capable of withstanding temperatures of up to 150°C and acceleration of up to 2000ms^{-2}. Those accelerometers are inexpensive, ideal for the environment and can be

easily found on the market. The vibration signal goes to an amplifier then to the data acquisition. The following Figure 4-6 [123] shows the accelerometer and Table 4-3 describes the specifications.

Figure 4-6 Accelerometer

Table 4-3 Accelerometers Technical Specifications

Accelerometers Specifications	
Features	Specifications
Type	TD-5-2
Sensitivity	45mv/ms^2
Acceleration	2000ms^{-2}
Frequency	0-15 kHz
Temperature Range	≤150°

4.4.2 Thermocouple

Figure 4-7 shows the thermocouple attached on top of the cylinder which records the measurement of the air temperature inside the cylinder. The thermocouples used are of 'K-type' with a linear response from -20 to 220°C. They are connected to an amplifier that is powered by a 240-volt supply and the output is then connected to the data acquisition channel. The monitoring of temperature in both the 1st and 2nd stages is vital for safety reasons and the protection of the sensors.

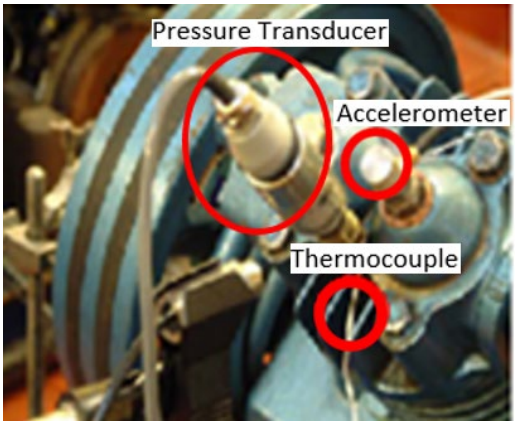

Figure 4-7 Accelerometer Thermocouple, Pressure Transducer

4.4.3 Dynamic Pressure Transducer

Two dynamic pressure sensors were used and they operate at a pressure of 4 MPa (40bar equivalent to 600 psi) and an upper-frequency limit of approximately 4 kHz. A small hole had to be drilled into each cylinder head and the (GEMS) type 2200 strain gauge pressure transducer fitted into the holes. These pressure sensors are economical and within the compressor and pressure limit. The maximum output of these sensors is 100 mV and Figure 4-8 shows the pressure transducer. It is being powered by a 10 Vdc power supply without amplification. The transducer is connected directly to the Data acquisition, Figure 4-9 shows the on-line raw data-trace of the dynamic pressure of the 1st and 2nd stage compression and Table 4-4 shows the technical specifications.

Figure 4-8 In-Cylinder Pressure Sensor

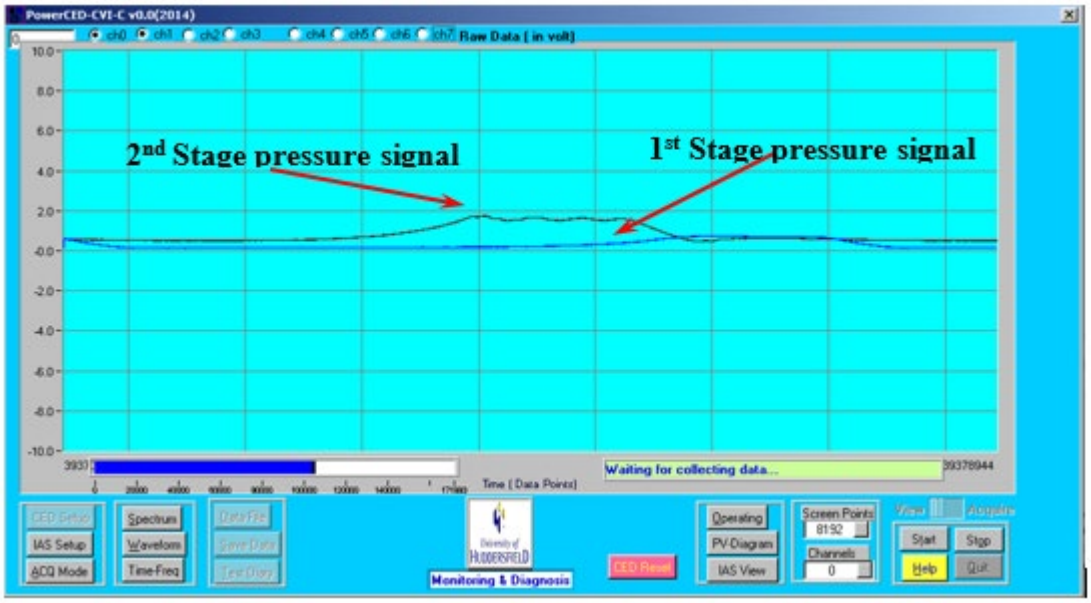

Figure 4-9 On-line Raw Data Trace of the Dynamic Pressure

Table 4-4 Pressure Sensor Specifications

Pressure Sensor Specifications	
Features	Specifications
Type	GEMS Type 2200 Strain gauge
Output	100 mV
Pressure Range	4 Mpa (600 psi)
Frequency Limit	4 kHz
Power Supply	4 Vdc

4.4.4 Static Pressure Transducer

The static pressure sensor as shown in Figure 4-10 is used on the receiver. It is a Sensor Technics, Type 'PS20000''V'

'V', functioning at a range of 0 to 1.35 MPa (13.5bar), at a maximum output of 100 mV with a supply of 15 Vdc and a temperature ranging from -20°C to + 105°C. The sensor switches the compressor motor cut off as and when required and triggers the data collection at various pressures according to the "Matlab" programme.

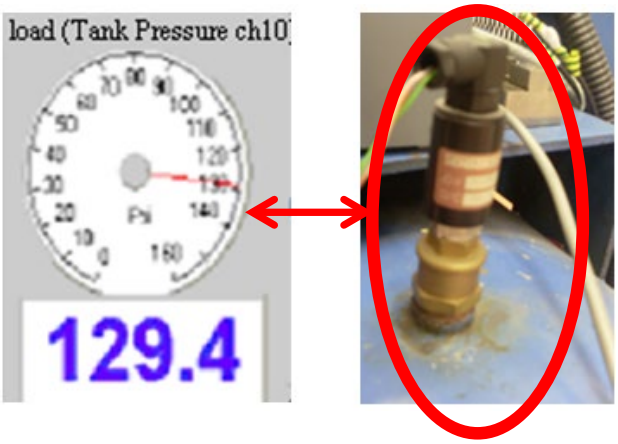

Figure 4-10 Static Pressure Sensor (Storage Pressure)

4.4.5 Shaft Encoder

The Shaft Encoder shown in Figure 4-11 is a (Hengstler) incremental optical encoder which is coupled to the driveshaft and is designed to measure the Instantaneous Angular Speed (IAS) at the optimum accuracy. The end of the crankshaft has 360 opaque segments evenly spread out around its perimeter to capture the small change in the shaft speed. The encoder is powered at 10 Vdc and connected to the Personal Computer (PC) via the Data Acquisition. This encoder is ideal for the application and is economical and Figure 4-12 shows the online raw encoder data.

Figure 4-11 Shaft Encoder

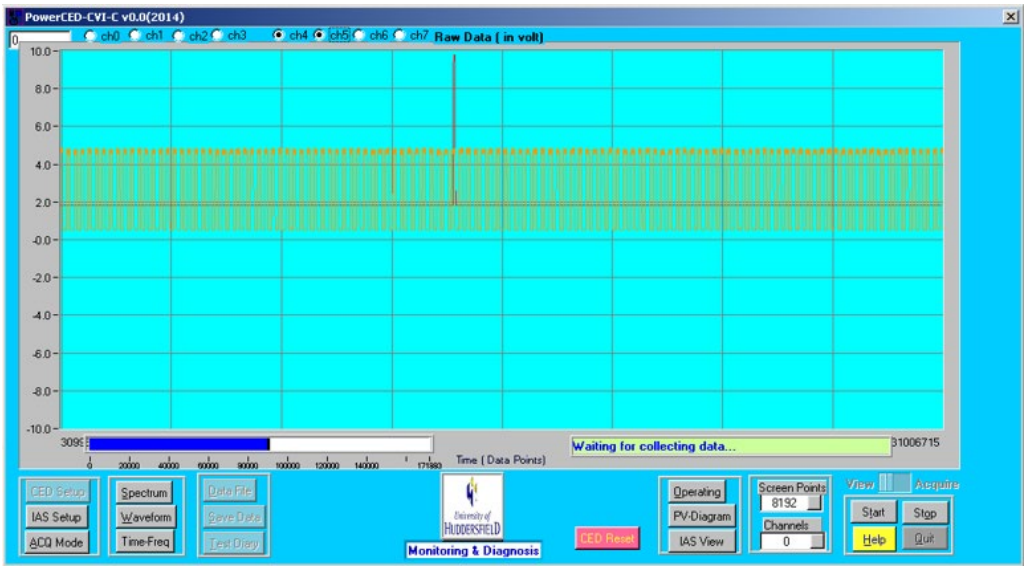

Figure 4-12 On-line Raw Encoder Data

4.4.6 Electrical Current and Power Measuring Devices

Previous researchers at the University of Huddersfield have worked on the capabilities of the power supply parameter to detect the fault in induction motors, gearboxes and pumps but not on a reciprocating compressor. There was already an instrument used by previous academics for the measurement of motor currents, voltages and power, Figure 4-13 shows the Three-phase measurement unit. The motor current and voltage in each phase was measured by a Mounting Hall Effect Current Transformer (MHCT) which will be explained later.

The measured value for the current in each line is fed into the measurement unit as presented in the schematic diagram in Figure 4-14 below, which makes the conversion into voltage measurement, filters the signal and feeds it to the data collection channel and Figure 4-15 shows the online motor current raw data.

The same device can also be used to measure the instantaneous current, voltage and power in each of the three phases. The maximum current of the phase current measuring unit is 5A, the voltage line to line is 12.8V and electrical power is 10 Vdc.

Figure 4-13 Three Phase Current Measuring Unit

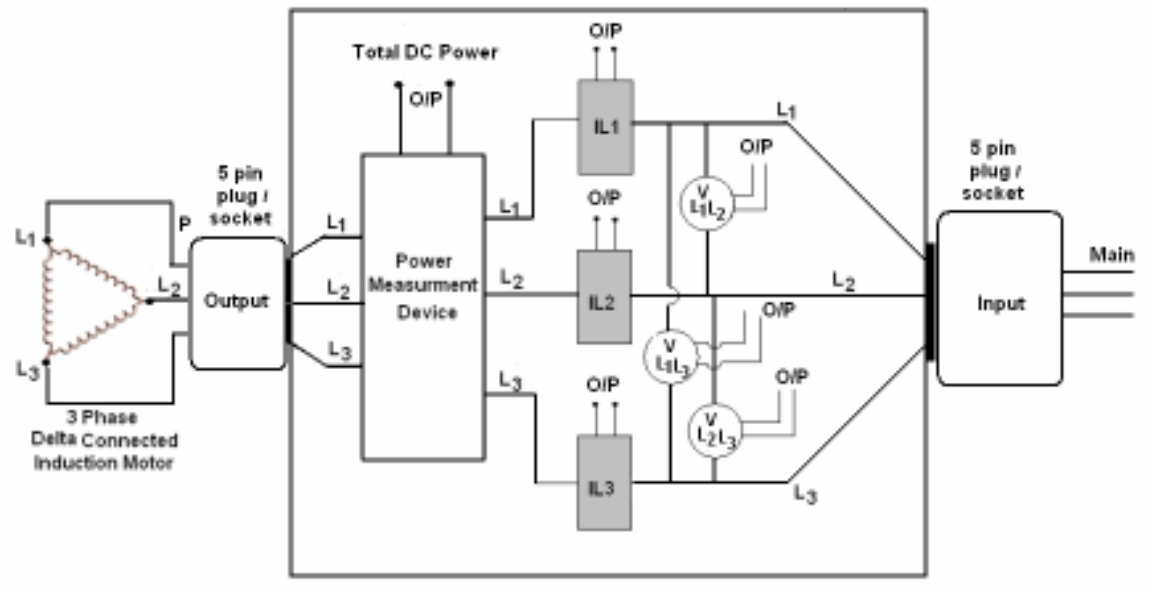

Figure 4-14 Three Phase Measurement Unit [124]

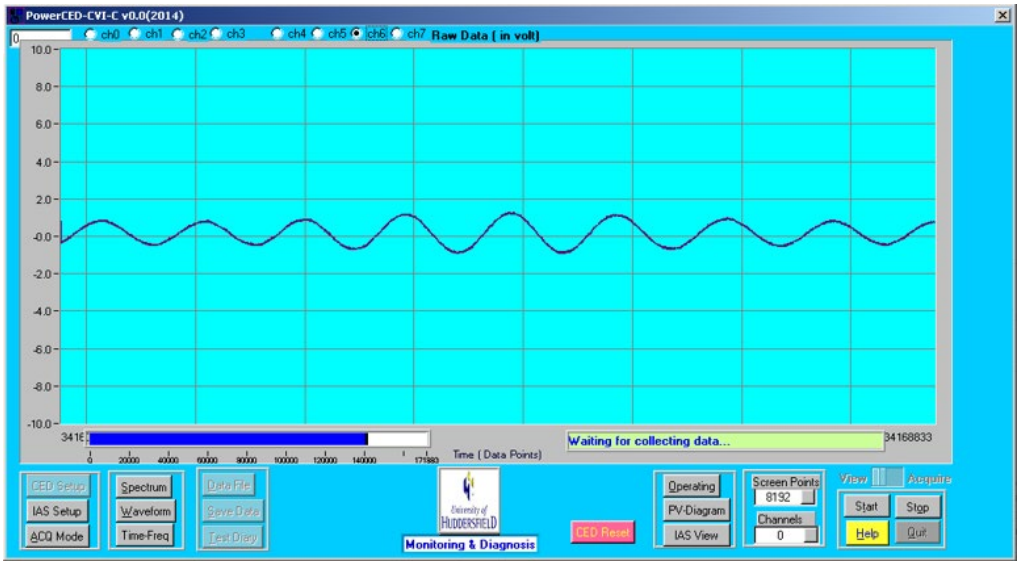

Figure 4-15 On-line Motor Current Raw Data

4.4.7 Stator Current Transducer

The stator current transducer is a Hall Effect current transducer, "RS number 286-327" which has now been discontinued. The part was inexpensive and even the equivalent product is very similar physically and economically however it is more performant, the 'RS' number is 180-7357. The device has an accuracy of ± 0.9 % and operates at a frequency bandwidth of DC to 200 kHz. Table 4-5 shows the Hall Effect Current Transducer specifications.

The input current ranges from 0 to 70 A, operating at a maximum temperature of ± 85° and a minimum temperature of -40°. The difference in this product compared to the previous discontinued current transducer is that the original one operates at a bandwidth of DC to 100 kHz and the operating temperature is 15° lesser.

Table 4-5 Hall Effect Current Transducer (RS 286-327) Technical Specifications

Hall Effect Current Transducer (RS 286-327) Specifications	
Features	Specifications
Supply Voltage	±15 Vdc, (±5%)
Operating Temperature	0°C to +70°C
Bandwidth	DC to 100kHz
Analogue Output Voltage	5 V
Response Time (Inst.)	< 1 µ sec

4.5 Data Acquisition System

The data acquisition used for this project is a Power 1401/2701 from the Cambridge Electronic Design (CED), which is illustrated in Figure 4-16**.** It is a robust, high-performance system for capturing and analysing different dynamic data. There are 16 input waveform channels on a standard Power 1401. Eight channels are available through a front panel Bayonet-Neil-Concelman (BNC) connector labelled as Analogue Digital Converter (ADC) inputs.

There are another eight through the rear panel Analogue Expansion D socket. These channels work at an input range of ±5V but can be configured to ±10 V if modified. The waveform input channels are buffered through amplifiers. The ADC can convert an input signal to a 16-bit digital value at approximately 800 kHz in one channel mode and 625 kHz if the channel is being interchanged [125]. The Power 1401 has an easy installation set-up for its software. Both the PC and the (Data Acquisition) DAC system should be switched on whilst carrying out this process. The provided Universal Serial Bus (USB) plug should be connected to both machines then the system will auto-detect the USB and will look for its driver followed by the instruction on the screen until it is finished [125]. For a simplified and automatic data acquisition of various test conditions, a software packet is developed on NI Lab windows platform. It allows the acquisition to be conducted automatically at given time intervals and specified discharge pressures. Seven channels have been used in this experimental study as shown in Table 4-6

Table 4-6 Type of Channel Used

Type of Data Channel Used	
Channel Number	Type of Data
Channel One	Pressure Data Collected from Fist Stage (Low Pressure) cylinder
Channel Two	Pressure Data Collected from Fist Stage (High Pressure) cylinder
Channel Three	First Stage Vibration Data
Channel Four	Second Stage Vibration Data
Channel Five	Data from Shaft Encoder
Channel Six	Measured Angular Data Position Marking TDC of Piston Position
Channel Seven	Motor Current Data from Current Transducer

Figure 4-16 Data Acquisition Cambridge Electronic Design (CED)

4.5.1 Data Management and Measurement System Procedure

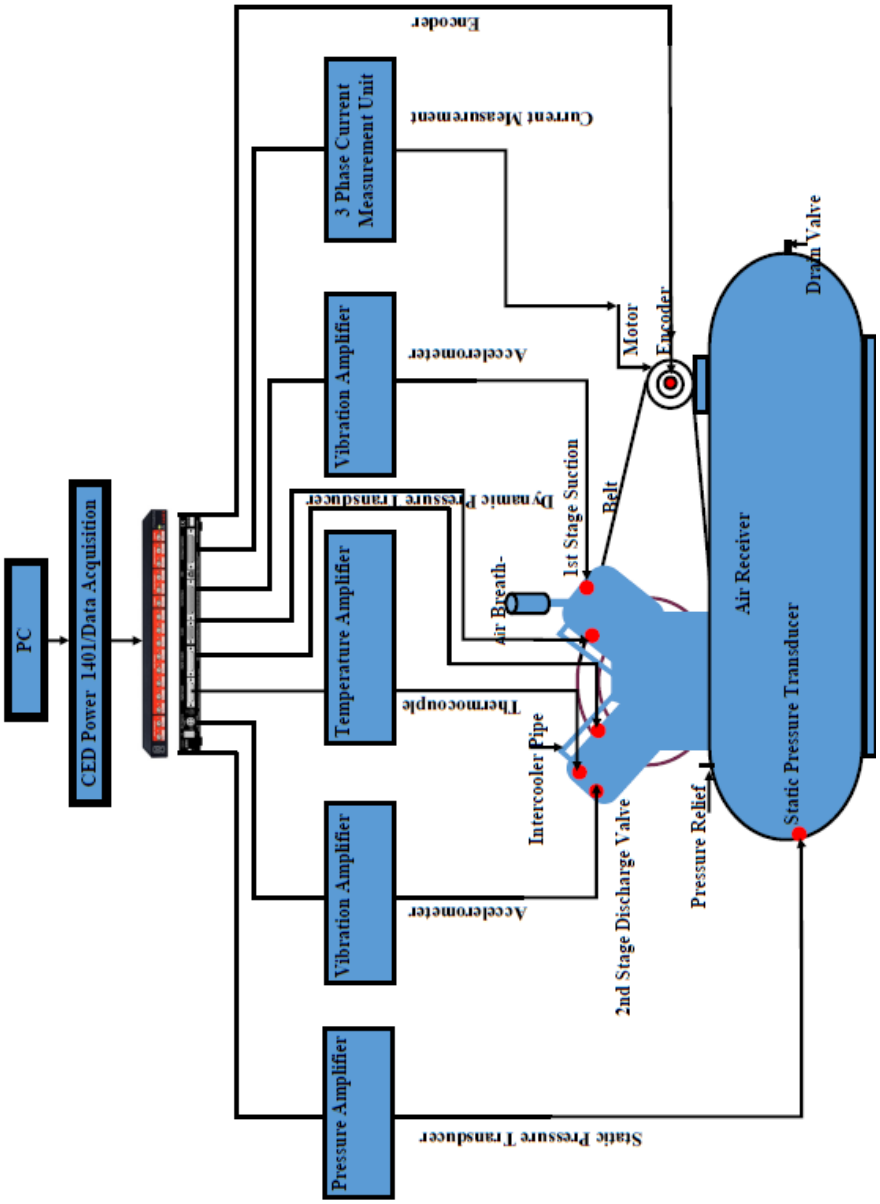

Figure 4-17 Test Bed Layout of the Experimental System

Figure 4-17, shows the Test Bed layout of the experimented system in which the sensor placement and signal flows are detailed. To achieve a high level of practical experience a test procedure was developed as follows; Four data files were collected for each set of the collected

sample from the test rig. As described above, from the type of data channel used each system was connected from the DAQ system to various part of the instrumentation of the RC under test. A directory was specifically created where the collected data was placed. A structured filename was also created for the identification of the related file numbers, specific test, compressor load and various faults conditions.

4.5.2 Test Procedure

The procedure to take the reading of the baseline was carried out in two separate stages, with a pressure transducer installed on the first and second stage. The transducers, in turn, carry the raw signal to the data acquisition and the signal is recorded by a computer for further investigation. These signals are then taken away to be computed offline in MATLAB.

Benchmarking the in-cylinder pressure trace from the RC was necessary and five sets of data were acquired from the test rig under the healthy conditions of the Baseline (BL). Similarly, five sets of data were collected for each of the four different faulty conditions (DVL, SVL, IL and LB). The test cases and operating conditions are detailed in Table 4-7. There are five tested cases, consisting of the healthy case or baseline (BL) and four faulty cases, which were tested one by one under three representative discharge pressures, corresponding the lower pressure operation of (40psi), the mid limit of (80psi) and higher limit of (120psi). Moreover, the faulty cases are the common problems in the RC, as reviewed earlier.

4.6 Pressure and Vibration Analysis during Valve Operation

There are four dynamic events in the operation: Suction Valve Open (SVO), Suction Valve Closed (SVC), Discharge Valve Open (DVO), Discharge Valve Closed (DVC) and two-position: Bottom Dead Centre (BDC), Top Dead Centre (TDC) and these events can be seen on a time trace of pressure and vibration. To comprehend the comparison of cylinder pressures, vibration and valve movement, it is necessary to understand the operation of the SVO, SVC, DVO, DVC and the position of TDC, BDC. The reason for this is to know when the suction discharge valve opens and closes and where the top dead centre and bottom dead centre are for further study.

In Figure 4-18 the TDC mark which shows 240 degrees is to be neglected as further work is required.

Also only the first and second stage healthy valve operation at 40psi is explained in detail.

4.6.1 First Stage Healthy Condition Valve Operation at 40, 80 & 120 psi

The following Figure 4-18 to Figure 4-20 describes how the changes in discharge tank pressure for the 1st stage at 40, 80 and 120 psi affect the opening and closing times of the valve's operation during its cycle.

1st stage valve operation

In the 1st stage, the low-pressure cylinder piston leads the 2nd stage by approximately 90°. When the 2nd stage piston is at TDC the 1st stage SVO open and DVO opens, the 1st stage valve operates at a healthy condition of a 40 psi as is shown in Figure 4-18 and operates as follows. On the 2nd stage, when the piston is at TDC, the 1st stage SVO and DVO opens. The time taken for the DVO to open and close depends a lot on the discharge pressure. If the discharge pressure is lower, the DVO opens later as a lower pressure in the discharge tank will need lesser pressure in the cylinder before the DVO open.

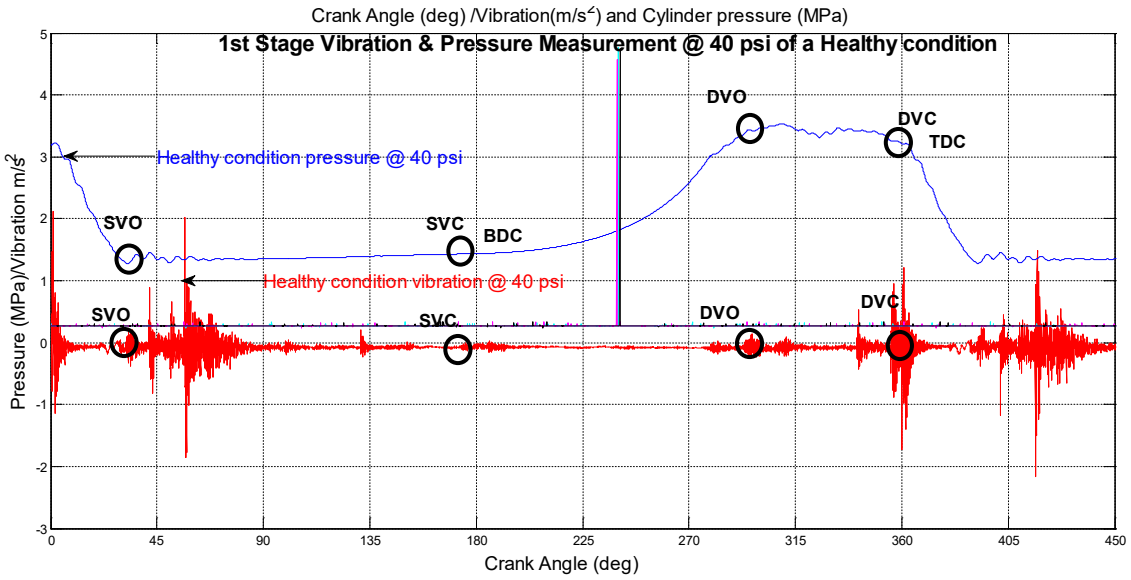

Figure 4-18 Healthy Condition 1st Stage Vibration & Pressure at 40 psi

1st Stage Valve Operation at 80 psi

From Figure 4-19, zero degrees (0º) corresponds to the (TDC) of the 1st stage the piston moving downward from 0º to about 30º approximately and from there the pressure decreases slightly then shows the expansion process. At this pressure, (SVO) the suction process starts.

At 31º onwards to about 179º, the pressure remains at the minimum constant level illustrating clearly the suction process. When (SVC) closes, marking the end of this process, the compression begins.

From 180º to about 295º the pressure increases gradually up to the maximum, showing the compression stroke. At this pressure, the discharge valve (DVO) is pushed open.

Beginning at 296º to approximately 358º the pressure remains slightly the same, showing the discharge process. At about 359º (DVC) closes and a new expansion process starts at TDC again.

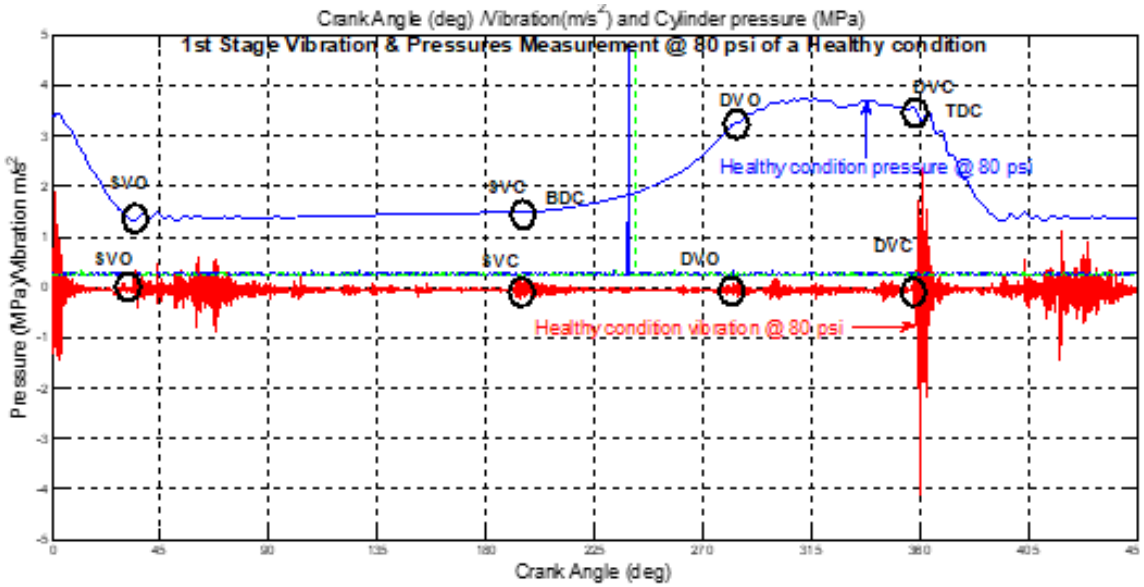

Figure 4-19 Healthy Condition 1st Stage Vibration & Pressure at 80 psi

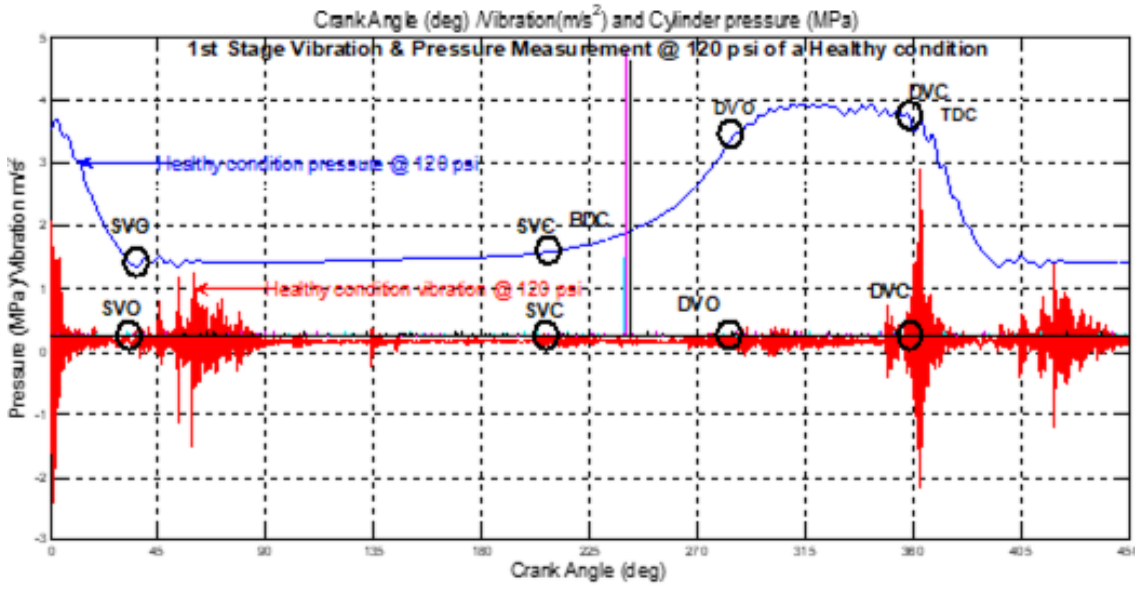

Figure 4-20 Healthy Condition 1st Stage Vibration & Pressure at 120 psi

Figure 4-19 and Figure 4-20 also clearly show how the impact in the discharge tank pressure affect the opening and closing times of the 1st stage valves which are obvious for all three discharge tank pressures: 40 psi, 80 psi and 120 psi. It is evident that the change in the crankshaft angle of the 1st stage-discharge valve closes with a decrease in discharge pressure and hence requires lesser work.

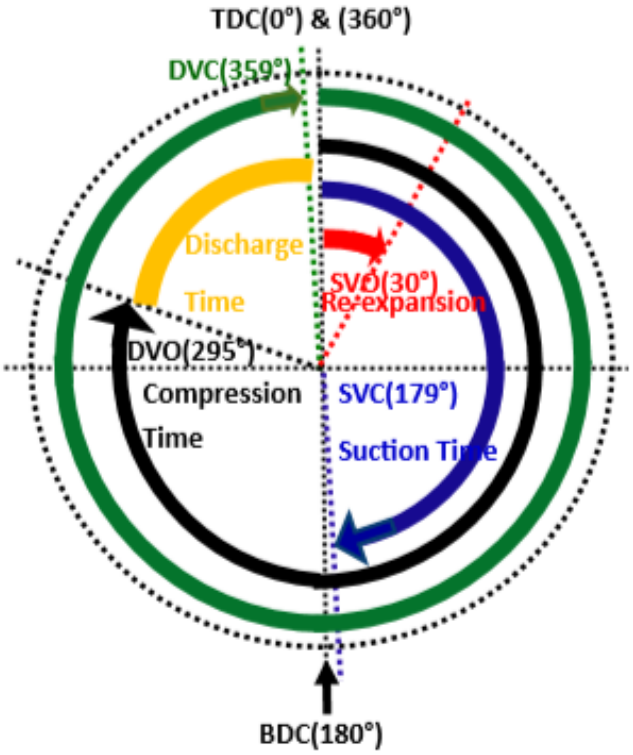

Figure 4-21 Operation of a Healthy Condition at 40 psi of a 1st Stage Valve

Figure 4-21 describes a brief operation of a healthy condition 1st stage at 40 psi. At 0° to 30° (SVO) shows the expansion phase. From 30° to 179° approximately is the (SVC) stage which is the suction process. From 180° to 295° more or less is the (DVO) compression process and then followed by the discharge process. However, this procedure will vary at 80 and 120 psi.

4.6.2 Second Stage Healthy Condition

Figure 4-22 shows how the changes in discharge tank pressure for the 2nd stage at 40 psi affect the opening and closing times and the remaining two discharge tank pressures. The 2nd stage 80 psi is shown in Figure 4-23 and Figure 4-24 shows the 2nd stage at 120 psi.

2nd stage valve operation

In the 2nd stage, the high-pressure cylinder piston leads the 1st stage by 45°. When the 1st stage piston is at TDC the 2nd stage SVC closes and DVC closes, the 2nd stage valve operates at a

healthy condition of 40 psi as is shown in Figure 4-22 and operates as follows; On the 1st stage, when the piston is at TDC, the 2nd stage SVC and DVC closes. The time taken for the DVO to open and close depends a lot on the discharge pressure. If the discharge pressure is higher, the DVO opens later as a higher pressure in the discharge tank will need higher pressure in the cylinder before the DVO springs open.

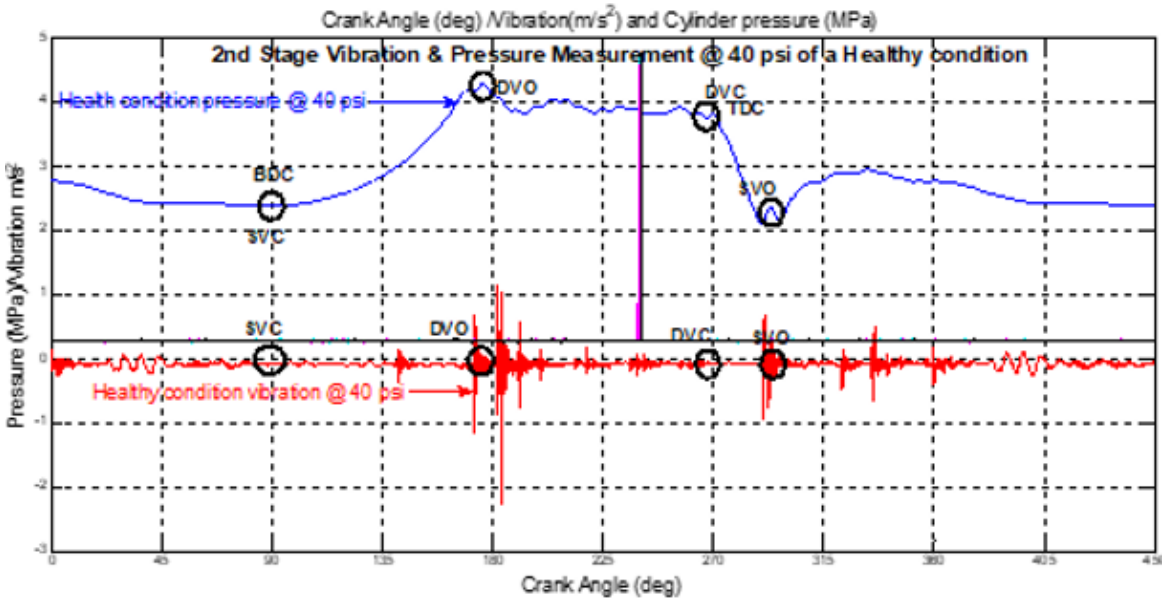

Figure 4-22 Healthy Condition 2nd Stage Vibration & Pressure at 40 psi

Figure 4-23 and Figure 4-24 also clearly show how changes in the discharge tank pressure affect the opening and closing times of the 2nd stage valves which are obvious for all three discharge tank pressures: 40 psi, 80 psi and 120 psi. It is clear that the change in the crankshaft angle of the 2nd stage-discharge valve opens with an increased discharge pressure and hence requires more work.

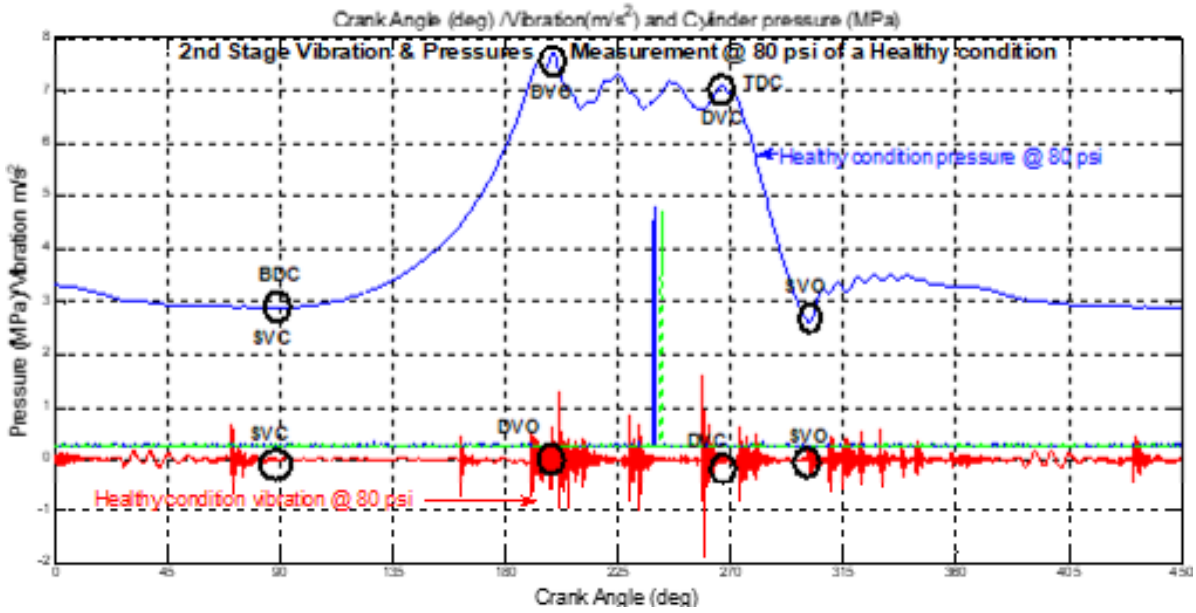

Figure 4-23 Healthy Condition 2nd Stage Vibration & Pressure at 80 psi

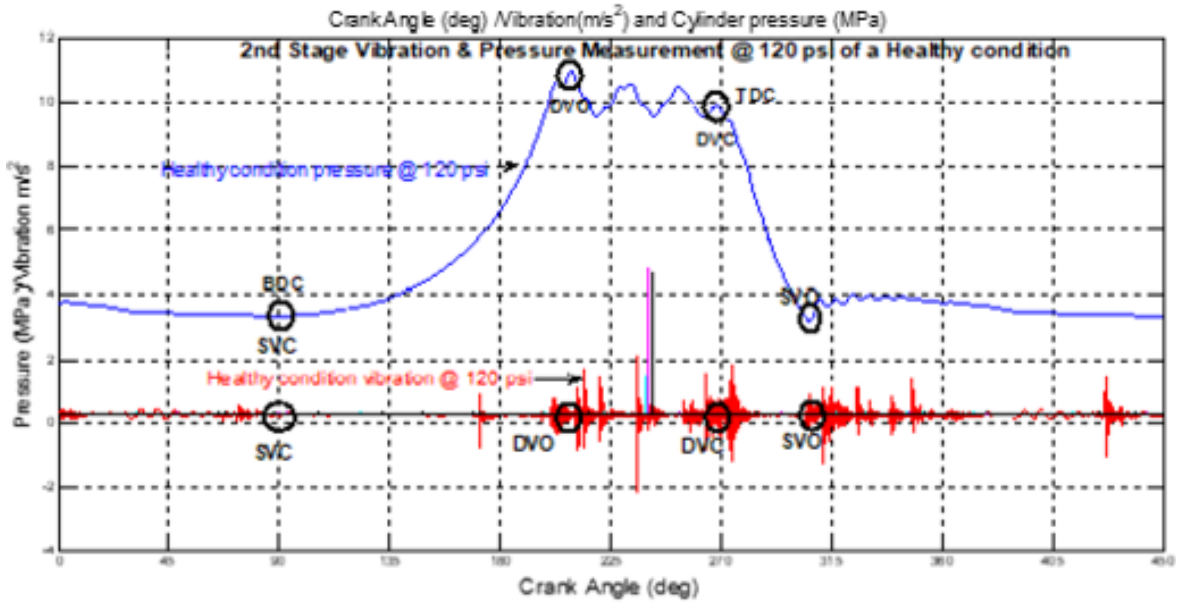

Figure 4-24 Healthy Condition 2nd Stage Vibration & Pressure at 120 psi

Healthy Conditions of a 120 psi, 2nd Stage Valve Operation

The 2nd stage valve operation of a healthy condition at 120 psi is shown in Figure 4-24

The (SVC), (DVO) & (SVO) on every discharge pressure on the 2nd stage varies whereas (TDC) is nearly always at the same position.

At 90° (SVC) of the second stage, the compression begins until (DVO) open. From 225° (DVO) till 270° the pressure reduces gradually with some irregularities. At 270°, (TDC) of the 2nd

stage, the piston moves downward from 271º to around 300º (SVO) and from there the pressure rises slightly to the expansion process.

Each case shows that less work is required in the suction stage whereas in the second stage (compression cycle) more work is required and the pressure oscillation is at a higher discharge pressure.

4.7 Healthy and Faulty Condition in-Cylinder Pressure Trace in Time Domain Analysis

Time-domain measurement is one of the simplest of the measurement techniques and requires relatively inexpensive and unsophisticated instrumentation for machine fault diagnostic [126]. The time-domain analysis uses the amplitude of the time signal to detect any abnormality in the machine operation as it holds useful information to study the changes in the machine operation [127]. The time-domain analysis calculates the characteristic features from the time waveform signals as a statistical measurement of the waveform.

To show the effectiveness and severity of the faults, this section analyses the change in cylinder pressures for both stages of a healthy compressor under different discharge pressure of (40, 80 and 120 psi) in the time domain. Figure 4-25 to Figure 4-33 shows the comparison of the following fault cases.

Table 4-7 Test Cases and Operating Conditions

Test Cases	Fault Locations	Fault Severity	Discharge pressures	Remarks
Healthy (BL)	n/a	n/a	Speed: 420rpm 40psi, 80psi, 120psi (2.8bar, 5bar, 8.3bar)	Good working operation see Figure 3-17
Discharge Valve leakage (DVL)	At 1st and 2nd stage-discharge valve	Figure 3-19 and Figure 3-20for the pressure diagram		Drilling 1 &2 mm hole on the plate as shown in Figure 3-18
Suction Valve Leakage (SVL)	At 1st and stage suction valve	Figure 3-22 and Figure 3-23 show the pressure diagram		Figure 3-21 shows the broken internal valve
Intercooler leakage(IL)	Intercooler	Figure 3-25 and Figure 3-26 represent the pressure diagram		The pipe joint is loosened by one revolution as shown in Figure 3-24
Loose Belt (LB)	Transmission belt	Figure 3-28 and Figure 3-29 for the pressure diagram		See Figure 3-27 for the loose belt

4.7.1 Baseline (BL) Test

A baseline signature for a healthy compressor under normal operating conditions is important as a point of reference when compared to a faulty RC system.

To achieve this, the RC was first thoroughly inspected and validated by the University technician and then a series of samples under different load conditions were being taken.

4.7.2 Changes in Cylinder Pressures under Healthy Condition for First and Second Stages

Figure 4-25 illustrates the waveform of the first and second stages cylinders pressure under different load discharge pressure of (40, 80 and 120) psi. It is obvious that the baseline of the first stage (suction valve) BL1 operates at a lower pressure than the second stage and that the 2nd stage cylinder pressure increases as the discharge pressure increases.

Pressure oscillates more at high discharge pressure. Each shows, in detail, that intake, compression, discharge, expansion and hence less current is required in the suction stage, whereas in the second stage (compression cycle) more work is required.

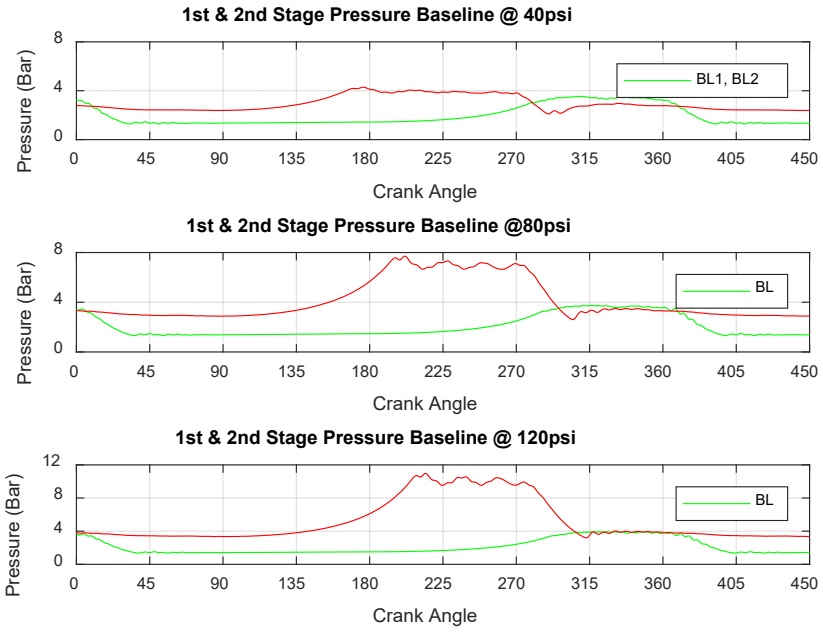

Figure 4-25 Pressure Trace of Both 1st and 2nd Stage Baseline (BL)

4.7.3 Changes in Cylinder Pressures under Discharge Valve Leakage

Different simulated cases of the cylinder pressure waveform effect for both the first and second stage cylinders at different discharge pressure is shown in Figure 4-26 and from observation it is obvious that the simulated faults have caused a change on the performance of the compressor especially at the higher discharge pressure.

From the 1st stage of Figure 4-26 for all three cases of the (SVO) 0° to about 30° and (DVO) 300° until the (DVC) 360°, the baseline is lower than the faulty discharge valve leakage and the pressure is nearly the same under all three conditions.

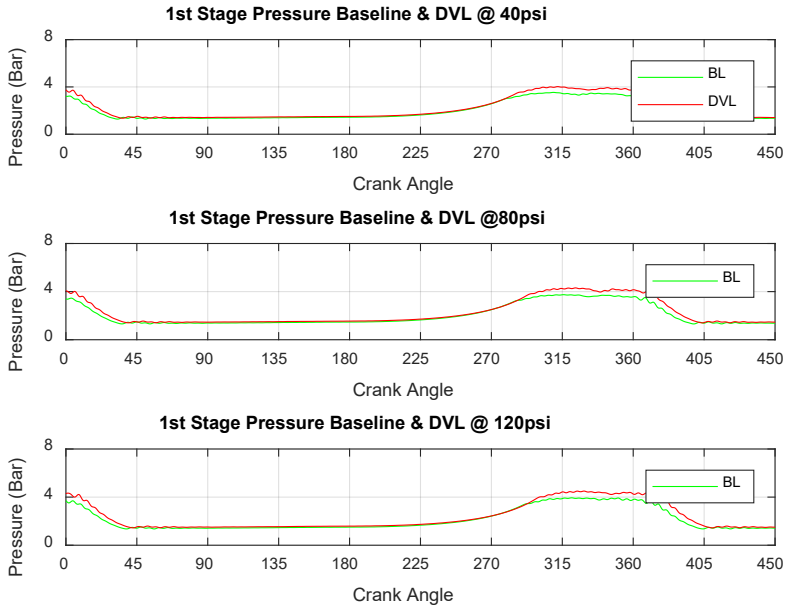

Figure 4-26 Pressure Trace of 1st Stage Baseline with Discharge Valve Leakage

On the 2nd stage at 80 psi from Figure 4-27, the pressure at DVO 180° is higher and from DVC 280° to SVC 300° is higher under 7 bar and approximately 11 bar at 120 psi DVO 200° because more work is required to compress the cylinder.

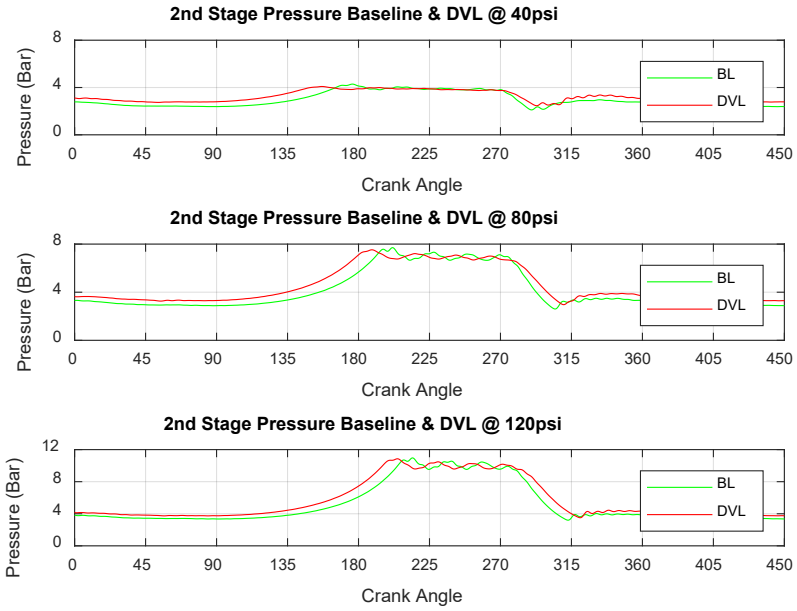

Figure 4-27 Pressure Trace of 2nd Stage Baseline with Discharge Valve Leakage

4.7.4 Changes in Cylinder Pressures under Suction Valve Leakage

On the 1st stage from Figure 4-28 SVO and DVO until the DVC, the baseline is lower than the suction valve leakage and the pressure differs under all three conditions, being much higher up to 7 bar at SVO and 8 bar at DVO at 120 psi.

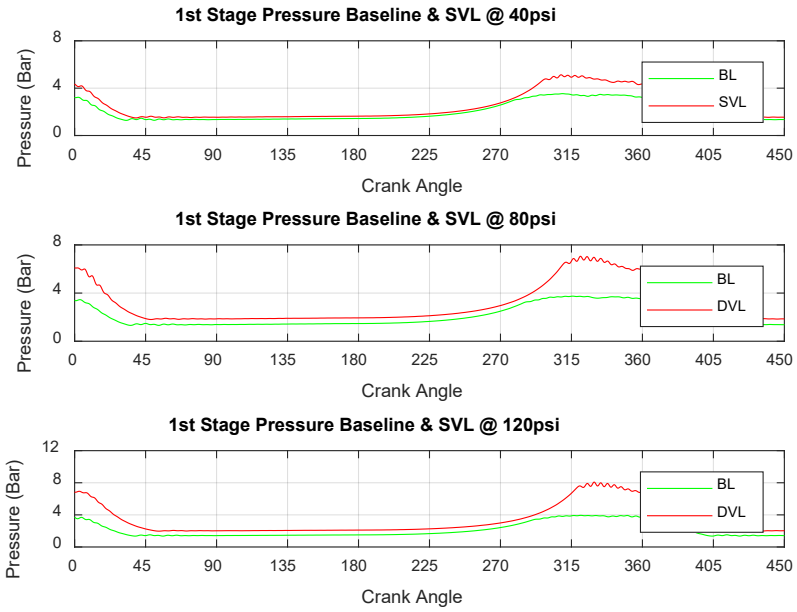

Figure 4-28 Pressure Trace of 1st Stage Baseline with Suction Valve Leakage

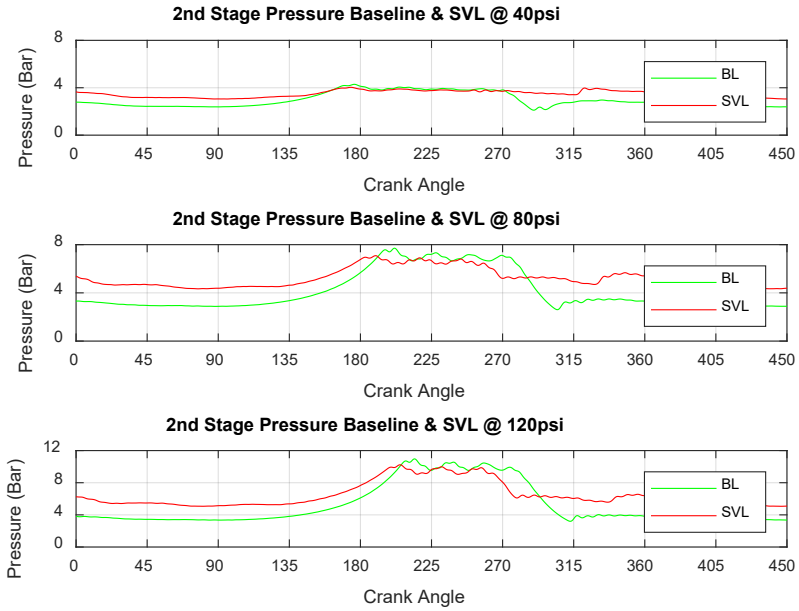

Figure 4-29 Pressure Trace of 2nd Stage Baseline with Suction Valve Leakage

From Figure 4-29 the 2nd stage, the pressure in between DVO and DVC is higher under 8 bar at 80psi and approximately 10 bar at 120 psi because more work is required to compress the cylinder when there is a faulty component.

4.7.5 Changes in Cylinder Pressures under Intercooler Leakage

From Figure 4-30 the 1st stage pressure from SVO and DVO until the DVC, the baseline is nearly the same as the faulty intercooler pipe and the pressure at 120 psi is slightly higher at SVO, just under 4 bar.

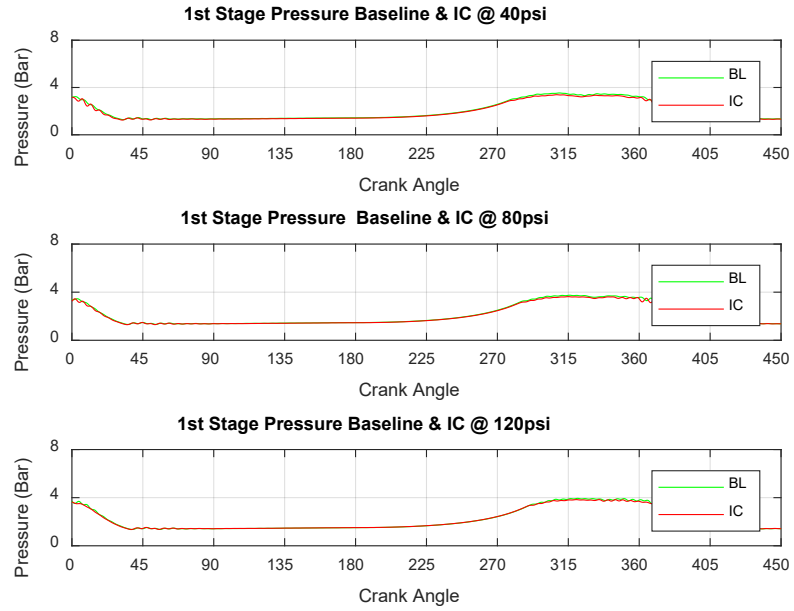

Figure 4-30 Pressure Trace of 1st Stage Baseline with Intercooler Leakage

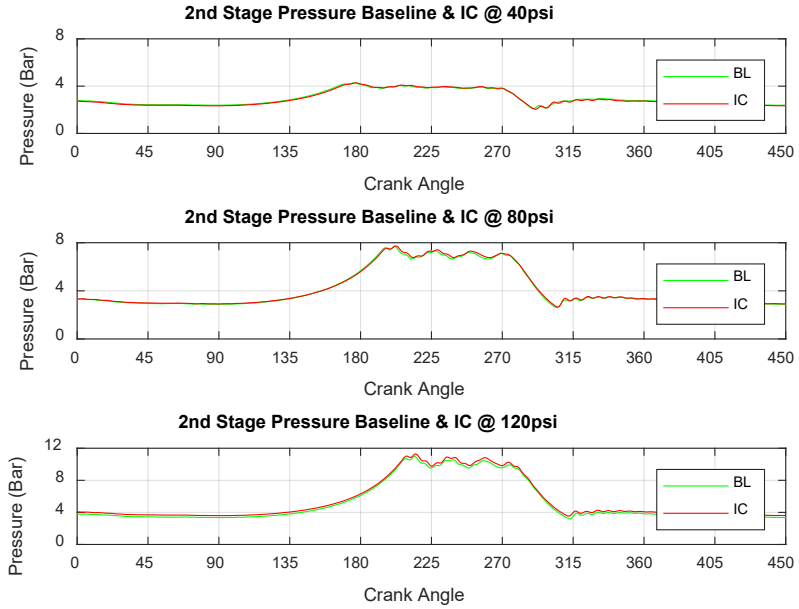

Figure 4-31 Pressure Trace of 2nd Stage Baseline with Intercooler Leakage

From Figure 4-31, the 2nd stage baseline pressure is slightly lower than the seeded fault under all three conditions. Between DVO and DVC, it is higher under 8 bar at 80psi and approximately 11.5 bar at 120 psi because more work is required when there is a loose pipe.

4.7.6 Changes in Cylinder Pressures under Loose Transmission Belt

Figure 4-4 gives an overview of the test procedure whereas Figure 4-32 and Figure 4-33 illustrates the trends of the healthy cylinder pressures with the introduction of a 5mm misaligned faulty belt on the 1st and 2nd stage-discharge valve.

4.7.7 Performance Characteristics of both the First and Second Stage with Loose Belt Transmission Pressure Trace

It can be seen from Figure 4-32 the 1st stage from SVO and DVO until the DVC, the baseline is virtually the same as the loose belt and the pressure at 120 psi is slightly higher at SVO just under 4 bar.

Figure 4-33 shows the baseline pressure of the 2nd stage is negligible in comparison to the seeded fault at 40 and 80 psi. Between DVO and DVC the pressure is higher under 8 bar at 80psi and approximately 11 bar at 120 psi because more work is required to compress the cylinder when there is a loose pipe.

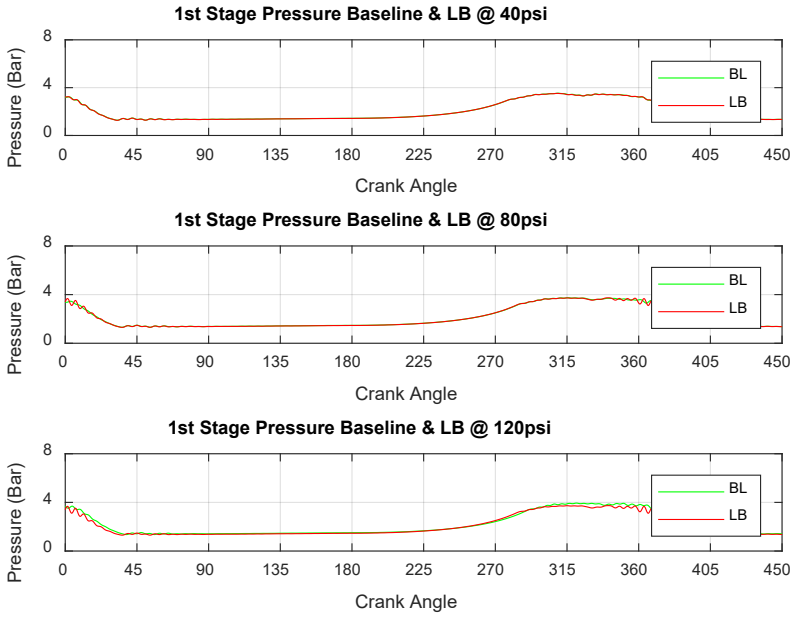

Figure 4-32 Pressure Trace of 1st Stage Baseline with Loose Belt Leakage

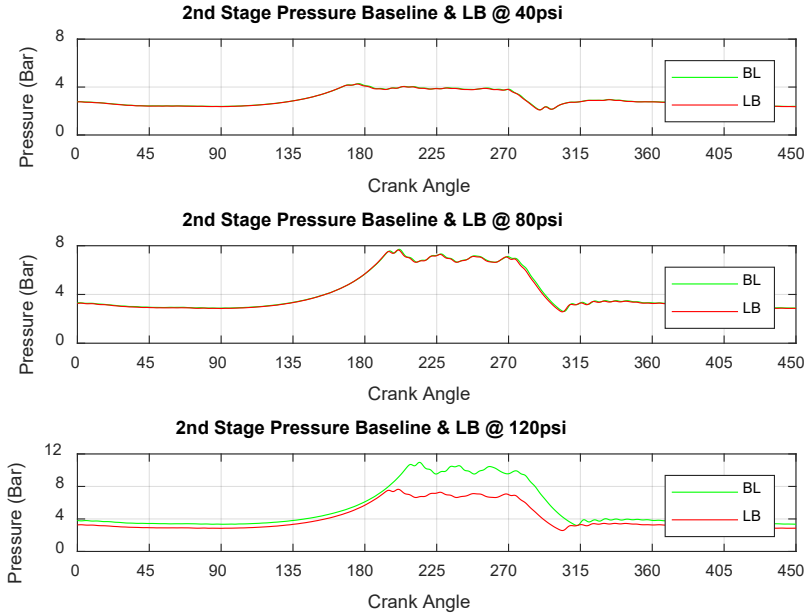

Figure 4-33 Pressure Trace of 2nd Stage Baseline with Loose Belt Leakage

4.8 Discussion

Overall, the discharge valve leakage in the second stage causes the pressure profile of the first stage to be slightly higher in the period of the suction process but higher for the discharge. This is due to the increased discharge pressure induced by the backflow of the leakage. Meanwhile, the pressure profile of the second stage shows a clear advance but with insignificant increases in amplitudes compared with the baseline.

For the suction valve leakage in the second stage, the pressure profile of the first stage is significantly higher for the entire operating cycle. This is because of the significantly increased discharge pressure induced by the increase in backflow from the leakage. Meanwhile, the pressure profile of the second stage shows a clear advance and increase during the suction process but with insignificant increases in amplitudes during the discharge process compared with the baseline.

For the leaky intercooler, the pressure profile of the first stage is slightly lower for the entire operating cycle, this is caused by a small leakage flow. On the other hand, because the leakage is very small, it causes invisible changes to the pressures in the second stages.

For the loose transmission belt, the pressure profile of the first stage under higher load is slightly lower for the entire operating cycle, this is also caused by a smaller leakage flow. On

the other hand, because the leakage is very small, it causes invisible changes to the pressures in the second stages of the suction process and significant changes in the discharge process.

Each case shows that less work is required in the suction stage whereas in the second stage (compression cycle) more work is needed and that the pressure oscillates higher at the discharge pressure.

4.9 Reciprocating Compressor Condition Monitoring Based on Common Non-Intrusive Measurements

This section focusses on different condition monitoring techniques including vibration-based Condition Monitoring (CM), Instantaneous Angular Speed (IAS), Current waveform, Root Mean Square (RMS) Envelope, Current Spectrum analysis in comparison for four common fault cases: Discharge Valve Leakage (DVL), Suction Valve Leakage (SVL), Intercooler Leakage (IL) and Loose Transmission Belt. Through this study, the behaviours of pressure, vibration and current differences of these faults can be identified as the basis for fault detection and diagnosis. To show the effects of each fault on the compressor, in-cylinder pressures are presented together with the vibration and electrical signals. Because compressors operate under different discharge pressures, the investigation is made up of three typical operating pressures: (40 psi) 2.8 bar, (80 psi) 5.5 bar and (120psi) 8.3 bar respectively under each fault to explore the changes and monitoring performance.

4.9.1 Vibration-Based Condition Monitoring

4.9.1.1 Vibration-Based Condition Monitoring of Discharge Valve Leakage

Discharge Valve Leakage Vibration at 2.8 Bar

As shown in Figure 4-34, a leaking discharge valve causes the change of vibration in the 1st stage to be negligible in the period from 0º of the TDC to about 30º of the SVO of the crank angle in the 1st stage cylinder. Following that sequence, the discharge valve leakage vibration signal is at its peak at about 60º of the crank angle but slightly lower than the baseline. In between the BDC and SVC of the cylinder from 135 º to 180 º, the vibration's signal is minimal. At about 285º of the DVO of the cylinder, the discharge valve leaking vibration signal is nearly equal to the baseline but slightly higher than at the BDC of the cylinder. Finally, at TDC and DVC, the leaking discharge valve vibration signal is about five times higher than the vibration signal at the DVO of the cylinder and is equal to the baseline.

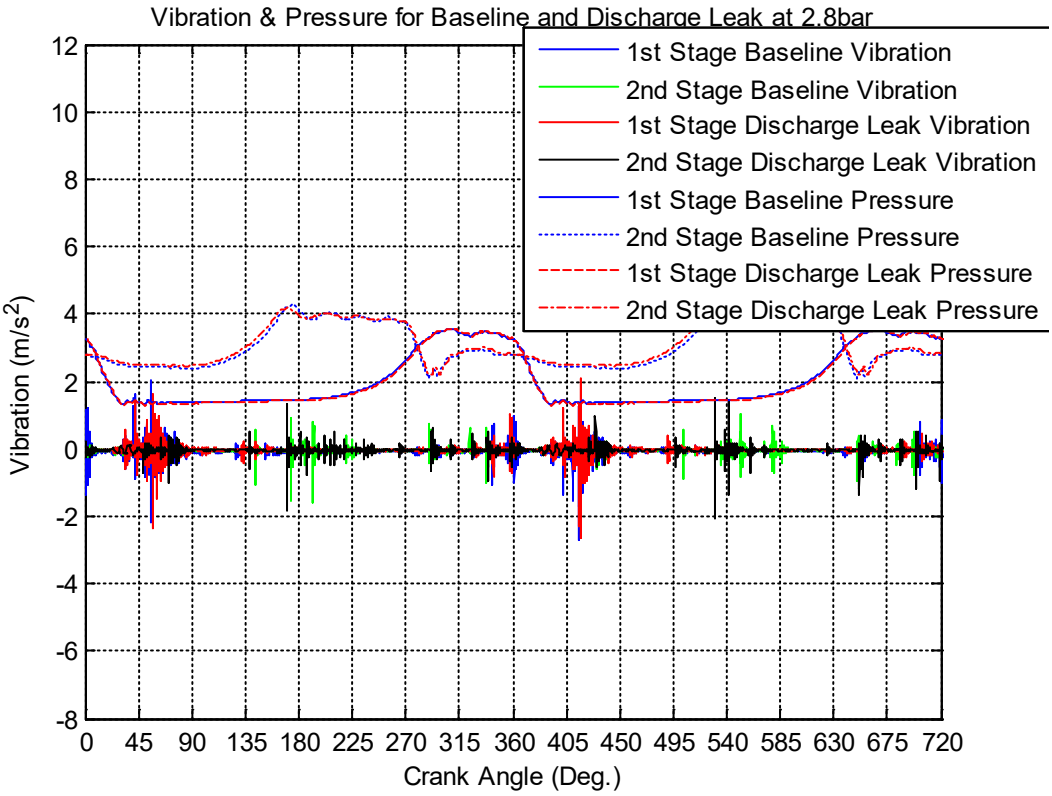

Figure 4-34 Discharge Valve Leakage Induced Pressure and Vibration at 2.8 Bar

The vibration signal of the 2nd stage, under the discharge valve leak in the compression process from 0º to 135º of the crank angle, is negligible. At about 165ºof the crank angle at DVO the discharge valve leak is slightly higher than baseline. Following that sequence at the TDC and SVC of the second stage cylinder, there is no vibration. Finally, at the SVO of the cylinder at about 290º of the crank angle, the discharge valve leak vibration signal is half of that at the DVO of the cylinder with the baseline equal.

Discharge Valve Leakage Vibration at 5.5 Bar

As shown in Figure 4-35, a leaking discharge valve causes the change of vibration in the 1st stage to be higher from the TDC of the cylinder at 0º to the full revolution of the crank angle. The only time where the leaking discharge valve is at its peak is at approximately 60 º just after the SVO and at the DVC and TDC of the cylinder where it is slightly lower than the baseline signal.

The vibration signal of the 2nd stage, under the discharge valve leak in the compression process from 0º to 180º of the crank angle, occurs at about 60º, just after the BDC and the SVC of the 2nd stage cylinder at about 190º of the crank angle at DVO of the cylinder discharge valve leak. Following that sequence at the TDC and DVC of the second stage cylinder, at about 270º of

the crank angle, the leaking discharge valve signal is lower than the baseline by half of its magnitude. Finally, at the SVO of the cylinder, at about 300º of the crank angle, the discharge valve leak vibration is minimal and higher than the baseline.

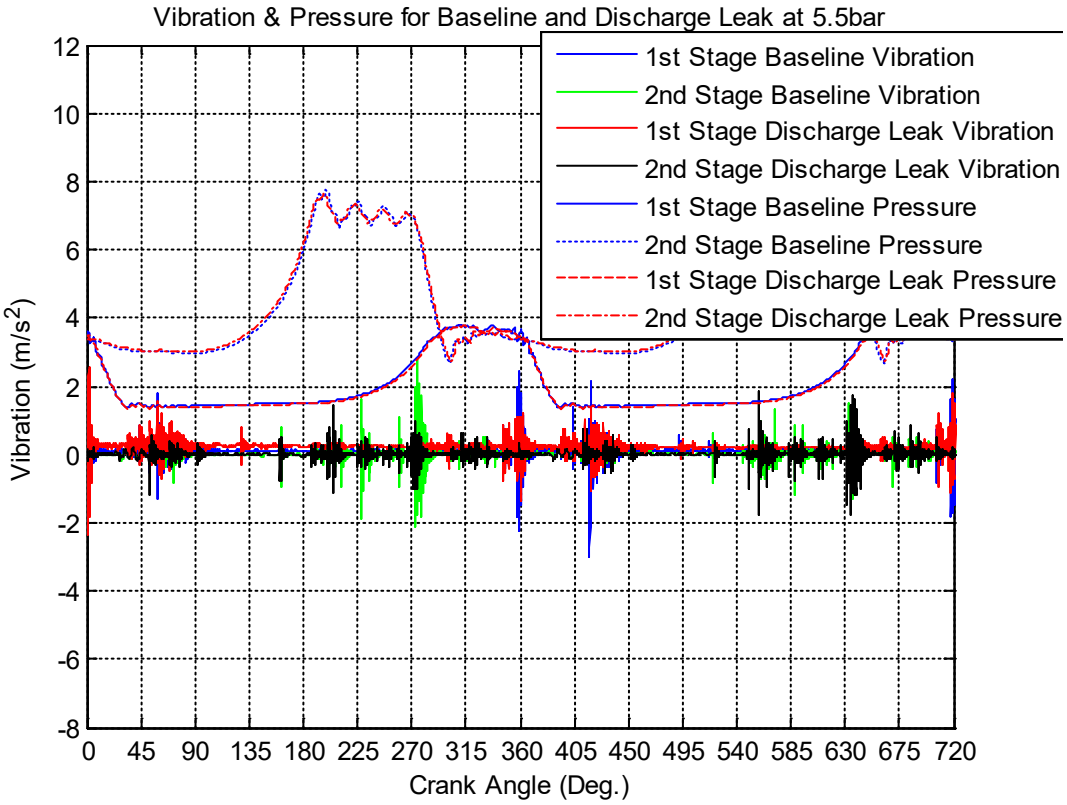

Figure 4-35 Discharge Valve Leakage Induced Pressure and Vibration at 5.5 Bar

Discharge Valve Leakage Vibration at 8.3 Bar

As presented in Figure 4-36, a leaking discharge valve causes the change of vibration in the 1st stage to be higher at the TDC of the 1st stage cylinder, reducing by 10º after the crank angle and rising again just after the SVO of the cylinder for about 60º and then reducing from about 90º of the crank angle which is at about the BDC and the SVC of the cylinder, until its full cycle at 360º of the crank angle at DVC and TDC where the discharge valve leak is at its peak and slightly lower.

The vibration signal of the 2nd stage, under the discharge valve leak in the compression process from 0º to 185º of the crank angle, occurs at about 75º just after the BDC and the SVC of the 2nd stage cylinder at about 200º of the crank angle at DVO of the cylinder, the discharge valve leak manifests again slightly lower than the baseline. Following that sequence at the TDC and DVC of the second stage cylinder, at about 270º of the crank angle, the leaking discharge valve

signal is lower than the baseline by half of its magnitude. Finally, at the SVO of the cylinder at about 310º of the crank angle, the discharge valve leak vibration is equal to the baseline and slightly higher than the 5.5 bar discharge leak valve signal from the previous figure.

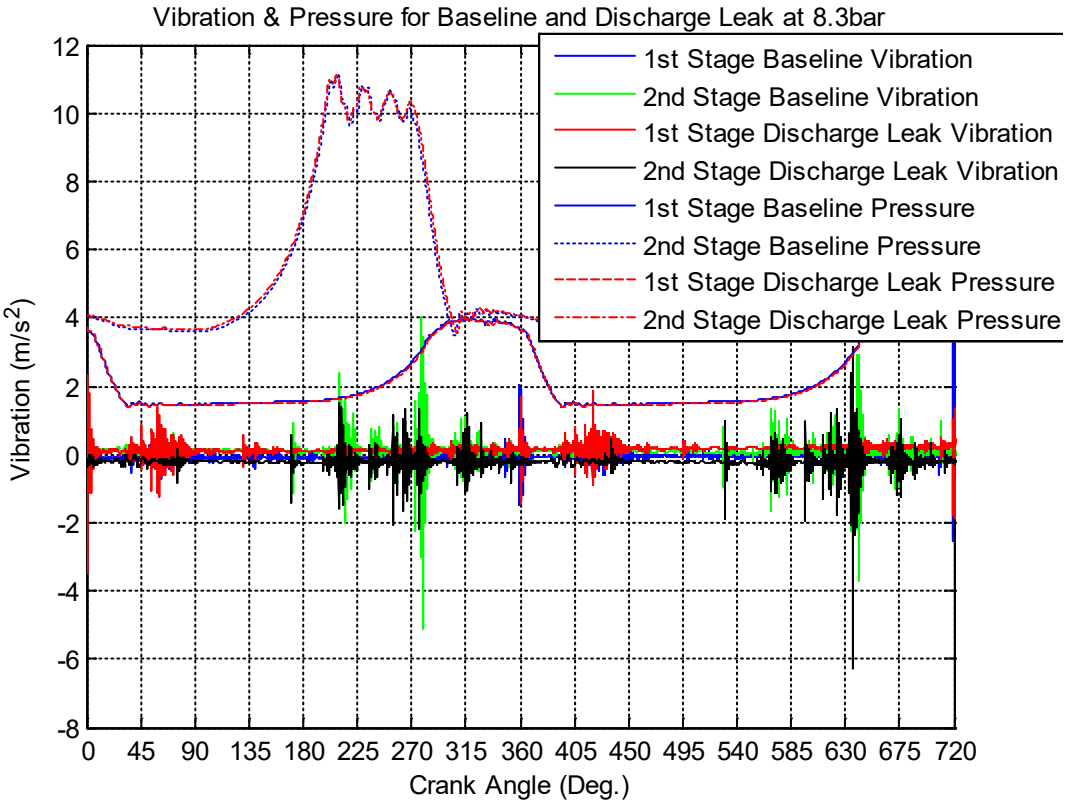

Figure 4-36 Discharge Valve Leakage Induced Pressure and Vibration at 8.3 Bar

4.9.1.2 Vibration-Based Condition Monitoring of Suction Valve Leakage

Suction Valve Leakage Vibration at 2.8 Bar

As illustrated in Figure 4-37, a leaking suction valve causes the change of vibration in the 1st stage to be at its peak at the TDC of the 1st stage cylinder, then after that process at about 60º. Just after the SVO of the cylinder, the signal is half the size of the signal at TDC and lower than the baseline signal. From the BDC and SVC of the cylinder to the full revolution, the suction valve leak is slightly higher but very minimal.

The vibration signal of the 2nd stage, under the suction valve leak in the compression process from 0º to 135º of the crank angle, is slightly higher but very minimal. At about 145º of the crank angle, just before the DVO, the suction valve leak is at its peak.

Following that sequence, the suction valve leak signal is randomly slightly lower to the baseline just after the SVO of the cylinder, at about 325º of the crank angle until the full revolution.

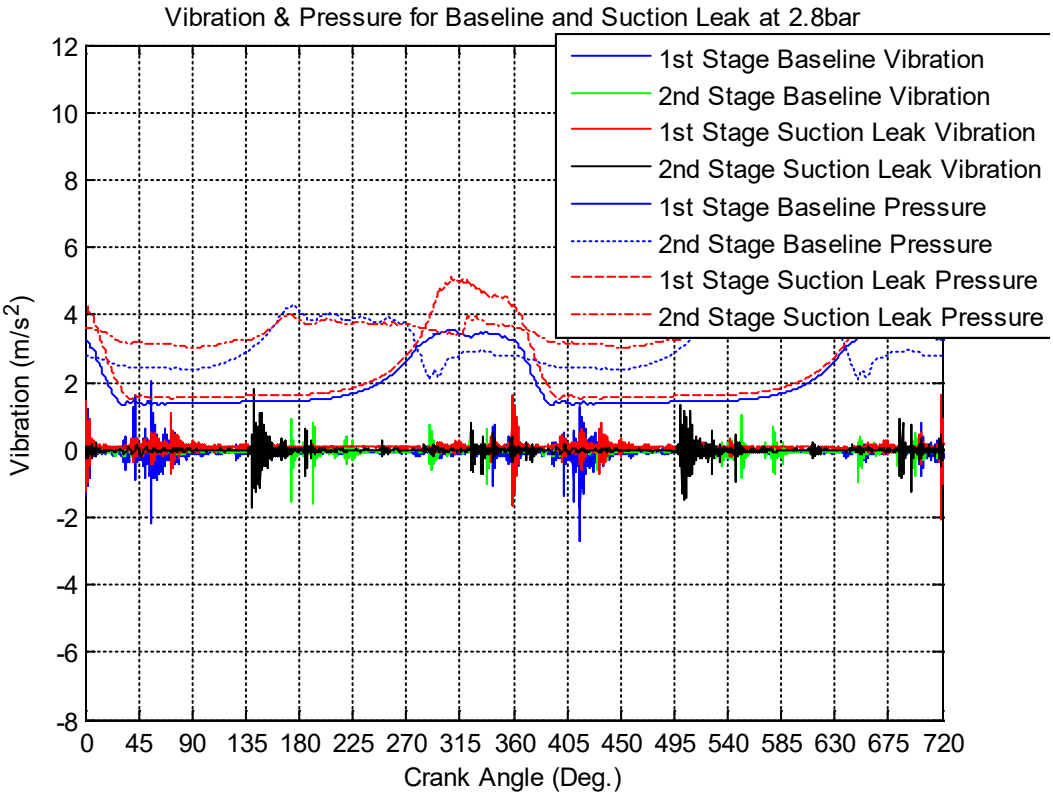

Figure 4-37 Suction Valve Leakage Induced Pressure and Vibration at 2.8 Bar

Suction Valve Leakage Vibration at 5.5 Bar

As shown in Figure 4-38 a leaking suction valve causes the change of vibration in the 1st stage to be at its peak at the TDC of the 1st stage cylinder then after that process, at about 60º, just after the SVO of the cylinder, the signal is below the baseline. From the BDC and SVC of the cylinder to the full revolution the suction valve leak is slightly higher but very minimal.

The vibration signal of the 2nd stage, under the suction valve leak in the compression process, from 0º to 130º of the crank angle, is slightly higher but very minimal. At about 130º of the crank angle, just after the BDC and SVC of the cylinder, the suction valve leak increases its magnitude slightly and goes to its peak at the DVO of the cylinder at about 200º of the crank angle. After that sequence, the vibration signal is up to the full revolution.

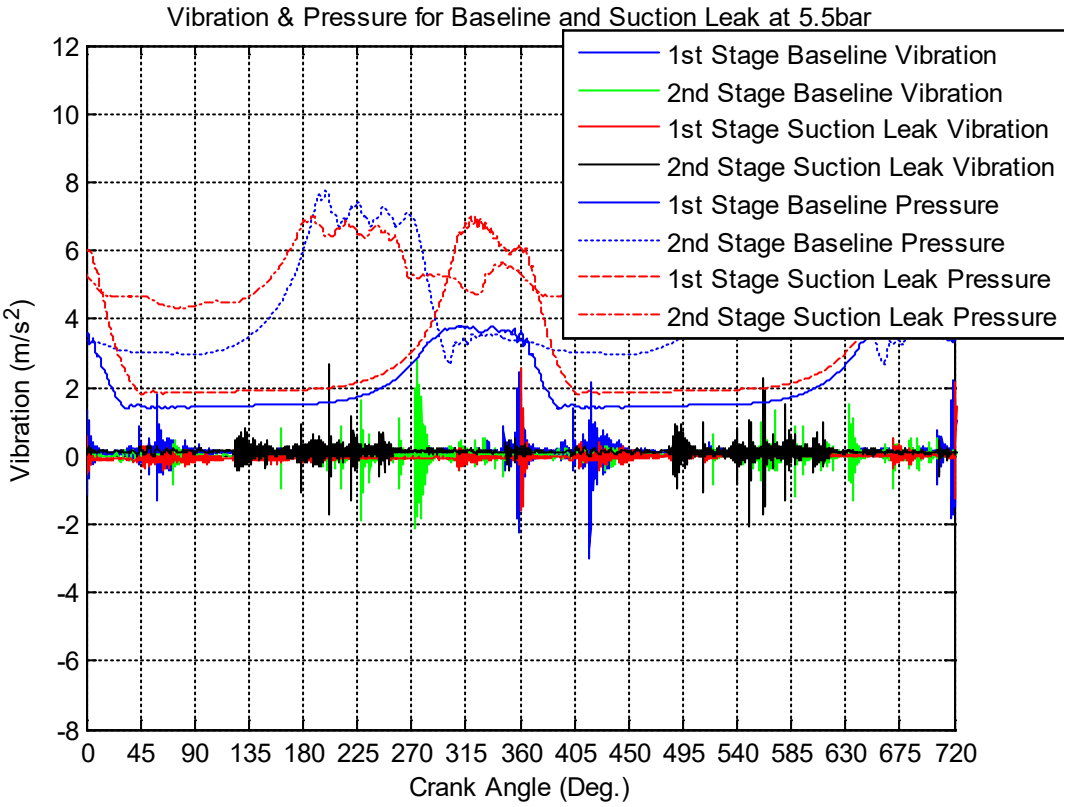

Figure 4-38 Suction Valve Leakage Induced Pressure and Vibration at 5.5 Bar

Suction Valve Leakage Vibration at 8.3 Bar

As shown in Figure 4-39, a leaking suction valve causes the change of vibration in the 1st stage to be at its peak at the TDC of the 1st stage cylinder then after that process, at about 55º just after the SVO of the cylinder, the vibration signal is minimal and approximately the same to the baseline signal in the rest of the cycle

The vibration signal of the 2nd stage under the suction valve leak in the compression process, from 0º of the TDC to 125º of the crank angle, is slightly lower but very minimal. At about 126º of the crank angle, just after the BDC and SVC of the cylinder, the suction valve leak increases its magnitude slightly and goes to its peak after the DVO of the cylinder is at about 210º of the crank angle, then goes slightly lower at 260º at the DVC and TDC of the cylinder and finally the suction valve leak signal goes down until the cycle is completed.

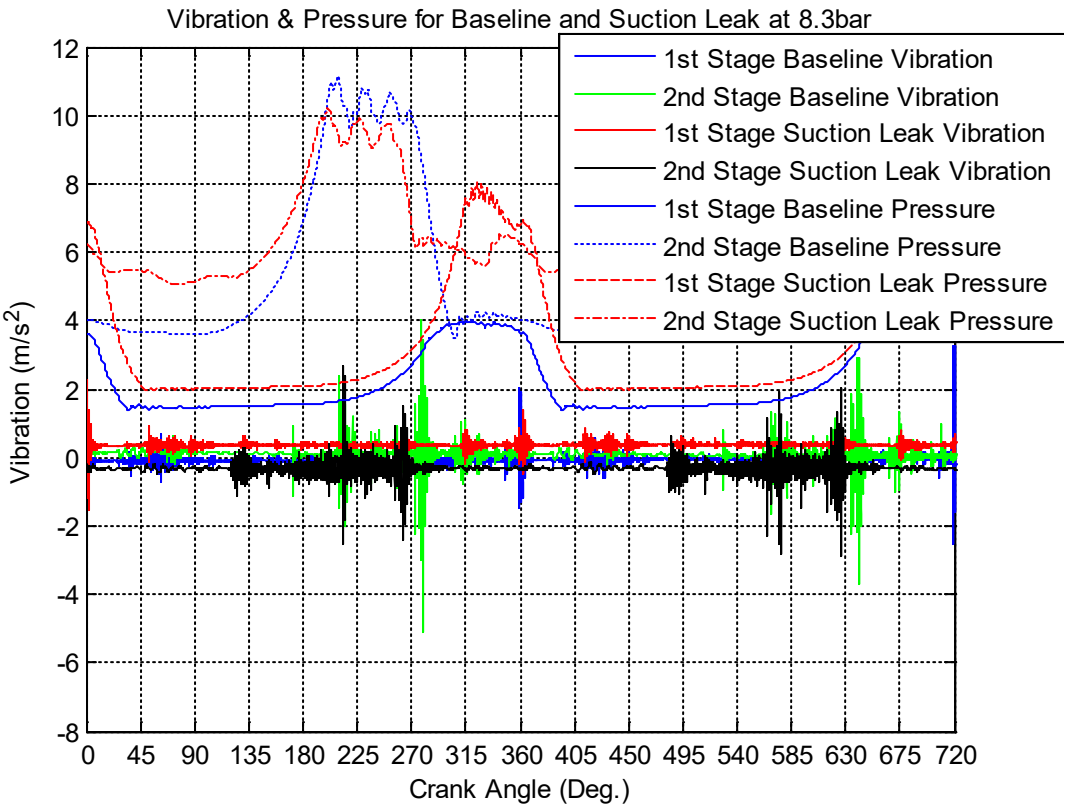

Figure 4-39 Suction Valve Leakage Induced Pressure and Vibration at 8.3 Bar

4.9.1.3 Vibration-Based Condition Monitoring of Intercooler Leakage

Intercooler Leakage Vibration at 2.8 bar

Figure 4-40 shows a leaking intercooler vibration in the 1st stage to be constant from the TDC of the cylinder until its full cycle without any variation. Whereas the baseline vibration signal is at its peak at about 50º of the crank angle.

The vibration signal of the 2nd stage, under the intercooler leak in the compression process from 0º of the TDC to 140º of the crank angle before the DVO, is nearly constant with minimal variation.

At about 178º of the crank angle at the DVO, the intercooler leak is at its peak. Following that sequence, the intercooler leak signal increases randomly but minimal, to its full cycle.

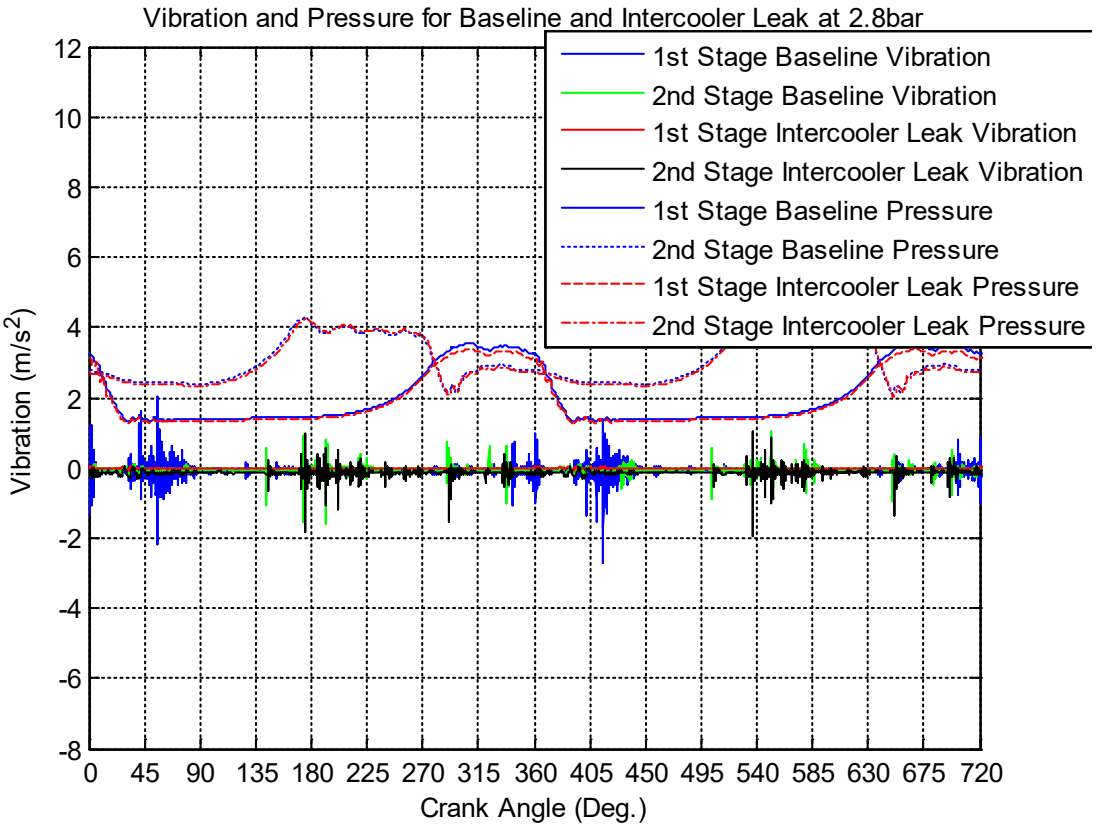

Figure 4-40 Intercooler Leakage Induced Pressure and Vibration at 2.8 Bar

Intercooler Leakage Vibration at 5.5 Bar

From the Figure 4-41 Intercooler Leakage Induced Pressure and Vibration at 5.5 Bar the leaking intercooler causes the change of vibration at the 1st stage to be constant from the TDC of the cylinder until its full cycle, without any variation. Whereas the intercooler leak vibration signal is at its peak at about 272º of the crank angle and slightly lower than the baseline.

The vibration signal of the 2nd stage, under the intercooler leak in the compression process, from 0º of the TDC to 160º of the crank angle just after the BDC and SVC, is nearly constant with minimal variation. At about 200º of the crank angle at the DVO, the intercooler leak is high. Following that sequence, the intercooler leak signal increases randomly until at the DVC where the vibration signal is at its peak and then reduces randomly and progressively to its full cycle.

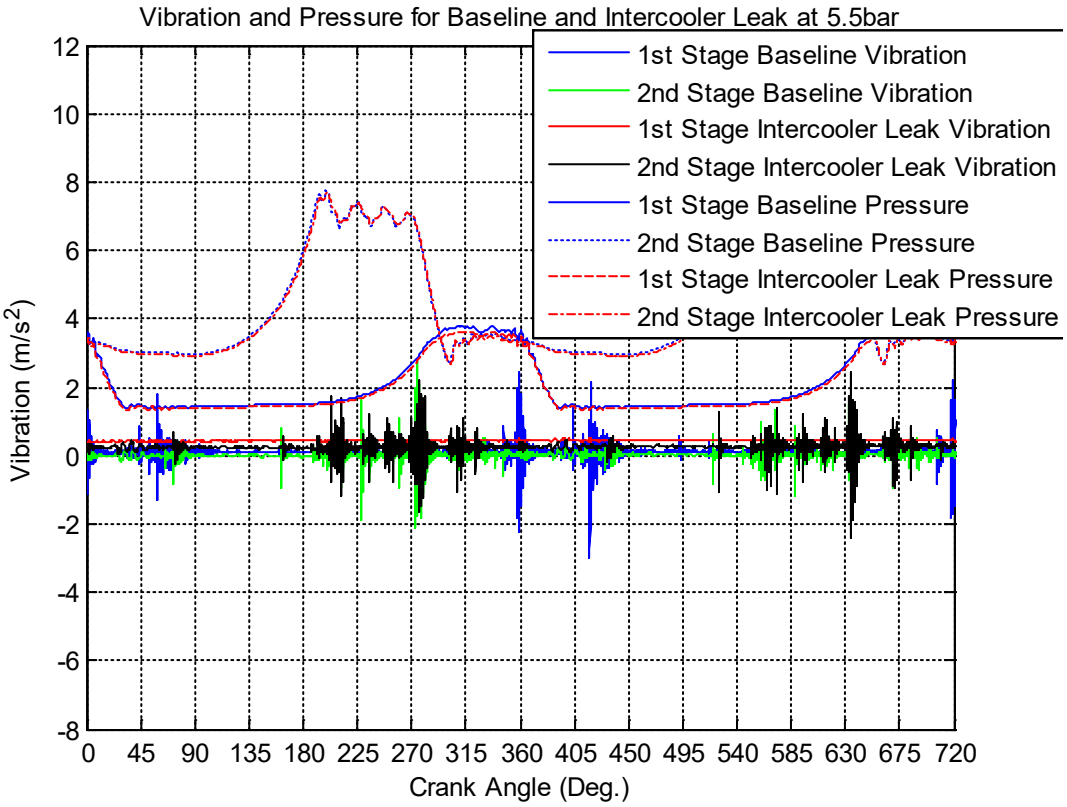

Figure 4-41 Intercooler Leakage Induced Pressure and Vibration at 5.5 Bar

Intercooler Leakage Vibration at 8.3 Bar

As can be seen from Figure 4-42 Intercooler Leakage Induced Pressure and Vibration at 8.3 Bar, the leaking intercooler causes the change of vibration at the 1st stage to be slightly higher at the TDC, 0º of the crank angle then is at its peak about 60º after the SVO. Following that sequence, the leaking intercooler vibration signal is minimal with very little vibration to the end of its cycle.

The vibration signal of the 2nd stage, under the intercooler leakage in the compression process, from 0º of the TDC to 178º of the crank angle just after the BDC, SVC is nearly constant with minimal variation. At about 179º of the crank angle before the DVO, the intercooler leak is high. Following that sequence, the intercooler leak signal increases randomly until at the DVC where the vibration signal is at its peak and then reduces randomly and progressively to its full cycle.

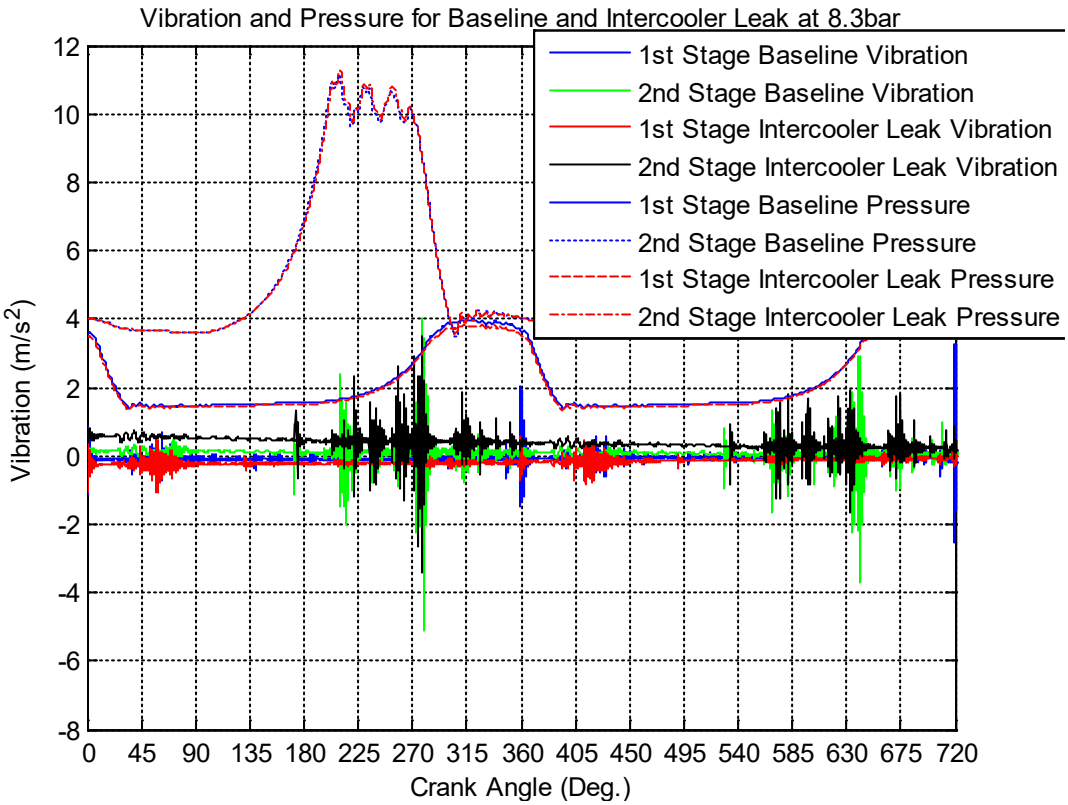

Figure 4-42 Intercooler Leakage Induced Pressure and Vibration at 8.3 Bar

4.9.1.4 Vibration-Based Condition Monitoring of Loose Belt

Loose Belt Vibration at 2.8 Bar

As shown in Figure 4-43 Loose Belt Induced Pressure and Vibration at 2.8 Bar causes the change of vibration at the 1st stage to be higher from the TDC of the cylinder at 0º to the full revolution of the crank angle. The only place where the loose belt is at its peak is at approximately 60º just after the SVO and at the DVC and TDC of the cylinder where it is slightly lower.

The vibration signal of the 2nd stage, under the loose belt in the compression process, from 0º to 145º of the crank angle is negligible. At about 146º of the crank angle, just before the DVO, the loose belt is slightly higher. Following that sequence after the DVO, at about 185º of the crank angle it is slightly higher and is at its peak at the DVC at 270º of the crank angle.

Subsequently, after that sequence, the intercooler leakage signal decreases progressively to its full cycle.

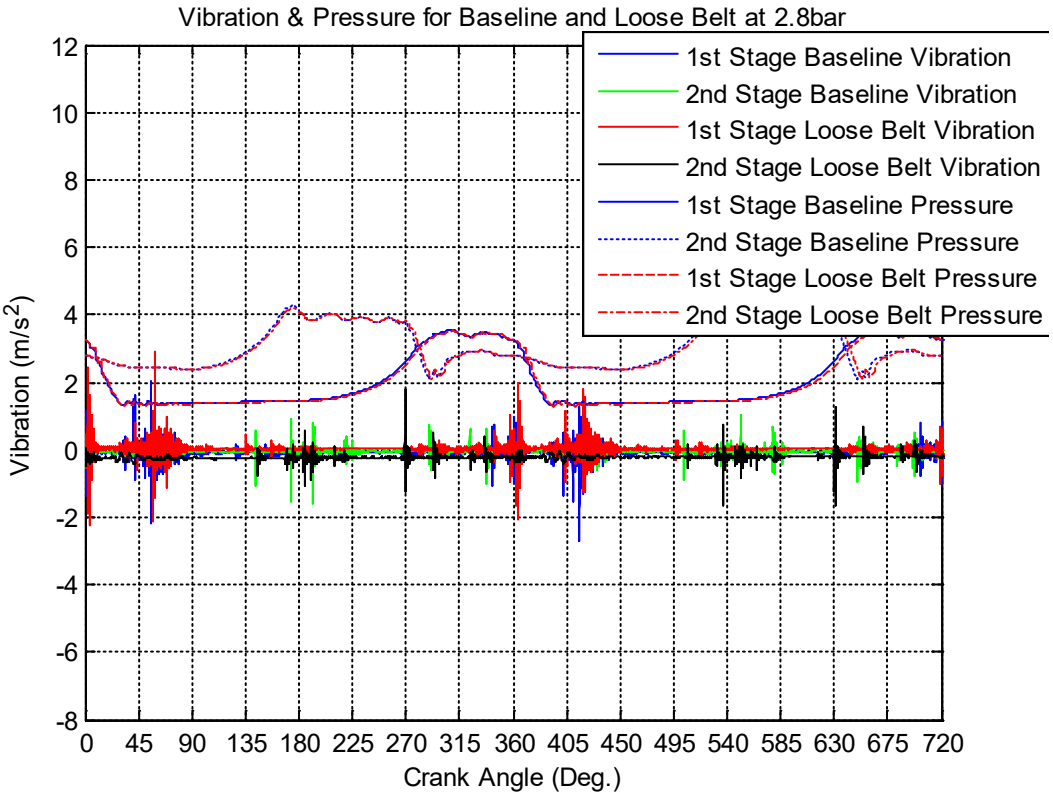

Figure 4-43 Loose Belt Induced Pressure and Vibration at 2.8 Bar

Loose Belt Vibration at 5.5 Bar

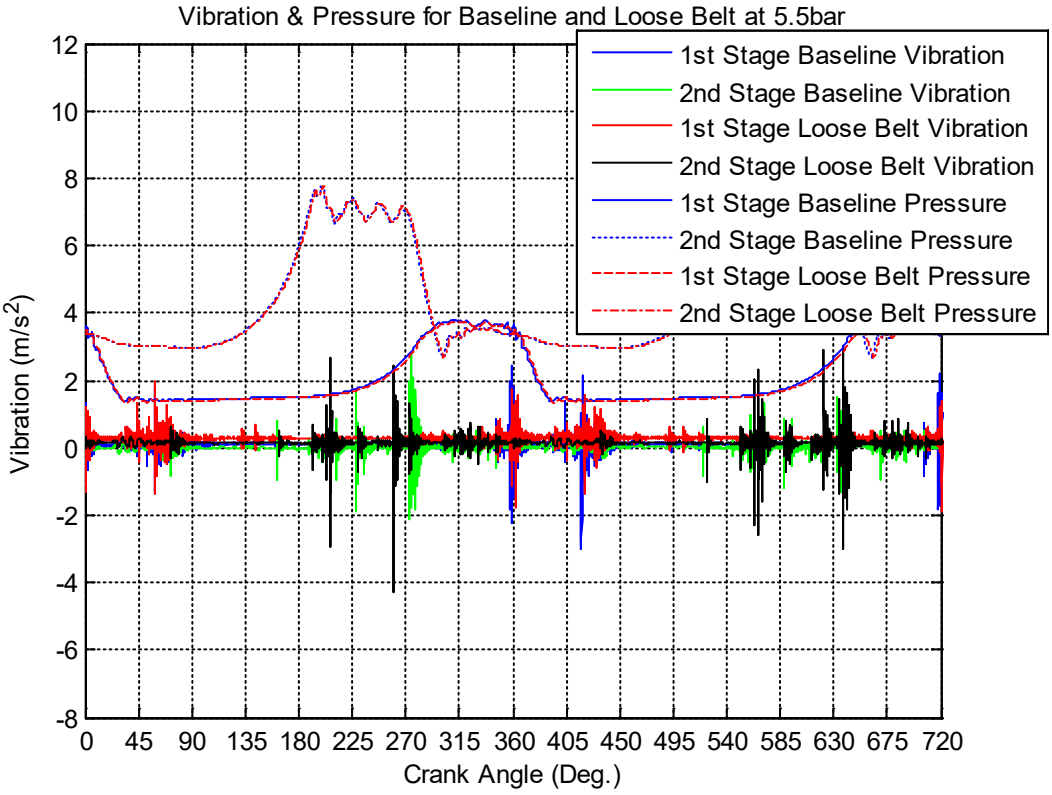

Figure 4-44 Loose Belt Induced Pressure and Vibration at 5.5 Bar

As shown from Figure 4-44 Loose Belt Induced Pressure and Vibration at 5.5 Bar, a loose belt causes the change of vibration at the 1st stage to be higher from the TDC of the cylinder at 0º to the full revolution of the crank angle. The only place where the loose belt is at its peak is at approximately 60º just after the SVO and at the DVC and TDC of the cylinder where it is slightly lower.

The vibration signal of the 2nd stage, under the loose belt in the compression process from 0º of the TDC to 70º of the crank angle, just after the SVO, is minimal and has slight variation until after the SVO where the vibration signal is slightly higher. Following that sequence, from 75º to the DVO at about 205º of the crank angle, the vibration signal is minimal and constant. The loose belt vibration signal is at its peak at about 206º and 265º just before the DVC. Following that sequence, the loose belt signal decreases randomly until at the DVC and then reduces randomly and progressively to its full cycle.

Loose Belt Vibration at 8.3 Bar

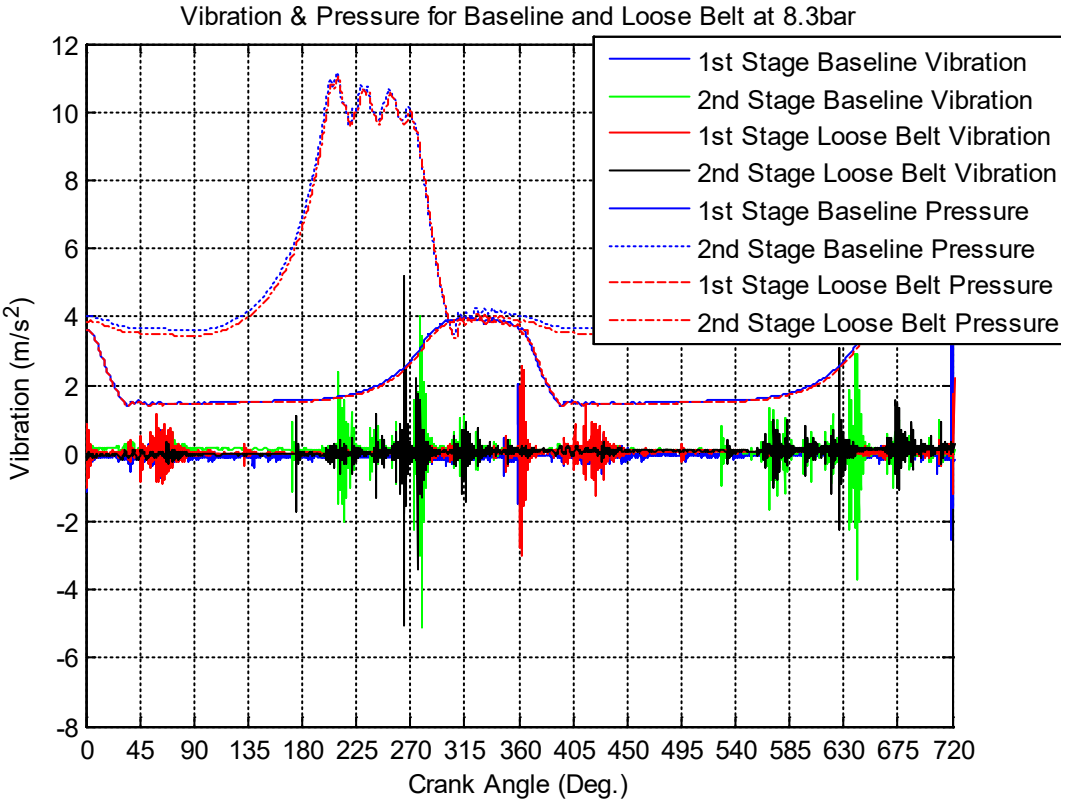

Figure 4-45 Loose Belt Induced Pressure and Vibration at 8.3 Bar

As shown from Figure 4-45 Loose Belt Induced Pressure and Vibration at 8.3 Bar, a loose belt causes the change of vibration at the 1st stage to be at its peak at the TDC of the cylinder at 0º to the full revolution of the crank angle. Following that sequence, just after the SVO at

approximately 60º of the crank angle, the vibration signal has a slight increase and then goes constant with no variation and very minimal change to its full cycle.

The vibration signal of the 2nd stage, under the loose belt in the compression process, from 0º of the TDC to 70º of the crank angle, just after the SVO, is minimal and has a slight variation until after the SVO where the vibration signal is slightly higher. Following that sequence, it is at its peak just before the DVC and the loose belt vibration signal decreases randomly to its full cycle.

4.9.2 Discussion

For the discharge valve leakage of the second stage, the vibration profile of the first stage is slightly lower for the entire operating cycle. This is because the slight decrease in discharge valve vibration is induced by a lesser backflow of the leakage. Meanwhile, the vibration profile of the second stage shows a clear picture of more vibration activities and increases progressively with a significant vibration increase in amplitudes during the discharge process, compared with the baseline under higher load.

For the suction valve leakage at the first stage, the vibration profile is insignificant for the entire operating suction cycle, this is because of the significantly increased suction pressure induced by the more backflow of the leakage. Meanwhile, the vibration profile of the second stage shows a minimal increase during the suction process but with higher increases in amplitudes during the discharge process, compared with the baseline.

For the leaking intercooler, the vibration profile of the first stage is slightly higher at the suction process operating cycle under higher load, this is caused by small leakage flows. Alternatively, the changes of vibration are significantly higher during the expansion process between the suction valve closing and discharge valve opening in the second stages.

For the loose transmission belt, the vibration profile of the first stage, under higher load, is lower for the entire operating cycle with more activities at the suction process, this is caused by a small leakage flow. On the other hand, the changes in vibration are significantly higher during the discharge valve process in the second stages.

Each case shows that less work is required in the suction stage whereas in the second stage (compression cycle) more work is needed and that the pressure oscillates higher at the discharge pressure.

4.10 Motor Current Signature Analysis Based Condition Monitoring

This section compares the motor current signature analysis of four compressor faults: discharge valve leakage, suction valve leakage, intercooler leakage and belt looseness. Through this comparison, the behaviours and differences of electric current signals between these faults, in comparison from the baseline (healthy compressor), can be identified as the basis for fault detection and diagnosis.

To show the effects of each fault on the compressor, in-cylinder pressures are presented together with the electric signals. This presentation also allows the changes in current waveforms to be explored in line with pressure changes.

Because compressors operate under different discharge pressures, the comparison is made at three typical operating pressures: (40 psi) 2.8 bar, (80 psi) 5.5 bar and (120 psi) 8.3 bar respectively under each fault to explore the changes and monitor performance under discharge pressures.

4.10.1 MCSA based Condition Monitoring Discharge Valve Leakage

MCSA of Discharge Valve Leakage at 2.8 Bar

As shown in Figure 4-46, a leaking discharge valve causes the pressure at the 1st stage to be slightly lower than that of the baseline by about 0.1 bar in the period from 0º to 280º of the crank angle at a starting pressure of about 3.4 bar at 0º of the TDC. Following that sequence, the discharge valve leakage then remains roughly the same to the end of the cycle with both waveforms at their highest at about 3.5 bar.

The pressure waveform of 2nd stage, under the discharge valve leakage, the compression process is slightly higher than the baseline from 0º to 170º, by about 0.2 bar, whereas the discharge process in the period of 171º to 191º the baseline pressure increases by about 0.2 bar and then it remains the same in the rest of the cycle. From observation, it is clear that the pressure at the 2nd stage illustrates a slight increase, which means the compressor shifts away from its optimal operation and may work at lower efficiency.

Corresponding to this change, the power supply current shows no difference for the leaking discharge valve current signal. This amplitude current also shows that it needs the same current consumption whilst delivering the same quantity of air, confirming that the compressor uses the same power and hence lower efficiency. The amplitude of the current signal is at the highest

after the DVO of the 1st stage at a crank angle of about 310º and lowest at a crank angle of about 180º, with the leaking discharge valve signal slightly lower.

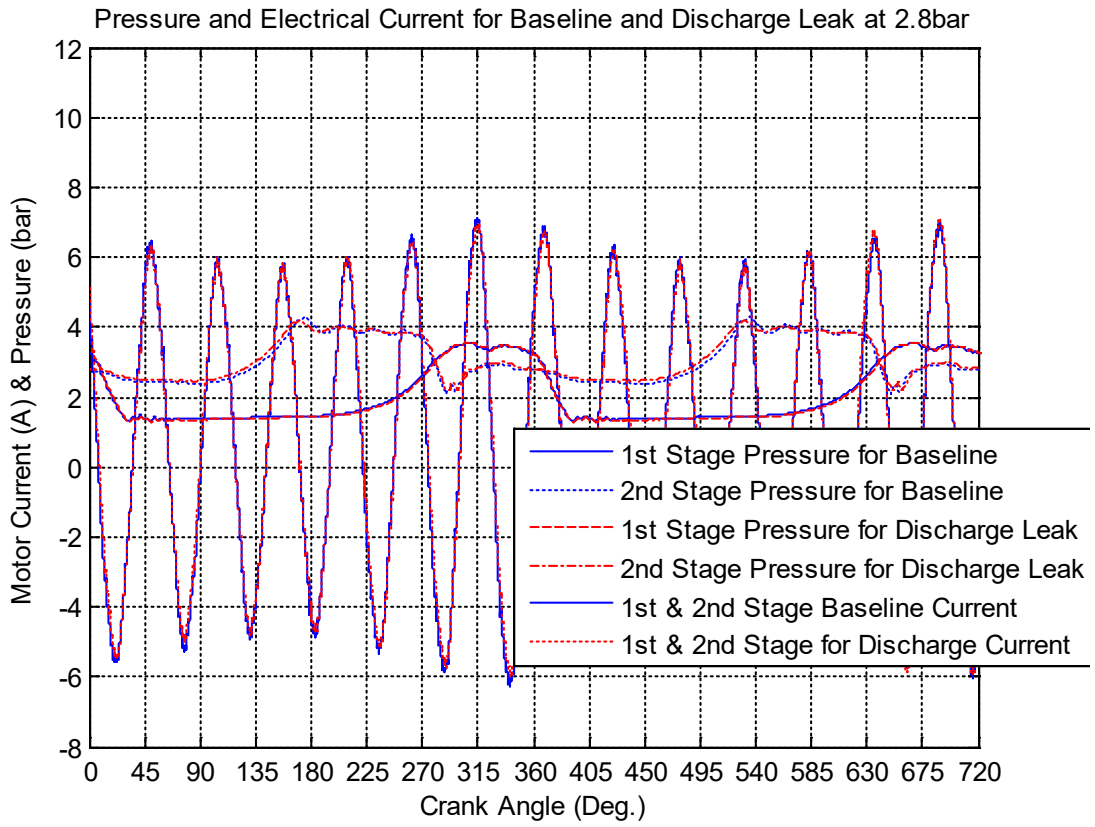

Figure 4-46 Current and Pressure Trace for Baseline and Discharge Valve Leak at 2.8 Bar

MCSA of Discharge Valve Leakage at 5.5 bar

As displayed in Figure 4-47, a leaking discharge valve causes the 1st stage pressure to be slightly lower than that of the baseline by about 0.1 bar in the period from 0º to 280º of the crank angle, at a starting pressure of about 3.5 bar at 0º of the TDC. Following that sequence, the discharge valve leakage then remains roughly the same to the end of the cycle with both waveforms at their highest at approximately 3.7 bar.

The pressure waveform of 2nd stage under the discharge valve leakage in the compression process, is visibly higher than the baseline from 0º to 195º, by about 0.1 bar and is at its peak at about 7.7 bar, whereas the discharge process in the period of 196º to 206º the baseline pressure increases by about 0.1 bar and then it remains roughly the same in the rest of the cycle. It is clear that the pressure at the 2nd stage shows a clear increase, which means the compressor shifts away from its optimal operation and works at a slightly higher efficiency.

Corresponding to this change the power supply current shows a slightly higher increase for the leaking discharge valve current signal. This slightly higher amplitude current also shows that it needs more current consumption whilst delivering a slightly higher quantity of air, confirming that the compressor uses more power and hence slightly higher efficiency.

The amplitude of the discharge current signal is at the highest after the DVO of the 1st stage at a crank angle of about 300º, phase-shifted leading the baseline by 5º and lowest at a crank angle of about 175º, with the discharge valve leakage current signal slightly lower and phase-shifted leading the baseline by 5º.

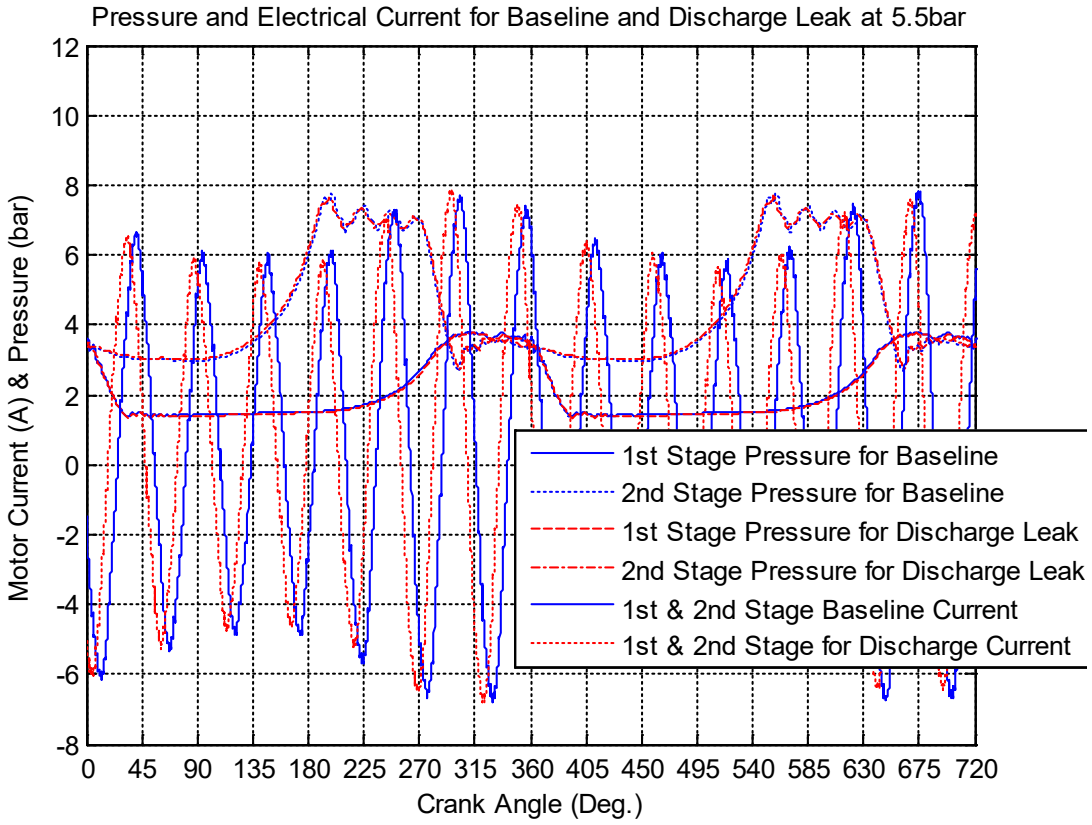

Figure 4-47 Current and Pressure Trace for Baseline and Discharge Valve Leak at 5.5 Bar

MCSA of Discharge Valve Leakage at 8.3 Bar

As presented in Figure 4-48, a leaking discharge valve causes the pressure at the 1st stage to be slightly lower than that of the baseline by about 0.1 bar in the period from 0º to 290º of the crank angle at a starting pressure of about 3.6 bar at 0º of the TDC. Following that sequence, the discharge valve leakage then remains roughly the same to the end of the cycle with both waveforms at their highest at about 3.9 bar.

The pressure waveform of 2nd stage under the discharge valve leakage in the compression process, is slightly higher than the baseline from 0º to 195º, by about 0.1 bar and is at its peak at about 11.2 bar, whereas the discharge process in the period of 196º to its full revolution, both the leaking discharge valve and baseline waveforms remain roughly the same in the rest of the cycle. From observation, it is clear that the 2nd stage pressure shows a clear increase, which means the compressor shifts away from its optimal operation and works at a higher efficiency.

Corresponding to this change the power supply current shows a slight increase for the leaking discharge valve current signal. This higher amplitude current also shows that it needs more current consumption whilst delivering a higher quantity of air, confirming that the compressor uses more power and hence higher efficiency.

The amplitude of the current signals is at the highest at DVO of the 1st stage at a crank angle of about 290º and lowest at a crank angle of about 160º with the discharge valve leakage current signal slightly lower.

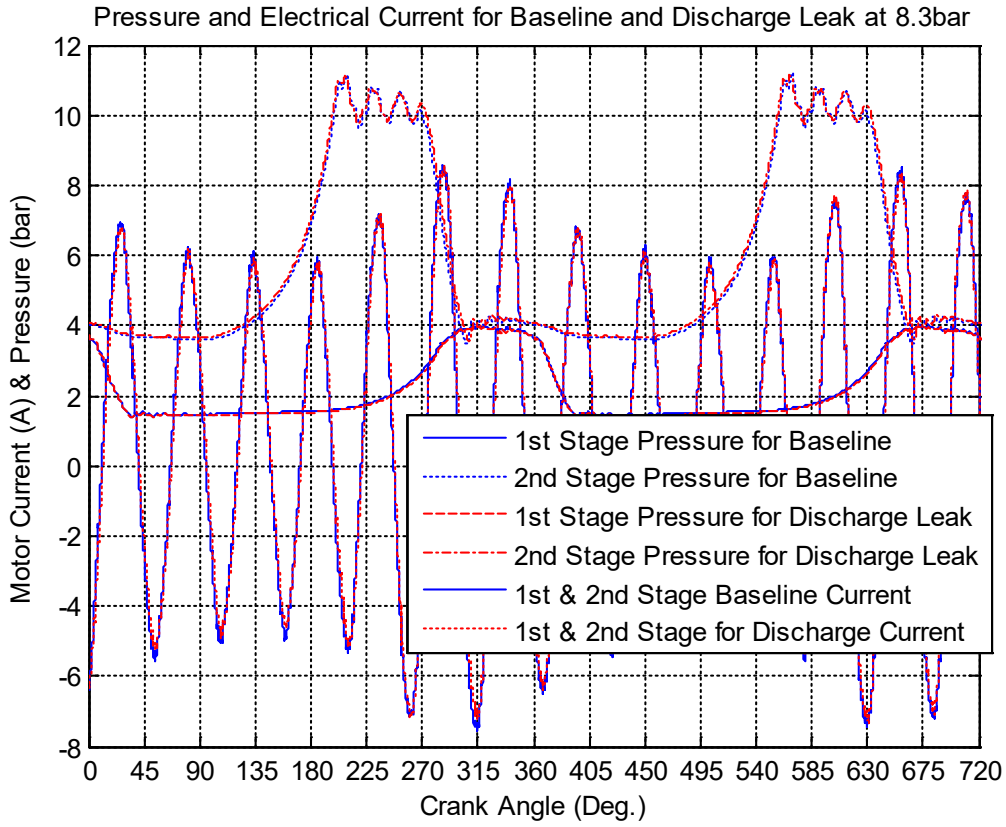

Figure 4-48 Current and Pressure Trace for Baseline and Discharge Valve Leak at 8.3 Bar

4.10.2 MCSA Based Condition Monitoring of Suction Valve Leakage

MCSA of Suction Valve Leakage at 2.8 bar

As illustrated in Figure 4-49, a leaking suction valve causes the 1st stage pressure to be higher than that of the baseline by about 0.8 bar at 0º of the TDC. The starting pressure of the leaking suction valve is 4.3 bar of the TDC which then converges with the baseline to approximately 30º of the crank angle, still slightly higher by about 0.3 bar in the period from 31º to 285º of the crank angle.

Following that sequence the suction valve leakage then climbs to its peak at about 5 bars at a difference of 1.5 bar higher than the baseline pressure signal then reduces to about 1 bar in the rest of the cycle. The pressure waveform of the 2nd stage under the suction valve leakage in the compression process is higher than the baseline from 0º to 155º, by about 0.8 bar. It is at its peak at 4 bars and lower than the baseline by about 0.4 bar at 170º, whereas the discharge process in the period of 180º to 270º of the crank angle, the leaking suction valve is lower than the baseline waveforms in the region of 0.3 bar and the leaking suction valve is higher by about 1 bar in the rest of the cycle. It is clear that the 2nd stage pressure shows a slight increase, which means the compressor shifts away from its optimal operation and may work at low efficiency.

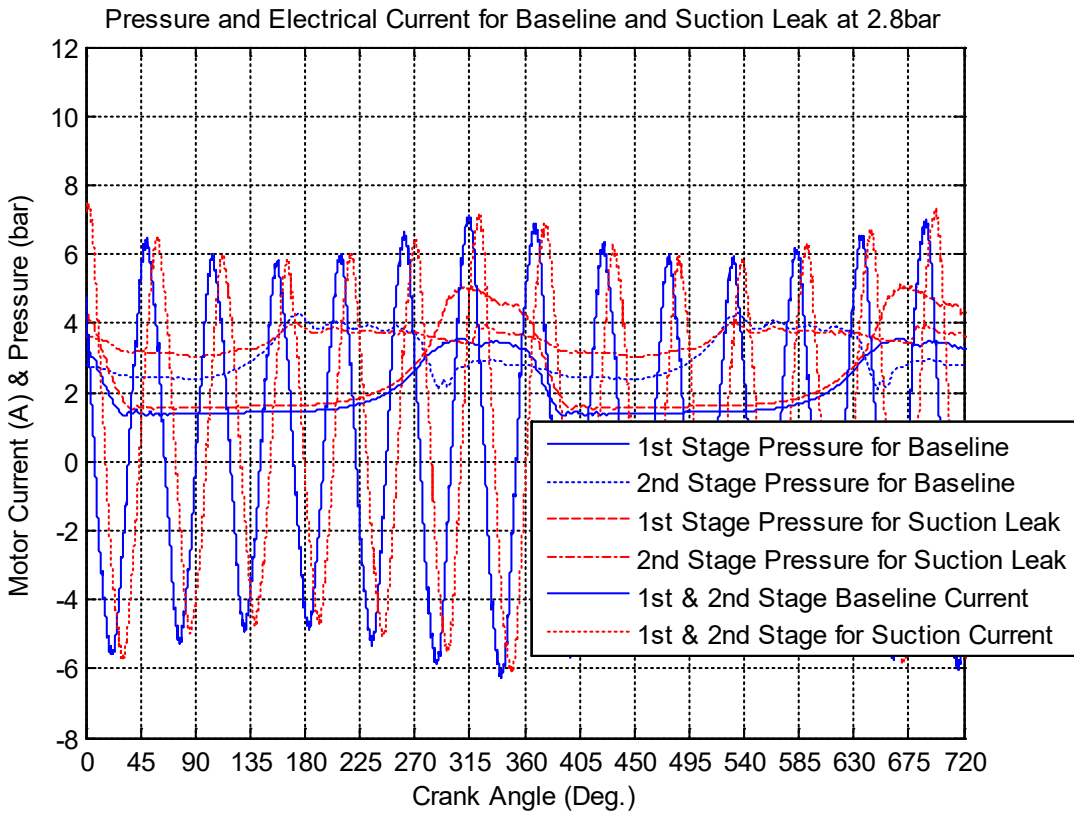

Figure 4-49 Current and Pressure Trace for Baseline and Suction Valve Leak at 2.8 bar

Corresponding to this change, the power supply current shows a slightly higher increase for the leaking suction valve current signal. This amplitude current also shows that it needs more current consumption whilst delivering the same quantity of air, confirming that the compressor uses more power and hence lower efficiency. The amplitude of the current signals is at the highest at a crank angle of about 320º angle with the suction valve leak current signal phase-shifted lagging by about 10º and at the lowest at a crank angle of about 195º with the suction valve leak current signal slightly higher and phase-shifted leading by about 10º.

MCSA of Suction Valve Leakage at 5.5 Bar

As shown in Figure 4-50, a leaking suction valve causes the pressure at the 1st stage to be a little higher than that of the baseline by about 2 bars at 0º of the TDC. The starting pressure of the leaking suction valve is 6 bars of the TDC then converges with the baseline to approximately 45º of the crank angle, still slightly higher by about 0.6 bar in the period from 46º to 285º of the crank angle. Following that sequence, the suction valve leakage then climbs to its peak at about 7.8 bar at a difference of 3.2 bar higher than the baseline pressure signal, then diminishes to about 2.8 bar in the rest of the cycle.

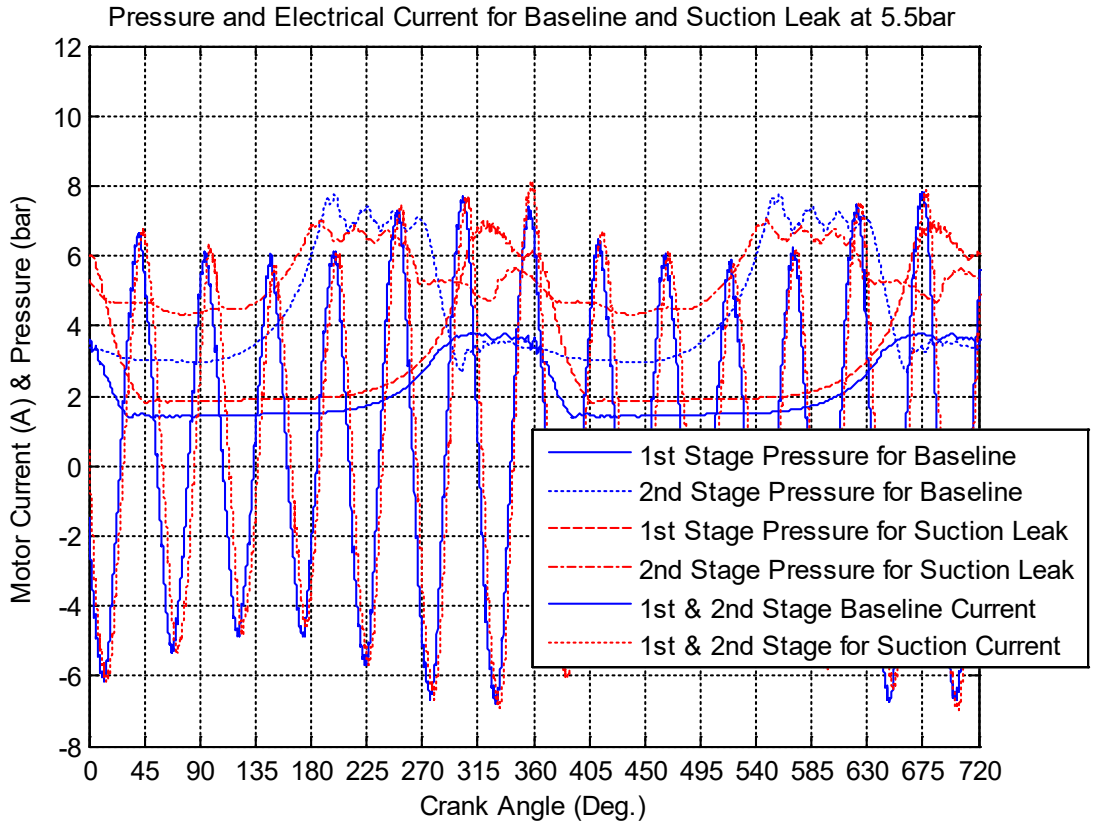

Figure 4-50 Current and Pressure Trace for Baseline and Suction Valve Leak at 5.5 bar

The pressure waveform of the 2nd stage under the suction valve leakage in the compression process is higher than the baseline from 0º to 180º, by about 2 bars.

It is at its peak at about 5 bars and lower than the baseline by about 0.8 bar at 190º whereas the discharge process in the period of 191º to 290º of the crank angle, the leaking suction valve is lower than the baseline waveforms in the region of 0.8 bar and the leaking suction valve is higher by about 1.8 bar in the rest of the cycle. From observation, it is clear that the pressure at the 2nd stage shows more increase, which means the compressor shifts away from its optimal operation and would work at a slightly higher efficiency with the suction valve leak at its peak at 7 bars lower than the baseline by about 0.8 bar.

Corresponding to this change the power supply current shows a slight increase for the leaking suction valve current signal. This slightly higher amplitude current also shows that it needs more current consumption whilst delivering a slightly higher quantity of air, confirming that the compressor uses more power and hence slightly higher efficiency. The amplitude of the current signals for the suction valve leak is at the highest at a crank angle of about 358º and lowest at a crank angle of about 175º with the suction valve leak current signal slightly lower and phase-shifted lagging by about 5º.

MCSA of Suction Valve Leakage at 8.3 bar

As described in Figure 4-51, a leaking suction valve causes the 1st stage pressure to be much higher than that of the baseline by about 3.2 bar at 0º of the TDC. The starting pressure of the leaking suction valve is 6.9 bar of the TDC then converges with the baseline to approximately 45º of the crank angle, still slightly higher by about 0.5 bar in the period from 46º to 290º of the crank angle.

Following that sequence the suction valve leakage then climbs to its peak at about 8.6 bar at a difference of 4.2 bar higher than the baseline pressure signal then diminishes to about 3.3 bar in the rest of the cycle.

The pressure waveform of the 2nd stage under the suction valve leakage in the compression process is higher than the baseline from 0º to 200º, by about 2.2 bar at TDC. It is at its peak at about 10 bars and lower than the baseline by about 1 bar at 200º whereas in the discharge process in the period of 201º to 268º of the crank angle, the leaking suction valve is lower than the baseline waveforms in the region of 1 bar. From 269º to 290º the leaking suction valve leads to 4 bars, higher by about 2.1 bar in the rest of the cycle.

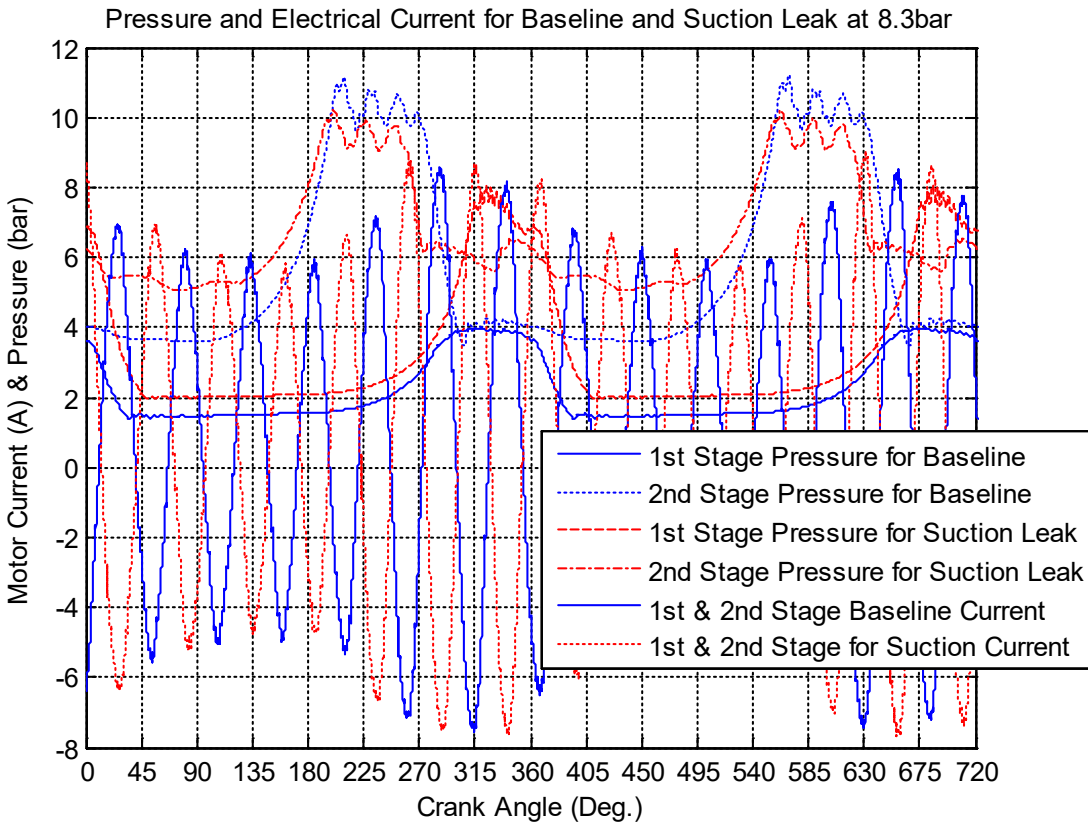

Figure 4-51 Current and Pressure Trace for Baseline and Suction Valve Leak at 8.3 bar

From observation, it is clear that the pressure at the 2nd stage shows a higher increase, which means the compressor shifts away from its optimal operation and works at high efficiency with the suction valve leak at its peak at 10 bars lower than the baseline by about 1 bar.

Corresponding to this change the power supply current shows a slightly higher increase for the leaking suction valve current signal. This higher amplitude current also shows that it needs more current consumption whilst delivering a higher quantity of air, confirming that the compressor uses more power and higher efficiency. The amplitude of the current signals for the suction valve leak is at the highest at a crank angle of about 260º and phase-shifted lagging the baseline current signal by about 30º and lowest at a crank angle of about 185º with the suction valve leak current signal slightly lower and phase-shifted leading by about 25º.

4.10.3 MCSA Based Condition Monitoring of Intercooler Leakage

MCSA of Intercooler Leakage at 2.8 bar

As shown in Figure 4-52, a leaking intercooler causes the 1st stage pressure to be slightly lower than that of the baseline by about 0.1 bar in the period from 0º to 280º of the crank angle at a starting pressure of about 3.4 bar at 0º of the TDC. Following that sequence, the intercooler

leakage then shows a difference of 0.2 bar lower than the baseline from approximately 281º to the end of the cycle and highest at about 3.5 bar.

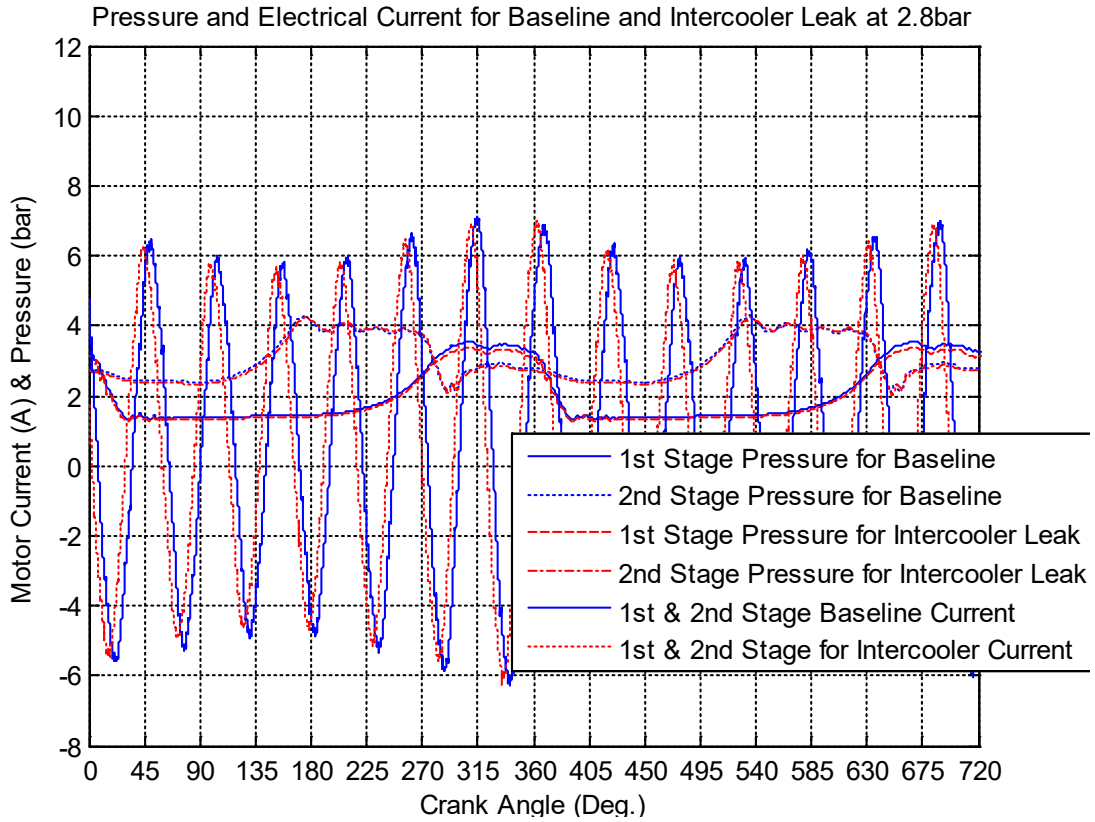

Figure 4-52 Current and Pressure Trace for Baseline and Intercooler Leak at 2.8 bar

The pressure waveform of the 2nd stage under the intercooler leakage in the compression process is slightly lower than the baseline from 0º to 170º, by about 0.2 bar, whereas the discharge process in the period of 171º in the rest of the cycle the baseline pressure remains roughly the same. From observation, it is clear that the pressure at the 2nd stage shows a slight increase, which means the compressor shifts away from its optimal operation and may work at low efficiency.

Corresponding to this change, the power supply current shows a slight increase in the leaking discharge valve current signal. This amplitude current also shows that it needs more current consumption whilst delivering the same quantity of air, confirming that the compressor uses more power and hence lower efficiency. As illustrated, the amplitude of the current signal is at its highest after the DVO of the 1st stage at a crank angle of about 360º and phase-shifted leading the baseline signal by about 5º and lowest at a crank angle of about 180º, phase-shifted leading the baseline by approximately 5º as well with the leaking discharge valve signal slightly lower.

MCSA of Intercooler Leakage at 5.5 bar

As presented in Figure 4-53, a leaking intercooler causes the 1st stage pressure to be slightly lower than that of the baseline by about 0.1 bar in the period from 0º to 280º of the crank angle, at a starting pressure of about 3.5 bar at 0º of the TDC. Following that sequence, the intercooler leakage then shows a difference of 0.2 bar lower than the baseline from approximately 281º to the end of the cycle, highest at about 3.7 bar.

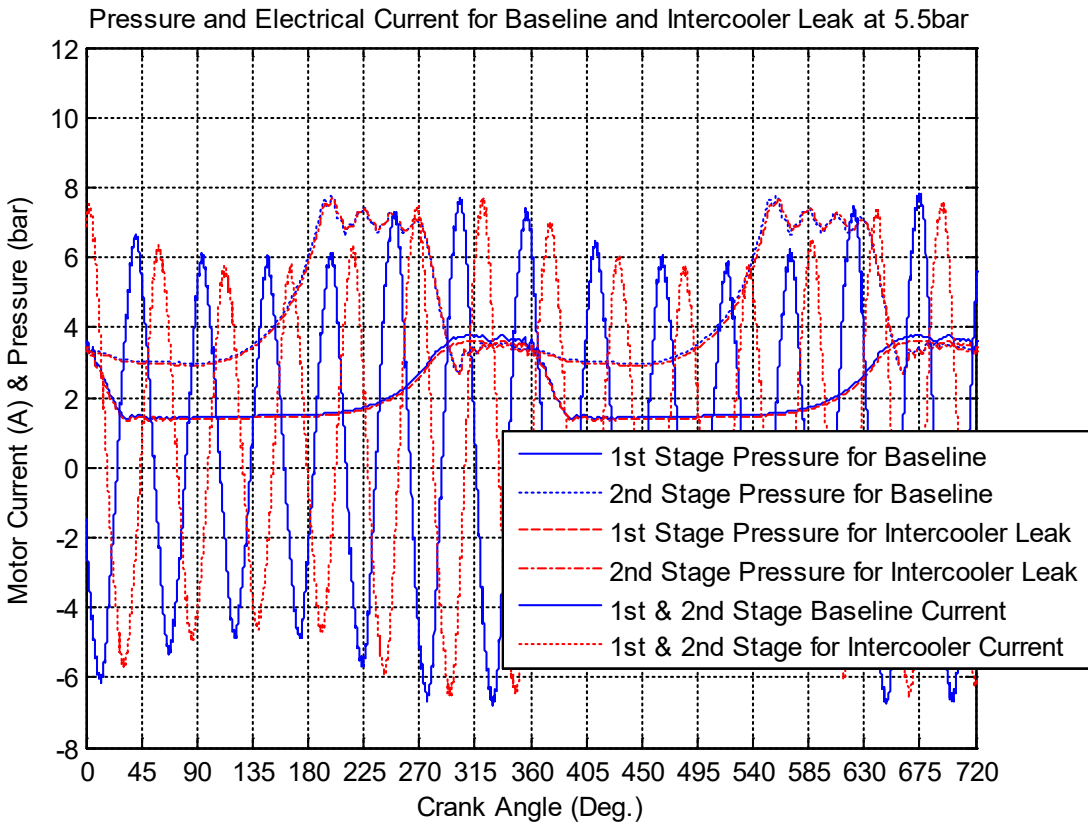

Figure 4-53 Current and Pressure Trace for Baseline and Intercooler Leak at 5.5 bar

The pressure waveform of the 2nd stage under the intercooler leakage in the compression process is slightly higher than the baseline from 0º to 195º, by about 0.1 bar and is at its peak at about 7.7 bar, whereas the discharge process in the period of 196º to 206º the baseline pressure increases by about 0.1 bar and then it remains roughly the same in the rest of the cycle. From observation, it is clear that the 2nd stage pressure shows a clear increase, which means the compressor shifts away from its optimal operation and works at a slightly higher efficiency.

Corresponding to this change the power supply current shows a slight increase for the leaking discharge valve current signal.

This slightly higher amplitude current also shows that it needs more current consumption whilst delivering a slightly higher quantity of air, confirming that the compressor uses more power and hence slightly higher efficiency.

The amplitude of the current signal is slightly higher after the DVO of the 1st stage at a crank angle of about 320º, phase-shifted lagging the baseline by about 20º and lowest at a crank angle of about 190º phase-shifted lagging the baseline by approx. 20º with the leaking discharge valve signal slightly lower.

MCSA of Intercooler Leakage at 8.3 bar

As shown in Figure 4-54, a leaking intercooler causes the 1st stage pressure to be slightly lower than that of the baseline by about 0.1 bar in the period from 0º to 280º of the crank angle at a starting pressure of about 3.6 bar at 0º of the TDC. Following that sequence, the intercooler leakage then shows a difference 0.2 bar lower than the baseline from approximately 281º to the end of the cycle and highest at about 3.9 bar.

The pressure waveform of 2nd stage under the intercooler leakage in the compression process is the same from 0º to 155º at a starting pressure of 5 bar, after that, the intercooler leakage is lower by about 0.05 bar from approximately 156º to 200º and is at its peak at 11.2 bar, whereas the discharge process in the period of 201º to 265º the intercooler leakage pressure increases by about 0.1 bar and then it remains roughly the same in the rest of the cycle. From observation, it is clear that the 2nd stage pressure shows a much higher increase which means the compressor drifts away from its optimal operation and may work at high efficiency.

Corresponding to this change the power supply current shows a slightly higher increase for the leaking discharge valve current signal. This higher amplitude current also shows that it needs more current consumption whilst delivering a higher quantity of air, confirming that the compressor uses more power and hence higher efficiency. The amplitude of the current signal is slightly higher after the DVO of the 1st stage at a crank angle of about 315º, phase-shifted, leading the baseline by about 25º and lowest at a crank angle of about 190º, phase-shifted, leading the baseline by approximately 20º with the leaking discharge valve signal slightly lower.

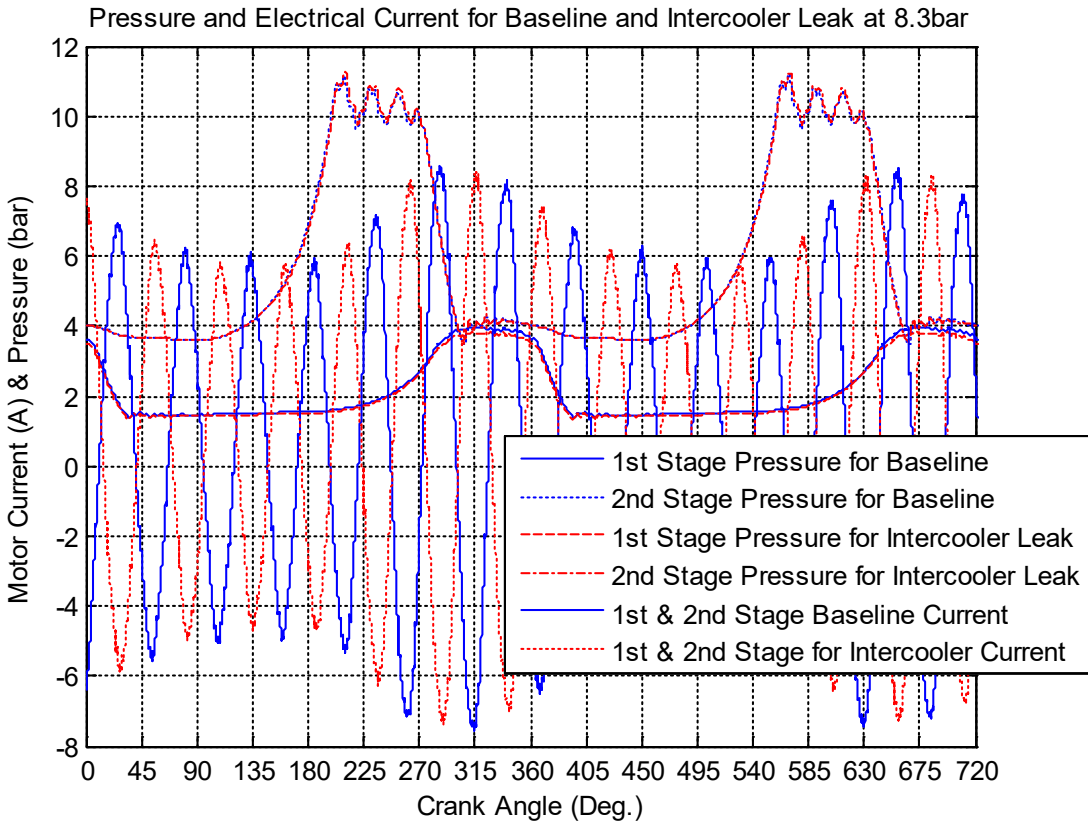

Figure 4-54 Current and Pressure Trace for Baseline and Intercooler Leak at 8.3 bar

4.10.4 MCSA Based Condition Monitoring of Loose Belt

MCSA of Loose Belt at 2.8 bar

As illustrated in Figure 4-55, the loose belt in the 1st stage pressure is the same from 0º of the TDC to 30º of the crank angle, at a pressure of approximately 3.6 bar. From 31º to about 300º of the crank angle the loose belt pressure is slightly lower by about 0.05 bar of the baseline. Following that sequence, the loose belt pressure then remains roughly the same to the end of the cycle with both waveforms at their highest at about 3.5 bar.

The pressure waveform of the 2nd stage under the loose belt in the compression process is the same from 0º to 110º at starting pressure of 2.8 bar then the loose belt pressure decreases by about 0.1 bar compared to the baseline from 111º to 190º of the crank angle and is at its peak at about 4.3 bar, whereas the discharge process in the period of 191º to the rest of the cycle the loose belt pressure remains roughly the same. From observation, it is clear that the 2nd stage pressure shows a slight increase, which means the compressor shifts away from its optimal operation and now works at a lower efficiency.

Corresponding to this change the power supply current shows a slight decrease in the leaking discharge valve current signal. This amplitude current also shows that it needs more current

consumption whilst delivering the same quantity of air, confirming that the compressor uses more power and hence lower efficiency.

The amplitude of the current signal is slightly lower after the DVO of the 1st stage at a crank angle of about 320º, phase-shifted, lagging the baseline by about 20º and lowest at a crank angle of about 190º, phase-shifted, lagging the baseline by approximately 20º with the loose belt signal slightly lower.

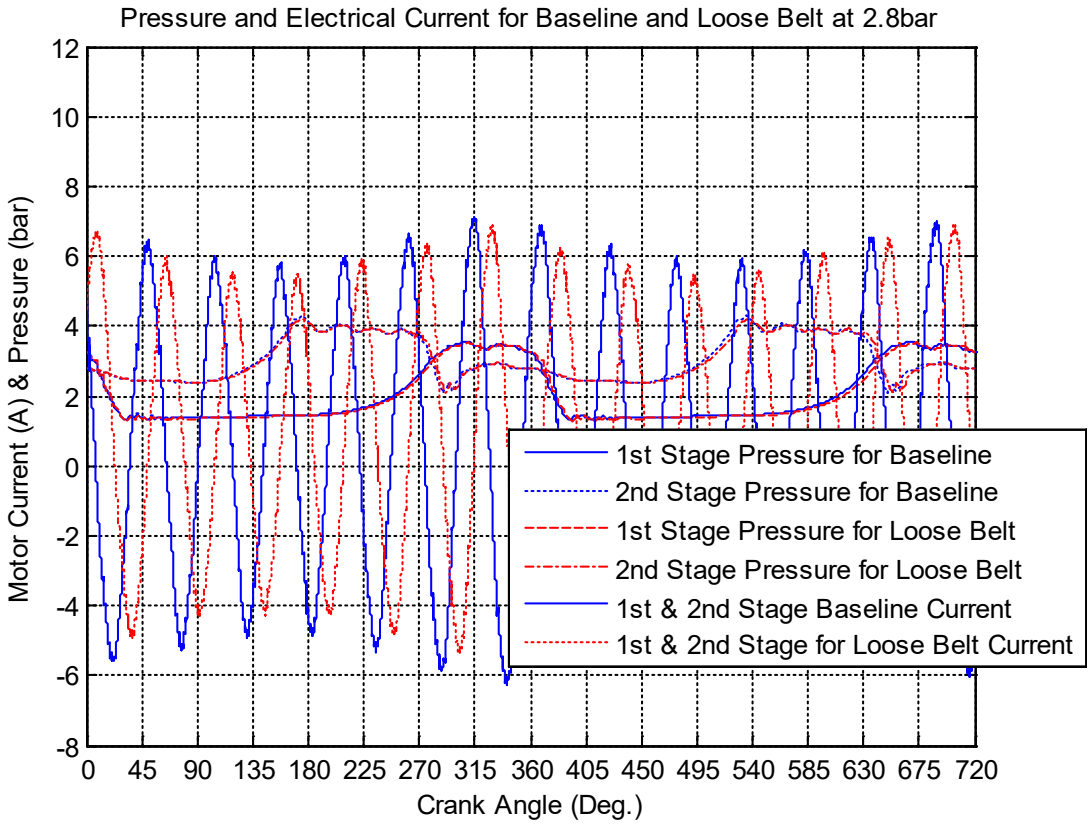

Figure 4-55 Current & Pressure Trace for Baseline and Loose Belt leak at 2.8 bar

MCSA of Loose Belt at 5.5 bar

As shown in Figure 4-56, the loose belt 1st stage pressure is the same from 0º of the TDC to 30º of the crank angle at a starting pressure of approximately 3.5 bar. From 31º to about 315º of the crank angle the loose belt pressure is slightly lower by about 0.1 bar of the baseline. Following that sequence, the loose belt pressure then remains roughly the same to the end of the cycle with both waveforms at their highest at about 3.7 bar.

The pressure waveform of 2nd stage under the loose belt in the compression process is the same from 0º to 135º starting at a pressure of 3.6 bar then the loose belt pressure decreases by about 0.05 bar from 136º to 191º of the crank angle and is at its peak at about 7.7 bar, whereas the discharge process in the period of 191º to the rest of the cycle the loose belt pressure remains

roughly the same. From observation, it is clear that the 2nd stage pressure shows a clear increase, which means the compressor shifts away from its optimal operation and would work at a slightly higher efficiency.

Corresponding to this change the power supply current shows a slight decrease in the leaking discharge valve current signal. This slightly higher amplitude current shows that the current consumption increases slightly whilst trying to deliver a slightly higher quantity of air, confirming that the compressor is trying to use more power and hence slightly higher efficiency.

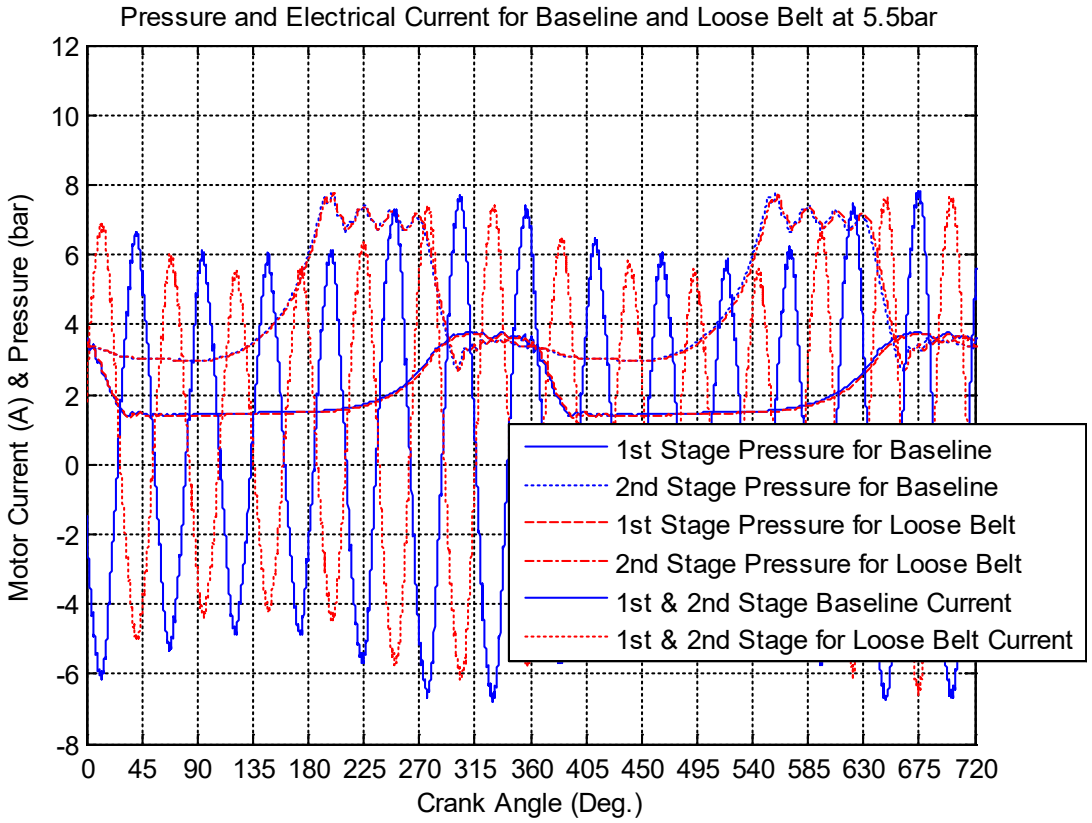

Figure 4-56 Current and Pressure Trace for Baseline and Loose Belt at 5.5 bar

The amplitude of the current signal is slightly lower after the DVO of the 1st stage at a crank angle of about 320º, phase-shifted, lagging the baseline by about 20º and lowest at a crank angle of about 150º, phase-shifted, lagging the baseline by approximately 25º with the loose belt signal slightly lower.

MCSA of Loose Belt at 8.3 bar

As shown in Figure 4-57, the loose belt of the 1st stage pressure is the same from 0º of the TDC to 100º of the crank angle at a starting pressure of approximately 3.6 bar. From 101º to about 300º of the crank angle the loose belt pressure is slightly lower by about 0.1 bar of the baseline.

Following that sequence, the loose belt pressure then remains roughly the same to the end of the cycle with both waveforms at their highest at about 3.9 bar.

The pressure waveform of the 2nd stage under the loose belt in the compression process is about 0.3 bar lower than the baseline from 0º to 135º starting at a pressure of 3.7 bar.

After that, the loose belt pressure decreases to about 0.1 bar from 136º to 191º of the crank angle and is at its peak at about 11.2 bar, whereas the discharge process in the period of 191º to the rest of the cycle the loose belt pressure remains roughly the same. From observation, it is clear that the 2nd stage pressure shows a higher increase, which means the compressor shifts away from its optimal operation and works at a higher efficiency.

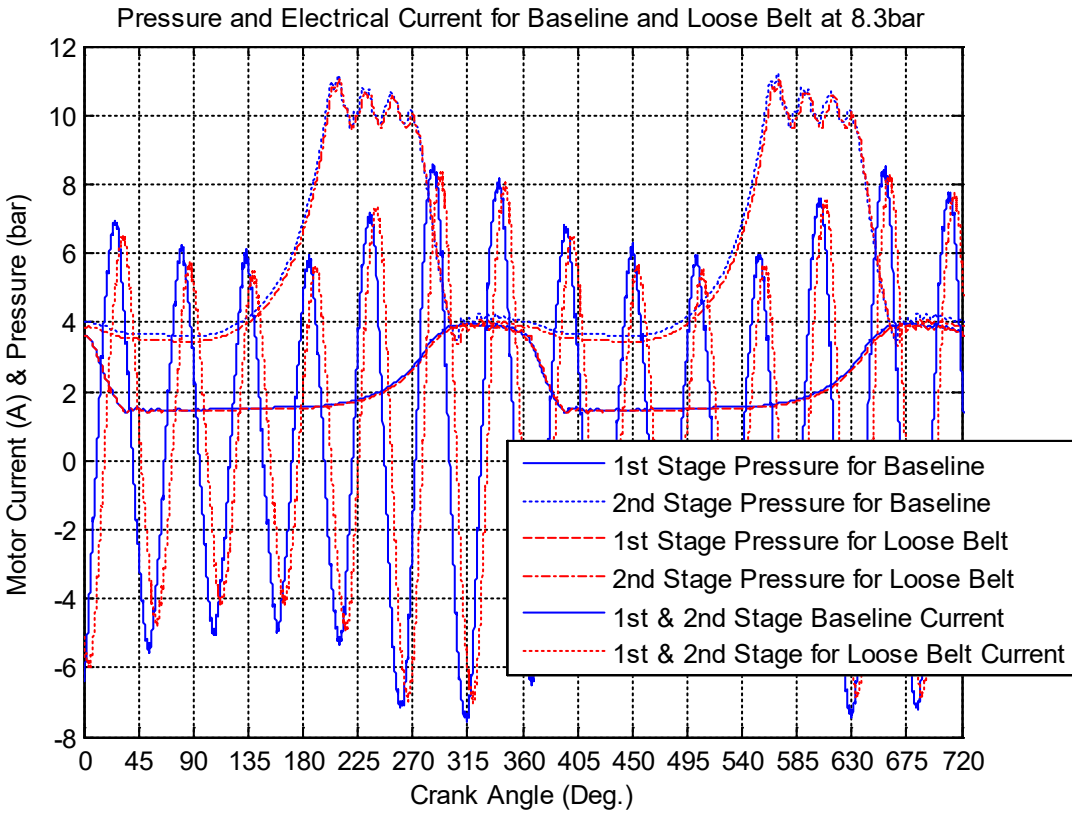

Figure 4-57 Current and Pressure Signals for Baseline and Loose Belt at 8.3 bar

4.10.5 Discussion

The power supply current shows a slight decrease in the leaking discharge valve current signal. The higher amplitude current shows that the current consumption is high whilst trying to deliver a higher quantity of air, confirming that the compressor is trying to use more power and hence higher efficiency. As illustrated in Figure 4-49, the amplitude of the current signal is slightly lower after the DVO of the 1st stage at a crank angle of about 300º, phase-shifted, lagging the baseline by about 10º and lowest at a crank angle of about 105º, phase-shifted,

lagging the baseline by approximately 10º with the loose belt signal slightly lower. Generally, the discharge valve leakage at the second stage causes the current profile of the first stage amplitude current to increase at its peak in the period discharge valve process. Whereas, the current profile of the second stage is behind but with a small decrease in the current amplitudes and slightly shifted compared with the baseline.

For the suction valve leakage at the second stage, the current profile of the first and second stage amplitude current increases at its peak in the period discharge valve process. Whereas, the current profile of both the first and second stage is leading the baseline current but at the same amplitudes and shifts significantly compared with the baseline at 5.5 bar.

For the leaking intercooler, the current profile of the first stage is slightly lower and the amplitude current increases at its crest in the period discharge valve process. Whereas, the current profile of both the first and second stage lags the baseline current but at the same amplitudes and slightly shifts compared with the baseline.

For the faulty transmission belt, the current profile of the first stage is slightly lower and the amplitude current increases at its crest in the period discharge valve process. Whereas, the current profile of both the first and second stage lags the baseline current but at same amplitudes and slightly-phase shifted compared with the baseline.

The amplitude current needs the same current consumption whilst delivering the same quantity of air, hence working at a different level of efficiency and being higher at the 2nd stage.

Each case shows that less work is required in the suction stage whereas in the second stage (compression cycle) more work is needed, and the pressure oscillates higher at the discharge pressure and hence uses more current.

4.11 IAS Based Condition Monitoring

An extra fault was introduced in this section as the opportunity arose to allow multiple faults to diagnose simultaneously.

The defective data is already explained previously in Table 4-7 Test Cases and Operating Conditions for only the Discharge Valve Leakage, Suction Valve Leakage, Intercooler Leakage and Belt Looseness.

Whilst the Defective Stator (DS) and both DS combine with DVL, these are new faults being seeded into the system. As cylinder pressure is the most vital parameter in measuring the operating performance of a Reciprocating Compressor (RC), these tests will give a clear

understanding of its performance under different pressure and load. It expresses all the functions and working processes in all the sub-systems components, such as valve movement in each stage, air-flow dynamics and motor speed-load signature.

4.11.1 IAS based Condition Monitoring of Crankshaft

IAS of Crankshaft Based Condition Monitoring Combined of 1st and 2nd Stage at 40, 80 and 120 psi

In this test the faulty stator winding, discharge valve leakage and both DVL and stator fault have been seeded. The main purpose of this exercise is to compare and localise failures at various steps of the compressor stages though the instantaneous angular speed. Figure 4-58 shows the 1st & 2nd stage pressure at 40, 80 and 120 psi over two revolutions of the compressor cycle and the consistency of the waveform is apparent. Figure 4-59 shows the comparison of the IAS signal and the pressure of the 1st & 2nd stage at 40, 80 and 120 psi respectively. From Figure 4-58,less work is carried out in the 1st stage between approximately 20° to 180° and more is done at approximately 220° to 320 °.

Minimum work is done during the 2nd stage expansion stroke, between crank angles of about 20° to approximately 90°, whereas maximum work is done between approximately 100° to 180° during the compression cycle followed by the discharge.

Considering the amount of work to be done in the 2nd stage as shown from Figure 4-59, at 120 psi the IAS speed is 20° to 70° throughout when both suction valves (SVO) are open and reach its maximum.

At about 100° when the 2nd stage suction valve closes, a gradual deceleration can be observed in the IAS performance as more work is needed to compress the 2nd stage gas.

The 1st stage suction valve closes at about 170° and now the machine starts to discharge the 2nd stage compress gas in the 1st stage cylinder. This carries on until to the 2nd stage (DVO) is at about 270° and a maximum deceleration of the IAS can be observed. Between 270° and 360° the 2nd stage goes through its suction stroke and 1st stage discharges gas to the cylinder. The shape of the IAS signal is very like a sinusoidal waveform. The maximum value of the IAS is approximately 90° of the crank angle and the minimum value is at 230°.

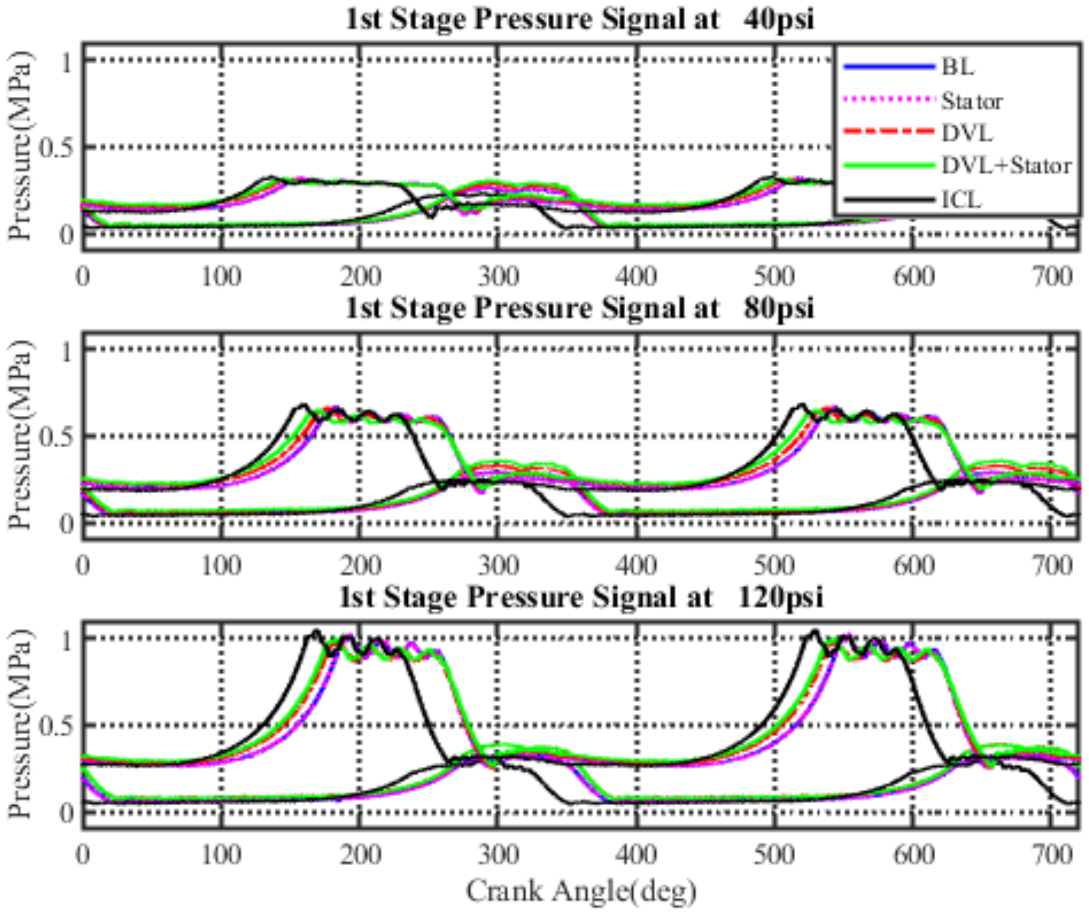

Figure 4-58 1st and 2nd Stage Pressure Signals at 40, 80 and 120 psi

The reason that the 2nd stage at 120 psi was considered for the above situation is that because it is the IAS that feeds back to the motor to produce variations in the motor current.

The process applies also to the stator, DVL, combine DVL and stator and baseline. The ICL is the only seeded fault that behaves differently during the IAS of the crankshaft at 40 and 80 psi while at 120 psi it's slightly lower by about 10 (rpm) from the suction valve open SVO up to the discharge valve open DVO.

From the DVO to the DVC it's remarkably higher and very like the trends.

Figure 4-59 illustrates how the IAS affect the pressure.

The greater the discharge pressure the greater the piston must work and the value of the IAS decreases as the discharge pressure increases. The maximum value of the IAS depends on the discharge pressure as it happens when both the 1st and 2nd stage suction valves are open.

The range in rpm is small compared with the inseminated fault but if those faults were of a higher magnitude the values would have made a bigger and catastrophic impact.

See also **Table 4-8** IAS of the Crankshaft at 40, 80 and 120 psi for the comparison.

Table 4-8 IAS Values of the Crankshaft at 40, 80 and 120 psi

	Baseline	Stator	DVL	DVL + Stator	ICL
40 psi	448	450	448	447	445
80 psi	447	449	446	445	442
120 psi	446	448	445	443	440

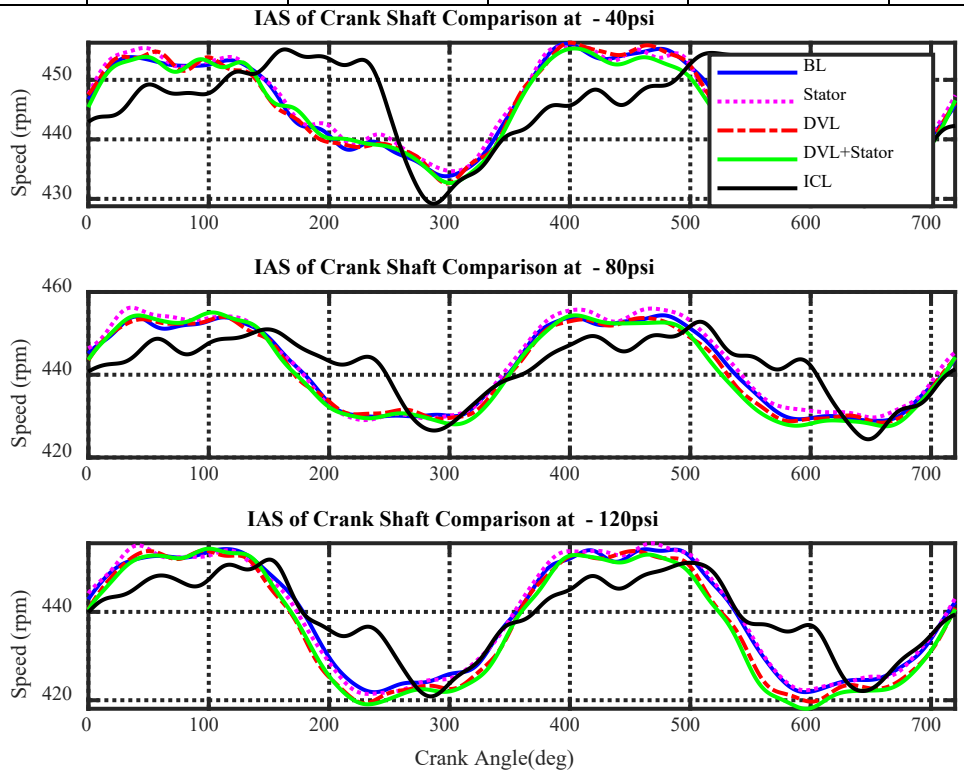

Figure 4-59 IAS of Crankshaft at 40, 80 and 120 psi

4.11.2 Current Waveform Based Condition Monitoring

The current fault of the baseline, faulty stator, faulty discharge valve together with the faulty stator and intercooler fault at 40, 80 and 120 psi can be compared in Figure 4-60 Current Waveform Comparison below.

The amplitude of the current of the crank angles discharge pressure from 100° to 225° approximately, lower than that from 250° to 360° and the amplitude increase with the discharge

pressure. This concludes that the current signal can be used to obtain valued information about the operation of the compressor.

The current can be an indication of the torque exerted by the motor, therefore, the maximum and minimum values of current correspond to an increase and decrease in the IAS.

Figure 4-61 RMS / Envelope Signal Waveform shows the Root Mean Square (RMS) values of the currents and is accompanied by the envelope signal for the baseline and the seeded faults for an accurate comparison.

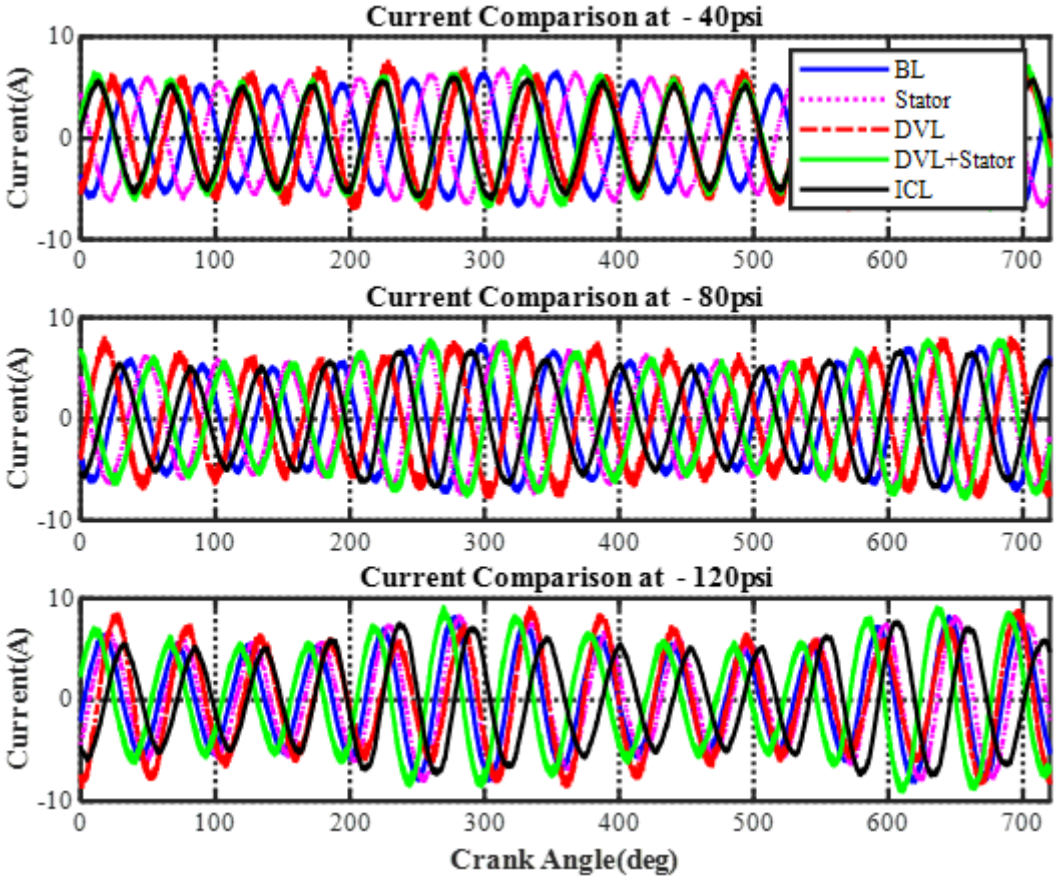

Figure 4-60 Current Waveform Comparison

4.11.3 RMS/Envelope Analysis

As illustrated in Figure 4-61, the RMS values are calculated for all the cases to quantify the differences for all individual faulty cases. The RMS values of the current signals change depending on the load fluctuation. At different operating discharge pressure such as 50 psi, the current signals are also changing with the different kind of faulty cases. The RMS signal under the faulty condition is higher than that of the baseline and the RMS value of the current signal of the intercooler leakage is lowest in the five conditions.

However, when the discharge pressure increases, the RMS values of the current signal increases accordingly under its conditions. This shows that if a failure is detected from the compressor, the load fluctuation characteristic will be different, consequently the RMS values and its change will be different to that of a healthy compressor with the increase of the discharge pressure. It should also be noted that this study mainly focuses on a higher-pressure range and based on this investigation failures can be identified and analysed by the RMS analysis in a relationship with the discharge pressures.

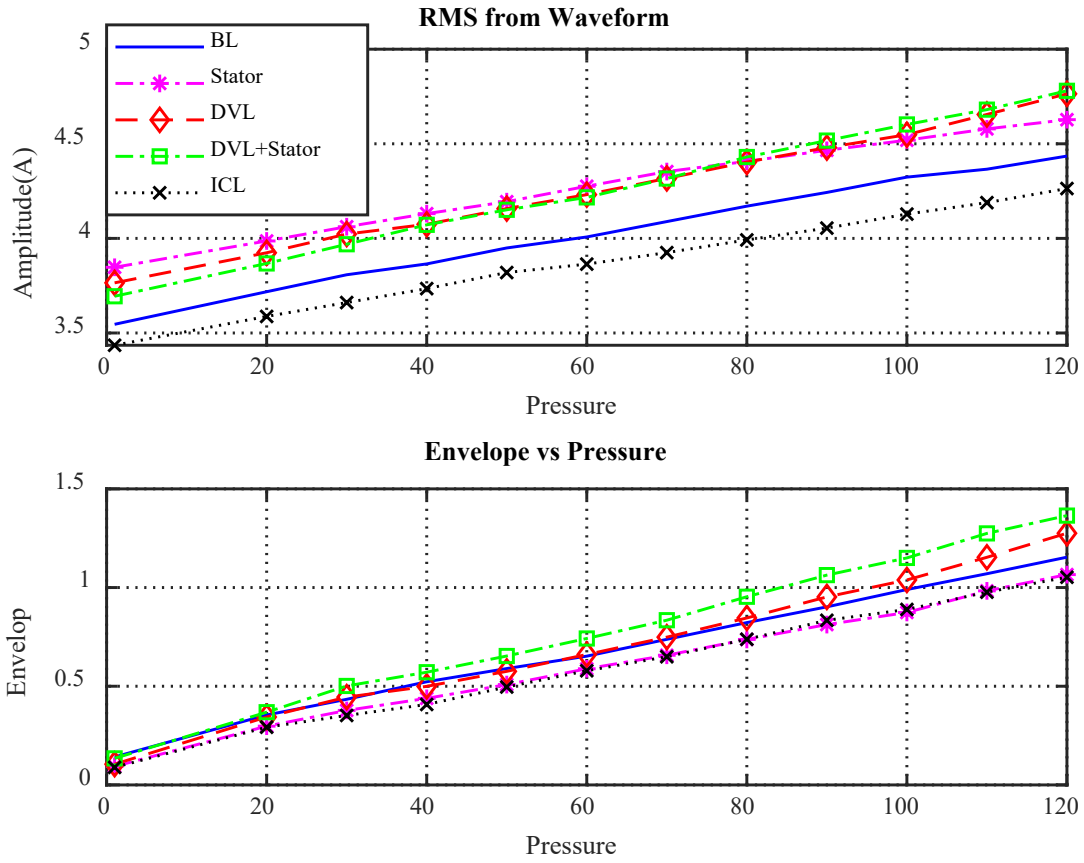

Figure 4-61 RMS / Envelope Signal Waveform

The envelope signal analysis has also proved it can allow a complete separation between the faulty conditions at different discharge pressures. The trends are very close to that of the RMS signal proving that it can capture the modulation characteristics with precision, however the envelope signal is slightly narrower than the RMS current signal.

4.11.4 Current Spectrum Analysis

An electric motor is a fundamental part of the conversion of electrical to mechanical energy in industries and the frequency analysis has proven to be better for the determination of motor condition such as eccentricity, misalignment, bearing deterioration and much more. A typical

motor drawing current will display the main component frequency at 50 or 60 Hz [128]. The supply frequency in this study is at 50 Hz as United Kingdom mains frequency is nominally 50 Hz and this can sometimes fluctuate between ±1% of 50 Hz. The main frequency is supplemented by a pair of sidebands of ±7.3 Hz which is the compressor operating frequency. Figure 4-62, shows the current spectra signal at 40, 80 and 120 psi for all five cases. From observation, the current spectra in all the three-discharge pressures plot the 50 Hz supply frequency and its harmonics are known as "sidebands" The spectrum displays a high level of Amplitude Modulation (AM). at 50 Hz fundamental and two sidebands $(F - f_1)\ and\ (F + f_1) \approx 42.7$ and 57.3 Hz. The first sidebands are slightly higher than the second sidebands showing the induced faults DVL combined with stator being at the peak trailed by the DVL with the assumption that the pressure of the RC increases in parallel with the amplitude of the sidebands.

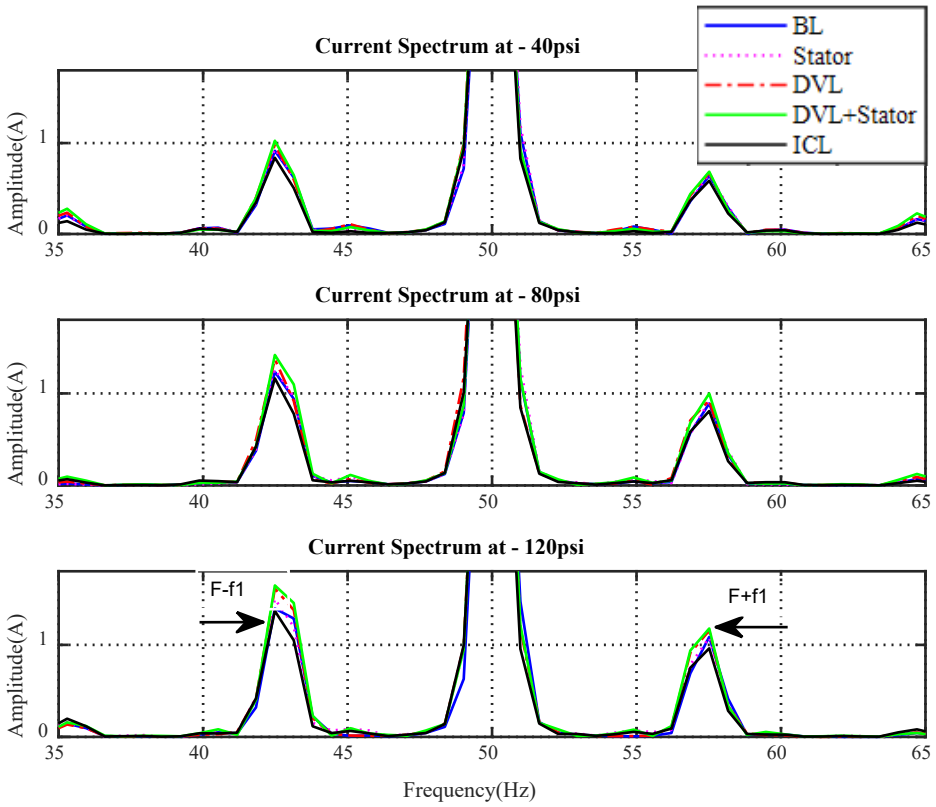

Figure 4-62 Current Spectrum Signal

4.11.5 IAS Spectrum Analysis

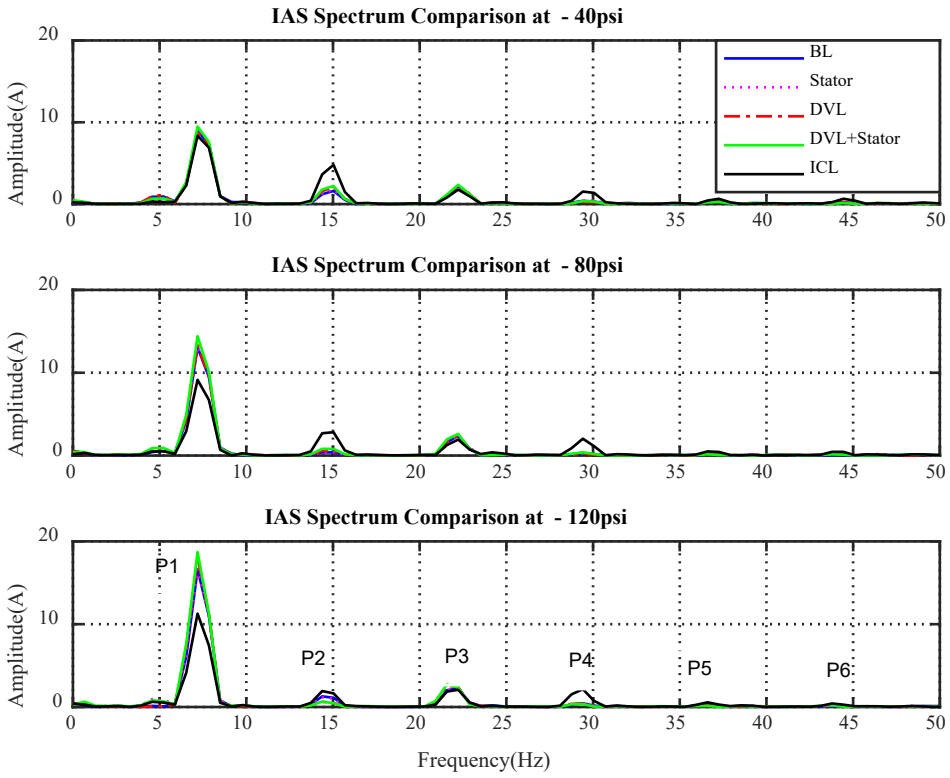

Figure 4-63 IAS Spectrum Comparison

Instantaneous Angular Speed (IAS) can offer useful information about the health and behaviour of a machine. Machinery such as RC rotates at a constant speed however in practicality the angular speed varies due to load fluctuations during operation. Any change in IAS indicates the presence of a fault and the possibility of failures. The spectral signatures, as shown in Figure 4-63, provide very important information concerning its frequency and fault conditions. The signals are closely related to the RC dynamics and have less noise however slightly demanding in the implementation phase due to the encoder mounting. Any failure is directly related to a frequency component and is displayed by a specific signature. At a discharge pressure of 40, 80 and 120 psi it is clear that the peaks, for all cases, are very similar in symmetry however the peak amplitudes vary and there are mixed spectral faults in peak 1 (P1) 1st harmonic 7.2 Hz, peak 2 (P2) 2nd harmonic, peak 3 (P3) 3rd harmonic, peak 4 (P4) 4th harmonic, peak 5 (P5) 5th harmonic and peak 6 (P6) 6th harmonic.

At 40 psi peak (P1) 7.2 Hz, DVL is at its peak and ICL lowest, Peak (P2) at approximately 15 Hz ICL is highest and BL the lowest, peak (P3) at 22.5 Hz DVL combined with Stator are at the highest and ICL lowest, at about 29 Hz peak (P4) ICL is highest and DVL combined with

the stator is the lowest and peak (5) and (6) at approximately 37 and 44 Hz the amplitudes is at its lowest with ICL slightly lower.

At 80 psi the trend is very similar to 40 psi however peak (P1) amplitude is higher compared to the 40 psi with ICL the lowest and the rest of the harmonics more or less similar to the 40 psi in exception of peak (P2) slightly lower that of peak (P2) 40 psi discharge pressure.

At 120 psi all five cases are at the maximum at peak (P1) compared to the 40 and 80 psi discharge pressure. At peak (P1) the DVL combined with the stator is at the upper limit, DVL and stator individually and baseline in the middle range and ICL at its lowest. The rest of the harmonics are more or less similar to the 80 and 40 psi discharge pressure with the exception of peak (P2) lower than the 40 and 80 psi discharge pressure.

The presence of low-frequency harmonics in the compressor could be associated with the shaft misalignment, imbalance, eccentricity cracks or bearing failure.[129].

4.11.6 Discussion

It has been found that the dynamic pressure, IAS and motor current monitoring allows full detection of all induced faults including different leakages of discharge, inlet and intercooler, driving belt looseness and motor stator asymmetries with moderate signal conditioning and analysis. However, both IAS and motor current monitoring provides good information regarding fault location and severity.

In this study only, the time domain application has been used for fault comparison of the cylinder under pressure at 2.8, 5.5 and 8.3 bar for the 1st and 2^{nd} stage. Four control parameters have been used; the baseline against discharge valve leakage, suction valve leakage, intercooler leakage and belt looseness.

So far, the time domain analysis result seems to be an easy method but not very accurate however it is still to be considered as the study of the frequency domain is left for future works.

In the meantime, vibration can provide both detection and diagnosis of these faults under the cost of high processing efforts. Considering those unacceptable intrusive disturbances of pressure monitoring and difficulties and safety issues of current transducers in production lines, it has concluded that IAS is relatively easy to be implemented because of the easiness of the sensor installation and low cost of the whole system. To composite its diagnostic deficiency, portable vibration monitoring system will be combined which needs to include more advanced signal analysis and diagnosis techniques.

Phase II

Applying Condition Monitoring to Industrial Liquid Ring Vacuum Pumps

Chapter 5

Analytic Modelling of a Liquid Ring Vacuum Pump

Chapter 6

A Preliminary Implementation of Vibration and Acoustics Monitoring to an Industrial Environment

Chapter 5. **Analytic Modelling of a Vacuum Pump**

This chapter presents an analytic analysis of the industrial target machine in Phase II which is the Liquid Ring Vacuum Pumps (LRVP) in a paper mill. It gives an in-depth understanding of the dynamic behaviour and operation of the machine and assists the monitoring and accurate diagnosis of the LRVP. Based on variation in key performance parameters such as pressure and flow rate, the behaviour of external dynamic responses such as acoustics, vibration and rotor IAS are understood qualitatively, which is sufficient for understanding the data characteristic in this preliminary study. As LRVP share the operation process of reciprocating compressors in terms of internal pressure oscillations, the qualitative results made in Reciprocating Compressor (RC) in Chapter 3 and Chapter 4 can be referred to LRVP data analysis.

5.1 Introduction

The Liquid Ring Vacuum Pump (LRVP) is a rotary type of pumps much like a vane vacuum pump and rotary piston vacuum pumps. Due to having liquid (water) seals LRVP has no exhaust valve, the friction surface and its compression is nearly isothermal or has little temperature change. With these distinctive features it is widely used in food, paper, pharmaceutical, metallurgy, petroleum, chemical and other industries to transport explosive gas with dust, non-condensable gas and water mixture.

In principle, LRVPs mainly consist of a vaned impeller and circular pump housing. The impeller is located eccentrically from the pump housing. When the impeller rotates, liquid (usually water) is fed into the pump casing and forms a moving cylindrical ring against the inside of the housing due to an effect of centrifugal acceleration. This liquid ring and the vane blades constitute a series of chambers. Working fluid such as gas or air is sucked into the chambers through an inlet port in the end of the housing. Pressures of fluid trapped in the chamber vary periodically as the volume changes when rotating the eccentric impeller. For an individual chamber, the pressure changes will be traditionally examined in three sub processes which includes **suction, compression and discharge.** This is very similar to that of a reciprocating compressor, see Figure 3-10, meaning that the force variation and dynamics of LRVP behave like a RC.

In addition, because the effect of liquid ring sealings, considerable power will be consumed through the frictional effects of fluids and interactions between fluid and stationary casing.

In general, dynamic behaviours of a LRVP can also be examined based on these gas impulsions and the friction excitations, which will then pave the fundamental for analysing measured vibration, acoustics and motors current signals to achieve fault detection and diagnosis.

As LRVP is a typical bladed rotor system, it can suffer from faults which commonly occur in such rotor systems. Typically, it can have impeller defects due to cavitation erosions, bearing defects, shaft seal malfunctions and various internal and external leakages.

There are high demands for condition monitoring of LRVPs to ensure the safety and efficiency of the production activities relying on LRVPs, which are evidenced by many general discussions and explanations on websites in relation to trouble shooting of LRVPs. However, extensive reviews have found little publications relating to LRVP dynamic modelling in

association with fault cases. This shortage of in-depth knowledge in the dynamic behaviours makes it difficult to implement vibro-acoustic based CM techniques on this machine.

To overcome this shortage, this chapter presents a study of the dynamic responses of LRVPs through modelling the air and water flow processes. A preliminary study has shown that LRVP operations share with a reciprocating machine the various sub-processes in terms of suction, compression, discharge and expansion. This study then focuses on analytic modelling in which the details of dynamic similarities are examined so that both the quantitative and qualitative results obtained based on the RC made in Chapter 3 and Chapter 4 can be referred in a greater degree for LRVP data analysis and CM implementation. This would avoid the repetitive studies made in Chapter 3 and Chapter 4. In addition, the dynamic effect of liquid ring frictions is also examined to understand its amplitudes and frequency characteristics when internal leakages occur due to faulty impellers.

5.2 Overview of Liquid Ring Vacuum Pump Models

A vacuum pump converts mechanical input energy of a rotating shaft, driven by an electric motor, into pneumatic energy by releasing the air contained within an enclosed space causing the internal pressure level to become lower than the atmospheric pressure. The volume released and the pressure difference produced will determine the amount of energy produced and the internal forces applied to the impeller, bearings, and shafts.

LRVP are well known for producing vacuum for the process industries. It is similar to the rotary positive-displacement pump but instead it employs water as the sealing element to formulate a series of compression chambers. Sub-process of suction, compression and discharge are formed by the circulation of a ring of liquid around the housing of the multi-bladed rotating impeller which is located in eccentricity between the pump housing and the rotating blade as explained in the above section. This operation is made possible due to the eccentricity of the rotating impeller. This can be elaborated more by the schematic of Figure 5-1 [130].

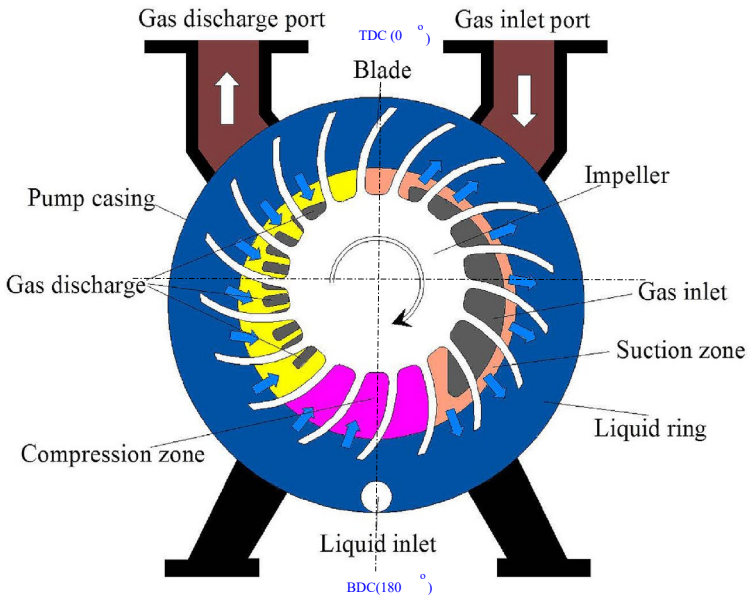

Figure 5-1 A schematic of liquid ring vacuum pumps [131]

The modelling of LRVP is an ongoing issue faced by academics as their theoretical results deviate from their actual performance due to a lack of fundamental study in the performance which limits its development in both reliability and performance. A universal theoretical model based on the operating cycle principle of the "suction-compression-discharge-expansion" performance of a liquid ring vacuum pump was implemented to solve the above issue by Si Huang et al. It was possible to accurately predict the liquid ring vacuum pump performance parameters such as shaft power, actual suction and discharge capacity and the global efficiency by the proposed theoretical model without the restriction of other important data such as the empiric range, the pump design and overall data. This model has proven to be a feasible tool for the application in the performances of the liquid ring pump due to its isothermal advantages of the compression process and the fluid acting as the seal [132].

A lot of work has been carried out on the industrial application and design of the LRVP however if compared to other types of compressors and pumps very little study has been done on the LRVP [132] [133].

Pfleiderer formulated an equation for the theoretical suction capacity in LRVP and drew a theoretical model of the compression ratio and the liquid ring area at each circumferential angle in the pump based on the ideal operating cycle theory of the "suction-compression-discharge" in Reciprocating Compressor (RC) [134].

Following that Schulz et al derived a relatively equivalent equation aimed at the theoretical suction capacity. It was found that both the equation of the theoretical suction capacity and its model has primarily been employed only during the designing stage of LRVP [135] [136].

Equation 5.1 to 5.3 below shows the theoretical suction capacity revealed by the impeller rotational speed and the geometric parameters stays the same, irrespective of the compression ratio of discharge pressure to suction pressure. The solution is not in line with the existing condition, especially when the compression ratio is quite high, however Prager [137] developed an empirical formula as shown in equation 5.4 and 5.5 for the actual suction capacity related on LRVP experimental data performance, but the legitimacy of the formula was limited by the amount of collected data and the maximum unidentified factual suction capacity. Powle [138] created Equation 5.6 for the ratio of the actual discharge capacity to the maximum actual discharge capacity, as the lowest suction pressure of the LRVP was too near to the saturated vapour pressure of the working liquid.

As shown in Equation 5-7 Bodik described a closer connection between the shaft power and the rotational speed of the LRVP.

Pfleiderer [134] : $q_{th} = \frac{1}{2}\mu\omega_2^2\ [(1-\alpha)^2 - v^2]$ (5.1)

$$q_s = \frac{\lambda}{\lambda_{max}} q_{s\,max} \tag{5.2}$$

Vacuum pumps: $\frac{\lambda}{\lambda_{max}} = 0.147\,X^3 - 1.297\,X^2 + 0.150X + 1$ (5.3)

Prager [137]

Compressor: $\frac{\lambda}{\lambda_{max}} = 0.707X^3 - 1.527X^2 + 0.1782X + 1$ (5.4)

$$X = \frac{\left({}^{P_d}/_{P_s} - 1\right)}{\left[\left({}^{P}/_{P_s}\right)_{max} - 1\right]} \tag{5.5}$$

Powle [138] $$q_d = \frac{q_{d\,max} P_a \left(P^m - P_V^{m+1} \,/_P \right)}{\left(P_a^{m+1} - P_V^{m+1} \right)} \quad (5.6)$$

Bodik [139] $$Au_2^3 + \mathrm{B}u_2 \quad (5.7)$$

5.3 Gas Flow and Pressure Pulsations

As briefly described above by Si Huang et al [132], his model was based on a analytic theoretical model of the operating cycle principle of "suction-compression-discharge-expansion" performance of an LRVP and was successful due to its isothermal advantages of the compression process and fluid acting as the seal, whereas Pfleiderer's [134] derivative for the "suction-compression -discharge" is based on the actual operating cycle of the LRVP and Figure 5-2 gives a brief overview of the Fundamental operation of the model. The model in Figure 5-2 (a) is structured into three processes; "suction, compression, discharge". The process starts with the suction stage at pressure PI_S curves 1-2 and stays constant until it attains q_{th} the highest suction capacity. The volume of the gas diminishes whilst the pressure rises till $\underline{PI_d}$ during the compression process curves 2-3. The discharge pressure $\underline{PI_d}$ during the discharge phase curves 3-4 stays constant until all the gas is released from the system. Figure 5-2 (c) relates to the zone in the LRVP and is partitioned into 4 segments in the following zonal order; segment *HCE* suction zone, segment *ECF* compression zone, segment *FCG* the zone, segment *GCH* the expansion stage, consequently some remaining gas q_0 which is remaining in the LVRP returns to the suction region after the gas has been discharged. The LVRP working principle is very similar to the RC. This remaining gas moves to q_e as shown in Figure 5-2 (b) and Figure 5-2 (c). In Figure 5-2 (b) it is shown as curve 4-1 and Figure 5-2 (c) represented as section *GCH, q*e which is also the expansion process.

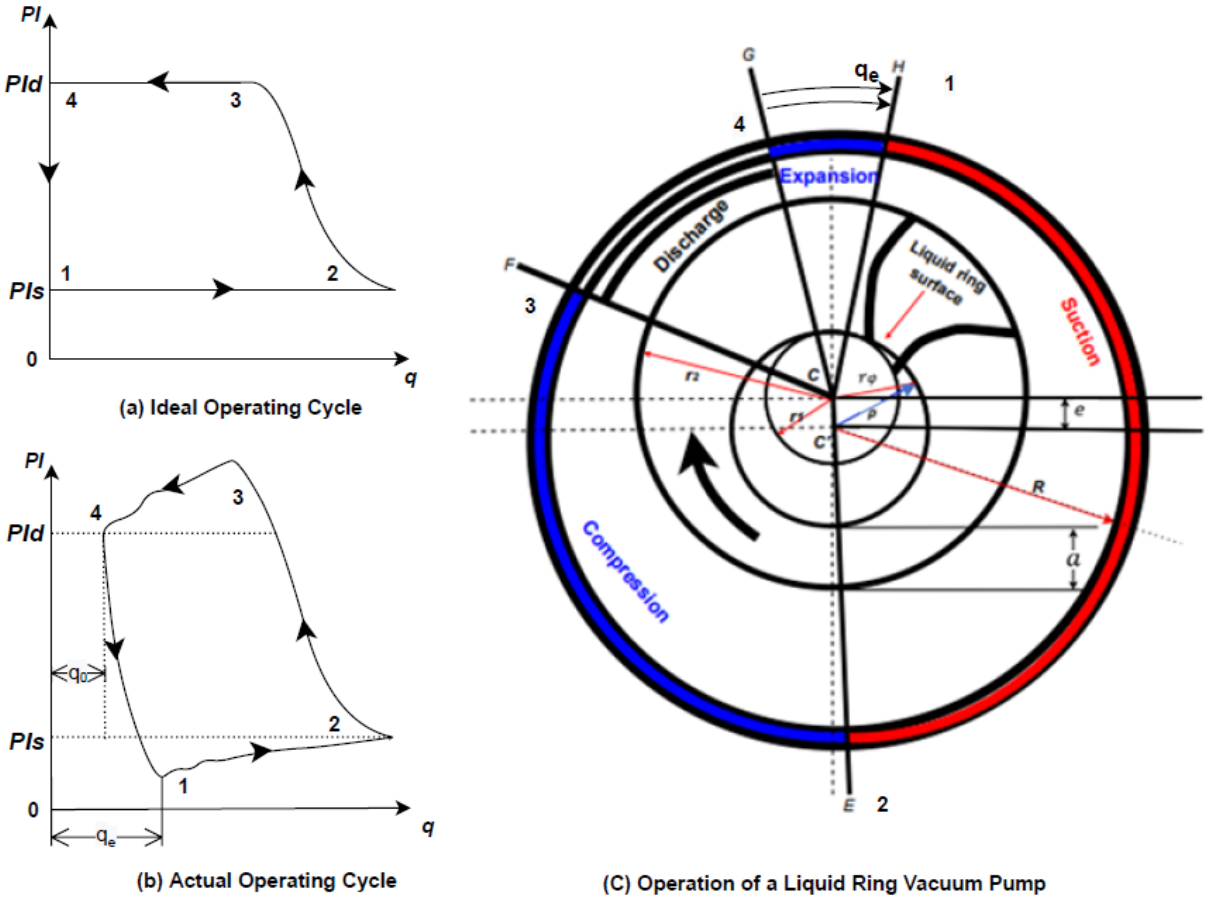

Figure 5-2 Operating Parameters of a Liquid Ring Vacuum Pump [132]

The suction volume in an LRVP equates to $q_s = q_{th} - q_e\ (if\ p_s \leq p_v, q_s = 0)$. The theoretical result differs from the practical as the remaining gas and its expansion phase were not take into consideration in the theoretical model from Figure 5-2 (a). From Figure 5-2 (c) the theoretical model includes an expansion stage based on Figure 5-2 (a) of the ideal operating model.

Each sector is briefly detailed and formulated below based on Figure 5-2 of the operating parameters of the LRVP.

1) Suction Phase

The distance from the centre of the impeller to any point on the LRVP surface in the suction area is described as:

$$r_{\varphi} = r_2 \sqrt{\frac{2(R-\rho)}{\mu r_2} + V^2} \tag{5.8}$$

Where,

$$\rho = r_2 \sqrt{1 + \left(\frac{e}{r_2}\right)^2 + 2 \ \frac{e}{r_2} \cos\varphi} \tag{5.9}$$

If the LRVP breathe-in to its maximum, the theoretical suction capacity q_{th} which is also described as the volumetric flow of gas passing through sector *CE* is:

$$q_{th} = \frac{1}{2} \mu\omega b r_2^2 \left[(1-\alpha)^2 - v^2\right] \tag{5.10}$$

2) Compression Phase

The distance from the centre of the impeller to any point on the LRVP surface in the compression area is defined as;

$$r_{\varphi} = r_2 \sqrt{\frac{(1-\propto)^2 + (\sigma - 1)\, v^2}{\sigma}} \tag{5.11}$$

The suction pressure to the compression ratio σ of the pressure at the angle of the circumference is;

$$\frac{1}{\sigma^2} = A^2 \left(1 - \frac{\sigma - 1}{\varepsilon}\right) \tag{5.12}$$

Where

$$A = 2(R-\rho)/\mu r_2 \left[(1-\alpha)^2 - v^2\right];\ \varepsilon = {g\omega^2 r_2^2}\Big/{2PI_S} \tag{5.13}$$

3) Discharge Phase

The distance from the centre of the impeller to any point on the LRVP surface in the discharge area is defined as;

$$r_{\varphi} = r_2 \sqrt{v^2 + \frac{2(R-\rho)}{\mu r_2} \quad \sqrt{\frac{1}{3}} \left(1 + \frac{1}{\varepsilon}\right)} \tag{5.14}$$

4) Expansion Phase

The distance from the centre of the impeller to any point on the LRVP surface in the expansion area can also be evaluated by (5.14). Consequently, the complete profile of the LRVP can be attained corresponding to equation (5.8), (5.11) and (5.14).

The volume of the return gas to the suction area of the LRVP is computed by equation (5.15) below where the circumferential angle is $\varphi = 2\pi$ to the middle of the blade and $r_{\varphi=2\pi}$ is the distance away from the surface of the liquid ring.

$$q_0 = \int_{r_1}^{r_{\varphi=2\pi}} \omega\, r b dr = \frac{1}{2}\mu\omega b\left(r_{\varphi=2\pi}^2 - r_1^2\right) \tag{5.15}$$

After a polytropic expansion procedure the volume flow of the gas alters from q_0 to q_e and goes through the following sequence:

$$q_e = q_0 \left(\frac{p_d}{p_s}\right)^{1/m} \tag{5.16}$$

The suction volume of the LRVP is now explained as:

$$q_s = \left(\frac{0}{\frac{1}{2}}\mu\omega b r_2^2[(1-\alpha)^{2-} v^2] - q_0 \left(\frac{p_d}{p_s}\right)^{1/m}\right) \quad \begin{matrix} p_s \leq & p_v \\ p_s > & p_v \end{matrix} \tag{5.17}$$

Now corresponding to the isothermal compression procedure, the discharge volume q_d can be expressed as:

$$q_d = \frac{q_s p_s}{p_d} \tag{5.18}$$

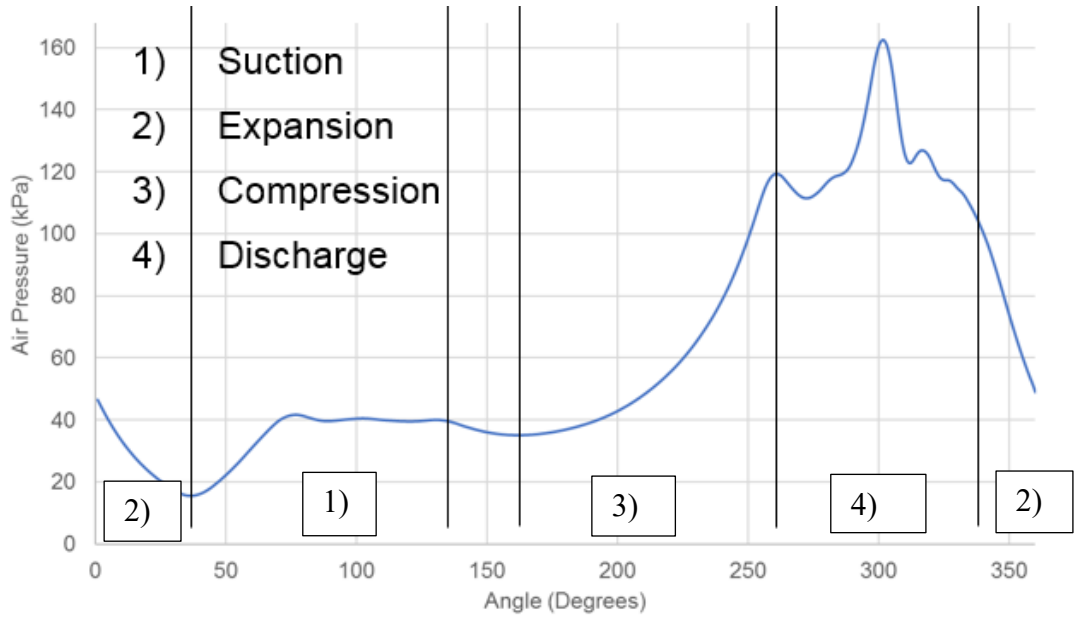

Figure 5-3 Gas pressure pulsations of a Liquid Ring Vacuum Pump [140]

Based on flow variations and pressure equations it is possible to obtain gas pressure pulsations in one impeller chamber. Figure 5-3 shows a typical pressure pulsation diagram from a Computational Fluid Dynamic (CFD) analysis. From this figure, it can be seen that the pressure

difference between suction and discharge phases are significant but is much smaller compared with a RC machine. Nevertheless, the pressure difference and flow vortex between the suction line and the suction port will couple acoustic waves into the suction line as does the discharge line and port. This effect will lead to acoustic vibration coupled not only to these two lines but to the housing structures and will produce vibrations.

Overall, as there are a series of intermittent such pressure pulsations, each being partitioned by the impeller blade, the total pressure pulsations, along with volume-flow rate, will still exist. Such pulsation will cause oscillations on the rotating shaft. Consequently, it will further lead to fluctuations of the impeller rotor system and thereby the Instantaneous Angular Speed (IAS) and motor current signatures.

5.4 Dynamic Effect of Liquid Ring

Due to the combined effect of centrifugal acceleration and gas pressures, the pressure distribution is not uniform. According to the Finite Element Analysis (FEA) based numeric study made by [140], quantitative pressure differences are typically in a range as depicted in Figure 5-4. The high pressure in the discharge phase can reach up to 320kPa and the low pressure just before such phase is as low as 210kPa. This biased pressure distribution means that there is a radial load applied to both the propeller rotor and the casing. Moreover, this load becomes higher at the tip of the impellers blade and lower at the gas chamber, which results in an impulsive force being applied to the casing and thereby induces casing vibration and acoustic radiations. Because of the higher pressure fluctuation and stronger fluid coupling this water ring induced vibration is much higher compared with that induced by gas pulsations. This water ring induced vibration can have a characteristic frequency f_w:

$$f_w = N_b f_r \pm f_r \tag{5.17}$$

Where N_b is the number of blade and f_r is rotor frequency. The sidebands are due to the biased pressure distributions. This shows that under steady operation the dynamic responses including casing vibration, airborne acoustics, rotor IAS and motor current will exhibit typical modulation contents which are common in many mechanical systems such as gear transmissions, rolling bearing and so on. Especially, this modulation becomes more significant when faults exist such as blade corrosions and increased bearing clearances which often cause further biased pressures.

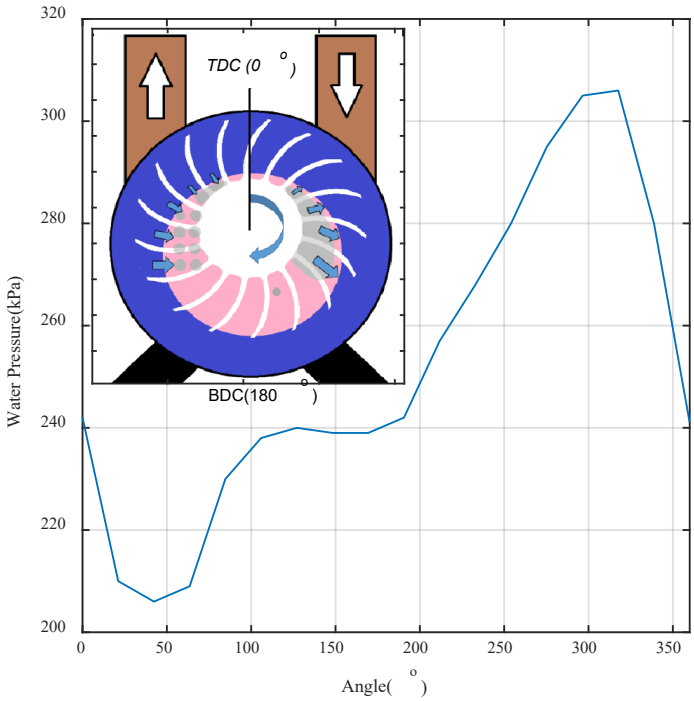

Figure 5-4 Water pressure pulsations of a Liquid Ring Vacuum Pump [140]

Another essential dynamic excitation is flow vortex. Because of interactions between water ring, blade tips, discharge ports etc there are strong vortices inside LRVP flow fields which are illustrated in Figure 5-5 from the FEA analysis carried out by [140]. These will be inevitably coupled to casing to generate vibration and acoustics. As the distribution of vortices are in a random and localised matter, the vibration induced often exhibit a broad band in a relatively high frequency range.

Overall, dynamic responses of a LRVP consists of both discrete and random components. The discrete or harmonic components are periodic according to blade number and rotation speed but modulated by rotation components. The random or irregular one is often in the high frequency range and can also be modulated by the rotation and blade components. As these high frequency components can often be magnified by the resonances of casing structures, it probably has a better signal to noise ratio for detecting and diagnosing faults due to defects in blade, casing and abnormal bearings.

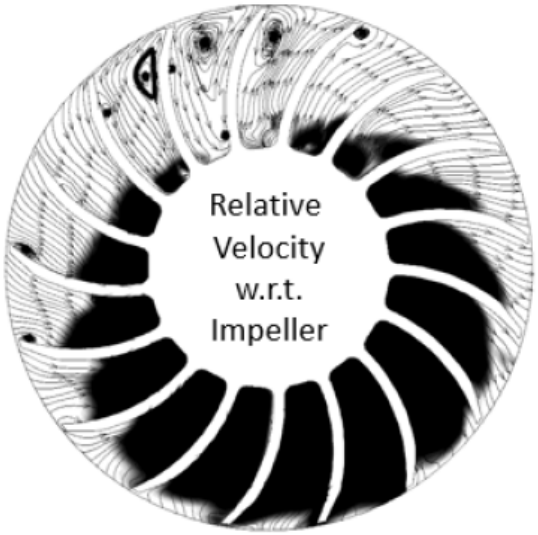

Figure 5-5 Flow fields inside of a Liquid Ring Vacuum Pump [140]

5.5 **Key Findings**

The Analytical Modelling analysis has not been reported on in as much detail as that of the RC in this chapter as these two types of fluid machines are both positive displacement pumps and most of the results from the RC can be applied to the LRVP studies. In particular they both share similar principles in terms of electrical, mechanical, fluid dynamic behaviours and operation to that of an RC in relation to the internal pressure oscillations as described partially in the qualitative results made in RC in Chapters 3 and 4. This can be referred to in conjunction to the LRVP data analysis. Section 3.8.1, Figure 3-10 demonstrates that the force variation and dynamics of the RC behave like an LRVP based on a single chamber where pressure varies in the suction, compression and discharge stages.

Chapter 6. **A Preliminary Implementation of Vibration and Acoustics Monitoring to an Industrial Environment**

This chapter gives an introduction of the industrial target machine in Phase II which is the Liquid Ring Vacuum Pump (LRVP), followed with a review of Condition Monitoring (CM) benefit, functionality and categories. An overview of the vacuum pump and its reliability is also explained followed by the current CM techniques applied to the target machine and a brief description of the actual CM used on the site. Moreover, it also presents the results of the preliminary study carried out for the three sets of vacuum pumps. In particular, high acoustic signals in the time domain allows the abnormal motor in one of the three sets to be indicated, which is confirmed by vibration analysis in both the frequency domain by spectrum and envelope analysis.

6.1 Industrial Target Machine

The LRVP is a key piece of equipment for many process industries such as petroleum, food and paper production, for creating vacuum. It is like a rotary positive-displacement pump but instead employs liquid as the main element in the gas compression. This compression is formed by the circulation of a ring of liquid around the casing of the multi-bladed rotating impeller which is eccentric between the pump casing and the rotating blade. During every revolution, each rotor chamber is partially filled and emptied creating a piston action within each set of the rotating impeller blades. This phenomenon is made possible due to the eccentricity of the design. The pump is designed in such a way that when the rotor chamber is emptying the liquid, it allows gas in and releases the gas when the compression is over. The LRVP uses only a certain amount of seal liquid to attain the vacuum and it's a one moving part with no metallic contact in the compression chamber [130],[141] as shown in Figure 5-1, chapter 5.2.

6.1.1 Vacuum Pump Categories

There are two main types of vacuum pump categories which are the gas transfer vacuum pumps and the trapping or entrapment vacuum pumps as shown below in Figure 6-1.

The following are just a brief overview of some of the vacuum pump types:

The Entrapment Vacuum Pump

The entrapment vacuum pump operates by trapping molecules within a confined space and may need regeneration as it is limited in its capacity [142].

The Gas Transfer Pump

The gas transfer pump is known as a positive displacement vacuum pump and the kinetic vacuum pump, using momentum to accelerate gas from the vacuum side to the exhaust side [142].

The Positive Displacement Pump

The positive displacement pump, suction side, has an expanded cavity on the discharge side. On the expansion of the suction side, cavity liquid flows into the pump, the cavity collapses and the liquid flows out of the discharge. The positive displacement vacuum pumps can be divided into two categories, namely the reciprocating displacement pump or the rotary vacuum pump [142].

Types of Vacuum Pump Used in Industry

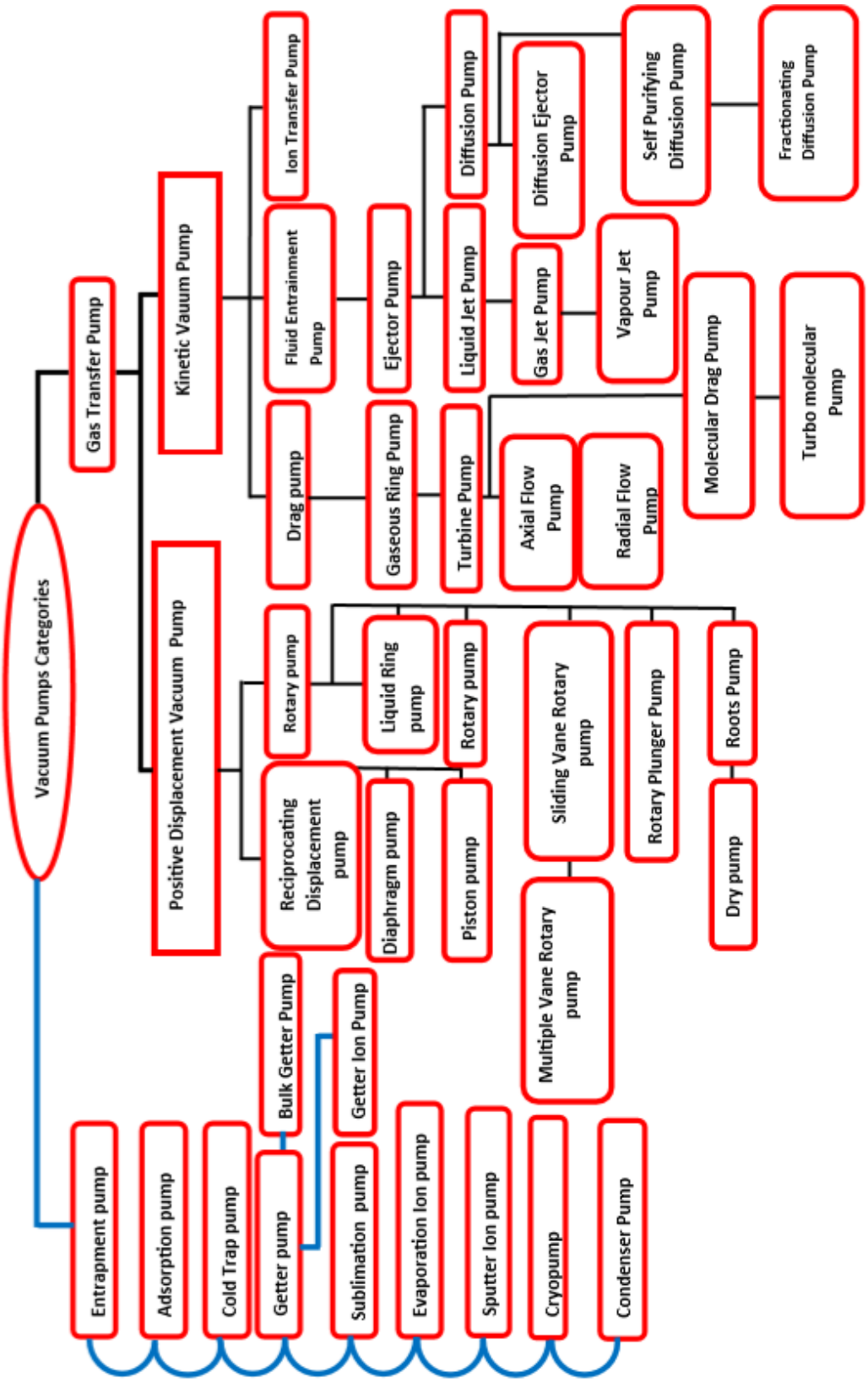

Figure 6-1 Types of Vacuum Pump [143]

The Kinetic Vacuum Pump

The kinetic vacuum pump is a pump in which the momentum is divulged to the gas or the molecules in such a way that the gas is transferred continuously from the inlet to the outlet [143].

There are two types of kinetic vacuum pumps, they are the fluid entrainment pumps and the drag vacuum pumps [143].

6.1.2 Common Failure Mode

In many systems, actuators are required to operate periodically so that some mechanical variable stays within a certain fixed range like a compressor or vacuum pump system. These systems are widely used in industrial facilities, aircraft and marine vessels and they have an air receiver or vacuum tank which ensures instant availability and provides for short periods of demand which is periodically charged by a compressor or pump creating a cycling system. These cycles create electrical power usage and follow a regular pattern of charging and discharging based on pressure.

The disadvantages that actuators can suffer in a cycling system is the detection of faults that cause the actuators to over operate. To alleviate this problem a model is developed to detect these effects and explain how changes in the controlled variable affect the operating schedule actuator [118]. Another disadvantage is that a common pump cannot be used due to different applications in different industries.

This has been made possible where there is both pressure and power in a representative cycling system aboard the USCGC Seneca. Whenever the (System Usage Event) SUE removes the vacuum from the system, a sharp drop is observed in the measurement of the vacuum pressure and when the number of SUE's increase, the discharge period shortens and the number of pump runs increases. However, the aim of Robert William Cox thesis was mainly to model the cycling system in determining the behaviour of the actuator under both faulty and non-faulty conditions [118].

Mahmud applied seven compressor fault types to a compressor mainly with valve, intercooler leakage, belt slippages and combined faults. The advantages of applying these faults may be useful to the vacuum pump with a belt but most vacuum pumps do not have a valve or intercooler hence these may not be possible [56].

At the 69th Conference of the Italian Thermal Machines Engineering Association, Stiaccinia, et al [119] developed a numerical model for the analysis of a reciprocating compressor coupled with its pipelines. The prime feature of the model is to couple the time-domain computation of the thermodynamic cycle of the reciprocating compressor with the frequency domain modelling of the pipeline systems.

The advantage of the multi-domain interaction is the possibility of modelling a compressor with a quasi-steady time-domain approach and the pipelines with an acoustic approach, this will allow the modelling of complex pipelines configurations with a linear equation system. The model proves that the computational tool is reliable and fast for the thermodynamic and acoustic analysis of the reciprocating compressor plants considering the mutual interaction between the compressor and its pipelines [119].

Zhen Dong presents the use of dynamic time warping (DTW) to process the motor current signal for detecting and quantifying common faults of a two-stage reciprocating compressor.

The advantage of using this technique is that the DTW suppresses the supply frequency component and highlights the sideband components, based on the introduction of a reference signal, which has the same frequency components as the power supply. The sideband components contain more useful information for the indications of faults and conditions of the monitored machine [120].

6.1.3 Condition Monitoring Benefit

LRVP's are used in a lot of process industries such as the petrochemical, pharmaceuticals, chemicals, food and paper industries as they are versatile machines and can handle "wet loads". The production of paper is a highly competitive industry and the mill cannot afford any unpredicted breakdowns which would lead to unscheduled downtime. To prevent this and ensure the smooth running of the production, the correct condition monitoring techniques should be applied to the machine.

The following savings, by avoiding the loss of production and unscheduled maintenance, means a very good and quick payback on the initial investment in monitoring the equipment. This will, in turn, create a big impact on high maintenance and operational costs.

If the LRVP is monitored by the appropriate techniques and inspected at the correct time intervals, the machine will be more reliable and not only be more efficient but the approximate time of when to send the pumps for refurbishment would be known instead of replacing the

pump earlier than its natural end of life. This would also reduce the maintenance budget and reduce the risk of any unscheduled downtime.

6.2 Current Monitoring Techniques used in Vacuum Pump

The current monitoring techniques used in the vacuum pump nowadays is vast. Some companies are now introducing an online vibration monitoring system that is easy to operate, easy to install and available at a price that would make it an option as standard equipment. An example is the 'Fag Smart check' which is good for the detection of problems such as bearing wear, unbalance, misalignment and caking on the vacuum pump depending on its application [144]. Like the above example, the 'Fab Works-iMS' is a web-enabled remote monitoring package for the Edwards vacuum pump [145], the 'EBANET3' which is for the monitoring of a dry vacuum pump [146]. 'PRUFTECHNIK' which has developed a monitoring system of the vacuum pump for paper machines aimed for Gardner Denver Nash Deutschland GmbH, that measure the frequency-selective recording of machine vibration, roller bearing monitoring, in-depth diagnosis using analysis of vibration spectra, envelope spectra and time signals, temperature measurement at pump bearings and water supply motor current and the rotational speed, pressure on suction and pressure sides [147]. Also, a vast amount of research has been done in the monitoring of a dry vacuum pump such as: using the statistical method [148], monitoring of dry vacuum pump characteristics by a mobile device [149], a (LabVIEW) based system for CM of a dry vacuum pump using AR modelling techniques [150], but there has been little work done on the wet liquid vacuum pump, more specifically in the field of Surface vibration and instantaneous angular speed based performance monitoring.

6.2.1 Reliability of Vacuum Pumps

There are multiple criteria which can influence the performance of a vacuum system. It is imperative to maintain the vacuum pump system and all its parts including the upstream and downstream pipeline. Any minor leakage will affect pump performance. Most of the common problems encountered in the vacuum system could be due to some of the following possibilities:

- A variation in the utility specification
- The malfunctioning of a part not doing what it is supposed to do
- An inconsistency in the process conditions and variations
- Loss of fluid in the system.

For the vacuum pump to operate in a good condition, care should be taken to ensure good operation of the vacuum system. Appadoo et al show a brief overview of some common problems and the causes and effects encountered in the liquid ring vacuum pump, together with a suitable troubleshooting approach which is explained through the failure analysis method [151].

6.3 Target Machine

At the paper mill facility, two measurements are recorded by the data collector at each point of the pump's system. They are the velocity and acceleration measurements. Each system is divided into three subsections, the motor, gearbox and pump and Figure 6-2 shows the existing facility layout of the pumps.

Figure 6-3 shows the layout of the three pumps position and gives the exact location of the data collection point of each pump.

Each system has nine points of readings that are taken and hence seventeen measurements per system which is explained below. As for position 1 DE from Figure 6-5 below, only one axial velocity data is captured. Samples will be taken on three different pumps; the M243 Dewatering Box Vac Pump, M256 Tail Cutter Box Vac Pump and the M242 the Trans Shoe/ "Uhle" Box Vac Pump.

Readings are taken at various positions on the motors.

At position 1 Non-Drive End (NDE) two sets of readings, the vertical velocity and vertical acceleration trend are being collected.

At position 2 Drive End (DE) two sets of readings are again taken, the vertical velocity and vertical acceleration trend and the motor have only one axial velocity reading taken at position 2 DE.

Position 3 is the Input Gearbox (GBI), horizontal velocity and horizontal acceleration trend.

Position 4 is (GBI), horizontal velocity and horizontal acceleration trend.

Position 5 is Output Gearbox (GBO), horizontal velocity and horizontal acceleration trend.

Position 6 is GBO, horizontal velocity and horizontal acceleration trend.

Position 7 is the pump DE, vertical velocity and vertical acceleration trend.

Finally, position 8 is the pump NDE, vertical velocity and vertical acceleration trend.

Figure 6-5 and Figure 6-6 below show the measurement of the three pumps taken on the 10th of July 2015 by the onsite CM team.

Samples were also taken by the author on that same date which is shown further in chapter six which will conclude the effectiveness of the measurement through a thorough analysis.

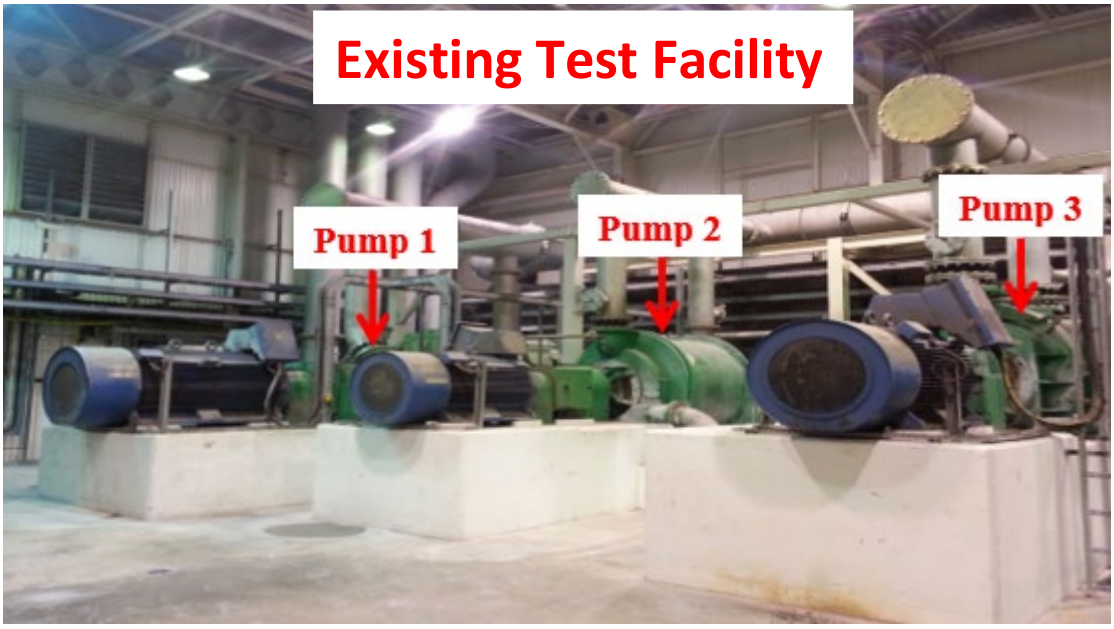

Figure 6-2 Existing Test Facility

The layout of the three Pumps and Sensors Position

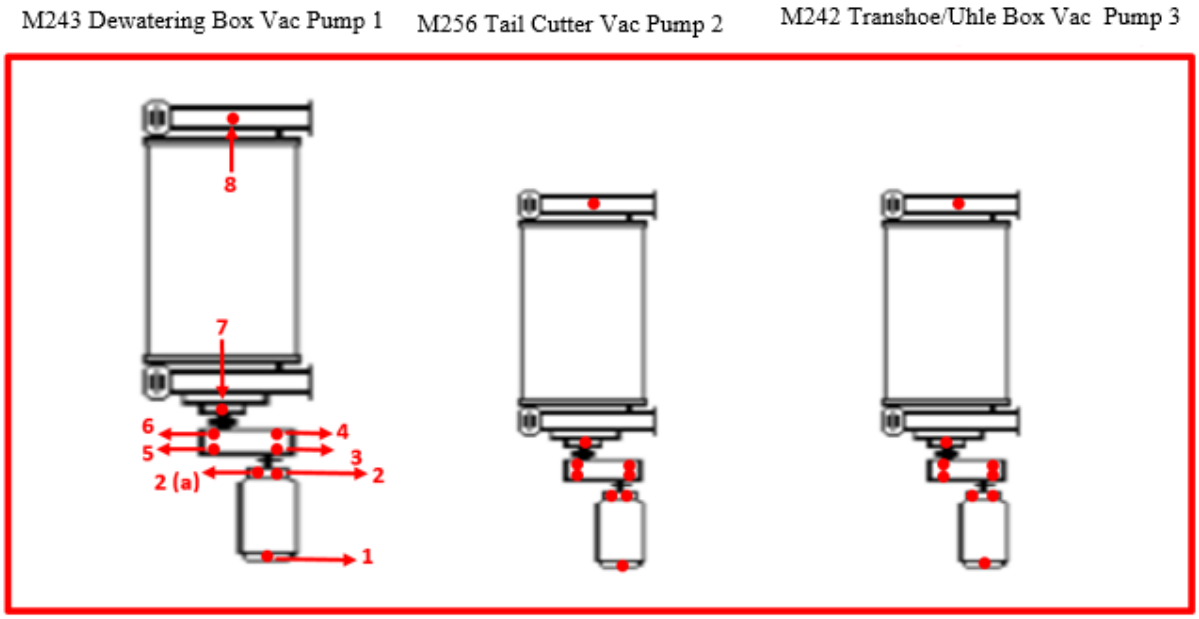

Figure 6-3 Pump and Sensors Position

6.3.1 The Data Collector Dynamix 2500

The Data Collector

Figure 6-4 The Data Collector Dynamix 2500

The 'Dynamix 2500' data collector as shown in Figure 6-4 is the device that the CM team used to gather all the information from the system in the existing test facility. This device is known to be good for the diagnostic and trending of machine vibration measurements on machines like motors, compressors, pumps, gearboxes, fans, mixers, centrifuges, hammer mills. It is also effective in the analysis of various operation such as unbalance in a machine, the remote analysis of time recordings of a machine's vibration and much more [152]. The device has a wide variety of features, it can operate in 10.50°C (14.122°f) temperatures ranges, it is also certified for "ATEX Zone 2" and "IEC Ex" for hazardous environments equipped with a sunlight-visible colour LCD, offers Mil-spec drop rating and "IP65" sealing.

6.3.2 M243, 2nd Dewatering Box Vac Pump Trend

Only the M243 velocity and acceleration trend captured by the CM team on site is shown here as an indication to the level of analysis.

Velocity Trend

Figure 6-5 shows the vertical velocity trend of position 1 and if the blue trend is lower than the yellow alarm level this indicates that there is no problem, however, if it is higher than the alarm level, then the frequency spectrum needs to be analysed as this trend will determine which part of the machine or components is causing the vibration to increase by the peaks Fast Fourier Transform (FFT), Ball Spin Frequency (BSF), Ball Pass Frequency Outer Race (BPOR), Ball Pass Frequency Inner Race (BPIR) and running motor speed.

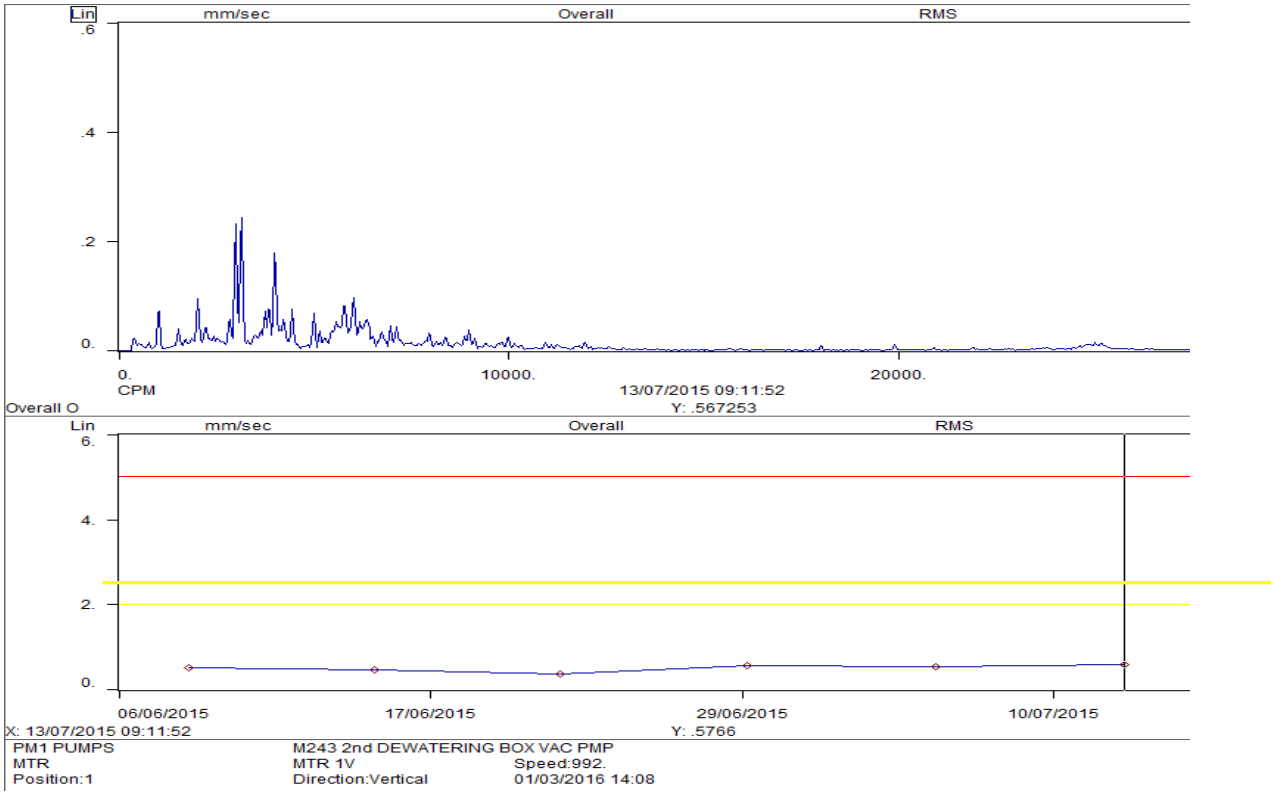

Figure 6-5 Motor Position 1 Velocity Trend

Acceleration Trend

The same applies for Figure 6-6 to the vertical acceleration trend of motor position 1. If the blue trend is lower than the yellow alarm level this shows that there is no problem but if it is higher than the alarm level then the frequency spectrum needs to be analysed as this trend will determine which part of the machine or components is causing the vibration to increase by the peaks (FFT, BSF, BPOR, BPIR and running motor speed).

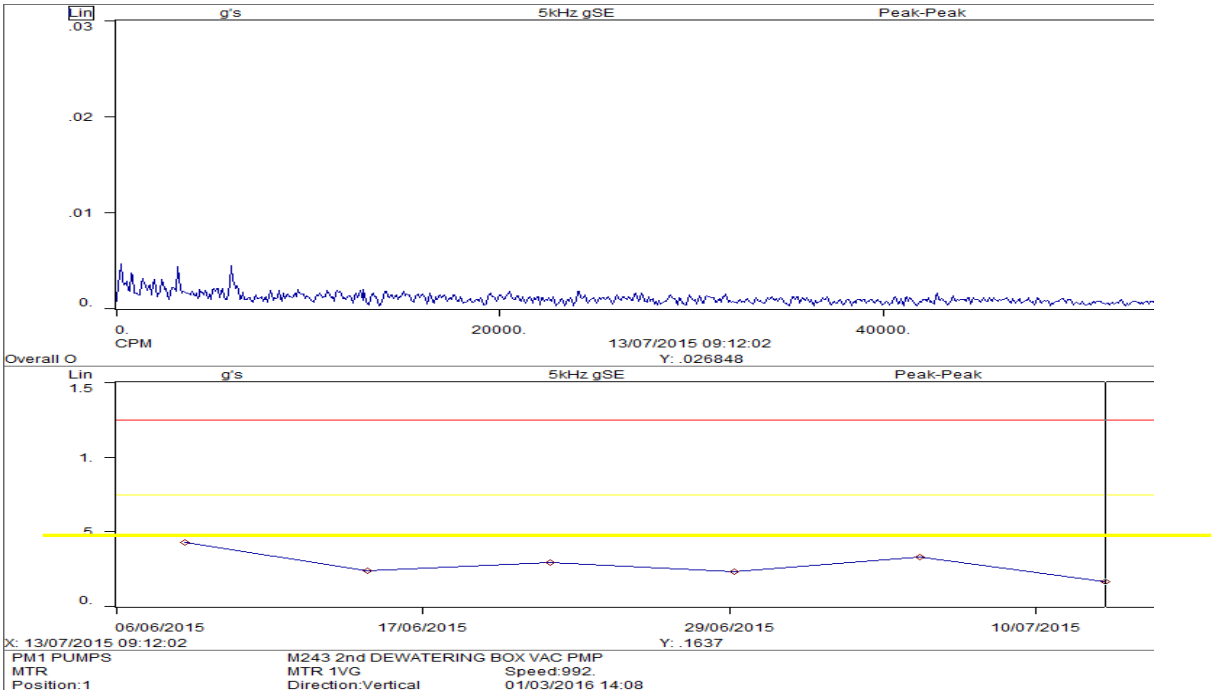

Figure 6-6 Motor Position 1 Acceleration Trend

6.3.3 On-Site CM Recommendation

See each position representation below:

- Position 1 vertical velocity and acceleration, NDE
- Position 2 vertical velocity and acceleration, DE
- Position 2 only one axial velocity, DE
- Position 3 input gearbox horizontal velocity and acceleration, GBI
- Position 4 input gearbox horizontal velocity and acceleration, GBI
- Position 5 output gearbox horizontal velocity and acceleration, GBO
- Position 6 output gearbox horizontal velocity and acceleration, GBO
- Position 7 pump vertical velocity and acceleration, DE
- Position 8 is the pump position vertical velocity and acceleration, NDE

M243, 2nd Dewatering Box Vac Pumps and for the remaining positions of this pump the trends are similar to the above Figure 6-5 and Figure 6-6 of the velocity and acceleration. The trend does not exceed the alarm level, yellow line.

Same as above applies for the M256 Tail Cutter Box Vac Pump 2 and M242 Transshoe/ "Uhle" Box Vac Pump where there is no discrepancy according to the CM report from the onsite team. The following report from Figure 6-7 dated 09/04/14 below explained of a recommendation that was made of the dewatering box vacuum pump where the bearing vibration level has increased. The pump bearing was supposed to be inspected at the earliest opportunity but as the CM report is generated every month the damage was quick to turn into a catastrophic failure causing the plant to ground to a halt at that time. See Appendix 1 for the picture taken on 24/04/14 of the damaged shaft impeller and build-up of limescale.

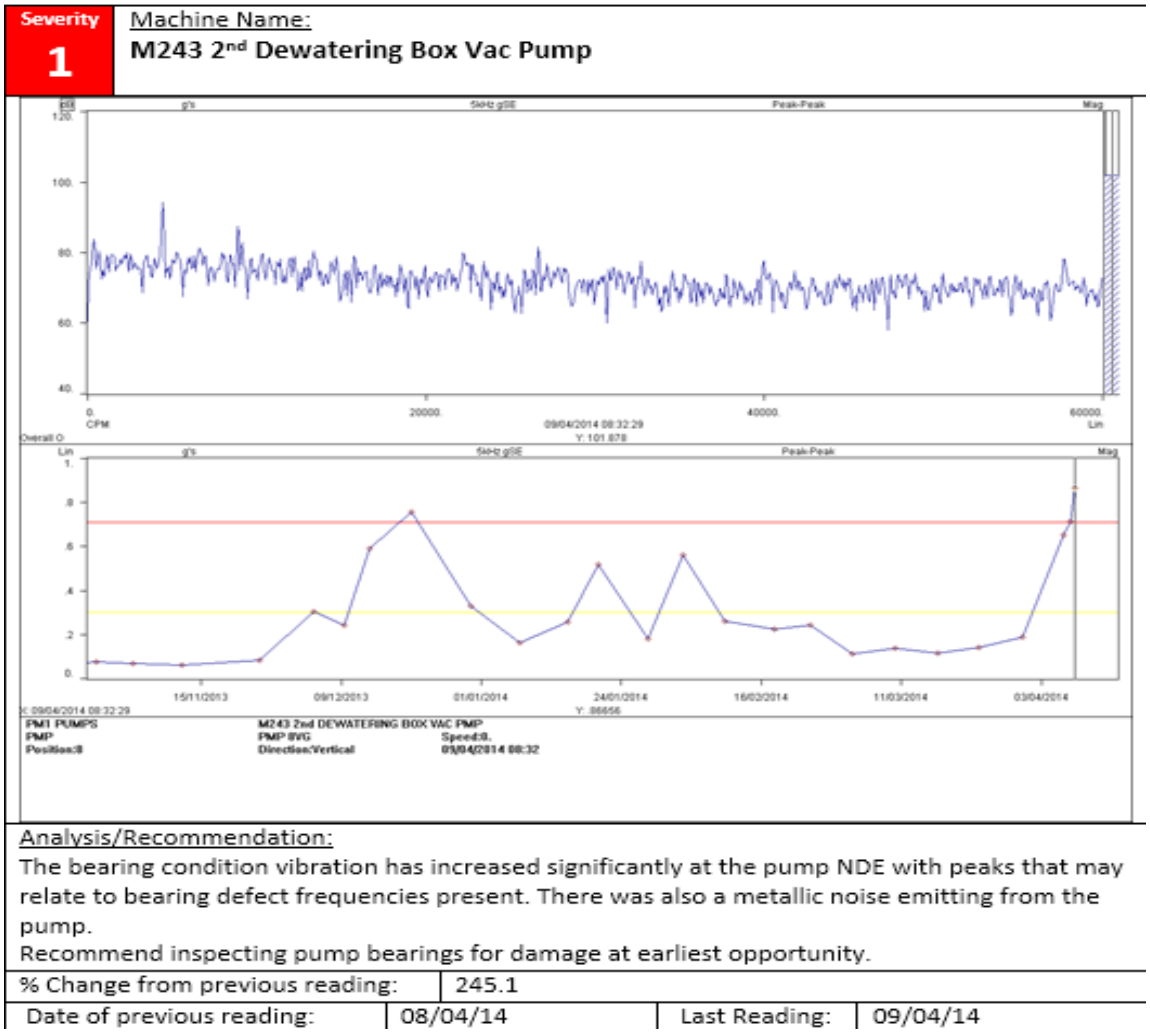

Figure 6-7 M243 Dewatering Vacuum Pump Report of 09/04/14

6.4 Discussion

Machine failures can easily occur causing an adverse effect on the maintenance costs and an increase in the loss of production therefore the level of interest in condition monitoring is vital. This system enables the company to monitor each critical piece of equipment and has its own

holistic and personalised condition management programme. This new technology data is accurate and the algorithms that are used are precise and reliable in assessing equipment condition enabling prediction and accurate diagnosis of equipment failure. In the meantime, many different techniques have been developed for condition monitoring. However the performance of techniques is highly application dependent. A huge variety of techniques have been developed to diagnose and monitor any dynamic and static machinery such as the Ultrasonic Analysis, Wear Debris Analysis, Oil Analysis, Vibration Analysis the Motor Current Signature Analysis which is the 'MCSA'.

The wet liquid ring vacuum pump remains an area where not enough research has been done in advance signal monitoring hence the reason this has led the author to embark into this area of research. Particular attention was also drawn to the incidents that occurred in 2014 as explained in Section 1.1 which has been a good motivational area of study. In Phase II of the preliminary research, after a qualitative study and fault mode analysis of these pumps, a field test was conducted to verify the feasibility of the scheme in terms of sensor installations, performances, data acquisition methods, system specification and fault diagnosis admissibility.

The reason for the three machines chosen is because one of those pumps had a serious issue in 2014 due to it degrading so fast and failing just in a matter of weeks soon after it was captured by the CM team on-site. The solution is to find a better approach to diagnosing and accurately localising the fault before it fails, to do a cross-comparison within the three systems and differentiate their condition based on the techniques that will be applied in the field implementation plan of Phase II and to prove the feasibility of the techniques by applying it to the target machines to examine the suitability and performance during the full course of a CM process by studying and applying the:

- Measurement system specification
- Data acquisition definition and implementation
- Data analysis method selection and evaluation
- Detection and diagnosis performance confirmation.

6.5 Implementation of Vibration and Acoustics Monitoring of the Industrial Machines

6.5.1 Test Facility

The plant room consists of three systems. Each structure has a set of equipment working together as part of a mechanism which transmits power to the Liquid Ring Vacuum Pump (LRVP) to operate. Every structure comprises of an electric motor, gearbox and vacuum pump. Samples will be taken from the three different systems. The first pump is driven by an 850kW motor and the remaining two are driven by two 400 kW electric motors. A risk assessment has been done before working with these machines and the area is regularly checked by the relevant engineering department to ensure safety is met.

6.5.2 Characteristics of the Vacuum Pump

Vacuum is used on different locations of the paper machine and at different stages in the papermaking. The three vacuum pumps are laid horizontally and the electric motors, gearboxes and pumps are shown in Figure 6-2 and Figure 6-3 respectively. The specifications of the systems are found in Table 6-1 and Table 6-2 correspondingly.

Table 6-1 Specification of the 850-kW Motor, H1 SH 13 type Gearbox Nash Model Pump 'P2620'

Motor Specification		Gear Box Specification		Pump Specification	
Power	850kW	Types	H1 SH 13 B	Nash Model	P2620
Voltage	3300V	N1	994	Pressure Differential Max	15 PSI
Frequency	50Hz	n2	245.43/min	Temp Design	60° F
Speed (rpm)	930	VG	320	Temp Max	200° F
Current	178A	Weight	2450Kg	Bearing Type	Timken Assy 092A4 both the Drive end and Non-Drive end
Bearings: Drive end:	6326/C3	Power	685 KW	Speed design	RPM 225/225
Non-Drive end	6324/C3	Oil	175		
Power factor	0.86			Speed Max	RPM 227/227
Phases	3			Speed Min	RPM 180/200
Weight	5600Kg				

Table 6-2 Specification of the 400kW Motor, H1 SH 9 B type Gearbox Nash Model Pump '904U1'

Motor Specification		Gearbox Specification		Pump Specification	
Power	400kW	Types	H1 SH 9 B	Nash Model	904U1
Voltage	3300V	n1	992/min	Pressure Differential Max	15 PSI
Frequency	50Hz	n2	244.14/min	Temp Design	60° F
Speed (rpm)	930	VG	320	Temp Max	200° F
Current	87A	Weight	2450Kg	Bearing Type	Timken Assy 092A4 both the Drive end and Non-Drive end
Bearings: Drive end:	6324/C3	Power	325 KW	Speed design	RPM 225
Non-Drive end	6319/C3	Oil	68		
Power factor	0.84				
Phases	3			Speed Max	RPM 227
Weight	3000Kg			Speed Min	RPM 180

6.5.3 Instrumentation and Measurement

Different types of measurement equipment were used to measure the target machine and positioned at different locations of the system depending on the context of use. Table 6-3 shows the equipment utilised during the study and each component will be briefly explained below.

Table 6-3 Equipment/Material used

Equipment		
Equipment/Material	Type of equipment	Quantity
4-Channel Data Acquisition	YE 6231	1
Vibration Sensors	CA-YD-185	3
Microphone	CHZ-211	1
Microphone Stand	Microphone Stand	1
Glue for vibration Sensor	Glue	1
Cables	Cables	50 meters

Piezoelectric Accelerometer/Vibration Sensors

Three of the vibration measurement sensors type "CA-YD-185" were utilised with a frequency range of 0.5 to 5,000Hz at three different sensitivities as shown in Table 6-4 below.

The sensors are capable of withstanding temperatures of up to 120°C and acceleration of up to 1000ms^{-2} and are ideal for this kind of environment. They were used for the motor Non-Drive End (NDE), motor Drive End (DE), Gearbox Input (GBI), Gearbox Output (GBO), pump Drive End (DE) and pump Non-Driven End (NDE) to measure the vibration level. These vibration signals are then transferred to the data acquisition to be recorded and Figure 6-8 below shows the accelerometer used during the investigation.

Figure 6-8 Vibration Sensor

Table 6-4 Vibration Sensor Specification

Characteristics of sensor CA-YD-185
Sensitivity: 20 ± 5° C
Sensor (1) =4.93; % mv/ms-2
Sensor (2) =4.98; % mv/ms-2
Sensor (3) =5.0; % mv/ms-2

The Microphone

The specific device used to measure the acoustic signal is a ½ inch microphone, type "CHZ-211" as shown in Figure 6-9 below with the frequency response characteristic of 20 to 20 kHz and the microphone specification is illustrated in Table 6-5 below. The microphone was selected due to its capability and suitability for the type of environment. The microphone was used to monitor the gearbox and pump airborne sound. The acoustic signals are then transferred to the data acquisition.

Figure 6-9 Microphone

Table 6-5 Microphone Specification

Microphone Type: CHZ-211
Sensitivity: 52.0 mV/Pa
Temperature -20° C to 60°C
Frequency range: 20-20kHz
Dynamic range: SPL blow which the total harmonic distortion < 3%: 146Db

4-Channel Data Acquisition

Figure 6-10 Data Acquisition

The data acquisition used for this project is a data logger and analysis system model YE6231 and is illustrated in Figure 6-10. It is a 4 channel, 24-bit resolution, synchronised acquisition at 100 kHz per channel with continuous sampling length and a maximum of four units can be used by one Personal Computer (PC).

6.5.4 Experiment Plan

The sensors and microphones have been positioned at different locations on the target machine during the data collection process and Figure 6-11 gives an overview of the precise locations of where the test samples have been taken.

Table 6-6 shows the legend and the measurement sensor position as described in Table 6-7

Three tests were being carried out on three different sets of machines.

Dewatering Box Vacuum Pump Experiment Plan

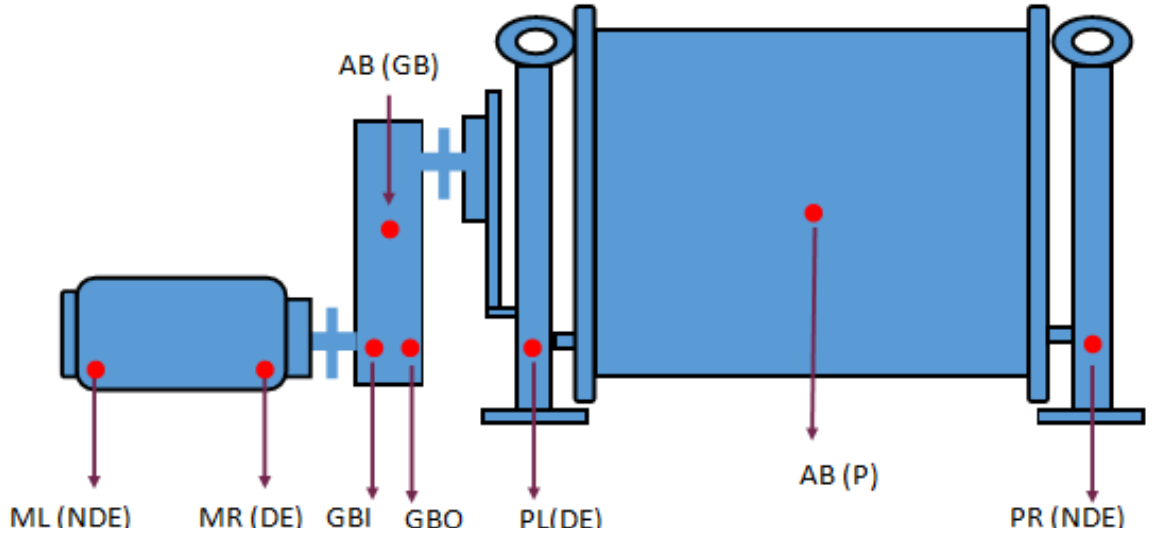

Figure 6-11 Dewatering Box Vacuum Pump

Table 6-6 Legend

Legend					
Motor		Gearbox		Pump	
ML (NDE)	Motor Left Non-drive end	GBI	Gearbox Input Left	PL (DE)	Pump Left Drive end
MR (DE)	Motor Right Drive end	GBO	Gearbox Output Right	PR((NDE)	Pump Right Non-drive end
		AB (GB)	Airborne Sound Gear Box	AB (P)	Airborne Sound Pump

Sensor Layout

Table 6-7 Measurement Sensor Position

Test No.	Position	Vibration	Acoustics
1	Left	VM1L, VG1L, VP1L	AG1
	Right	VM1R, VG1R, VP1R	AP1
2	Left	VM2L, VG2L, VP2L	AG2
	Right	VM2R, VG2R, VP2R	AP2
3	Left	VM3L, VG3L, VP3L	AG3
	Right	VM3R, VG3R, VP3R	AP3

The acronyms are explained as follows :

- VM1L: Vibration Motor 1 Left
- VM1R: Vibration Motor 1 Right
- VG1L: Vibration Gearbox 1 Left
- VG1R: Vibration Gearbox 1 Right
- VP1L: Vibration Pump 1 Left
- VP1R: Vibration Pump 1 Right

6.5.5 Data Collection and Processing Procedure

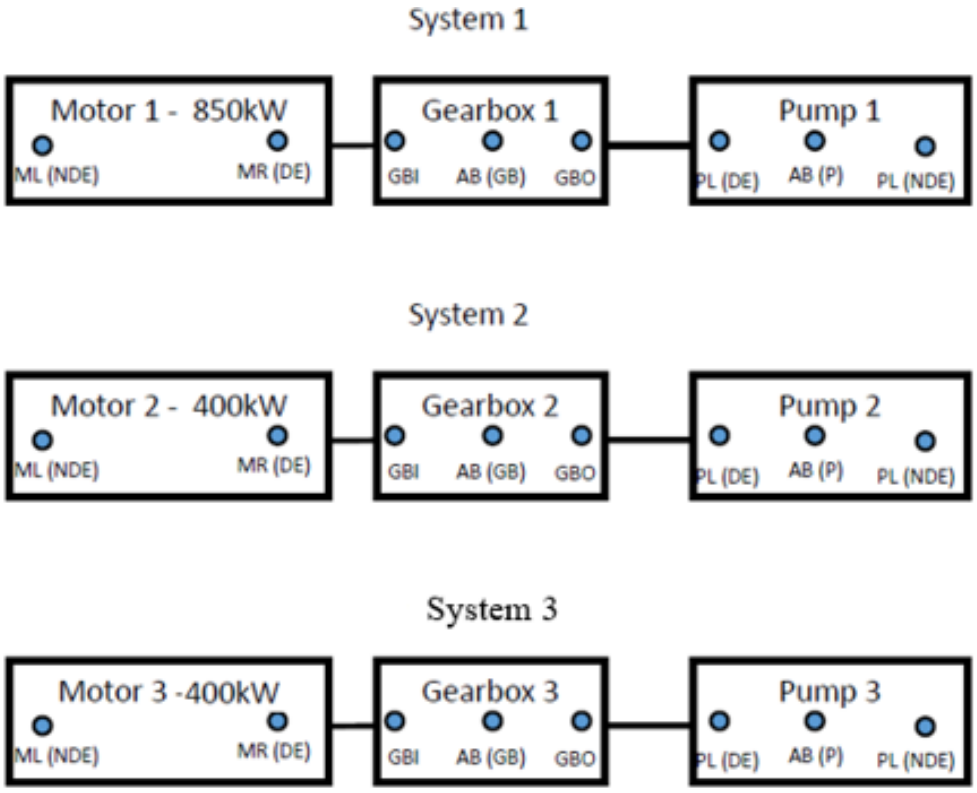

Legend					
Motor		Gearbox		Pump	
ML (NDE)	Motor Left Non-drive end	GBI	Gearbox Input Left	PL (DE)	Pump Left Drive end
MR (DE)	Motor Right Drive end	GBO	Gearbox Output Right	PR((NDE)	Pump Right Non-drive end
		AB (GB)	Airborne Sound Gear Box	AB (P)	Airborne Sound Pump

Figure 6-12 General System Layout

The data was collected on the actual machines whilst they were running, below is the process for the data collection. Figure 6-12 shows the general system layout of the test system and Figure 6-13 illustrates the Schematic of the Data Acquisition.

The test has been performed according to the following sequences as shown from Figure 6-14 to Figure 6-21. This gives a visual understanding of the geographical position of the sensors laid on the machine whilst under observation.

The data recording time for the data collection process is 30 seconds at a sampling rate of 96 kHz, the higher the sampling frequency used the better with 96 kHz being the highest on that data acquisition.

To achieve advanced signal processing, the average of the signal is required and will be separated into numerous segments. To obtain a higher frequency resolution the signal should be recorded for a longer period.

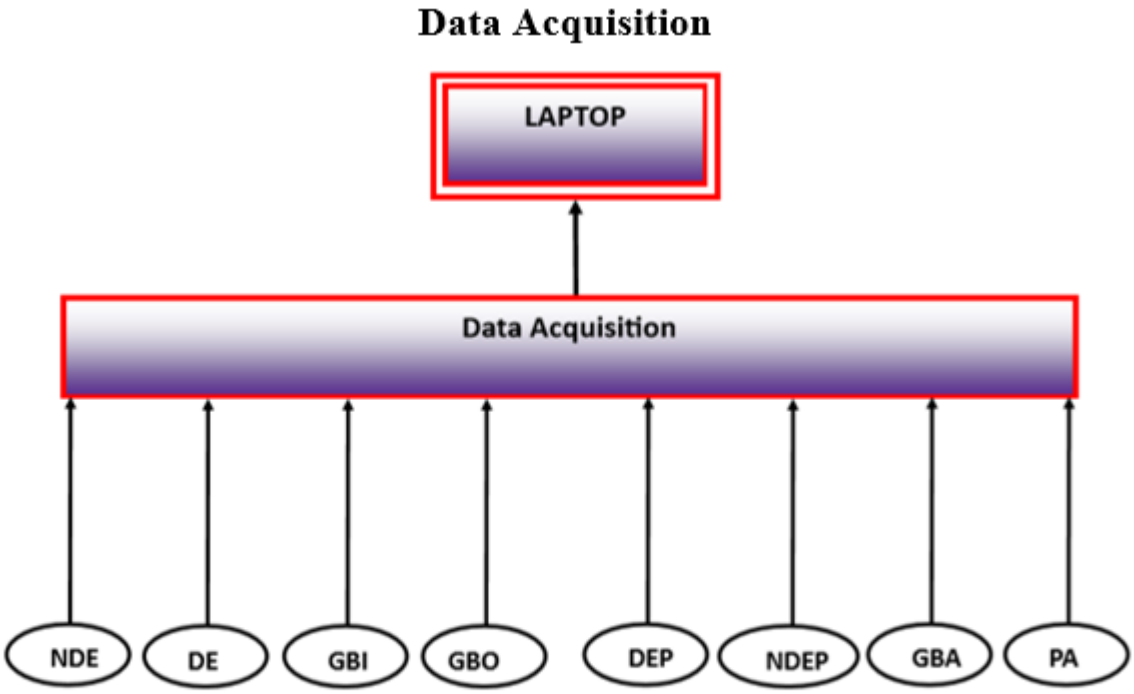

Data Acquisition Legend	
NDE: Non-Drive Motor	DEP: Drive End Pump
DE: Drive End Motor	NDEP: Non-Drive End Pump
GBI: Gearbox Input	GBA: Gearbox Acoustics
GBO: Gearbox Output	Pump Acoustics

Figure 6-13 Schematic of Data Acquisition

In this experiment, three sets of tests have been carried out. Each test is repeated five times to secure a reliable and accurate result and this will be explained fully in the following sub-section of this chapter.

For the test system no. 1, the Motor 1, Gearbox 1 and Pump 1 were under observation and the samples were taken in the following order:

1.1) Vibration of Motor 1 left (NDE), Gearbox Input 1 left, Pump (DE) 1 left; Acoustics for Gearbox 1

1.2) Vibration of Motor 1 right (DE), Gearbox Output 1 right, Pump (NDE) 1 right; Acoustics for Pump 1

The following test system no. 2, the Motor 2, Gearbox 2 and Pump 2 were under observation and the data taken in the following order:

2.1) Vibration of Motor 2 left (NDE), Gearbox Input 2 left, Pump (DE) 2 left; Acoustics for Gearbox 2

2.2) Vibration of Motor 2 right (DE), Gearbox Output 2 right, Pump (NDE) 2 right; Acoustics for Pump 2

Finally, for the test system no. 3, the Motor 3, Gearbox 3 and Pump 3 were under observation and the samples logged in the respective order:

3.1) Vibration of Motor 3 left (NDE), gearbox input 3 left, pump (DE) 3 left; acoustics for gearbox 3

3.2) Vibration of Motor 3 right (DE), gearbox output 3 right, pump (NDE) 3 right; acoustics for pump 3.

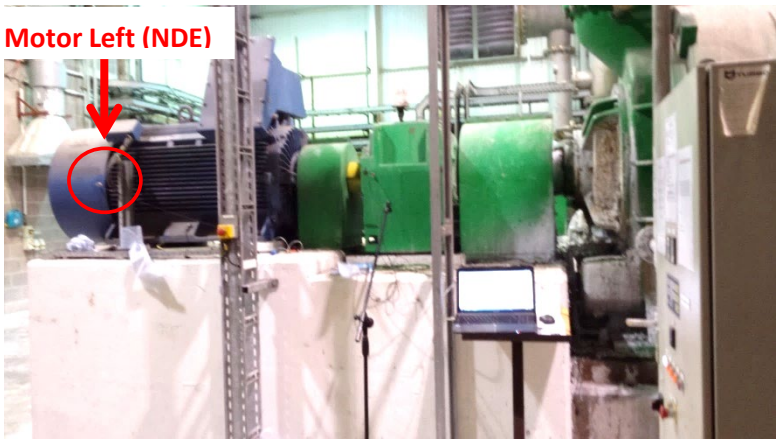

Figure 6-14 Motor Left (NDE)

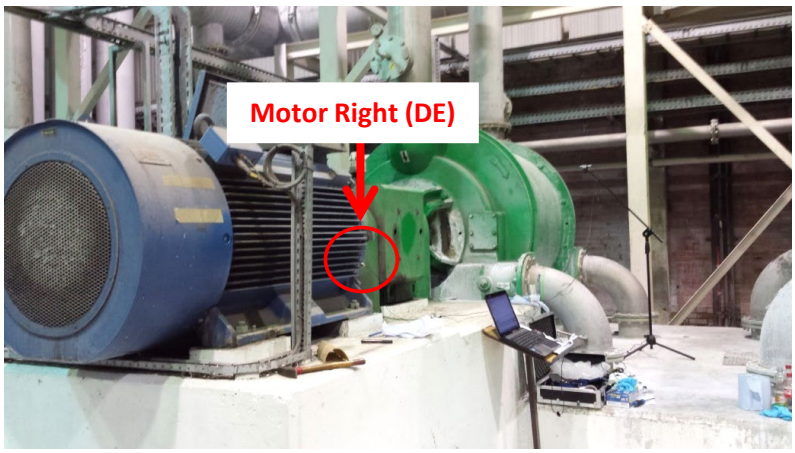

Figure 6-15 Motor Right (DE)

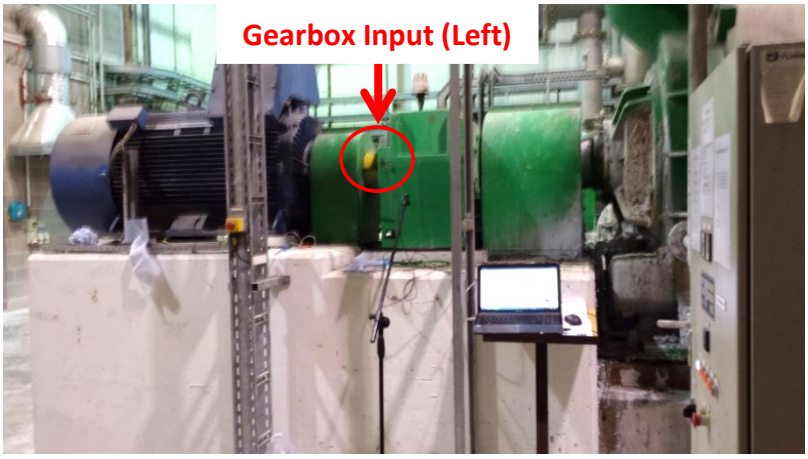

Figure 6-16 Gearbox Input Left Position

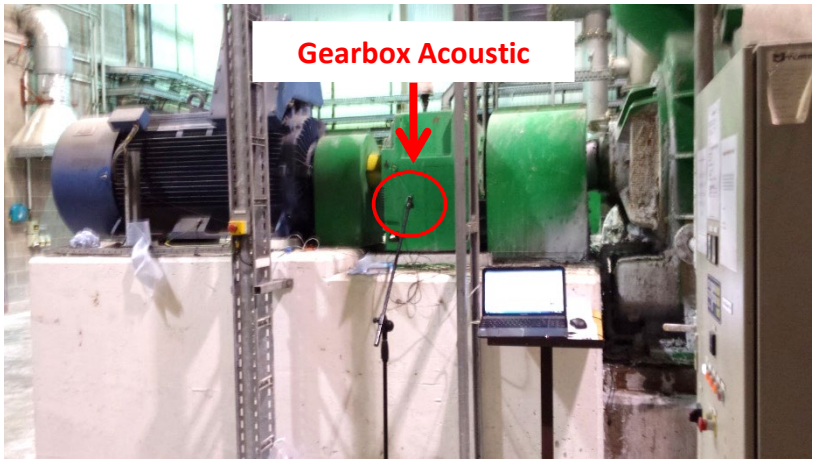

Figure 6-17 Gearbox Acoustic

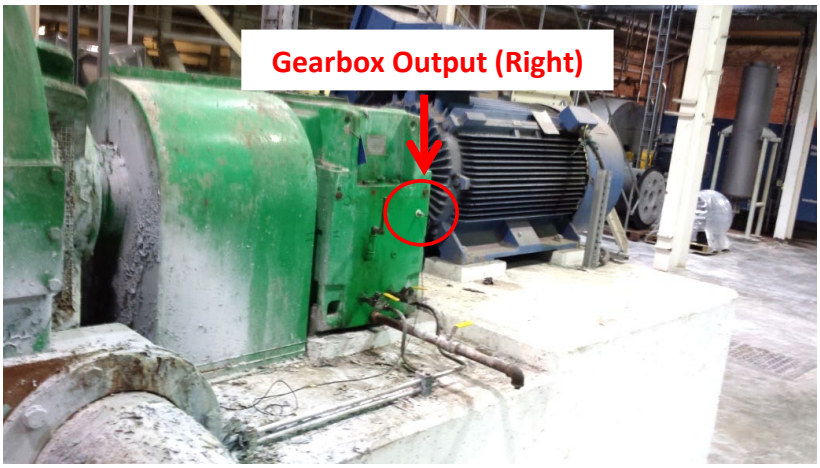

Figure 6-18 Gearbox Output Right Position

Figure 6-19 Pump (Drive End)

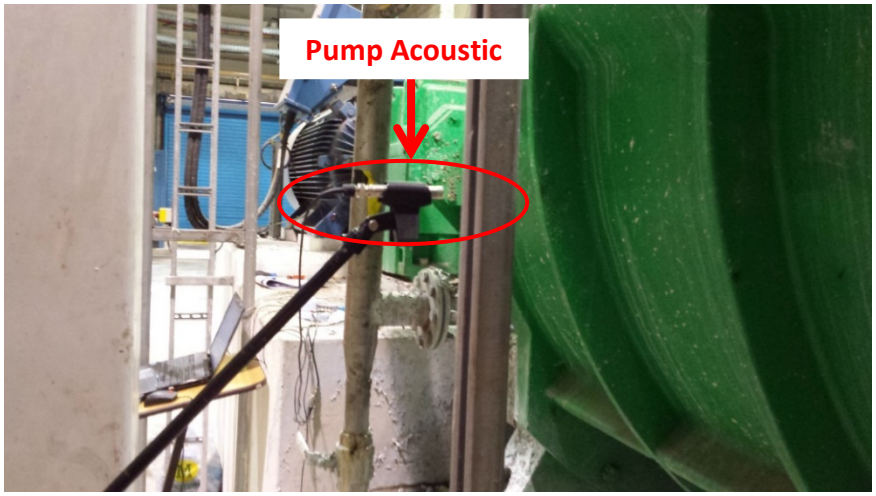

Figure 6-20 Acoustic Sensor positions for Pump

Figure 6-21 Pump (Drive End) Position

6.6 Vibration and Statistical Data Signals in the Time Domain

The vibration signal in time domain processing is a sector in applied mathematics and engineering that works with operation on or analysis of signals in either continuous or discrete time. The desired signal may include images depending on the type of measurement, it could be sound or sensor data signalisation [153]. All rotating and reciprocating machines such as electric motors, compressors and vacuum pumps generate a wide range of vibration frequencies. The total spectrum of frequencies is called a machine signature [4, 6, 7]. Each peak on the spectrum has its fundamental reason and if there are lots of machine faults the shape of the peak levels in the signatures will change considerably.

An example is a rotor which can develop basic frequencies. The amplitude of the signal at these frequencies will normally increase if the machine develops a fault [4]. An imbalanced shaft which is constantly exciting the assembly, as another example, will develop a forced damped vibration due to the driving force. The amplitude of the forced vibration is highly determined by the magnitude of the driving force. If the forcing frequency coincides with a natural frequency of the system, the resulting amplification leads to an extremely high and destructive level of vibration and this is called ‘resonance’.

If a fault produces a signal at a known frequency then the magnitude of that signal is expected to rise as the fault develops [4].

The technique used in this phase is the vibration signal in the time domain for all three motors, gearboxes, pumps, airborne sound data for gearboxes and pumps. Time-domain measurement is often considered the simplest of the measurement techniques and requires relatively inexpensive and unsophisticated instrumentation.

In the time domain, defect condition is often detected and evaluated using statistic descriptors of the vibration signal such as the peak value, Root Mean Square (RMS), Crest factor or Kurtosis [109].

Kurtosis is one of the useful and widely used statistical parameters. This method is normally used to indicate and detect spikiness in the signal [154]. Any healthy machine will generally exhibit a “Gaussian” or normal amplitude density. As the machine begins to deteriorate it starts to generate amplitude distribution signals that deviate from Gaussian. The kurtosis is a means of measuring the deviation from the normal distribution which can be calculated in real-time from the signal [155].

RMS, which is also the value of the vibration signal, is a time analysis feature that is the measurement of the power contained in a vibration signature. This feature is good to track the overall noise level, but no information is provided on which part is failing. It is ideal to detect any major out of balance in any rotating system [156].

Mean absolute is another popular and easy method of measuring forecast error. It is the average of the difference between the forecast and actual demand [157].

Peak-factor or crest value is another parameter that can indicate if there is a significant change in the waveform of the signal. According to Bruel & Kjaer application notes in detecting a faulty rolling element, the crest factor is equal to the peak amplitude of a waveform divided by the RMS value. This can give an idea of how much the waveform is affected. The impact can be associated with roller bearing wear, cavitation and gear tooth wears [158].

This study also uses the vibration signal in the time domain which is then compared to the statistical data vibration techniques.

6.6.1 Motor Vibration Signal

In this study, the vibration signal in the time domain is made possible due to the signals obtained by the accelerometers and the microphone.

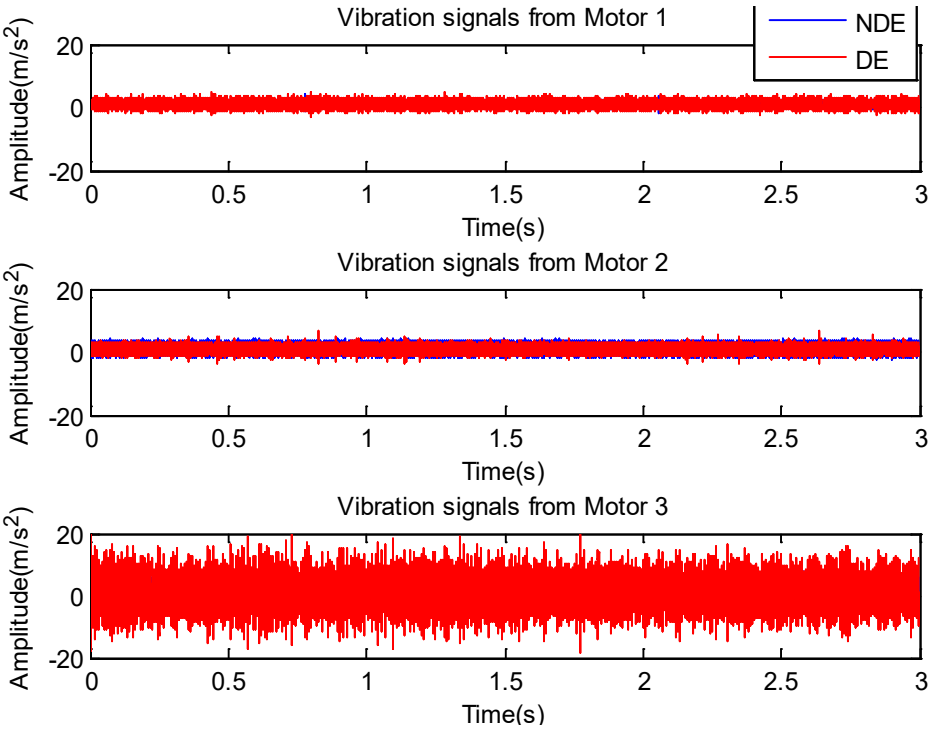

Figure 6-22 Signals in Time Domain of all Three Motors

Figure 6-22, Figure 6-24 and Figure 6-26 represent the measured vibration signals in the time domain for Motors, Gearboxes and Pumps respectively.

From Figure 6-22 it can be seen that the vibration signal of Motor 1 at DE is greater than the NDE and much lower compared to Motor 2 and 3 though Motor 1 is a bigger motor in size.

The vibration signal of Motor 2 NDE is higher than the DE but signal is lower compared to Motor 3.

The Motor 3 vibration DE is higher in comparison to Motor 2 DE. Motor 3 vibration signal is much higher even that both Motor 2 and 3 are both of similar size. When compared to Motor 1 the vibration level much lower. This means that motor 3 could potentially have some internal component failures and needs attention.

Statistical Data of Motor Vibration

The statistical data properties and quality of the tested data of the vibration for all three motors, gearboxes, pumps and airborne sound were selected to do a comparison with the vibration techniques as they are easy and simple to understand. This includes the application of kurtosis, measurement of Root Mean Square (RMS), mean abs and the peak or crest factor as described in Section 2.1.

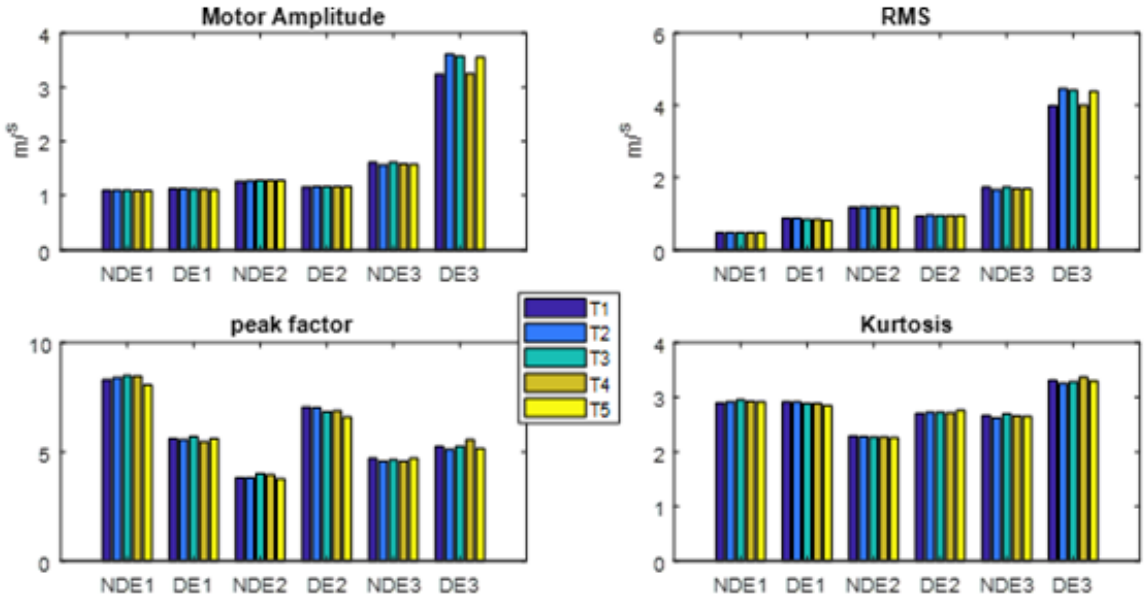

Figure 6-23 Motors Vibration Data Statistics

Figure 6-23, Figure 6-25 Figure 6-27 show the quality of the motors vibration data statistics of Motors, Gearboxes, Pumps and Airborne sound. Each test was repeated five times to get a more

reliable result as it improved data robustness and captured any data that may have been accidentally missed.

For this study (DE1) signal is measured on the drive end of Pump 1 and (NDE1) signal is measured on the non-drive end of Pump 1. Similarly, (DE2) and (NDE2) is for Pump 2, (DE3) and (NDE3) for Pump 3.

The variation in the measurement and majority of the data is stable in Figure 6-23 except for the DE3 of motor 3 where there is a slight discrepancy in the vibration on the motor RMS and motor amplitude from the five sets of data. This indicates a small degree of unbalance of the shaft or bearing wear.

6.6.2 Gearbox Vibration Signal

Figure 6-24 shows the vibration signal of the Gearboxes 1, 2 and 3 in the time domain and the Gearbox Input (GBI) vibration represented in blue is greater than the Gearbox Output (GBO) in red.

Gearbox 1, GBI vibration level is higher than the GBO and for gearbox 2 the vibration level of the GBI is greater than the GBO. For Gearbox 3 the vibration level is lower than both gearbox 1 and 2 and it is apparent that gearbox 1 and 2 GBI has a problem which needs addressing.

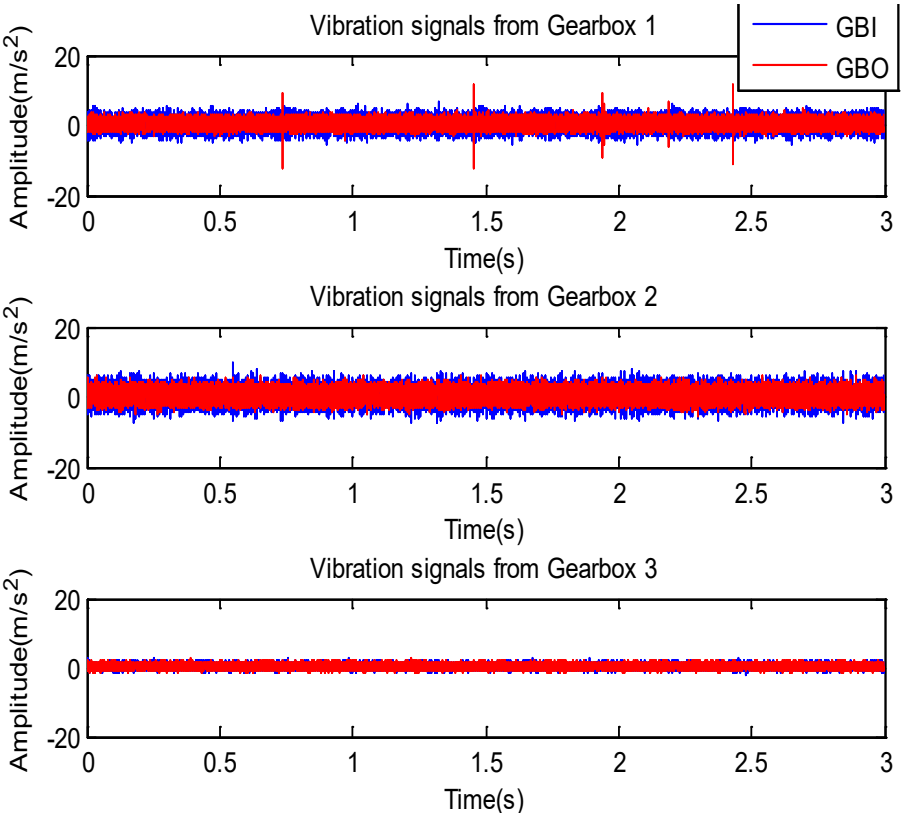

Figure 6-24 Vibration Data from all Three Gearboxes

Statistical Data of Gearboxes Vibration

From observation, the repeatability of most of the data looks good, excluding the kurtosis and peak factor value for the Gearbox Output from Figure 6-25. This means that there are some random impulses in the measured vibration signal on the gearbox 1 input. This is an indication of the beginnings of deterioration in the gearbox output where attention is required.

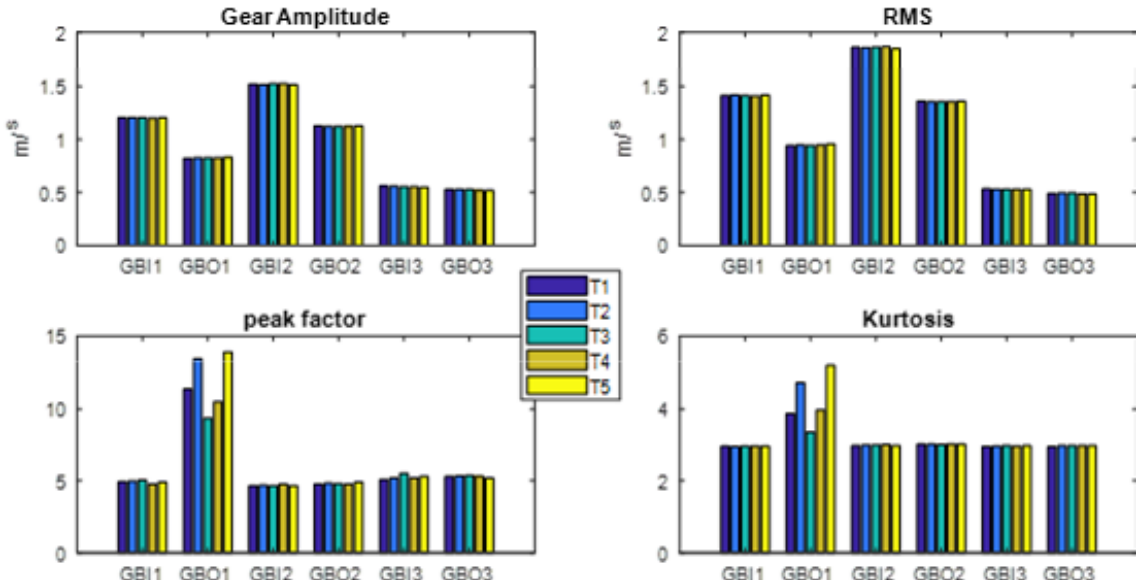

Figure 6-25 Gearboxes Vibration Data Statistics

6.6.3 Pump Vibration Signal

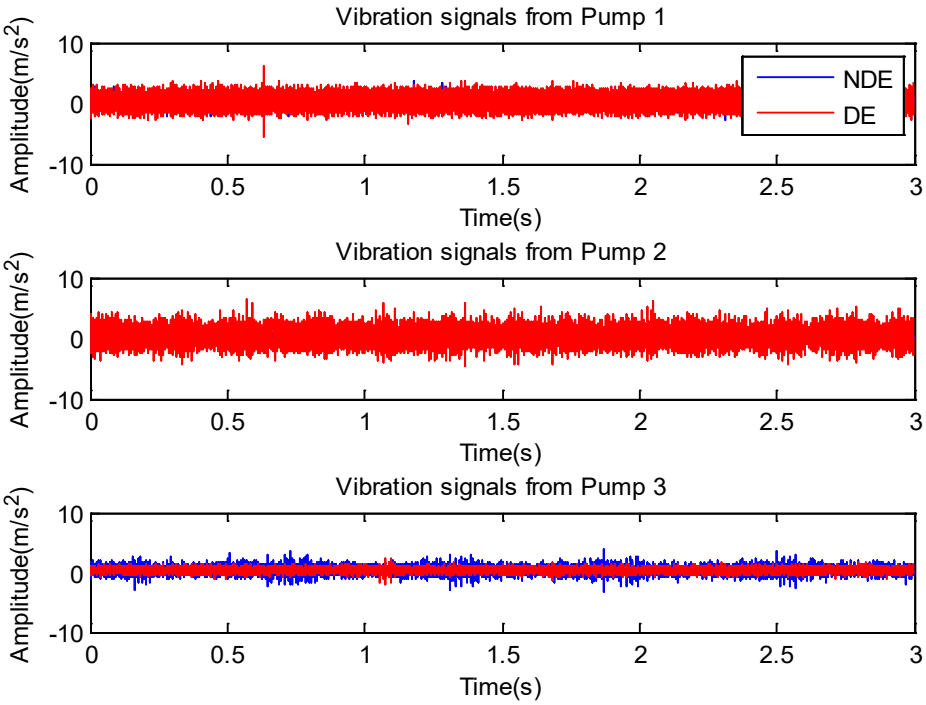

Figure 6-26 Vibration Data of all Three Pumps

Figure 6-26, displays the vibration data of Pumps 1, 2 and 3 in the time domain. For Pump 1, the DE vibration level is higher than the NDE and the same applies for pump 2 whereas, for Pump 3, the vibration level of the DE is lower than Pump 1 and 2.

The NDE vibration level here is slightly higher than the DE therefore Pump 2 needs more attention as there may be a fault in the impeller or other internal components of the pump.

Statistical Data of Pumps Vibration

Figure 6-27 below shows some random minor impulses in the measurement of the vibration signal from all the pumps. There is a slight instability on the peak factor, possibility indicating early wear in a bearing or the rotor for all of the three pumps.

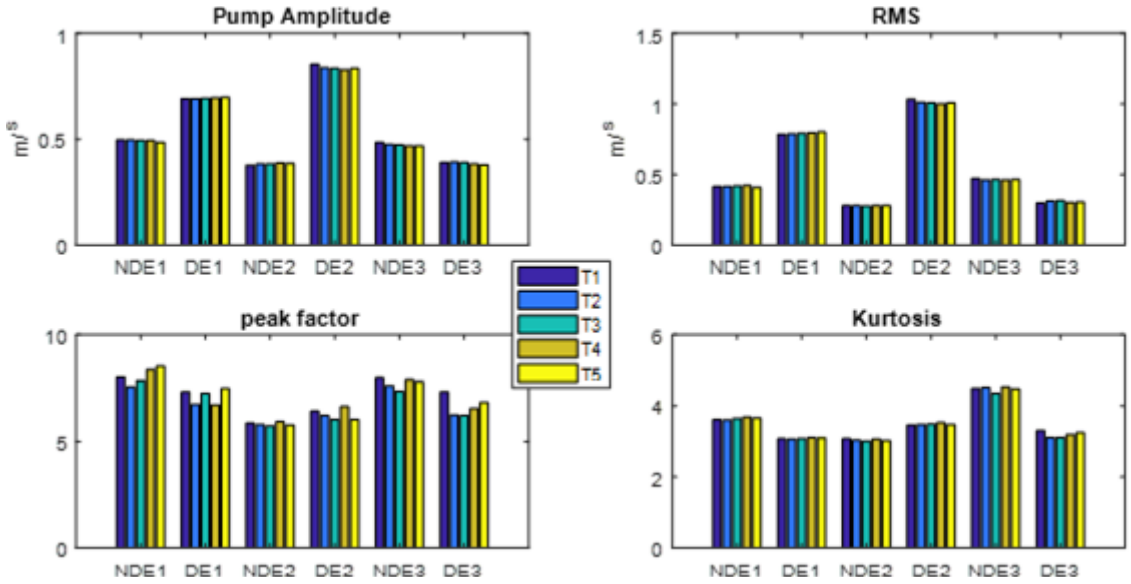

Figure 6-27 Pump Vibration Data Statistics

6.7 Airborne Sound Data for Gearboxes

Airborne sound can measure the sound of the machine and its environment. It contains different kinds of information and measures noises more than vibrations.

The first sensor is put near the gearbox, the second one is located near the pump. The airborne sound of Gearbox 1 has a slight variation at 0.5 s as seen in Figure 6-28. Airborne sound on Gearbox 2 is random and slightly higher than Gearbox 1 whereas Gearbox 3 sound level is more inconsistent and higher than Gearbox 1 and 2 which means there is a possibility of gear tooth wear or misalignment.

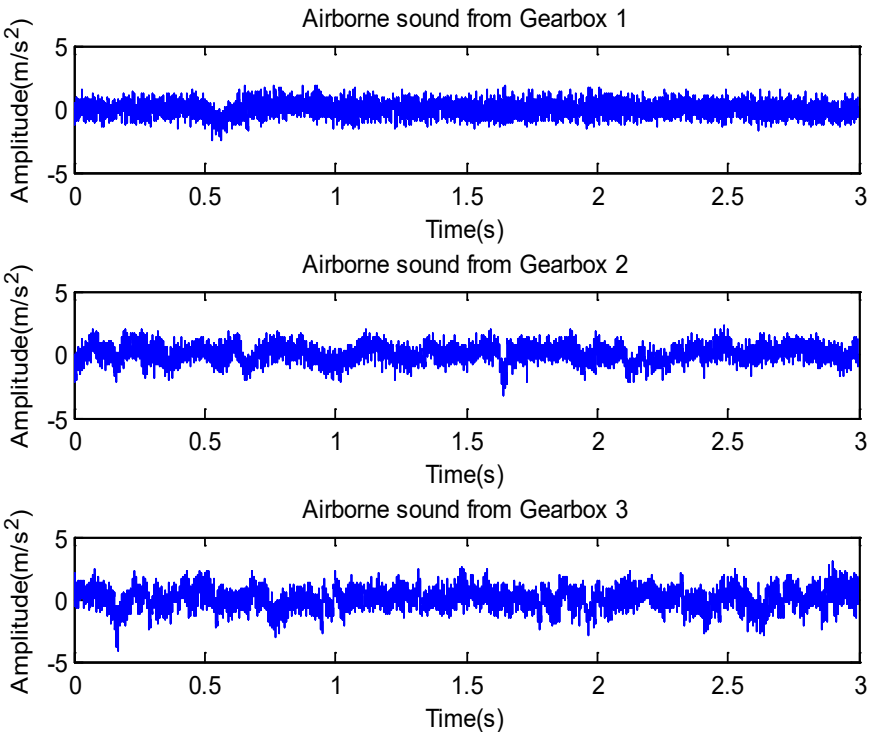

Figure 6-28 Airborne Sound Data for all Three Gearboxes

6.7.1 Airborne Sound Data for Pumps

Figure 6-29, shows the airborne sound data from Pumps 1, 2 and 3. Sound from Pump 1 and Pump 2 is similar but Pump 3 has some variations, probably misalignment or bearing failure.

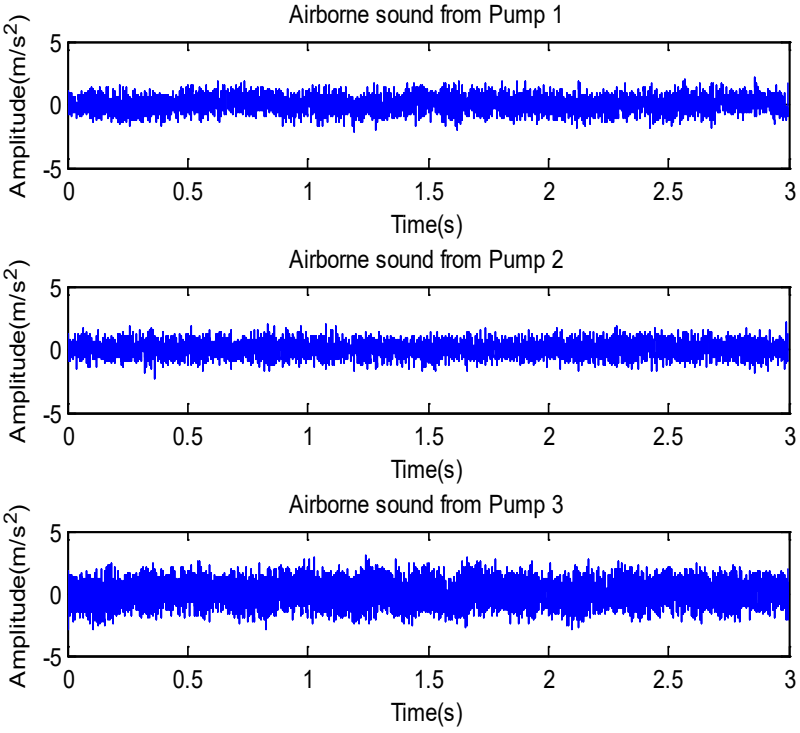

Figure 6-29 Airborne Sound Data of Pumps 1, 2 and 3

Statistical Data of Airborne Sound for Both Gearboxes and Pumps

Figure 6-30 shows the Airborne Sound data statistic of all the three gearboxes and pumps.

This reliable data shows a slight change that could be the external noise around pump 3 which affects the mean abs and peak factor marginally.

The vibration signal proves that the DE of Motor 3 could potentially have some internal component failures and needs attention.

The variation in the statistical data measurement also proves that the DE of Motor 3 has a slight discrepancy in the vibration on the motor RMS and sound amplitude from the five sets of data.

This indicates a small degree of unbalance of the shaft or bearing wear.

Overall, for the motor vibration, the motor 3 drive end is higher in comparison to both motor 1 & 2 which proves that motor 3 could potentially have some internal component failures and needs attention.

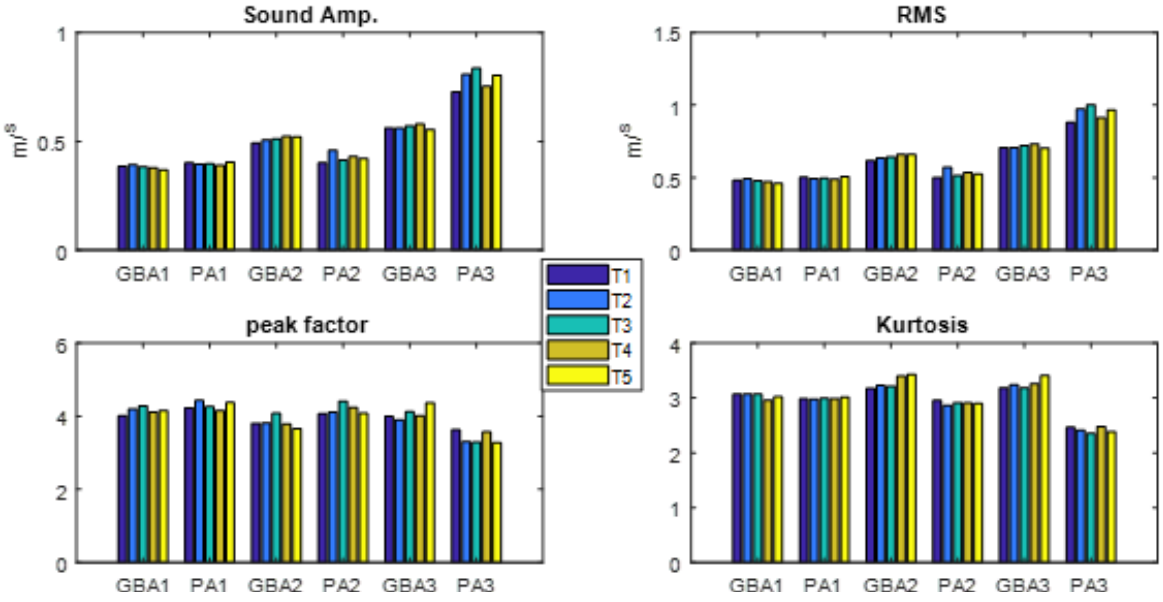

Figure 6-30 Airborne Sound Data Statistics

For the gearbox statistical data properties, the variation in the measurement and majority of the data is stable, excluding Motor 3, where there is a slight discrepancy in the vibration on the motor, this indicates a small degree of unbalance of the shaft or bearing wear.

For the Gearbox vibration, gearbox 1 and 2 input have some problems which need addressing.

From the gearbox statistical data, some random impulses are measured in the vibration signal of gearbox 1 input which indicates the beginning of the deterioration of the tooth.

For the pump motor vibration, Pump 2 needs more attention as there might be a fault in the impeller or other internal components of the pump.

For the pump statistical data, there is a slight instability on the peak factor possibly indicating early wear in bearing or rotor for all of the three pumps.

For the Airborne sound data for gearboxes, Gearbox 3 sound level is more inconsistent and higher than Gearbox 1 and 2 which means there is a possibility of gear tooth wear or misalignment, whereas the airborne sound data from pump 3 seems to have more variations and there may be a possibility of misalignment or pump bearing failing that needs attention.

6.8 Vibration Signals and Acoustic Spectra in the Frequency Domain

The frequency-domain can be analysed through a computer-based programme called the Fast Fourier Transform (FFT) or a frequency analyser. This technique will show one or more discrete frequencies around which energy is focussed.

The intention of using frequency domain analysis in the diagnostic of machinery is to find the key frequency component that reflects the mechanical condition of the machine. The frequency component of the vibration signal is always linked to the dynamic and mechanical condition of the equipment.

The most widely and commonly used method for examining the spectrum of the vibration signal in rotating machines is the frequency domain. In terms of fault detection, any change in the mechanical condition of the machine is most likely to result in a change in the vibration signal. The vibration produced by the normal and damaged components consists of the fundamentals and harmonics of the meshing frequencies. Localised faults produce a short pulse in the vibration signal and this creates an amplitude modulated signal. Their effect is visible by the low-level sidebands of the rotational speed of the faulty components [154].

6.8.1 Spectra of Vibration Signal from Motors

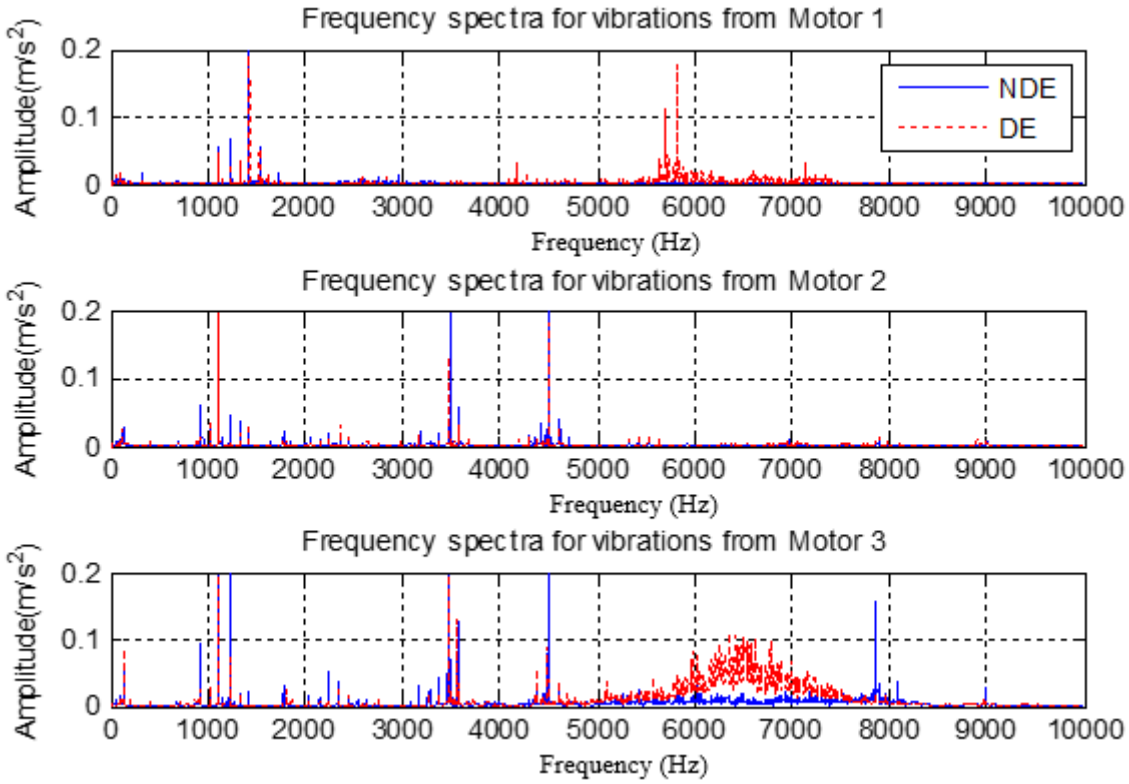

Figure 6-31 Spectra of Vibration Signals from Motor 1, 2 and 3

The spectra of the vibration signal from all three motors are shown in Figure 6-31.

In Figure 6-31, there are some discrete frequencies in the spectrum of the motors vibration signal, this also confirmed the presence of the shaft rotational frequency, rotor bar pass frequency and bearing characteristic frequencies.

In the motor 3 DE, the vibration is slightly higher and a couple of additional resonance frequencies can be observed due to the vibration transfer path difference which indicates a small degree of the unbalanced shaft, bearing wear or damaged impeller. There is more frequency resonance in the higher frequency band for motor 3 whilst motor 2 vibration is the lowest.

6.8.2 Spectra of Vibration Signal from Gearboxes

Figure 6-32, illustrates the spectra of vibration from the gearboxes. It can be seen in the figure that there are many discrete frequencies, including shaft frequencies, meshing frequencies and bearing characteristic frequencies and gearbox 2 vibration is higher whilst gearbox 3 is the lowest. The difference between the measured signals may be induced by bearings due to the bearing type being different.

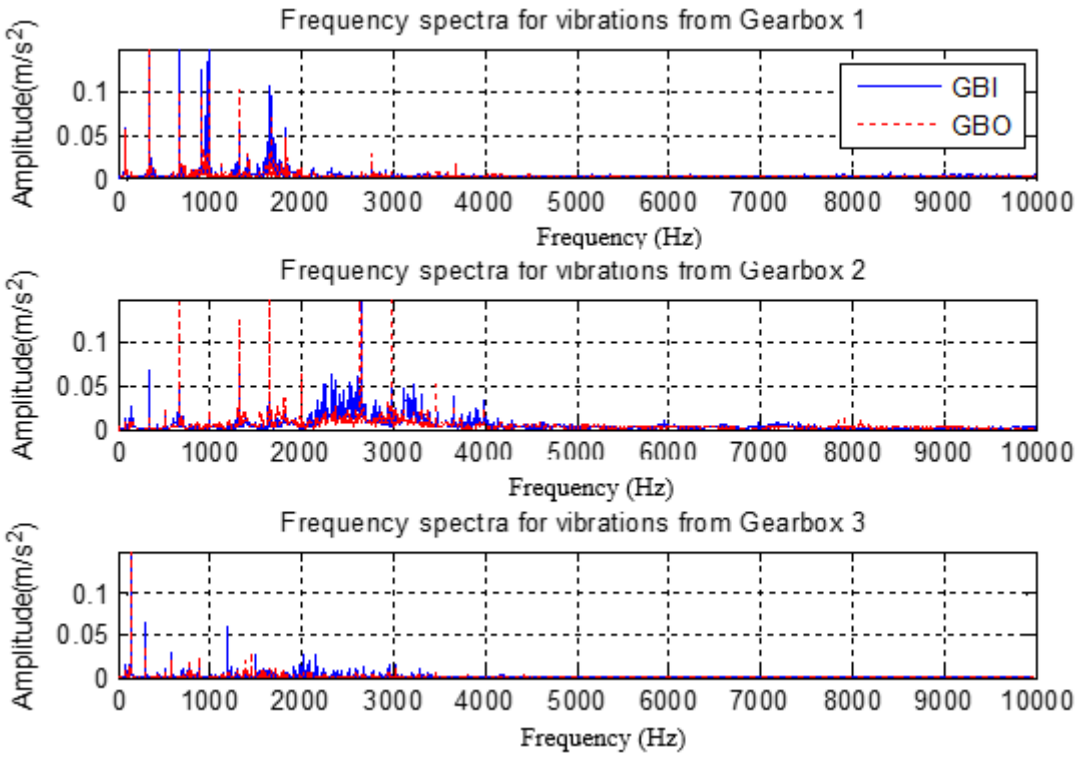

Figure 6-32 Spectra of Vibration Signals from Gearbox 1, 2 and 3

6.8.3 Spectra of Vibration Signal from Pumps

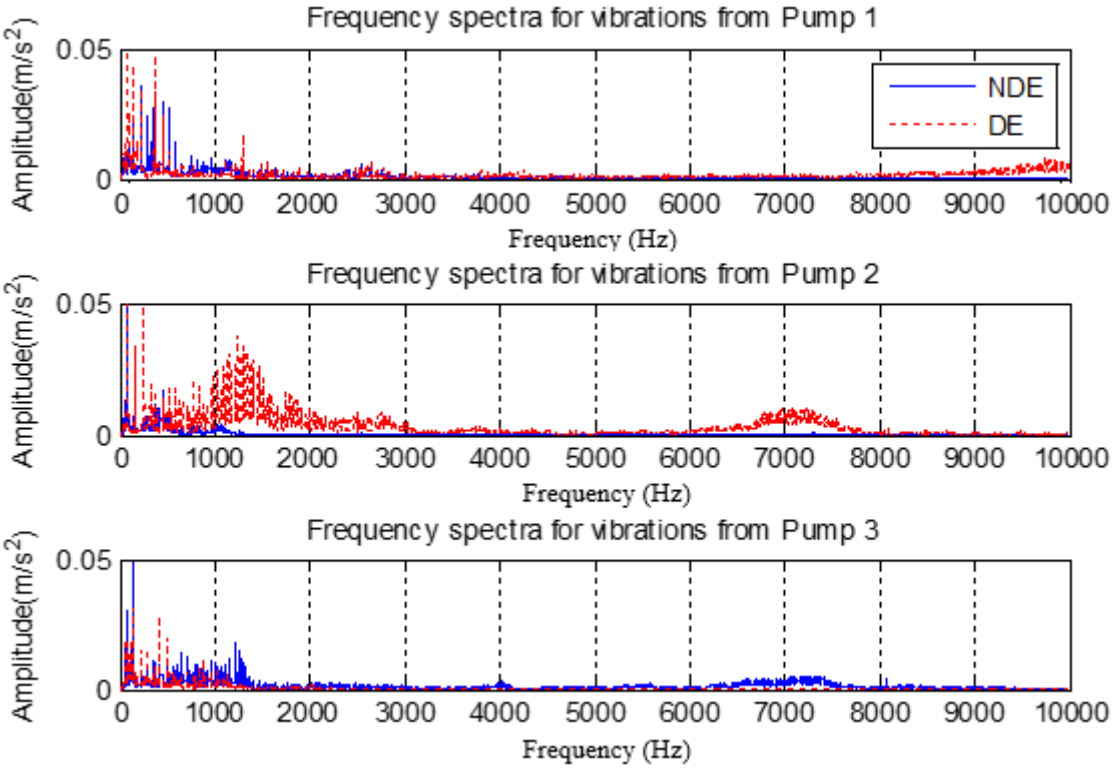

Figure 6-33 Spectrum of Vibration Signals from Pumps 1, 2 and 3

Figure 6-33, represents the spectra of vibration from pump 1, 2 and 3. There are some discrete frequencies in the low frequency which are related to the shaft and pump rotational frequencies. As the pump's components are different and sensors are not all located at the same position this could be a contributory factor for the variation in frequencies which in turn cause the vibration differences. For both pumps 1 and 2 their spectrums have revealed that the DE is in a critical situation with pump 3's vibration being lower in comparison and pump 3's DE being higher.

6.8.4 Acoustic Signals for Gearboxes and Pumps

Figure 6-34, shows the Spectra of the Acoustic signals for Gearboxes and Pumps

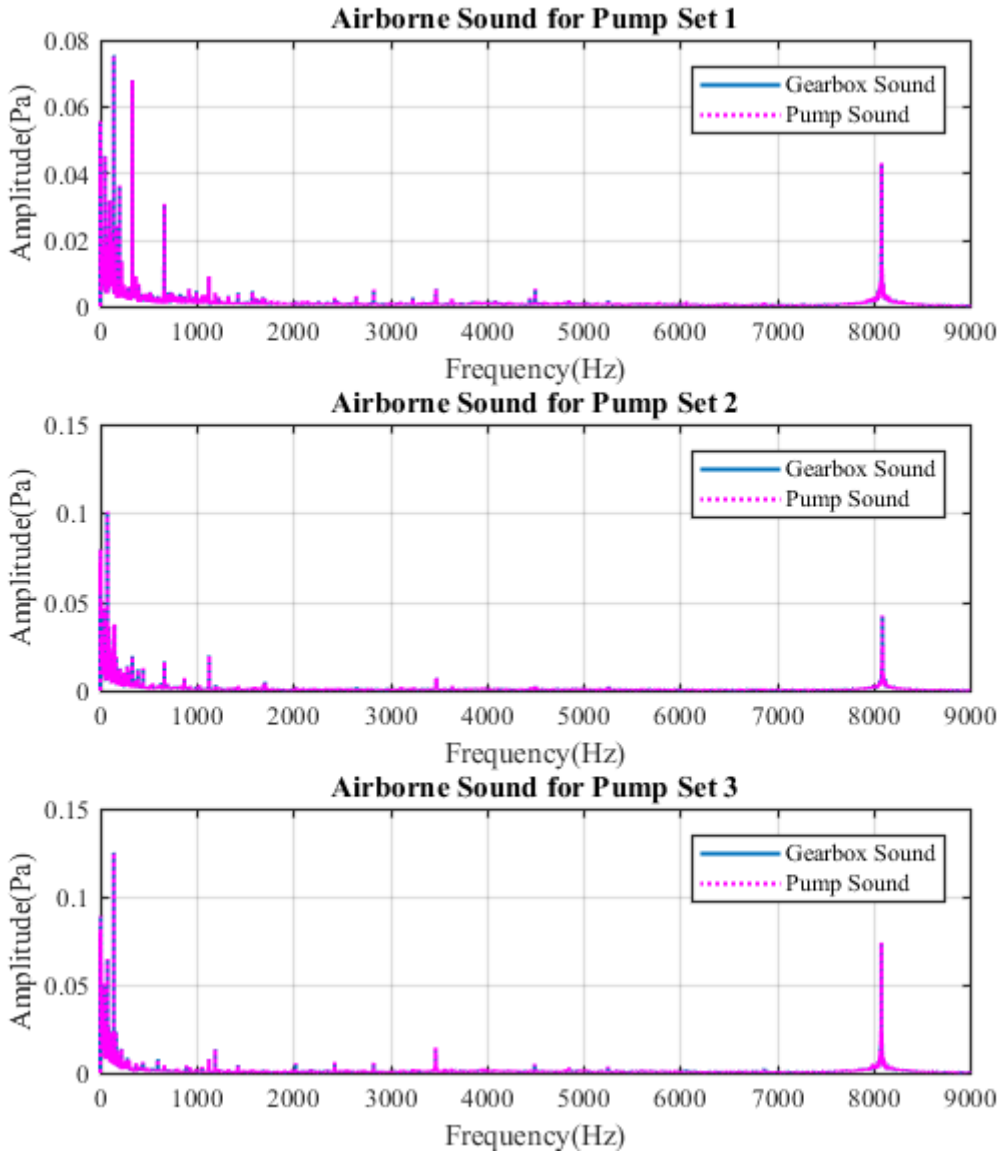

Figure 6-34 Spectra of Acoustics for Pumps and Gearboxes

There are distinctive discreet components in the low-frequency range, most of them being correlated to the operational physics of the motors, gears and pumps, even though high background noise can be observed due to room reflections. This shows the high feasibility to use remote AS measurement for monitoring such equipment. Besides, there is a high-frequency tone at 8100Hz from all three-pump sets comprising of the gearboxes and motors which may come from the electronic noises of the variable motor speed, pump set 2 sound being the lowest.

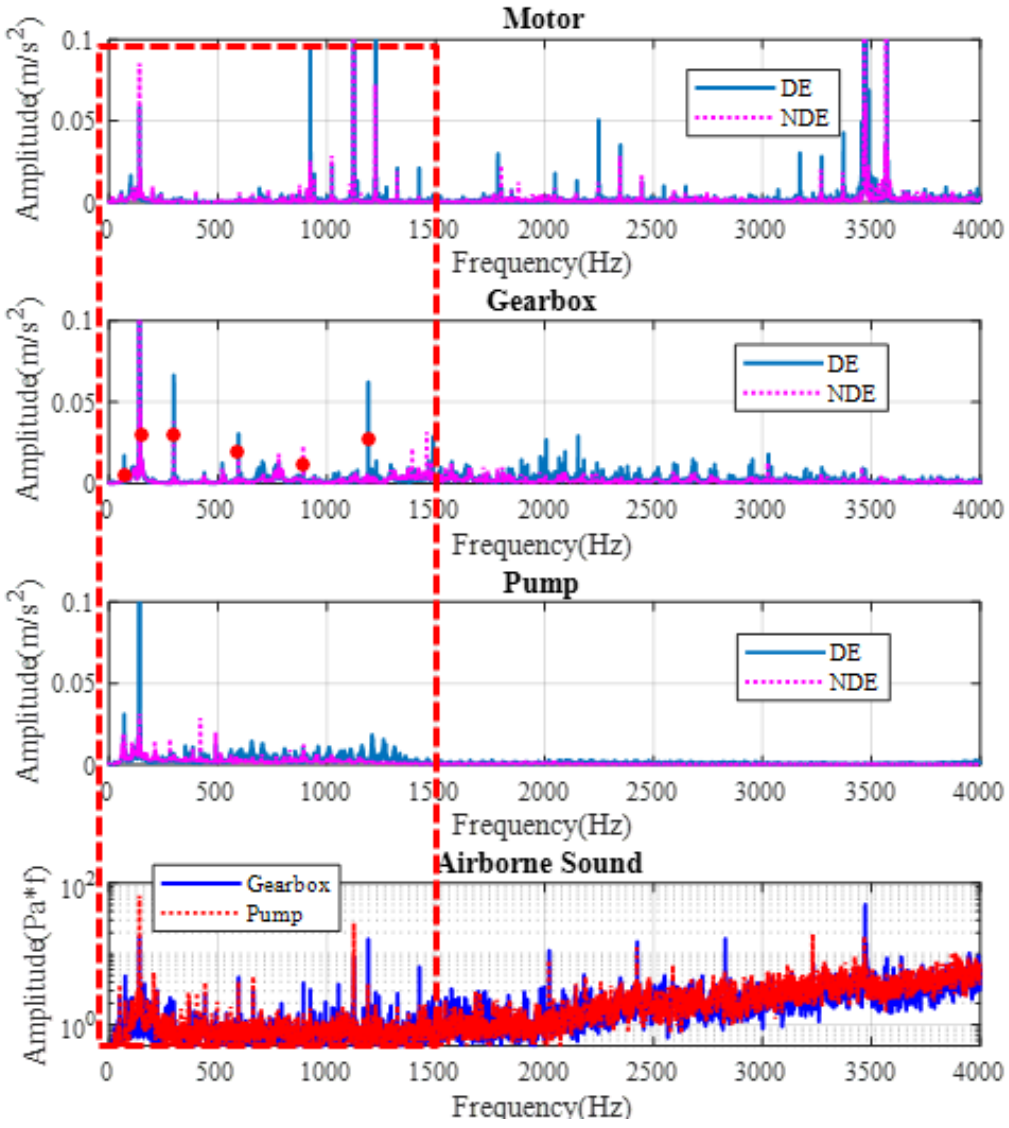

Figure 6-35 Spectrum of vibration and airborne sound for Pump Set 3

For more detailed analysis, a direct comparison of the Spectra between the Vibration and Airborne sound (with a multiplication of frequency) for pump set 3 is shown in Figure 6-35. There are some distinct similar frequencies in the pattern whilst at its peak amplitudes at about approximately 50, 100, 250, 600, 900, and 1200 Hz.

This further confirms that there is a good correlation between the spectrum vibration and the airborne sound. It is inexpensive and also an easy deployment technique to apply.

Based on the spectrum comparison, it is possible to use remote sound to indicate the health conditions for all the machines as the same frequency content in low frequency exists.

6.9 Envelope Spectra of Vibration

Envelope spectra analysis involves spectral analysing of the envelope or amplitude modulation component of time history. It can be very useful in providing diagnostic information regarding the early failures of bearings [109] and gears [156].

An impulse is produced each time a loaded rolling element contacts a defect or another surface in the bearing or when a faulty gear tooth get in contacts with another tooth. This impulse has a very short impact compared to the interval between the pulses. The energy from the defect pulse will be distributed at a very low level over a wide range of frequencies which in turn makes the bearing or tooth effects difficult to detect by conventional spectrum analysis when they are in contact with the presence of vibration from other machine components.

Fortunately, the impact usually excites a resonance in the system at a much higher frequency than vibration generated by the other components. This structural energy is usually concentrated into a narrow band that is easier to detect than the widely distributed energy of the bearing defect frequencies. With a wearing part and breakage, the sideband activity near-critical frequencies, such as the output shaft frequency, is expected to increase. The whole spectrum contains very high periodic signal associated with the gear mesh frequencies [145].

6.9.1 Envelope Spectra of Motors

Figure 6-36 shows some discrete frequencies in the envelope spectra which may have been caused either by an imbalanced shaft, faulty bearing or damaged impeller. It is obvious from the envelope Spectra of Motor Vibration that there is one more frequency resonance in the higher frequency band for motor pump set 1 and 3 compared to motor pump set 2 with motor pump set 3 being the more critical. Figure 6-37 and Figure 6-38 shows the Envelope Spectra Vibration for all three gearboxes and pumps.

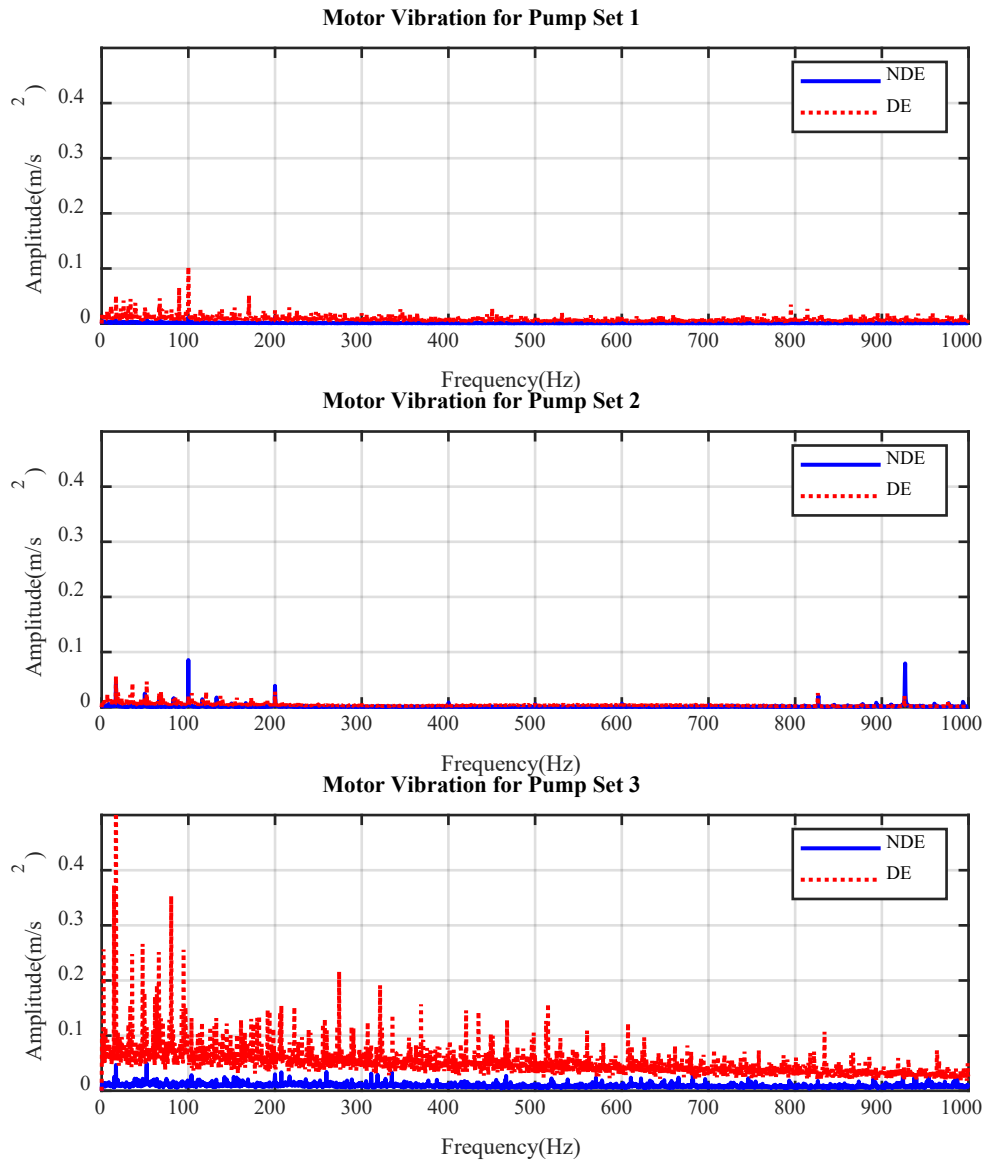

Figure 6-36 Envelope Spectra of Motor 1, 2 and 3

6.9.2 Envelope Spectra of Gearboxes

There are several discrete frequencies in the vibration on the Envelope Spectra of the Gearbox pump set 1 and 2, as shown from Figure 6-37, which include shaft frequencies, meshing frequency, and bearing characteristic frequencies. The difference between the measured signals is induced by bearings because the bearing type and gear tooth number are different.

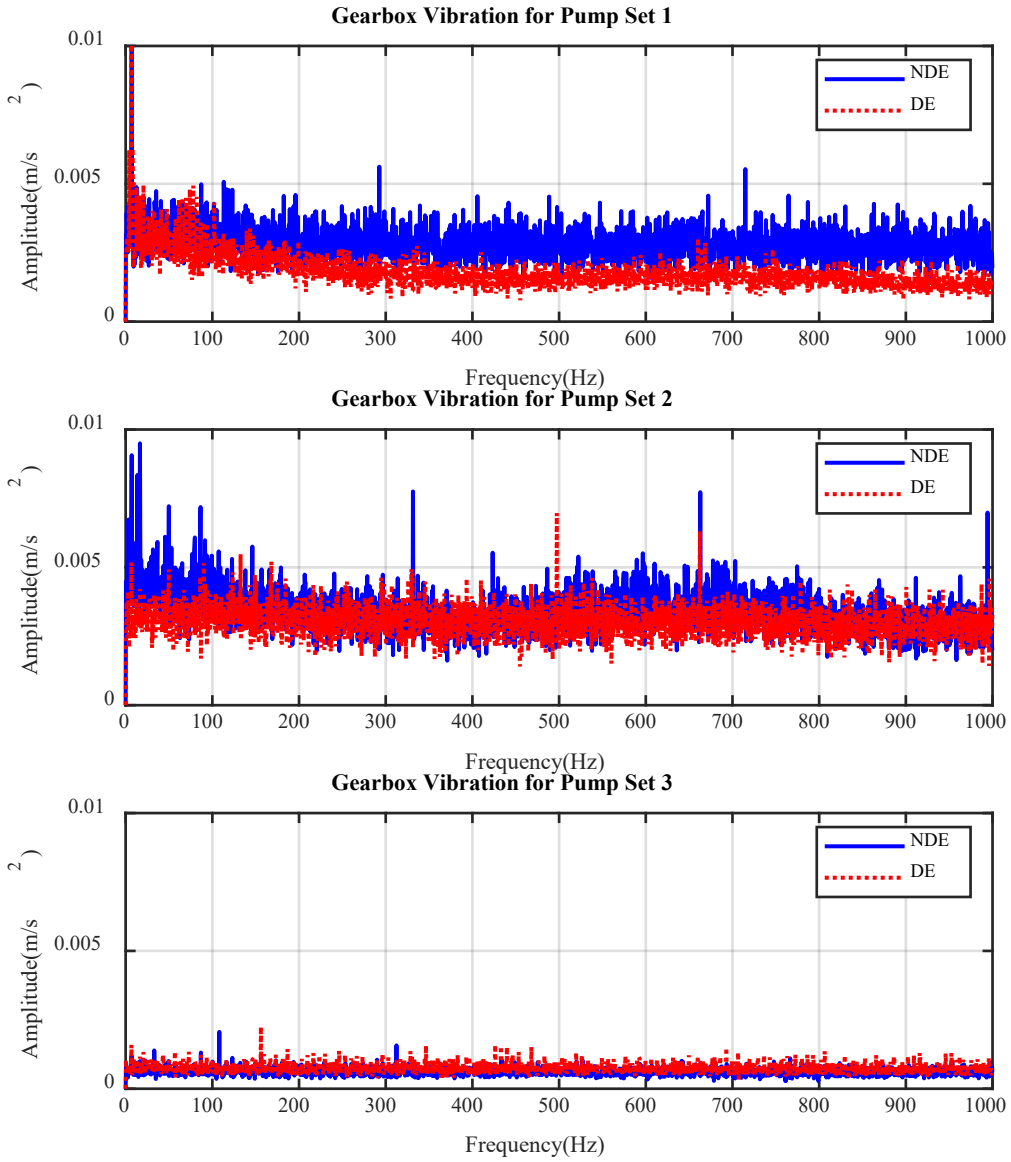

Figure 6-37 Envelope Spectra of Gearboxes 1, 2 and 3

6.9.3 Envelope Spectra of Pumps

According to Figure 6-38 of the Envelope Spectra vibration, of the pump set 1, 2 and 3, pump set 1 condition seems less severe. The higher pitch frequencies on pump set 2 DE and 3 NDE could be because of the pump blade rotational frequency, bearing wear, misalignment and other associated components and require assistance.

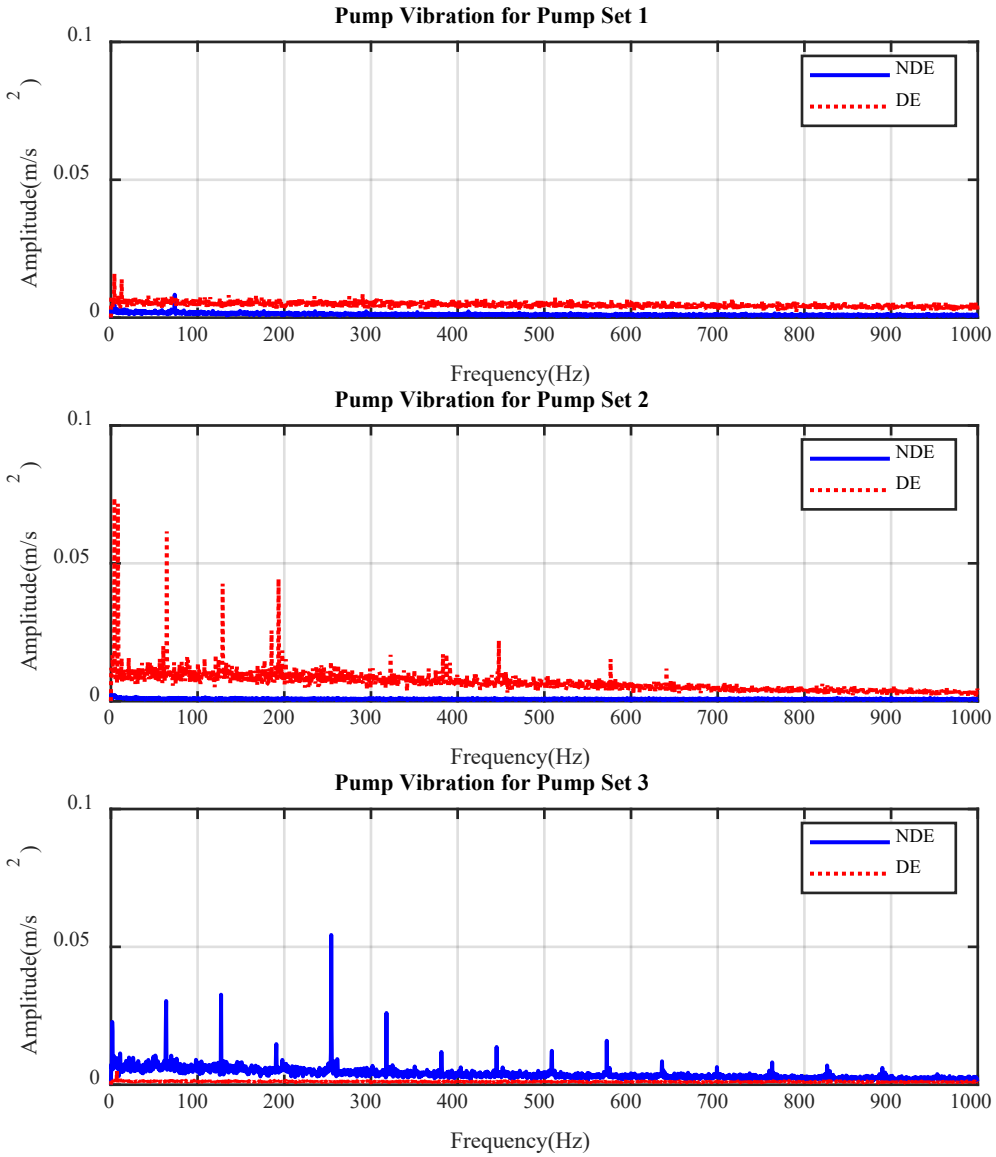

Figure 6-38 Envelope Spectra of Pumps 1, 2 and 3

6.10 **Discussion**

Due to the environment being noisy, low frequency background noise can be observed due to room reflections. However, as the analysis was quite in-depth with various techniques it was proven that all the three motors results on the motor vibration are relatively similar to the results of the motor vibration data statistics. Nevertheless, even whilst motor three being half the size of motor one, it indicates a higher vibration amplitude and for the three gearboxes and pumps their results were quite consistent.

Based on the Airborne sound study on the gearboxes and pumps it can be seen that the airborne sound of gearbox 1 has a slight variation. Airborne sound on gearbox 2 is random and slightly lower than gearbox 3 whereas gearbox 3 sound level is more inconsistent and higher which means there is a possibility of gear tooth wear or misalignment. The sound data for pump 1 and pump 2 are similar however pump 3 has some variations, probably misalignment or bearing failure.

In the spectra vibration analysis, it was found that motor 3 vibration is higher and some additional resonance frequencies can be observed. For the spectra of vibration gearbox 3, vibration is lower than gearbox 1 and 2 whereas pump 2 spectra vibration is higher than pump 1 and 2.

Based on the vibration on the Envelope Spectra motor 3 DE, the vibration is higher which indicates a degree of the unbalanced shaft, bearing wear or damaged impeller. There is more frequency resonance in the higher frequency band for motor 3. There are many discrete frequencies in the vibration on the Envelope Spectra of the Gearboxes which may include shaft frequencies, meshing frequency and bearing characteristic frequencies. The difference between the measured signals may be induced by bearings because the bearing type and gear tooth number are different. It was found that gearbox of pump set 1 and 2 is higher than the gearbox of pump set 1. Analysis shows pump set 2 DE and pump set 3 NDE show higher pitches.

Phase III

Investigating Acoustic Condition Monitoring based on the Laboratory Compressor

Chapter 7

Acoustic Monitoring of the Laboratory Compressor based on Conventional Analysis

Chapter 8

Acoustic Monitoring of the Laboratory Compressor with State-of-the-Art Convolutional Neural Networks

Chapter 7. **Acoustic Monitoring of the Laboratory Compressor Based on Conventional Analysis**

To address the difficulties of using vibration for field applications, this chapter focus on the studies of using remote acoustic monitoring based on a laboratory environment. It provides an in-depth understanding of the signal generation mechanisms from the compressor deficiency in loss of performance and its possible potential knocking effect. A brief overview of "noise sources" and their dynamic characteristics is explained together with a summary of the type of faults and wear in a compressor. A review of the acoustics monitoring study using conventional analysis techniques has been undertaken. The general system set up and of how this investigation has been progressed, the sound imaging, sound localization and frequency analysis and its Root Mean Square (RMS) values followed with a discussion has also been explained.

7.1 Acoustics Monitoring in Compressor

Review of Acoustics Monitoring Study using Conventional Analysis Techniques

Acoustic monitoring is a powerful tool that has entered a new era, an age of complex and precision engineering [51]. With evolution, several diagnostic techniques using sound signatures and data processing have been designed but have not been used widely which causes great difficulty in the interpretation of sound signals. The instrumentation technique is like the vibration analysis but the fundamental problem lies between the transmission [159]. Airborne acoustic can be used for the measurement and detection of defects in the rolling element bearings [42], gearbox system [43] and much more. It contains different kinds of valuable information and measures noise more than vibration. It is more practical than vibration as it does not need to be attached to the machine and is considered as Non-Destructive Testing (NDT). The benefits of sound monitoring are immense as they are non-contact, low-cost implementation and flexible application. Based on the characteristics of sound propagation, such as reflection and diffraction, the position of the microphone has a great influence on the monitoring results which is demonstrated in this study. In this chapter, the position of the microphone is changed to collect the noise signal for comparison. A combination of the vibration signal and the acoustic camera analysis is implemented to comprehend the influence of the microphone position. The analysis results show that the signal attenuation and frequency distribution differ from different locations and is greatly affected by the environment.

Airborne acoustic monitoring has the possibilities of replacing the need for several vibration sensors that need mounting at various locations on the machine and the potential of being detached from the machine surface. The airborne acoustic, by nature, is a non-contact system and is good in high frequency and short wavelengths [43]. Another advantage of acoustic monitoring is when noise is under investigation, this technique provides a more direct source of noise and generation mechanisms [160]. However, there remains a problem with acoustic monitoring as the signals may be contaminated by any background noise, which may include influences such as parasite and interference from related sound sources. Nevertheless, scholars such as Zafar et al. claim that noise filtration in airborne acoustic data of a machining process shows a promising future [161].

Acoustic Emission (AE) was originally developed for the non-destructive testing of static structures, however, due to the extension of its application in recent times, it is now possible to monitor rotating machinery.

Elasha et al. presents a new technique for the application of AE in the monitoring of a large helicopter (CS-29) main gearbox and postulated that their results demonstrate that AE can detect a small bearing anomaly within the helicopter gearbox [162]. The primary task in the condition monitoring of the gearbox, as described by Sharma et al, is to identify the presence of defect to avoid any sporadic failures. In their experimental investigation on AE generated during the meshing of gears of a healthy and a well-cracked gear, it was strongly argued that AE technique is capable of diagnosing a crack in the gear tooth at different load conditions proving that AE technique has the potential for the assessment of the condition of gearbox [163], this is in very close to Elasha et al. findings [162].

Elamin et al. also strongly agree that the acoustic emission signal is shown to be effective for the detection of exhaust valve faults in a diesel valve engine. They posit that AE is an extremely powerful condition monitoring tool and that the variation in the signal indicates the presence of an engine failure [164]. Wang et al describe their work based on the Fault Diagnosis of Reciprocating Compressor Valve using Acoustic Emission and prove that the fault of a crack in a valve disc has not been possible to diagnose by acoustic emission signal effectively [165]. Elamin describes that AE signals are unlikely to be influenced by noise from a long distance but will need to be reduced and be more localised as damping of different sources is critical in attaining a good sensor location. Previous scholars [166], have established that AE source characteristic is quite complex and is becoming more complicated by the factor which affects AE wave transmission and attenuation which includes internal damping, reflection, conversion mode and diffraction [166].

Based on those assumptions and previous research, there lies a gap in the knowledge in the characteristics of sound propagation, such as reflection and diffraction. This study shows how those microphones influence the placements for the condition monitoring of reciprocating compressors. This study proves that the sensor microphones have a great impact on the monitoring results.

7.1.1 Sound Generation

A compressor is made of several key components that require to be maintained and cared for through a good maintenance system. To be able to develop a good acoustic monitoring program for the machine, a thorough understanding is required of faults in compressors which generate sound with a knocking effect. In general, problems with reciprocating compressors fall into one of the following broad categories: failure to run, loss of capacity, noise and vibration [105].

“Noise” which also known as “Knocks” is often described as a mechanical, or friction-related sound [105]. Noise is omnipresent in any operating compressor. Faults in the compressor can originate from bearing, crankshaft, motor, crankcase, cylinder, loose belt, and valve. When these parts start to deteriorate noise can be heard from the compressor which also shows a sign of potential mechanical failure. These faulty components in the compressor will produce noise and these forces can cause a rise in the acoustic level which can also reduce the performance of the compressor. Similarly to vibration, in acoustics, the source of noise in a compressor system can be attributed to the compressor internal or external components, gas motion in the compressor itself and any associated piping system. In an ideal world, the flow of air would be steady without any pulsation, however in practice, the discharge pressures are not steady due to the valve motion and contained high temperature due to the second stage cylinder high compression actions.

7.1.2 Sources of Noise

Noise sources depend on their dynamic characteristics and would usually instigate from components such as:

Cylinder Knocks

Cylinder knock may happen through loose pistons, insufficient head clearance, broken piston rings, loose rider bands, loose or broken valves, moisture carryover of “liquid slugging”.

The frame or Running Gear Knocks

A knock or noise in a compressor running gear is usually caused by a loose or worn bearing that has too much clearance.

- Loose flywheel or sheave
- Worn or loose bearings
- Large clearance on crosshead pin-to bushing
- Loose mechanical gland packing
- Connecting rod hitting end of the piston rod in the crosshead
- Belt misaligned, causing the motor rotor to “weave” and bump

Squealing Noise

Whereas squealing noise in the compressor is caused by the following:

- Compressor or motor bearing too tight
- Lack of oil
- Belt slipping or worn
- Leaking joint or gasket [105]

The following chapter demonstrates how sound is generated and localised.

7.2 Methodology

This work presents a high level of signalisation techniques with identification to quantify and qualify the best location to capture the acoustic signal from a machine. Four sensors/microphones have been used at four different distances and heights from the compressor to get the ideal position for a proper analytical exploration into the signal. A computational algorithm has been developed in MatLab software code for the comparison of different sensors in contrast with the correct location. Two separate data acquisition systems were used during the data collection process. In total 16 channels of data were collected. The two systems were necessary as the CED 16 channel unit (model 1401), as shown in Figure 7-2, does not support acoustic monitoring hence the reason the Sinocera 16 channel unit (model YE6232B) as shown in Figure 7-1, was utilised and coupled to CED (model 1401).

See Table 7-1 and Table 7-2 below which shows the specification for the data acquisitions

Table 7-1 Data Acquisition 1

Data Acquisition 1	
Manufacturer/Software	Sinocera/YE7600
Type	YE6232B
No. of Channels	16CH, selectable voltage/IEPE input
A/D conversion resolution	24 bits
Input range/Power Supply	≤±10VP/4mA/+24VDC
Gain	x1, x10, x100
Filter	Independent Anti-filtering
Sample Rate (Max)	96kHz/CH, Parallel

Figure 7-1 Data Acquisition 1

Table 7-2 Data Acquisition 2

Data Acquisition 2	
Manufacturer	Cambridge Electronic Design
Type	Power 1401/CED 2701
No. of Channels	16CH
Input range	Selectable to ±5V or ±10V
Interface	USB 2.0
A/D conversion resolution	16 bits
Memory Expandable to	1 Gbyte to 2 Gbytes
1 Ch Mode	800kHz

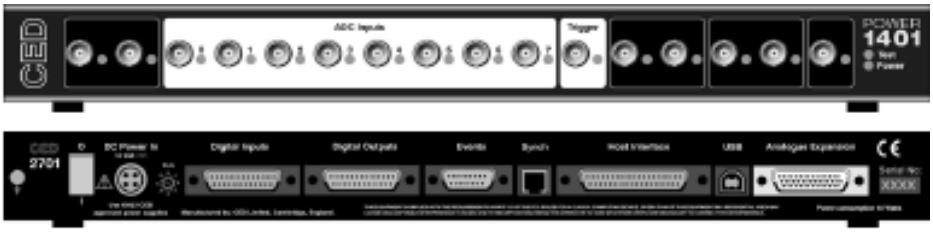

Figure 7-2 Data Acquisition 2

7.2.1 Measurement System Layout

As previously described, 16 position signals have been captured by four similar microphones varied at four different distances and heights from the compressor to compare the airborne signal. Figure 7-3 below shows the system layout of those microphones.

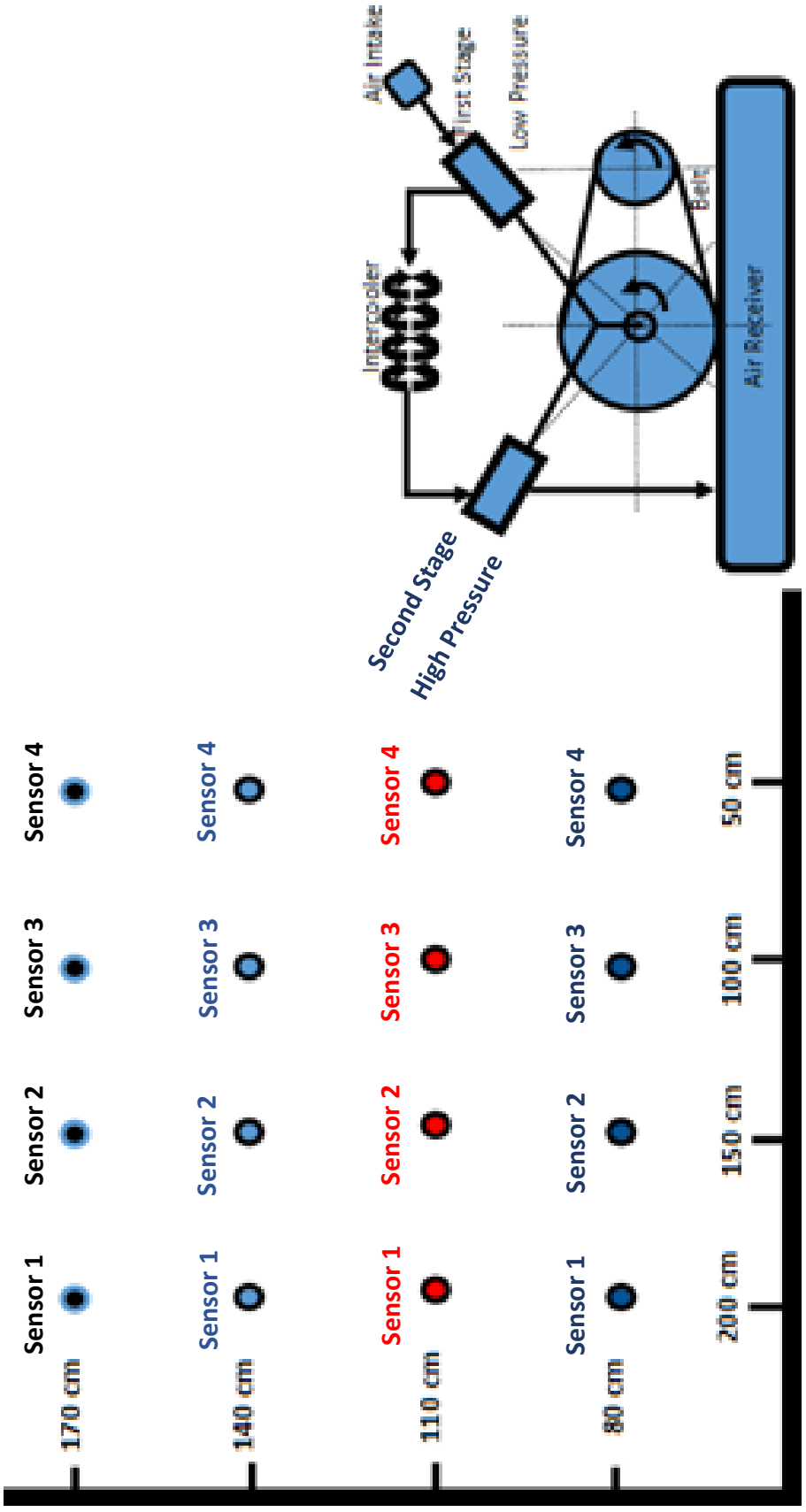

Figure 7-3 System Layout

Sensor Arrangement

A Broomwade TS-9 compressor has been used as shown in Chapter 4 with the Compressor Specification Table 4-1.

The simulation test was conducted with four acoustic sensors as described below in Table 7-3.

Sensor 1 is a “BAST YG201” serial no. 07228 is set at 50, 100, 150 and 200 cm and height of 1.7 m from floor level known as channel 5 from the data acquisition.

Sensor 2 is a “BAST YG201” serial no. 07066 set at 50, 100, 150 and 200 cm and height of 1.4 m from floor level known as channel 6 from the data acquisition.

Sensor 3 is a “BAST YG201” serial no. 07198 set at 50, 100, 150 and 200 cm and height of 1.1 m from floor level known as channel 8 from the data acquisition.

Sensor 4 is a “BAST YG201” serial no. 100252 set at 50, 100, 150 and 200 cm and height of 0.8 m from floor level known as channel 10 from the data acquisition.

Table 7-3 Acoustic Sensor

Sensor 1, 2, 3 & 4	
Serial Number	07228, 07066, 07198, & 100252
Microphone Type	BAST YG201
Sensitivity	± 0.5 dB
Temperature	-40° to + 85°C
Frequency Range	16 Hz to 100 KHz

General System Set up

Figure 7-4 shows the System set up with an array of four sensors/microphones positioned vertically which can be moved at different distances and Figure 7-5 shows the Test Bed layout in which the sensor placement and signal flows are detailed.

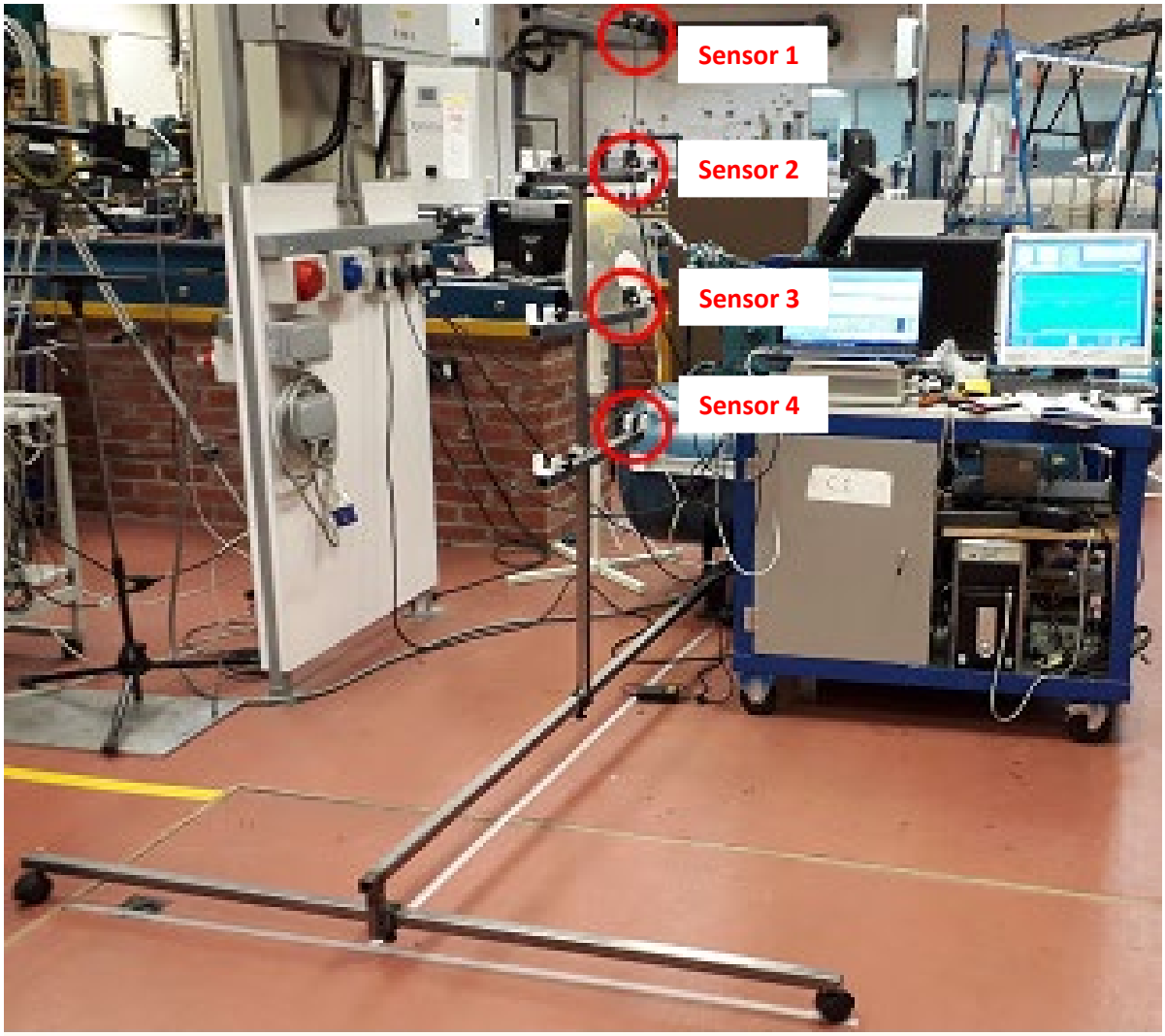

Figure 7-4 System Set up

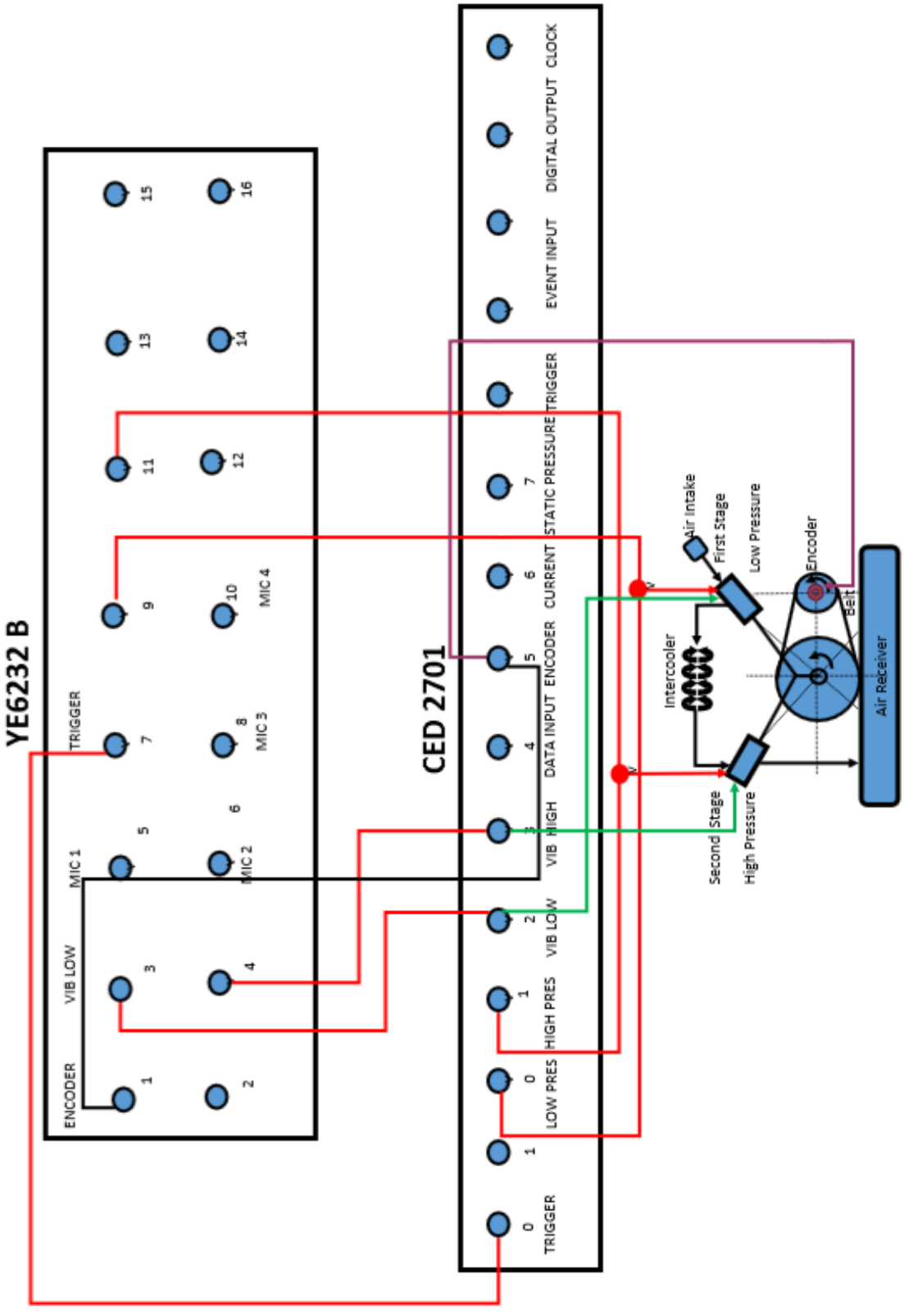

Figure 7-5 Test Bed Layout

7.2.2 Test Cases and Procedures

To study the acoustic monitoring techniques, a series of tests were carried out while the machine was in operation. The test cases and operating conditions are detailed in Table 7-4.

Table 7-4 Test Cases

Test Cases	Fault Locations
Healthy (BL)	n/a
Discharge Valve leakage (DVL)	At 2nd Stage Discharge Valve
Suction Valve Leakage (SVL)	At 1st Stage Suction Valve
Intercooler leakage (IL)	Intercooler
Loose Belt (LB)	Transmission belt

7.2.3 Sound Imaging

Figure 7-6 Spiral Array Acoustic Camera displays a Spiral Array Acoustic camera with 64 microphones. This device can display a sound field like an image and hence can visualise the position and shape of the field [167]; it assists in the localisation of acoustic signal generation mechanisms, in this case, from the compressor under study. Table 7-5 shows the Spiral Array Specification.

Table 7-5 Spiral Array Specification

Spiral Array	
Acoustic Imaging	
Sensors	64
Aperture	1 m
Sensitivity	50mv/Pa
Dynamic	34dB-140dB

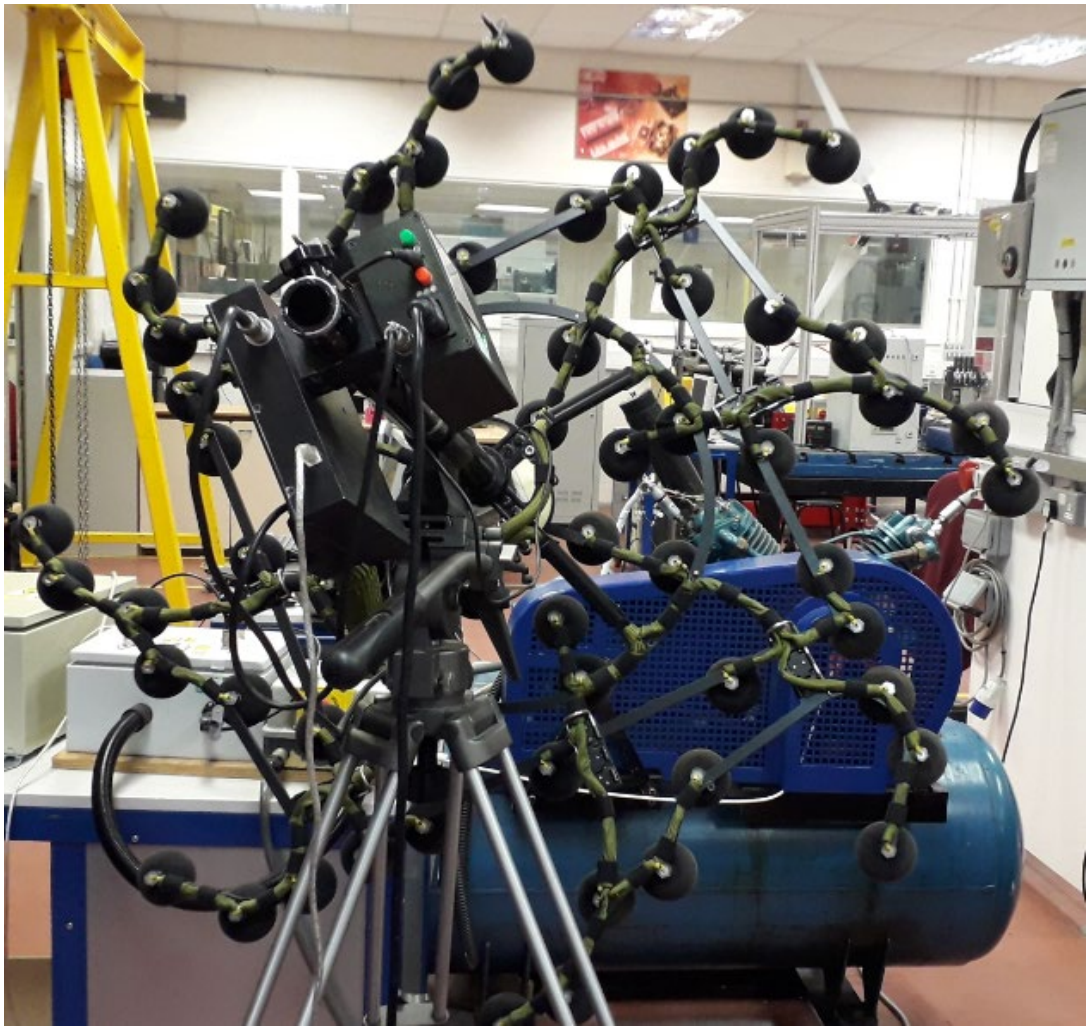

Figure 7-6 Spiral Array Acoustic Camera

7.3 Techniques Evaluation

This section proved the feasibility of the acoustical condition monitoring technique and its possibilities of extracting features without the need for attaching any equipment to the machine whilst in operation, also known as Non-Destructive Testing (NDT). For this study, the Discharge Valve Leakage (DVL) is compared with the Baseline (BL) to demonstrate its operation and how it can affect the performance of the Reciprocating Compressor (RC). The area of study is Root Mean Square (RMS) comparison, Vibration against the Acoustic Spectrum, Short-Time Fourier Transform (STFT) and the sound frequency analysis. Acoustic imaging is also studied and its effectiveness has proven to be possible. The technology of acoustic imaging has the capability of visualizing and localizing the source of sound position in the various frequency bands to alleviate any noise intrusion.

7.3.1 RMS Analysis in Time Domain

The RMS analysis is shown in Figure 7-7, the values are calculated for all the cases to quantify and qualify the differences of the acoustic signal in comparison to pressure at 0.8, 1.1, 1.4 and 1.7 m height from the floor level and 50, 100, 150 and 200 cm away from the compressor.

RMS Analysis of 50, 100, 150 200 cm away from Compressor

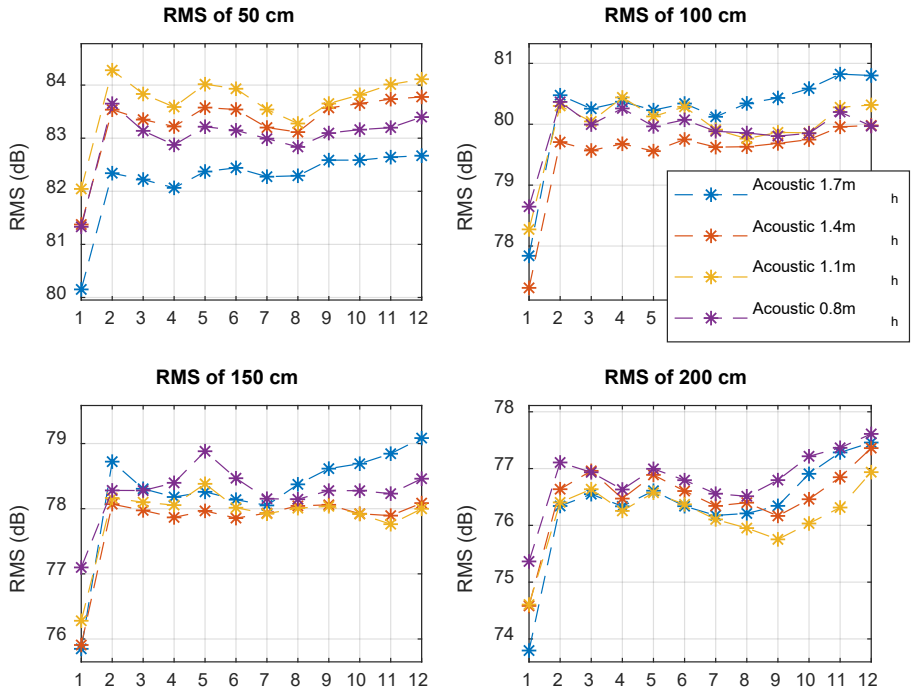

Figure 7-7 RMS Analysis

The RMS values of the sound pressure variation are dependent on the load fluctuation of the operation of the machine.

The RMS of sound pressure value at 50 cm is higher in comparison to the remaining three distances at 100, 150 and 200 cm under all operating discharge pressure conditions. RMS of 50 and 100 cm reveal that the amplitude of the acoustic signal is at its peak when the acoustic sensor is at a height of 1.1m from the ground. In this location it reveals most detail about the sound propagation and location of the noise sources under all operating discharge pressure conditions. However, the RMS acoustic signal of the sound pressure decreases when the microphones are further away from the compressor. Based on this method, it defines that if the distance to the object is increased, then the RMS height is decreased. Nevertheless, at acoustic of $1.1m_h$ in yellow colour at 50 cm away from the source, it seems to be the location in this analysis that generates more noise from the RC.

RMS Comparison of Baseline against Discharge Valve Leakage

Figure 7-8 demonstrates the RMS comparison of BL against DVL in respect to the sensor height and its distance away from the compressor. From this study, it is possible to tell when the DVL is deviating and see how the trend of the sound generation from the RC is affected. It is noticeable that the RMS signal is prone to be influenced by the measuring distance. This comparison also clarifies that if the distance to the object is increased the RMS height decreases.

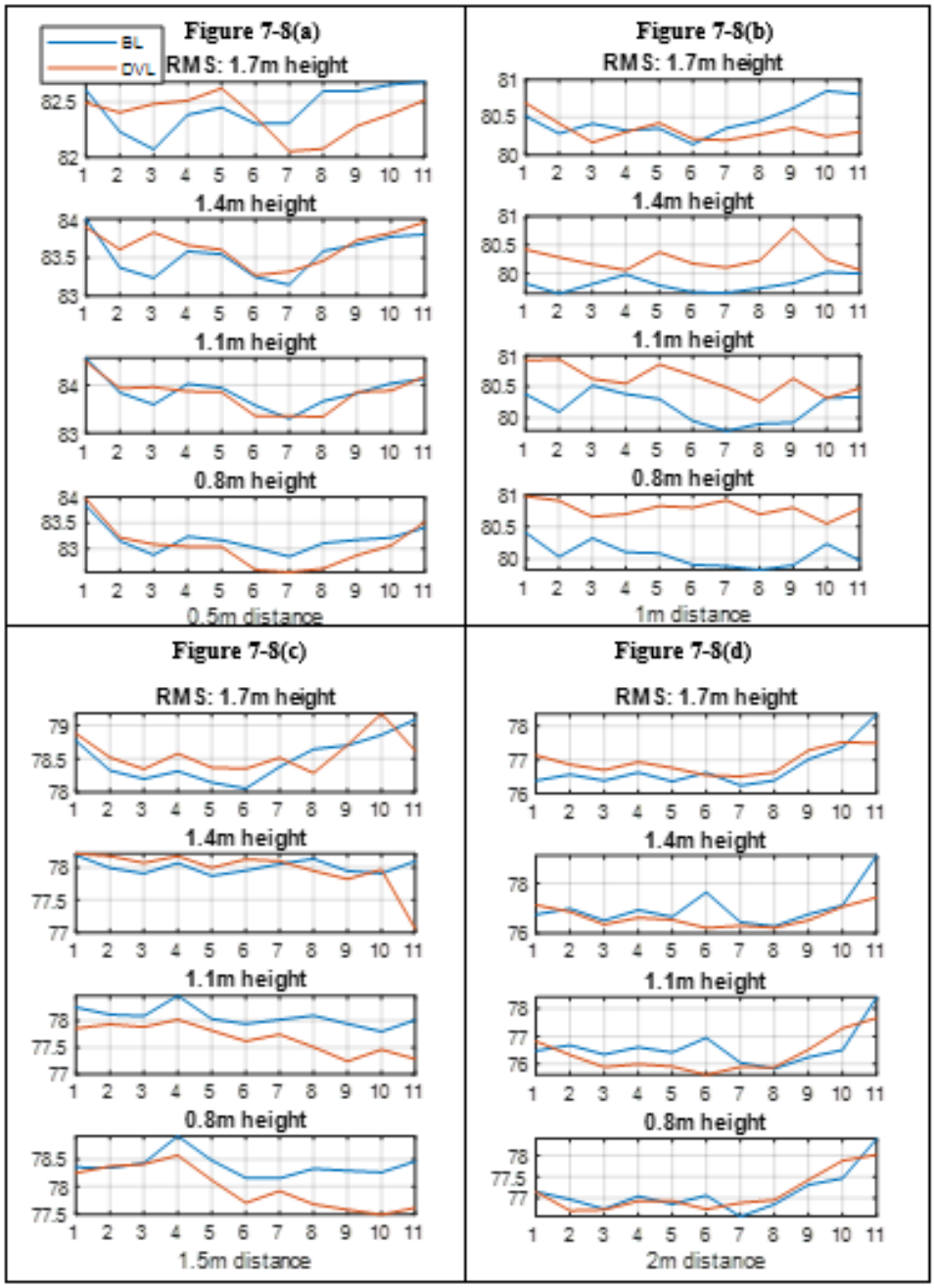

Figure 7-8 Comparison between Baseline and Discharge Valve Leakage

7.3.2 Vibration Spectrum VS acoustic spectrum in Frequency Domain

From both the vibration and acoustic spectrum of the RC as shown in Figure 7-9, there are some discrete frequencies in the low frequency under 1500Hz especially under the 600Hz which are related to discharge leak valve due to its high impact velocity. The flow of gas to and from the leaking valve travelled around the enclosure in an erratic flow pattern, through cylinder openings and cavities under and above the valve. The uneven distribution of gas flow can affect and cause other plate valves to wobble during the opening and closing motion creating an abnormal mechanical action and hence the reason the noise level increases.

Frequency of Vibration Spectrum VS Acoustic Spectrum

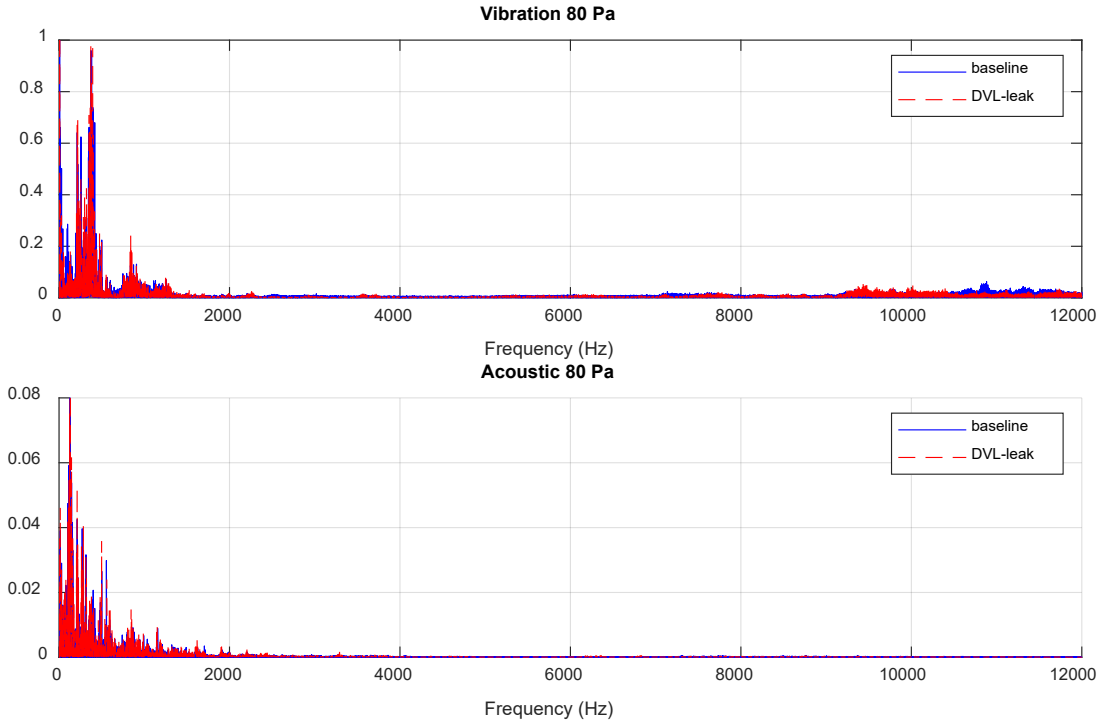

Figure 7-9 Frequency of Vibration and Acoustic Spectrum

Figure 7-10 displays an unevenly spread into 4 intervals. The acoustic signal contains the vibration components but it is different in acoustic. Due to the reciprocating nature of the machine and the residual imbalance the peak is aligned with the harmonics of the rotational frequency of the crankshaft. The correlation under 500 Hz between both the acoustic and vibration looks dissimilar.

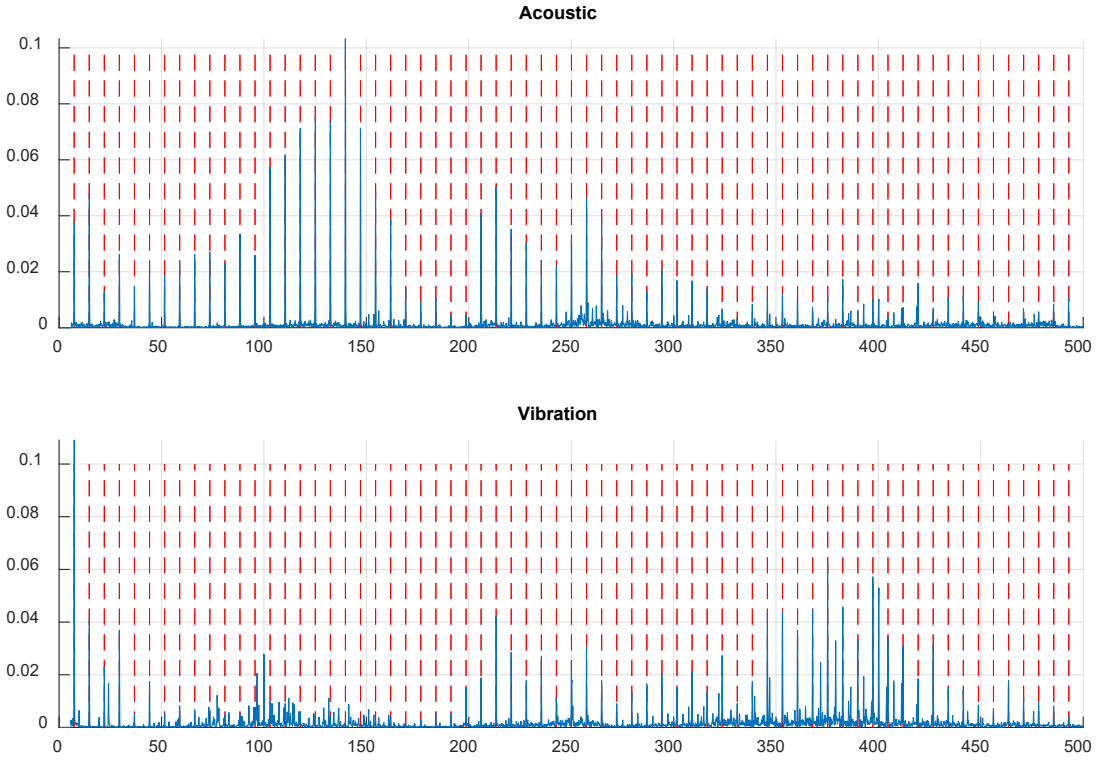

Figure 7-10 Frequency of Vibration and Acoustic Spectrum

7.3.3 Short-Time Fourier Transform from 0 to 110 psi

Short-Time Fourier Transform (STFT) is implemented at a high level to observe the frequency change of vibration and acoustic from Figure 7-11.

The data shown demonstrates a combination of how the components change based on the vibration and acoustic signal against time and frequency. The changes for both vibrations occur within the range of 0.32 to 0.345 kHz whilst for acoustic it is within 0.22 to 0.23kHz. This indicates that STFT Vibration has a number of visible spectral components in the frequency range of 0.32 to 0.345 kHz compared to the acoustic signal. Both SFTT plots demonstrate valuable feature trends of the RC baseline against DVL and the harmonics decrease linearly with the pressure. However, vibration STFT appears to be better than acoustic for this exercise and further works are required in simulating and studying all the seeded faults on the RC such as DVL, intercooler and suction leakage.

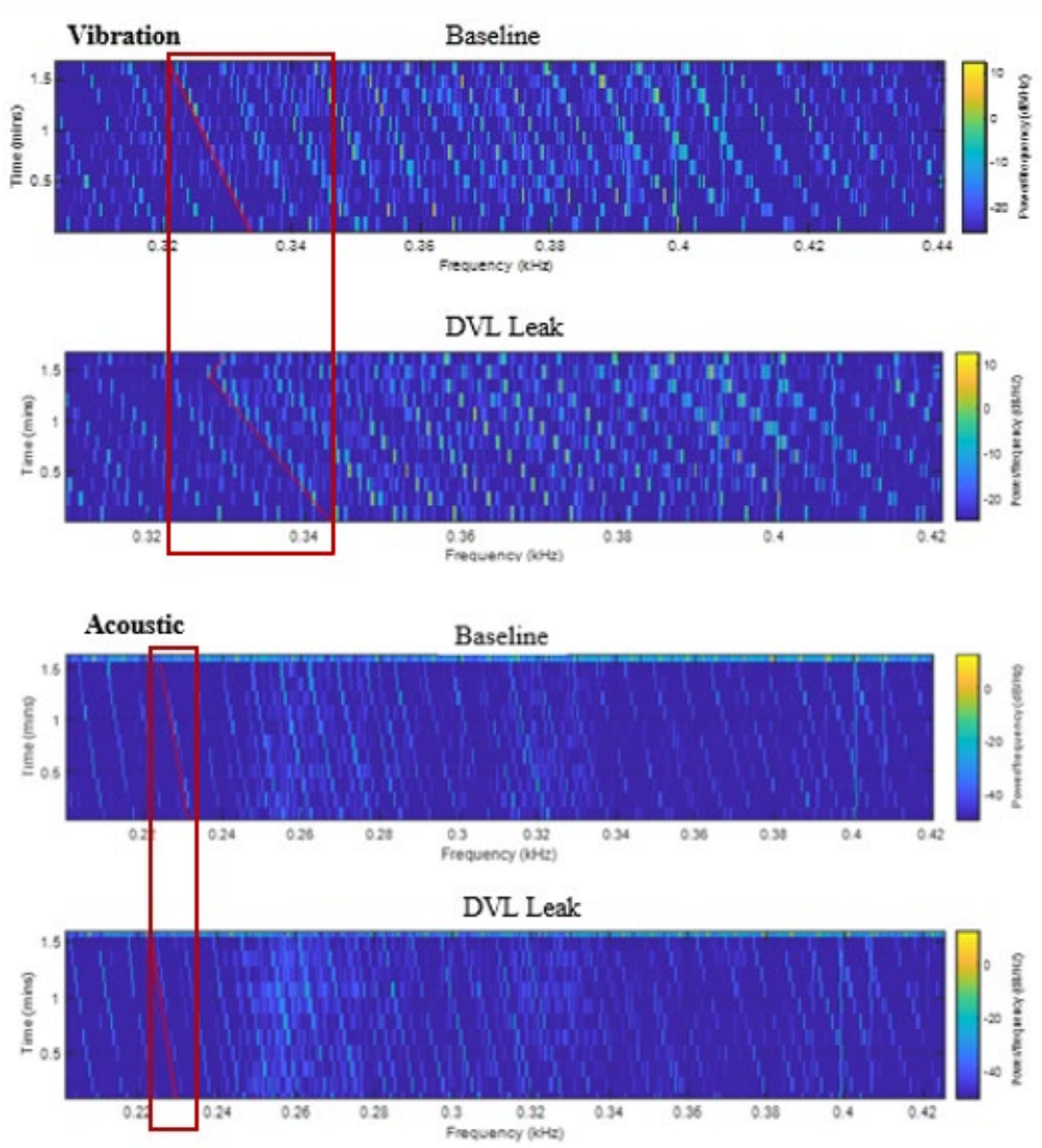

Figure 7-11 Acoustic in Short Time Fourier Transform

7.3.4 Rotational frequency

The vibration of the shaft mechanism usually happens at the rotational frequency of the machine shaft and when the system is changing state. The environment where the measurement is taken can also have an impact on the way the sound travels. Figure 7-12 details the rotational frequency of three sets of tests for BL and DVL of the RC. For each parameter and pressure two instantaneous values were recorded. This was repeated on a minimum of three separate occasions and the results were averaged to those data points. It is obvious that on baseline and DVL the sound pressure levels decay linearly.

The noise level of the DVL is lower compared to baseline which was recorded by the microphones. The fluctuation of the three sets of data of baseline and DVL can be attributed to a range of compressible factors. The sound pressure level of the RC operates steadily, the rotational speed converges and as the faults decrease the efficiency of the compression, hence increasing the load. Further works are suggested with an emphasis in analysing all the seeded faults as suggested for the STFT vibration above.

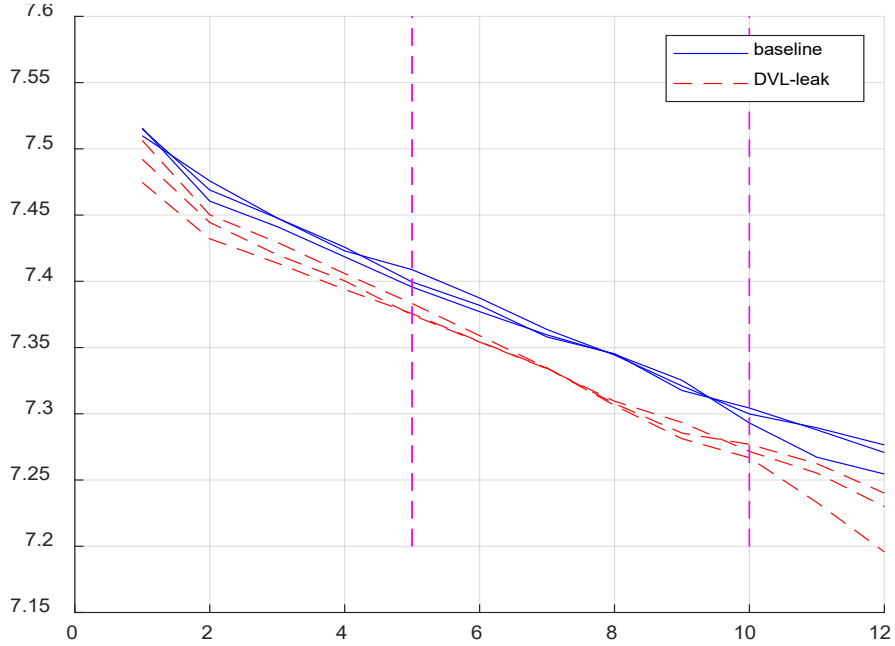

Figure 7-12 Rotational Frequency

7.3.5 Sound Localisation through Acoustic Imaging Technology

This study aims to identify the exact noise sources location from the RC through the acoustic imaging and frequency analysis by computing RMS value in the frequency domain. The Sound Imaging was found to be the best approach as it allows the connection between the frequency with acoustic signal generation mechanisms.

Test Procedures

As described in Figure 7-6 Spiral Array Acoustic Camera with 64 microphones was used as the device has the capability of displaying a sound field like an image, hence can visualise the position and shape of the field. The test procedure is similar to that as described in Section 7.2.2, however, in this exercise, only the second stage, Discharge Valve Leakage (DVL) was under test. The DVL has a 2 mm hole drilled as explained in Section 4.3.2.1 Simulation of Valve Leakage and Figure 4-3 shows the faulty valve plate.

Valve Leakage Simulation

Discharge valve leakage is more critical than the Suction Valve Leakage (SVL) as the valve works at high pressure and is more exposed to impacts and wear therefore it is obvious that at this stage a higher sound level will be generated. The Spiral Array Acoustic Camera was placed at 2 metres away from the RC. Four sensors were placed at different heights as described in chapter 7.2.1 in the Measurement System Layout which collects and analyses the raw acoustical signal as explained in Chapter 7.2.

Frequency Range Analysis According to Sound Localisation.

There is a variety of reasons for the valve to generate sound as explained in Chapter 7.1.1 and the discharge valve is amongst them. The frequency analysis study has made it possible to identify the noise sources where the distributed noise pattern radiates and at a known frequency. After a series of tests and analysis, it has been possible to locate the noise generation from the RC, where the distributed noise pattern radiates and at a known frequency. Figure 7-13 shows the frequency ranges from 125 to 3300Hz. The investigation started at a low frequency of 125 to 200 Hz initially and slowly progressed up to 3300 Hz. From observation, the sound is produced from the entire compressor and its surroundings and the reflection can be taken as the area source. At 312 to 600 Hz a big spot can be jumping up and down in front of the compressor and its surroundings. At 600 to 900 Hz below it is obvious that the compressor cylinders, both first and second stage crankshaft and motor radiate the noise. It is more visible and excited by an eccentric wheel at 900 to 1200 Hz. At 1200 to 1500 Hz shows noise radiation slightly below the head of the first and second stage compressor and is inclined more toward the driving belt. From 1500 to 2400 Hz the noise sources are detected at both stage cylinder heads and moving around this area. At frequency ranges from 2400 to 3300 Hz the noise sources are coming from the second stage cylinder, intercooler and the crankshaft. However at frequency ranges of 3000 to 3300 Hz below it is clearer that the compressor cylinder second stage radiates the noise and is much sharper. The acoustic imaging has been able to segment the frequency band and distinguish where the noise source is being generated from the RC.

Relationship of the Frequency Analysis to the Cylinder Pressure and Vibration Analysis

This shows a clear indication that the DVL of the RC requires more work. This also demonstrates a correlation to Section 4.7.3 Changes in Cylinder pressure under Discharge Valve Leakage at 120 psi and Section 4.9.1.1 Vibration-based Condition Monitoring of the Discharge Valve Leakage Vibration at 8.3 bar of the 2nd stage cylinder, where DVL operates

at its highest pressure and oscillating at approximately 11 bar at 120 psi and requires more compression. This supports the finding in this study of the RMS Frequency Range Analysis where the detection of the cylinder knock generates more noise from the compressor 2nd stage.

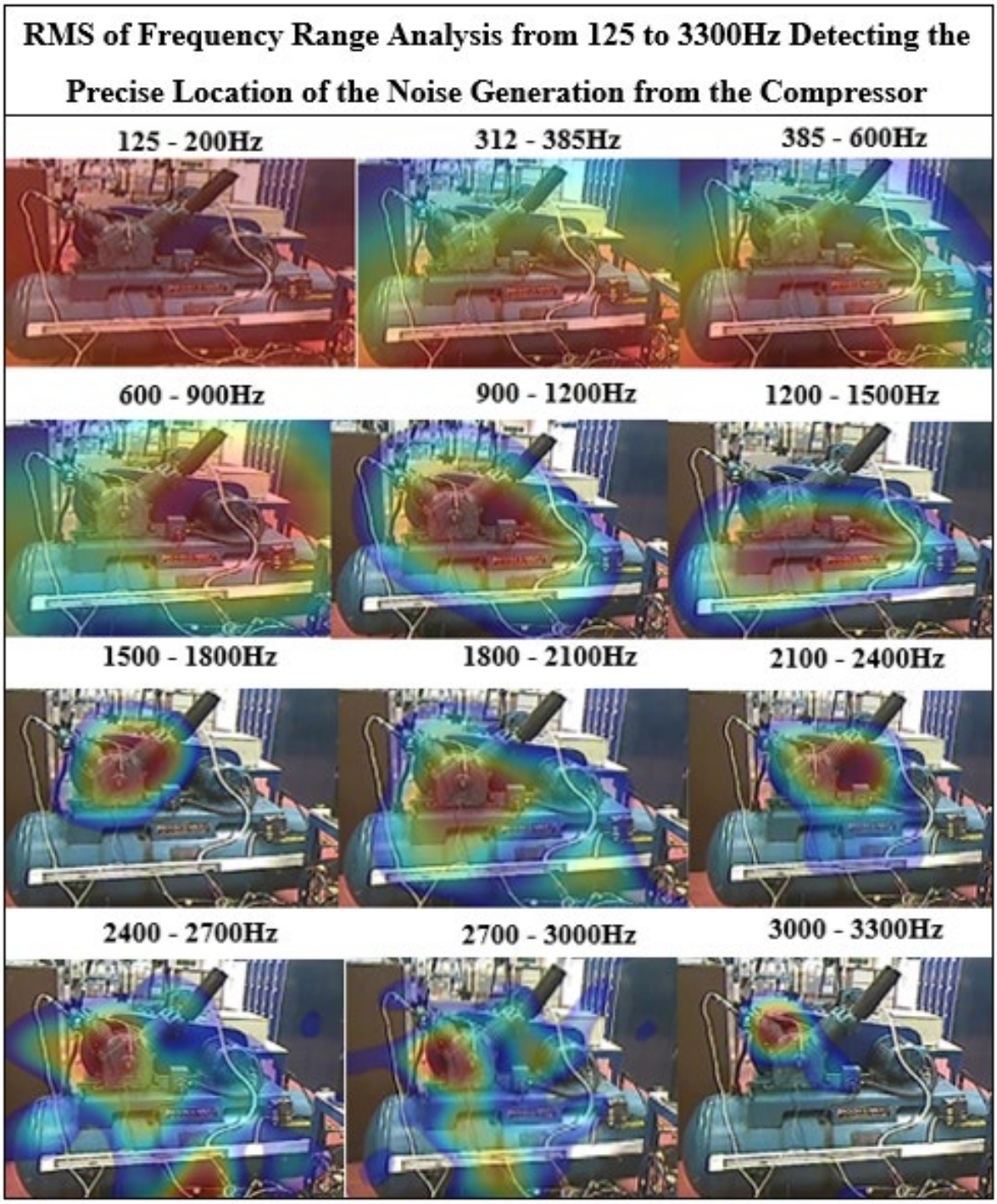

Figure 7-13 Frequency Range Analysis from 125 to 3300Hz

7.3.6 3D Column Chart Analysis

The 3D column chart from Figure 7-14 to Figure 7-19 shows the difference in RMS when the baseline is subtracted from the DVL readings, over the frequency range 0 to 12kHz and for a range of sensor heights and distances from the target machine. Frequency Range from 2100 to 3300Hz shows a good distribution in sequence at 0.5 metres.

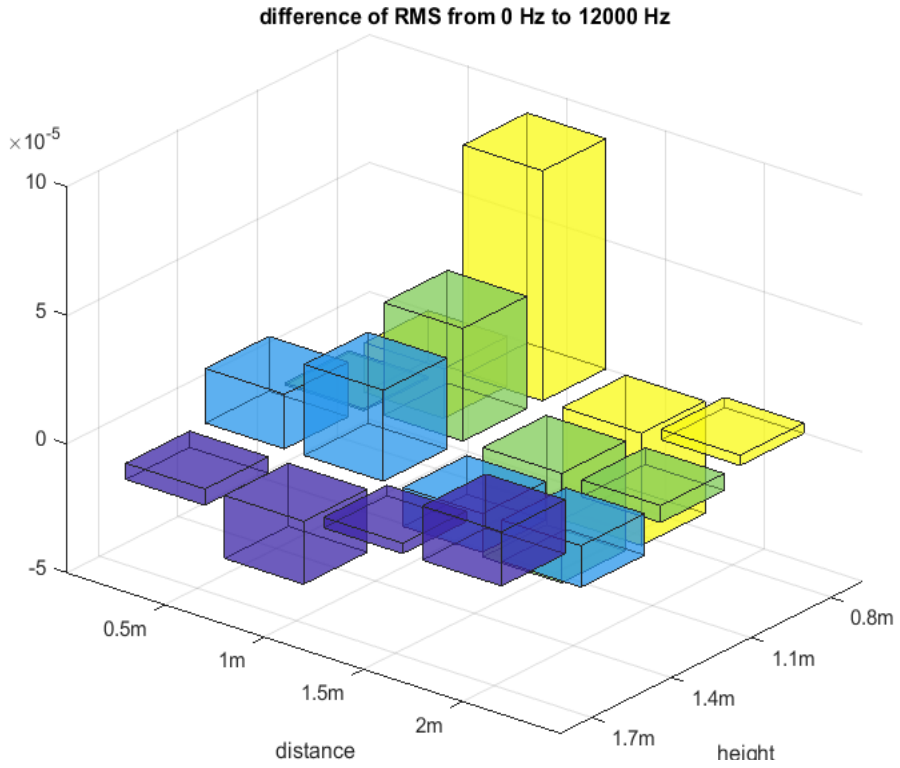

Figure 7-14 Bar Diagram from 0 to 12000 Hz

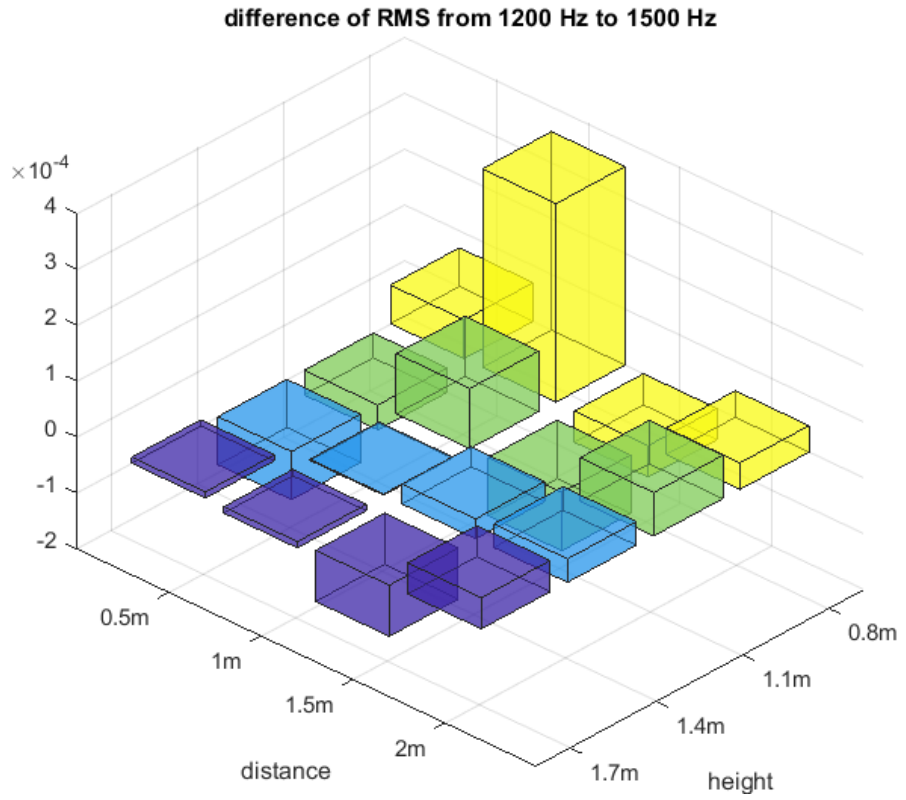

Figure 7-15 Bar Diagram from 1200 to 1500 Hz

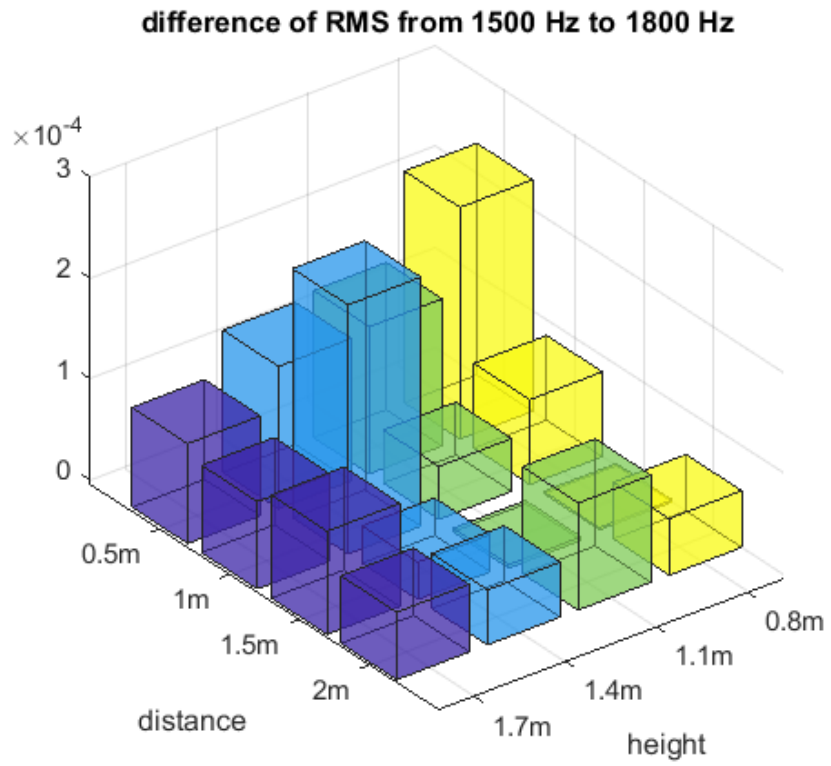

Figure 7-16 Bar Diagram from 1500 to 1800 Hz

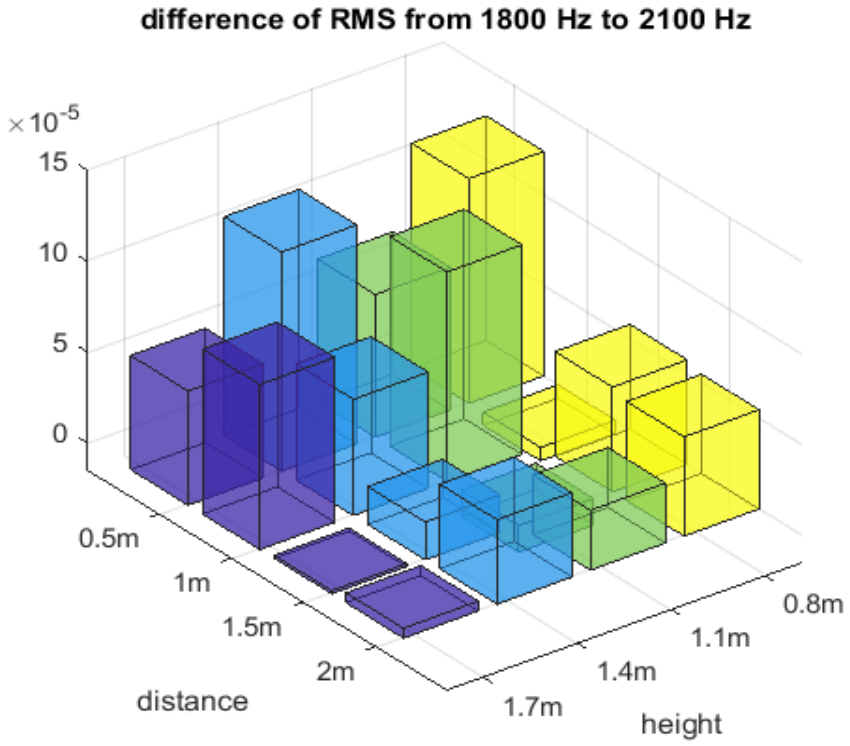

Figure 7-17 Bar Diagram from 1800 to 2100 Hz

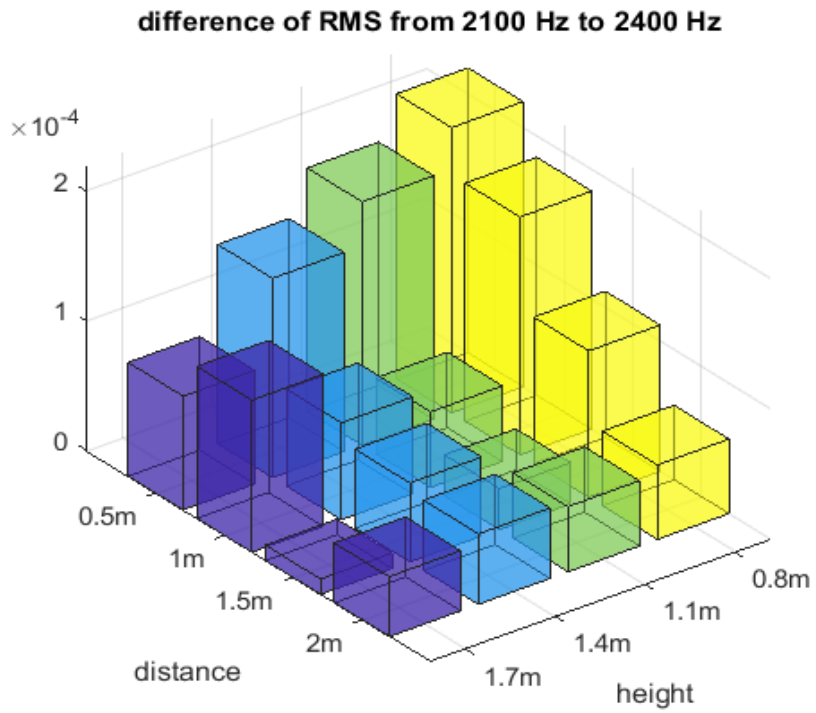

Figure 7-18 Bar Diagram from 2100 to 2400 Hz

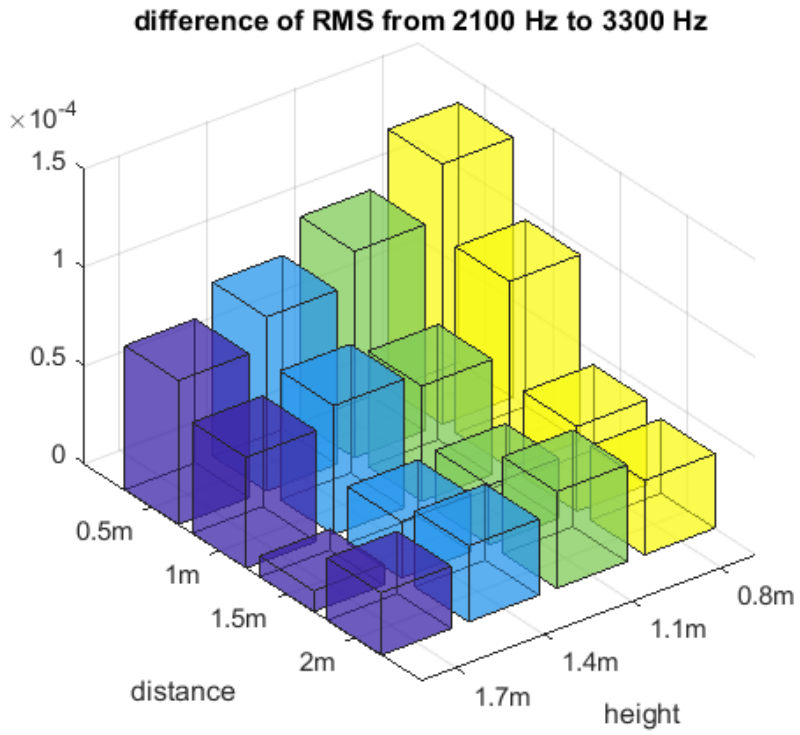

Figure 7-19 Frequency Range from 2100 to 3300Hz

7.4 Discussion

From the Time Domain RMS Analysis, the acoustic signal at 1.1m height, 50 cm away from the compressor, shows a good indication of the sound propagation and for locating noise sources under all operating discharge pressure conditions. However, the RMS acoustic signal of the sound pressure decreases when the microphones are further away from the compressor. The Spiral Array can locate sources of airborne sound at a higher frequency. Based on this finding it is clear that the second stage cylinder valve was generating more noise as it was seeded with a faulty valve. This faulty discharge pressure was also not steady due to the faulty valve motion and contained a high temperature due to the second stage cylinder high compression actions. This caused a rise in the acoustic level which reduced the performance of the compressor. The harmonics shift can indicate an abnormal operating state caused by the faults. RMS of the specific frequency range can indicate the faults which are consistent with the sound localisation from the sound imaging device. Based on 7.3.5 of the Sound localisation it is evident that at high-frequency ranges of 3000 to 3300 Hz the compressor cylinder second stage radiates more noise and is much sharper. It was possible to section the frequency band and differentiate where the noise source is being generated from the RC. To end, the 3D Column Chart Analysis Figure 7-19 at 2100 to 3300Hz shows a good distribution.

Chapter 8. **Acoustic Monitoring of the Laboratory Compressor with State of-the Art Convolutional Neural Networks**

For efficient acoustic data analysis, Chapter eight is the final part of Phase III and focussed on the Convolutional Neural Networks (CNN). As a state of the art technology, CNN can be applied to raw data for extracting optimised diagnostic information, which avoids the inefficiency of signal analysis based feature extraction and optimisation. CNN will be used to mine acoustical data from a Reciprocating Compressor (RC) and locate an optimal position away from the RC for the data collection, demonstrating which signal has a good indication of sound propagation and locating of noise sources under four operating discharge parameters. CNN architectures and training procedures are detailed. The results show this CNN based scheme allows high diagnostic accuracy, as well as the determination of the most suitable microphone localisation.

8.1 Acoustic Signal from Reciprocating Compressor

The acoustical signal emanating from RC is time-varying because various components manifest a significant change with time and this can increase frequency modulation. These unveiled modulation frequencies proved the roughness, impulsive, abrupt change of amplitude with time, varying wideband and harmonic [168]. The non-stationary process is common when equipment runs under various loads and conditions. The reciprocating compressor is a good example where there are transient signals generated during the various stages in the process, including the stop and start of the motor. These signals can be in the form of acoustic, vibration, current and much more. The acoustic signal in the RC can be regarded as a tough non-stationary signal due to its harsh operation and can also contain critical information of the compressor condition and its mechanism. These non-stationary processes can provide a good indication of the state of the equipment which cannot be realised by a stationary signal.

8.1.1 Common Feature Analysis Methods

To conduct an effective diagnosis and prognosis, the most significant and responsive features should be chosen. The lack of accuracy in this process selection can reduce the effectiveness and reliability of the study. To reach a good agreement in this pre-arrangement, a brief explanation is given below by using common feature analysis methods to explain the 'Time Domain Analysis', 'Spectral Analysis' and 'STFT Analysis', which will reveal the signal characteristics and also express the advantages of the Short-Time Fourier Transform (STFT).

Time Domain Analysis

Time-domain parameters such as kurtosis, Root Mean Square (RMS), crest factor, peak to peak and skewness is generally known as statistical parameters and time-domain features, they can provide an unsteady time-varying signal and are normally used for the non-stationary signal.

Kurtosis is a well used feature, it is based on the distribution of signal data with time series random variable [169]. It is a measure of the distribution intensity. The time-domain techniques normally relate to a specific change of the waveform signal in time.

The signal of the Root Mean Square (RMS) and crest factor are well known and the easiest features in the time domain analysis. RMS is very effective in finding any imbalance and other associated faults in the rotating machine. The downfall is that it cannot detect a deteriorating part [169]. RMS technique characteristic is to have a good time resolution at the same time

keeping a poor frequency resolution whereas crest factor is usually explained as the ratio of peak value over RMS value of a given signal and can indicate the shape of the waveform.

Peak-to-peak is the variance between the maximum and minimum amplitude of the signal whereas skewness is generally defined as the characteristic parameter qualifying the asymmetry degree of signal distribution. Defects can highly influence the distribution symmetry and intensify the level of skewness.

Spectral Analysis

The Frequency domain analysis gives spectral facts of signals and is achieved by altering the time domain signal into the frequency domain. The advantage of this analysis is that it can isolate a certain frequency of attention. Fast Fourier Transform (FFT) can provide the frequency domain of a steady signal but not for Time Varying signal and is mainly used for stationary signal and "windowing", however FFT is simple to implement compared to STFT. Nevertheless, the FFT analysis has some serious shortfalls. One of them is that time information is lost in the transformation to the frequency domain [170]. FFT is a stationary signal that cannot identify when an event has taken place, this is not generally used in the time domain parameters.

Short Time Fourier Transform Analysis

Signal processing is present in a variety of applications. Its main objective is to provide underlying information on specific problems in the decision making process and the use of the correct approach is fundamental. The popular technique used for studying non-stationary signals is the STFT and for this reason it has a fundamental place in the time frequency domain. The signal is non-stationary if the spectral contents or frequency changes with respect to time. STFT works in choosing a localised window function in the time frequency function and the signal is divided into smaller time intervals in respect to the moving window function. This technique is called "Windowing" the signal. Each interval is analysed with the Fourier Transform which will then determine the frequency at which the interval exists [171].

STFT is described as a form of collaboration between the time and frequency based views of a signal. It explains what is happening in both situations, at what frequencies and the occurrence of a signal. The precision of this information is determined based on the size of the window. The shortcomings are that as soon a particular size for the time window is selected these frequencies will apply for that specific window. Signals come in various forms and some may

need a more flexible method [172]. The spectrogram remains to be the main technique used as it can be easily calculated as the magnitude squared of the STFT of the time-frequency analysis [173].

In Fourier Transforms the sum of the sinusoids of different frequencies are separated from the waveform, the amplitudes are identified and a frequency amplitude of the signal is obtained. The STFT is also a Fourier Transform that is dependent on time [174].

8.2 Data Mining Based on Convolutional Neural Networks

In this study, CNN is used which is a combination of artificial neural networks and recent deep learning methods. Artificial Intelligence (AI) endeavour to give machine human-like capabilities such as the use of Neural (NN) [175]. This technology has been used for a lot of image and pattern recognition tasks in recent years. CNN's are a type of multi-layer neural networks mainly built for the processing of two-dimensional data. This technique has proven to be feasible by previous researchers such as Xiaofeng et al and they deeply endorse that if the training speed of a network is increased and the models have improved, a higher level of convolutional neural networks in image recognition is attainable and can be applied in a variety of fields [63]. Simard et al also propose that CNN can be used in many visual issues if a bigger training set is utilised and that the technique is simple and can give a good evaluation [65]. Chapter 2.4 give an in-depth literature review of CNN and its application.

Some of the core keywords used in this study are briefly explained below for clarification.

CNN uses convolutional layers to filter inputs for valuable data. This process of convolution is about merging input data, also known as the feature map, with a filter or convolution kernel to create a transformed feature map. The filters are altered based on the learned parameters to extract the most important information for a specific job. CNN fine-tunes itself automatically in finding the best feature based on the job [176]. A neuron usually works by applying non-linear filtering to a weighted sum of its inputs. Neurons are small computational elements organized in a layered structure applied as CNN inputs [177].

Convolution layers are formed by neurons known as kernels which perform a non-linear filtering operation by moving a small context window, also recognised as the kernel's receptive field on the layer's input. This also computes a series of activations as the windows cover it sequentially. Local connectivity also known as localised filtering represents a key feature in obtaining invariance against shifts of recognizable input patterns. It is vital in image

recognition that a target object is recognized regardless of its position in the input picture. The activations computed by each kernel are collected in matrices called feature maps which is also represented as the actual convolutional layer's output. The networks can achieve shift invariance at the price of losing the entire original input because of the small dimension of field receptivity.

This problem can be solved with the implementation of the sequential stacking of more convolution layers, however, the pooling layer between two sequential convolutional layers is most widely used as it can quickly achieve wider overviews. This process fundamentally subsamples each feature map, reducing its dimension and extracting the highest value from a window that moves along each feature map and this is called max-pooling. The network can learn higher level features on a wider input overview without the requirement of many convolutional layers due to the pooling layers. This, in some situations, can be an overfitting issue of result to the large number of parameters to be trained. The last CNN layer will reveal the actual network's prediction. It is usually made of fully connected neurons and each of them will immediately precede the entire layer output.

Finally, due to classifications difficulties, it is normal to use the softmax function as neurons' nonlinearity, subsequently linking each of the possible classes to a specific neuron [178].

8.2.1 Preferred Classification

Supervised Learning

The supervised learning method is used in this experiment to analyse and evaluate the collection of signals data to find out which position and signal proved to be a good indication of sound propagation under the four operating discharge pressure conditions. This method is used to process the labelled datasets where the data is transferred to the datasets so that the neural network learns the correlation between label and data. This type of classification is known as supervised learning which is a powerful instrument where classification tasks are dependent on various labelled datasets [58]. Simard et al. also postulate that the quality of a learned system is dependent on the size and quality of the training set [65] with a higher degree of accuracy. This type of Artificial Intelligence (AI) learning can also identify a person in images, recognize facial expressions, detect faces, identify objects in images, recognise gesture in the video, identify speakers, transcribe speech to text voice recognition and more [58]. These have also been briefly described in chapter 2.4.7.

8.3 Determination of the Best Sound Acquisition Position Based on Convolution Neural Networks

As described in Section 7.2.1 of the Measurement System Layout, sixteen position signals have been captured by four similar microphones, varied at four different distances and heights from the compressor, to compare the airborne signal against data validation training accuracy. Figure 7-3 shows the System Layout of those microphones "acoustic sensors" concerning the compressor. The result also enables to qualify and quantify the ideal acoustic signal location where data can be taken which will enable us to identify the ideal location for the data collection. The system layout gives an overview of how the 16 sensors are positioned.

8.3.1 General System Set up

Section 7.2.1 Figure 7-4 is the same System Set up with an array of four microphones vertically, as explained earlier, which can be moved to different positions and Figure 7-5 shows the same Test Bed layout being used for this chapter.

8.3.2 Test Simulation

In this experiment the same "Broomwade TS-9" compressor has been used as shown in Section 4.3.1, Figure 4-1. Three common fault cases have been seeded into the system at four different operating parameters: Baseline (BL), Discharge Valve leakage (DVL), Suction Valve Leakage (SVL) and Intercooler leakage (IL) and the acoustical data is collected for further processing. CNN technique is preferred as the CNN network supervised learning methods will satisfy the criteria to handle a large number of learning samples, train them and give good accuracy [65] [66].

For clarification, this study is not for fault classification. The objective is to be able to extract the acoustical data of the four test cases at various positions away from the compressor, and through the implementation of CNN, be able to locate the best position away from the RC for the data collection, demonstrating which signal has a good indication of sound propagation and locating of noise sources under the four operating discharge parameters. This is achieved by the aid of four microphones that will be moved at different heights and distances from the observed machine.

Sixteen points of data collection will be taken as explained in Chapter Seven and the following; Figure 7-1 Data Acquisition 1, Figure 7-2 Data Acquisition 2, Figure 7-3 System Layout,

Figure 7-4 System Set up, Figure 7-5 Test Bed Layout and Figure 7-6 Spiral Array Acoustic Camera are applied to this study.

8.3.3 Test Procedures

To collect acoustical data, a series of tests were carried out while the machine was in operation. The data was taken from the four test cases and the operating conditions are detailed in Table 8-1 below.

Table 8-1 Four Test Cases

Test Cases	Fault Locations
Healthy (BL)	N/A
Discharge Valve Leakage (DVL)	At 2nd Stage Discharge Valve
Suction Valve Leakage (SVL)	At 1st Stage Suction Valve
Intercooler Leakage (IL)	Loose Intercooler

8.4 Data Preparation

This study has used the original acoustical data from chapter seven where four microphones have been used at four different distances and heights from the RC under four different operating working conditions as explained in 8.3 above. To attain an optimal result, the handling of the datasets gained from the microphones requires great care and a high level of pre-processing precision.

8.4.1 Pre-processing Steps

The pre-processing procedural steps are as follows:

1) The sample data taken from the RC is converted into images and arranged into one main folder called “CNN train” as shown in Figure 8-1, “CNN train folder”.

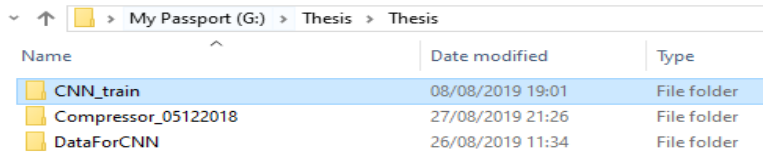

Figure 8-1 CNN Train Folder

2) It is then divided into16 folders, “Step30 Data 11 to 44” as illustrated in Figure 8-2.

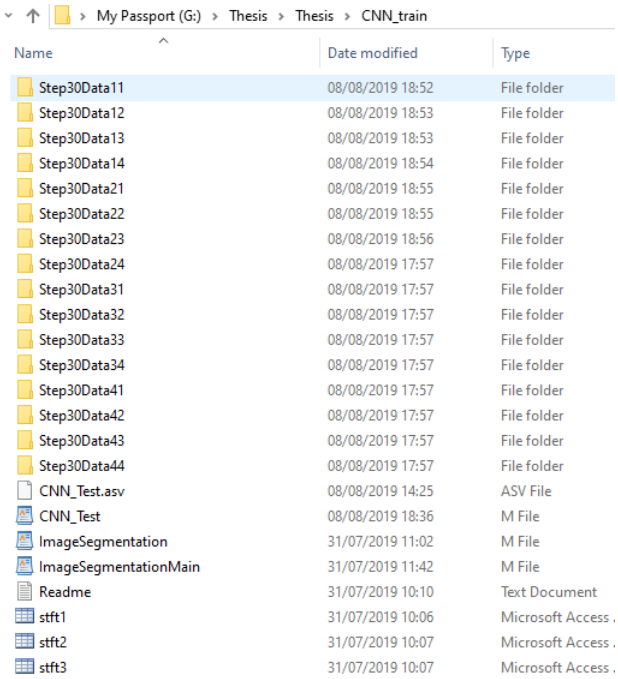

Figure 8-2 Step 30 Data 11 to 44 Folder

3) The 16 folders are now subdivided into four subfolders as shown in Figure 8-3.

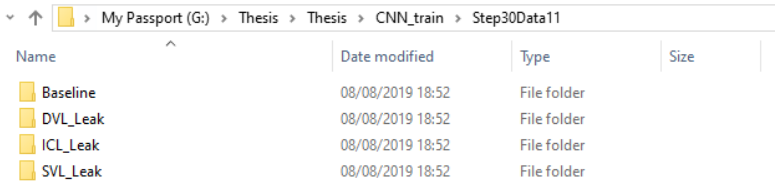

Figure 8-3 Divided Four Subfolders

4) Each subfolder will have (12 X 63) = 756 Images as presented in Figure 8-4.

Figure 8-4 Image Subfolder

5) Sixteen different networks need training hence (756 X 4) = 3024 Images. Each network will require 3024 images. For the 16 CNN, a total of (3024 X 16) = 48384 images are required. These images are now ready for training.

6) However before the training process, a MatLab algorithm was computed in the STFT program to get FFT and the following operation is performed internally (nfft = 256*4, winx **= Kaiser(nfft,18), overlap = round(0.9*nfft)), take the modulus of the complex number** and form a two-dimensional image, the size of the image is 513*1967 = 1009071

Data frequency domain after the STFT process.

The Spectrogram Figure 8-5 shows the data frequency domain after the STFT process.

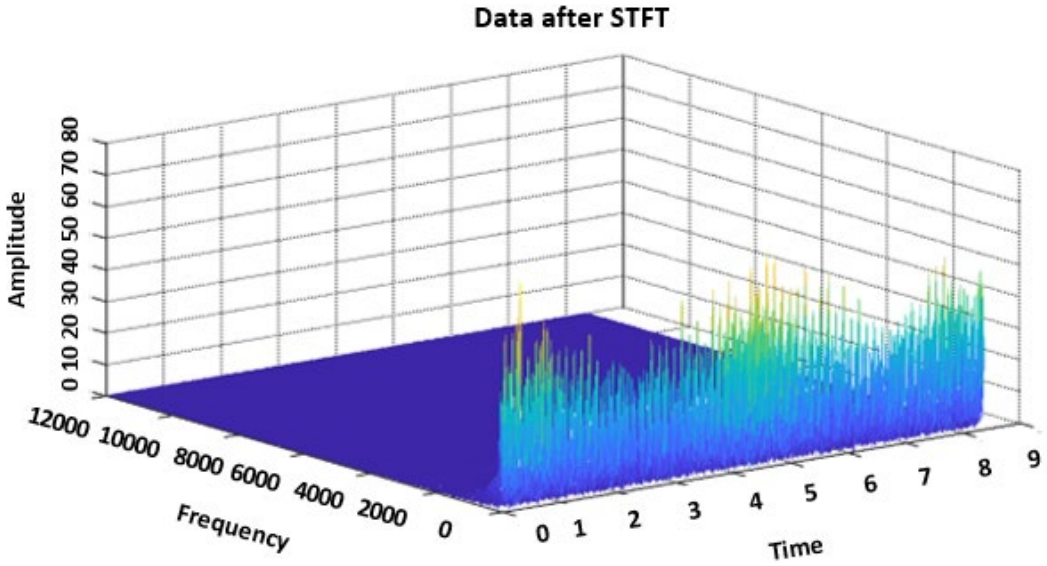

Figure 8-5 Data after STFT

Further processing is required to obtain the data in the frequency domain as shown in Figure 8-6. The image has been narrowed by (image .^ 0.5) The images are normalised to hexadecimal depth to highlight the changes in detail: (image =image/(max(max(image))))*65535.

Note: For Figure 8-5 and Figure 8-6 a majority of the frequencies between 2000-12000Hz are almost zeros as the interest is on the amplitude difference in time and frequency domain not the absolute value of the amplitude, therefore, the values are not negligible because the amplitude value in some frequency ranges are too small.

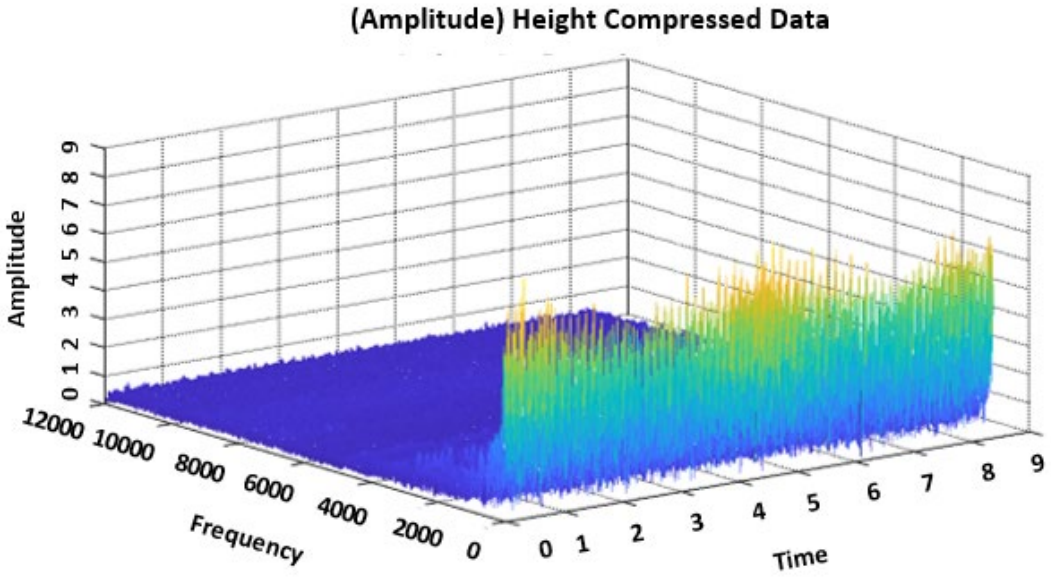

Figure 8-6 Amplitude Height Data

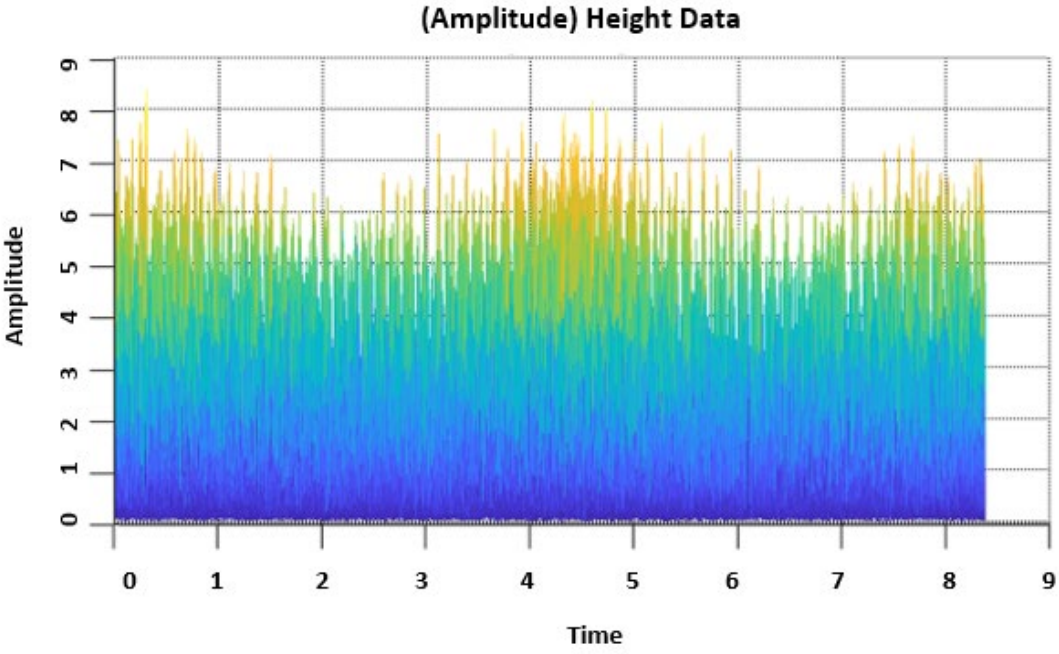

Figure 8-7 Data in Frequency Domain Changes on the Time Axis

The above Figure 8-7 shows the side view of the data in the frequency domain. The figure proves that the frequency changes on the time axis.

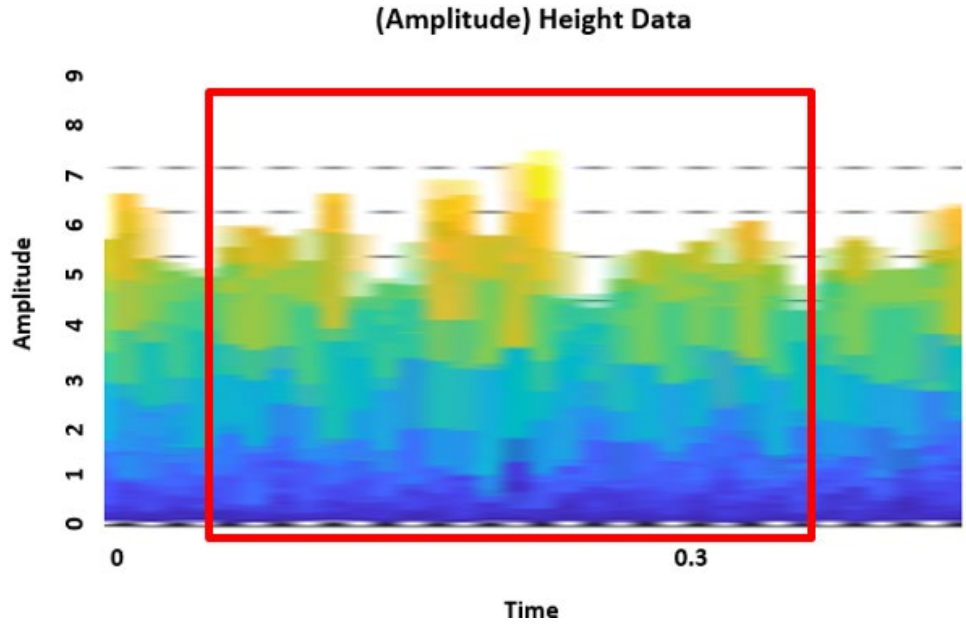

Figure 8-8 Waterfall View in the Time Axis

Figure 8-8 shows the waterfall view in the time axis and it is evident that there are 3 peaks and 3 periods. Each period of the signal is approximately 30. If the width of each image is cut to 101, which covers the three periods and the offset between the two consecutive images is 30, therefore the length of 1967 will have to be offset by 30 but this can vary depending on size. To get the number of partial images from the spectrogram, the length (1967-101)/30= 63 partial images.

63 images were picked up for each condition, distance, height, pressure and the size of each image is 513*101. All images are divided into 16 categories based on the distance and height (4x4=16).

These images are now ready for training. After training the data set size of the network the network/validation accuracy can be found.

8.5 CNN Design and Training Processing

CNN Design

This study is to find the most suitable signal acquisition position from the RC though CNN and the spectrogram obtained by the STFT as described in the time-frequency characteristics of the acoustical signals, however, it still requires further extraction to distinguish more features for the classification and identification of various signal. The acoustical datasets obtained from the microphones need thorough preparation before the CNN training. The evaluation of the acoustical images is done through the CNN deep learning network technique. The captured

images have relevant information in localising the most suitable signal acquisition position. As previously described CNN is ideal for image classification and pattern recognition in assisting for the accurate feature extraction [58], [126], [179]. In this investigation, the CNN network architecture and design was not straight forward and to achieve an optimal result and understanding of the relationship between training and validating the accuracy of the network, the key parameters were changed by four sets of trial and error exercises in accordance with the following sequential structure as illustrated in Figure 8-9. The concept is to try to get more width network with smaller convolution kernels from an initial stage.

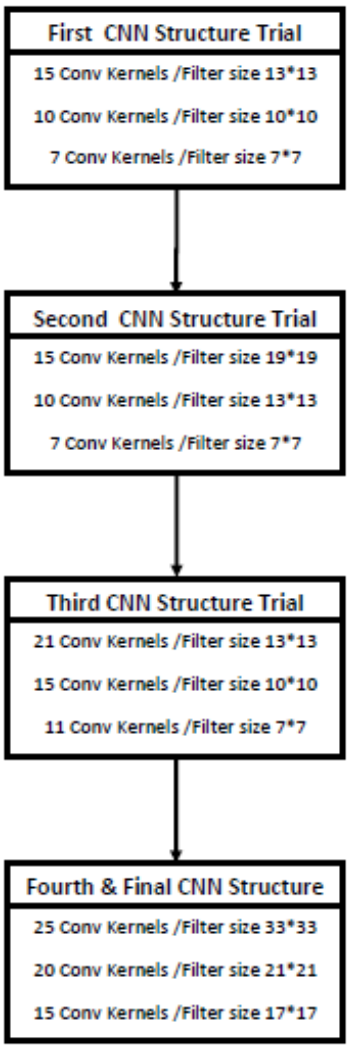

Figure 8-9 CNN Structure Trial

In order to extract more information from the images, only the first and second training trial will be briefly explained further and were arranged into three convolution kernels. Each convolution layer is accompanied by the normalised (can be trained) and pooling layer. The first convolutional layer contains fifteen convolutional kernels; 13*13 filter size, the second

convolution layer was organised into ten convolutional kernels; 10*10 filter size and the third convolution layer arranged into seven convolutional kernels; 7*7 filter size. The size of the convolution kernels also defines the information of the image and in the second structure only the first two convolutional layers filter size were changed while the kernels was unchanged.

8.6 Analysis based on Randomness Training

Network Structure Impact on the Results

The Table network representation displayed 16 networks and each network is classified as (Distance, Height) in cm as shown in Table 8-2.

Table 8-2 Validation Table Network Representation

Height in cm / Distance in cm	Network	Training of Dataset							
		N 1	**80**	*N 2*	**110**	*N 3*	**140**	*N 4*	**170**
50	*N 1*	*N(1,1)*	(50,80)	*N(1,2)*	(50,110)	*N(1,3)*	(50,140)	*N(1,4)*	(50,170)
100	*N 2*	*N(2,1)*	(100,80)	*N(2,2)*	(100,110)	*N(2,3)*	(100,140)	*N(2,4)*	(100,170)
150	*N 3*	*N(3,1)*	(150,80)	*N(3,2)*	(150,110)	*N(3,3)*	(150,140)	*N(3,4)*	(150,170)
200	*N 4*	*N(4,1)*	(200,80)	*N(4,2)*	(200,110)	*N(4,3)*	(200,140)	*N(4,4)*	(200,170)

The separation of the dataset preparation for the Network*s* and the evaluation was repeated twice, the validation accuracy of the 16 networks are derived as shown from Table 8-3 and Table 8-4 which will be briefly further below. To achieve the highest accuracy the dataset had to be first evaluated. During the import of the labelled dataset, the images were fragmented into 70%/30% where 70% of the images data is used for training the data set size and 30% is used for the validation purposes/network testing. The key parameters used during the training process are the Learning Rate = 0.01, and MaxEpochs = 3. The test for the first trial and second trial are shown in Table 8-3 and Table 8-4 where *N(4,1)* is 25% and *N(4,2)* is 44.5% on the first attempt and the second attempt *N(4,1)* is 25% and *N(4,2)* is also 25%.

Table 8-3 First Validation Test using 30% Dataset

Height in cm / Distance in cm	Network	First Validation Test using 30% Dataset							
		N 1	**80**	*N 2*	**110**	*N 3*	**140**	*N 4*	**170**
50	*N 1*	*N(1,1)*	0.25	*N(1,2)*	0.8513	*N(1,3)*	0.9515	*N(1,4)*	0.25
100	*N 2*	*N(2,1)*	0.9504	*N(2,2)*	0.7214	*N(2,3)*	0.9394	*N(2,4)*	0.8689
150	*N 3*	*N(3,1)*	0.7963	*N(3,2)*	0.7863	*N(3,3)*	0.9504	*N(3,4)*	0.7555
200	*N 4*	*N(4,1)*	0.25	*N(4,2)*	0.4449	*N(4,3)*	0.25	*N(4,4)*	0.25

Table 8-4 Second Validation Test using 30 % Dataset

Height in cm / Distance in cm	Network	Second Validation Test using 30% Dataset							
		N 1	**80**	*N 2*	**110**	*N 3*	**140**	*N 4*	**170**
50	*N 1*	*N(1,1)*	0.8293	*N(1,2)*	0.7423	*N(1,3)*	0.9868	*N(1,4)*	0.4559
100	*N 2*	*N(2,1)*	0.9108	*N(2,2)*	0.2478	*N(2,3)*	0.9835	*N(2,4)*	0.6619
150	*N 3*	*N(3,1)*	0.2489	*N(3,2)*	0.9372	*N(3,3)*	0.25	*N(3,4)*	0.8733
200	*N 4*	*N(4,1)*	**0.25**	*N(4,2)*	**0.25**	*N(4,3)*	0.2533	*N(4,4)*	0.6553

As this is only at an initial stage and the result is not great, more testing is required. The training process for the 16 datasets took two days in total to be completed.

To ensure that the low accuracy is not due to short training time, *N(4,1)* training was carried out for a second time with Max Epochs = 8. Figure 8-10 shows the progress of the second set of training of *N(4,1)* at a longer time with max epochs 8 to ensure a higher accuracy is reached. Table 8-5 shows the result of the validation accuracy which is regrettably lower therefore unfortunately the validation accuracy did not change with a lengthier training time of 108 min 6 sec.

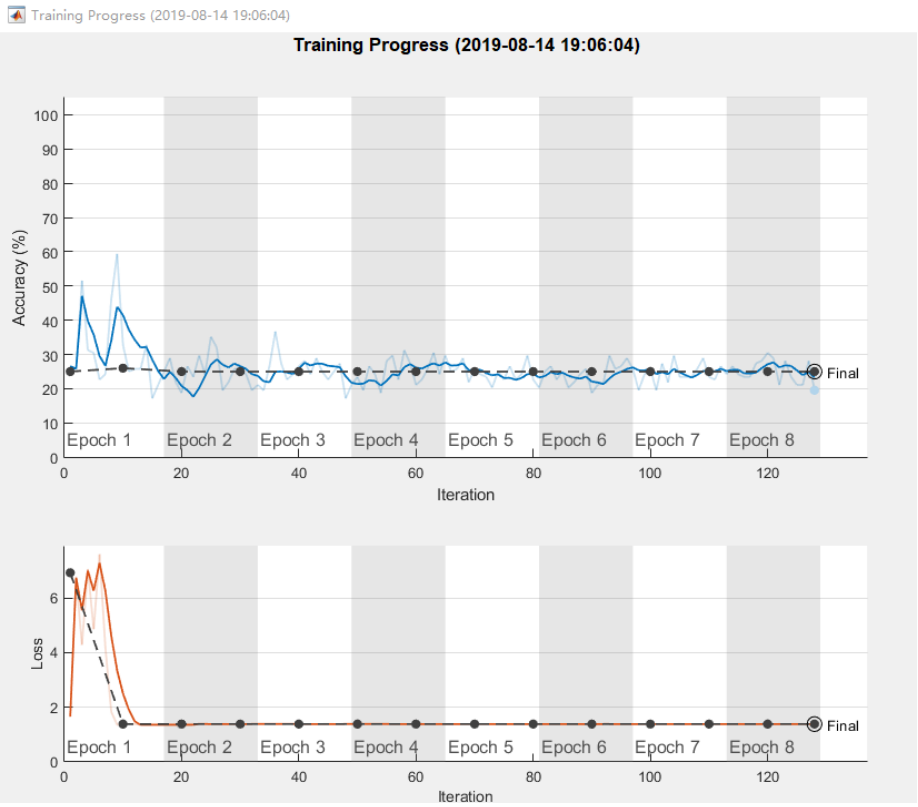

Figure 8-10 Training of Network (4,1) in Progress at a Longer Time

Table 8-5 Validation Accuracy of Network (4,1) at a Longer Training Time

Results	
Validation accuracy:	25.00%
Training finished:	Reached final iteration
Training Time	
Start time:	2019-08-14 19:06:04
Elapsed time:	108 min 6 sec
Training Cycle	
Epoch:	8 of 8
Iteration:	128 of 128
Iterations per epoch:	16
Maximum iterations:	128
Validation	
Frequency:	10 iterations

Subsequent CNN Structure Trial

To understand the relationship between the training and network dataset size, key parameters were changed in the second set of trial and error CNN Structure accordingly, with the first convolutional layer now containing fifteen convolutional kernels; 19*19 filter size, the second convolution layer was prepared into ten convolutional kernels; 13*13 filter size and the third convolution layer arranged into seven convolutional kernels; 7*7 filter size.

The aim is to get a new network with bigger convolution kernels in the first two layers. *N (4,1)* and *(4,2)* were trained again and their training progress are shown below in Figure 8-11 and Figure 8-12.

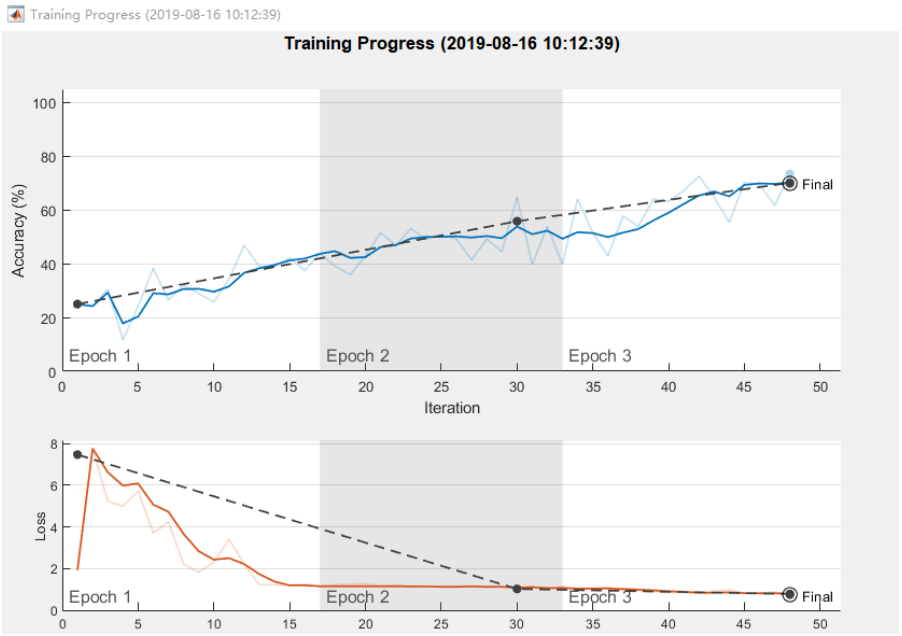

Figure 8-11 Second Training Progress of Network (4,1)

From Table 8-6 the validation accuracy of the network (4,1) was carried out at a shorter time of 22 min 56 sec with max epochs 3. It was found that if the training time is shorter the validation accuracy is slightly increased however this still needs improvement.

Table 8-6 Validation Accuracy of Network (4,1) at 69.93 % at a Smaller Training Time

Results	
Validation accuracy:	69.93%
Training finished:	Reached final iteration
Training Time	
Start time:	2019-08-16 10:12:39
Elapsed time:	22 min 56 sec
Training Cycle	
Epoch:	3 of 3
Iteration:	48 of 48
Iterations per epoch:	16
Maximum iterations:	48
Validation	
Frequency:	30 iterations

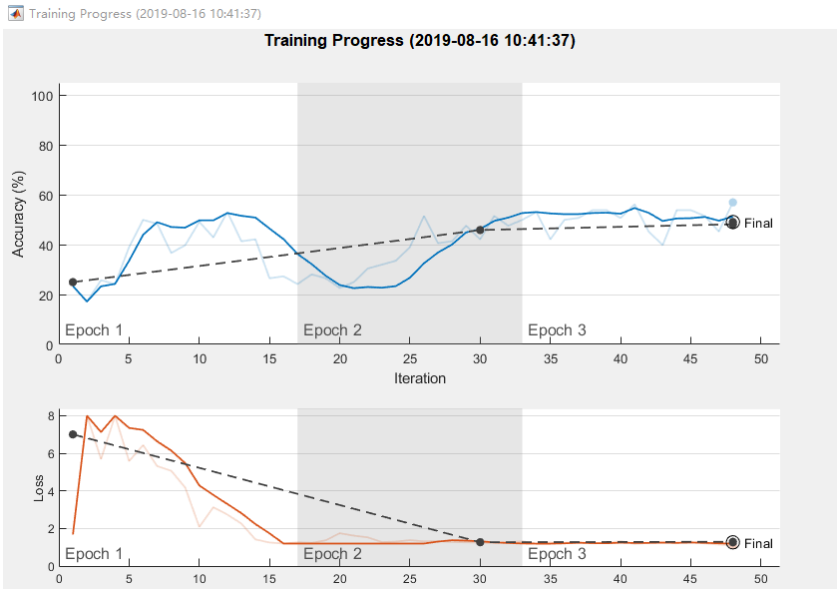

Figure 8-12 Training of Network (4,2) in Progress

Table 8-7 shows the validation accuracy of the network (4,2) at a much shorter time of 21 min 31 sec with max epochs 3. The validation accuracy is still lower and requires more work.

Table 8-7 Validation Accuracy of Network 44 at 49.12 % with a Smaller Training Time

Results	
Validation accuracy:	49.12%
Training finished:	Reached final iteration
Training Time	
Start time:	2019-08-16 10:41:37
Elapsed time:	21 min 31 sec
Training Cycle	
Epoch:	3 of 3
Iteration:	48 of 48
Iterations per epoch:	16
Maximum iterations:	48
Validation	
Frequency:	30 iterations

To explore if a smaller network with smaller convolution kernels can have higher accuracy, *N(4,1)* and *(4,2)* were trained for a longer time (MaxEpochs = 8) as shown below in Figure 8-13 and Figure 8-14.

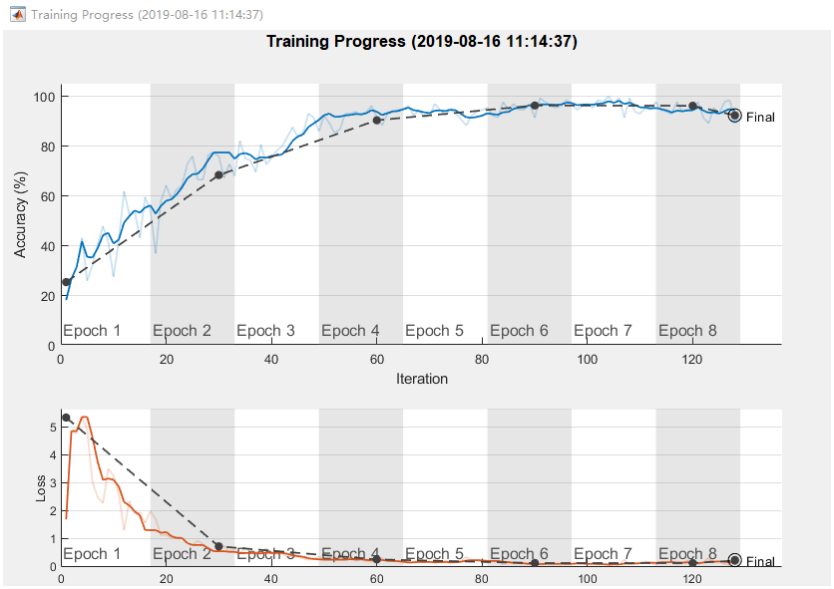

Figure 8-13 Training of Network (4,1) in Progress

Table 8-8 shows the validation accuracy results at 92.29% where the training time is increased to 56 min 55 sec. It also shows the training of the network with a longer period with max epochs 8 to ensure a higher accuracy closer to 100% but still needs enhancing. *N(4,2)*

Table 8-8 Training Processing of Network 41 (Smaller Convolution Kernels and Longer Training Time)

Results	
Validation accuracy:	92.29%
Training finished:	Reached final iteration
Training Time	
Start time:	2019-08-16 11:14:37
Elapsed time:	56 min 55 sec
Training Cycle	
Epoch:	8 of 8
Iteration:	128 of 128
Iterations per epoch:	16
Maximum iterations:	128
Validation	
Frequency:	30 iterations

Figure 8-14 were also trained for a longer time as explained briefly above at (Max Epochs = 8). It was found that *N(4,1)* made significant progress as shown in Table 8-8 whilst the validation accuracy of *N(4,2)* made little improvement at a validation accuracy of 25% from Table 8-9.

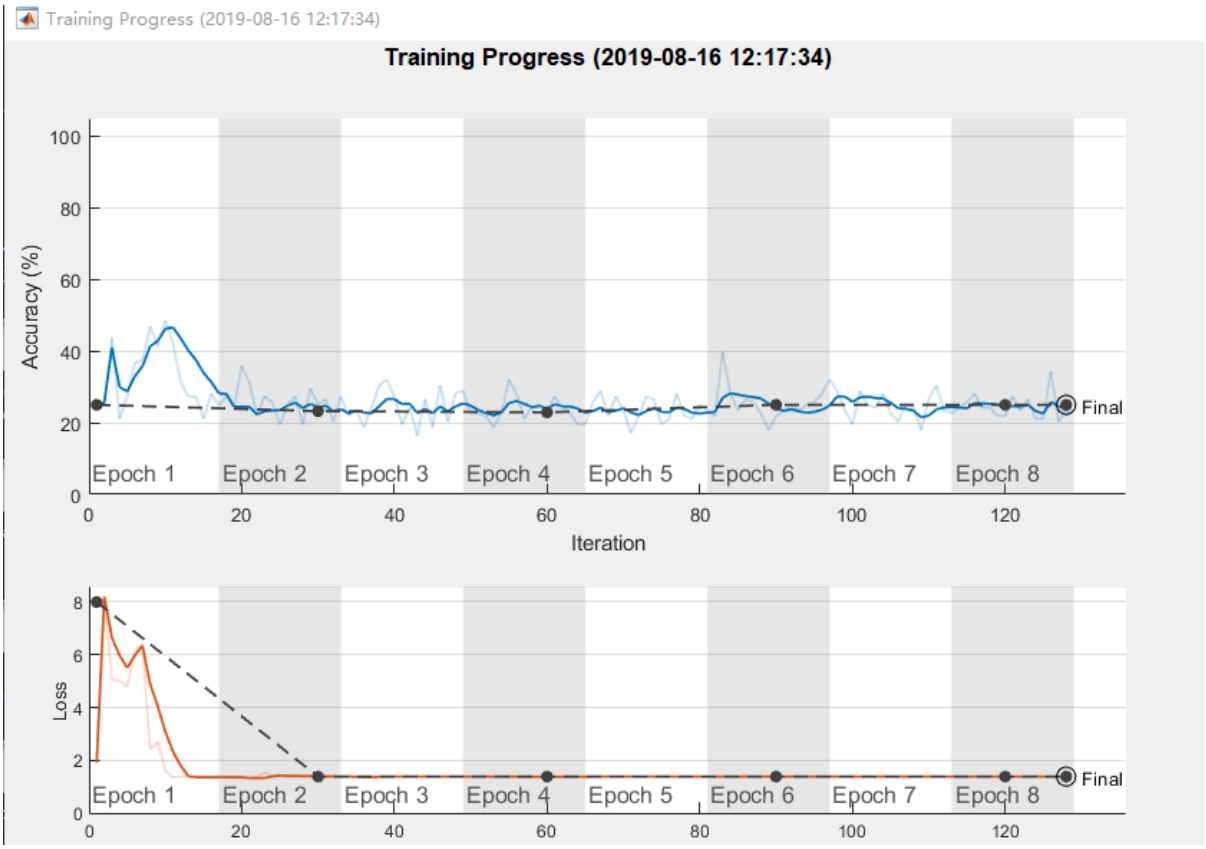

Figure 8-14 Training of Network (4,2) in Progress

Table 8-9 Training Processing of Network42 (Smaller Convolution Kernels and Longer Training Time)

A third trial was carried out with the following CNN Structure, with the first convolutional layer being twenty-one convolutional kernels; 13*13 filter size, the second convolution layer was organised into fifteen convolutional kernels; 10*10 filter size and the third convolution layer arranged into eleven convolutional kernels; 7*7 filter size, still the validation accuracy shows no improvement and are not described any further.

Note:

The above analysis illustrates the principles of the training in full of chanciness, therefore it is difficult to complete effective training for a certain network. Different figures record the training process of the collected acoustical data from various positions. The difference in accuracy verifies that the information quantity of the collected signals at various positions is different. Finding a suitable acquisition position is the purpose of this study.

8.6.1 Final CNN Training Phase

Finally, based on previous analysis inaccuracies, the fourth CNN training structure has a bigger structure where the first convolution layer is comprised of twenty-five convolutional kernels, the second convolution layer contains twenty convolutional kernels and the third convolution layer arranged into fifteen convolutional kernels. The filter sizes of the convolution kernels are set in the following arrangement: the first layer is 33*33, the second layer is 21*21, and the third layer is 17*17. Figure 8-15 illustrates the CNN Design Architecture. The wider and deeper the network, the better training effect, however it takes longer. It was unfortunate to state that aside from a lot of practice, there is no direct way to determine the right size of

network and that it is vital that computers with good computing power are essential for the training.

Figure 8-15 CNN Design Architecture

These convolution layers will be used to extract the images features and they use the linear rectification technique for activation whereas the pooling layers use the maximum pooling technique which picks only the active feature in a pooling region. The nodes of the convolution and pooling layers are connected to the target nodes through the fully connected layer after the activation process. Finally, the fully connected layer, which is the last output of the neuron, is followed by the softmax function and the final CNN structure is illustrated in Figure 8-16 supplemented with a more rational explanation.

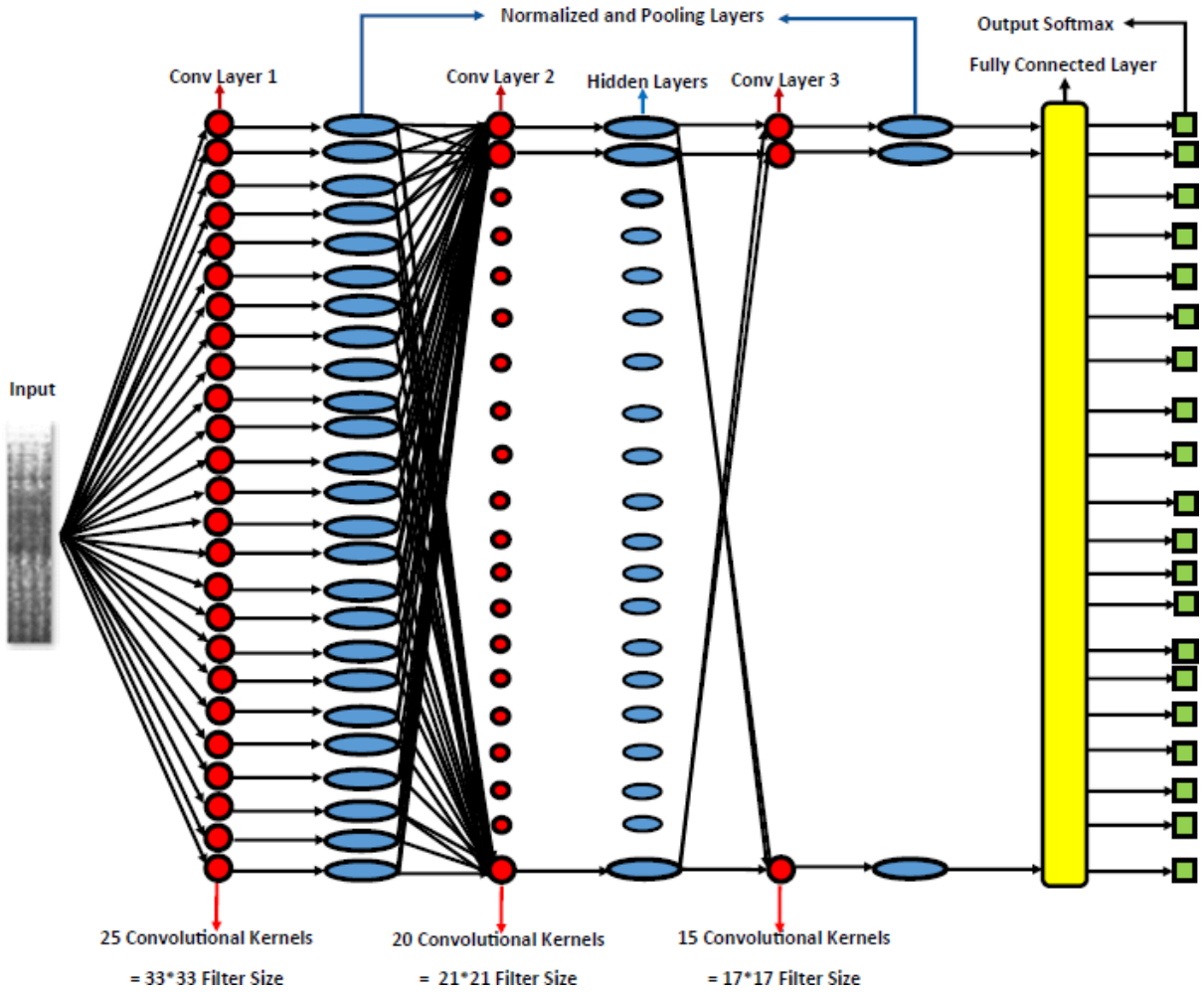

Figure 8-16 Final CNN Structure

The input datasets comprise of 48384 images with the size of the two-dimensional image at 1009071 and designed into three convolution kernels. Each convolution layer is accompanied by the normalised (can be trained) and pooling layer. The convolutional layers (33*33), (21*21) and (17*17) are used to extract the features of the images at different stages. All the convolutional layers use the linear rectification method as shown in Figure 8-16 even though the pooling/(hidden) layers uses the maximum pooling method. The nodes of the convolutional and pooling layers are linked to the target node via the fully connected layer after the activation phase, whereas the output layer returns to the softmax function. The acoustical data sets obtained from the microphones need thorough preparation before the training of CNN to gain a reliable high-performance accuracy in finding the most suitable signal acquisition position.

8.7 Final CNN Structure Validation Accuracy using various percentage Dataset

Accuracy Achieved through Convolution Neural Networks

Machines emit noise whilst in operation but for the case of the RC and due to its age, more noise is generated. This comes mainly from the cylinders as the pistons are the only main moving mechanism. Each acoustical signal will show a different trend depending on its noise severity and the position away from the compressor. Knowing the best location to collect this data through a non-intrusive diagnosis technique based on a combination of acoustic and CNN, the difference in accuracy is described below and has proven to be an effective technique in finding the most suitable signal acquisition for the RC.

A quantitative approach is used to explore the validation accuracy as described in Table 8-10 based on the final CNN Structure, with the convolution layer consisting of twenty-five, twenty and fifteen convolutional kernels, with filter size of convolution kernels set to 33*33, 21*21, and 17*17 as previously described in Figure 8-16.

The study uses 5 different proportions of the total available data set for training purposes. The specific percentages are 5, 10, 20, 30 and 70% of the data set size. In each case the remainder of the data set (95%, 90%, 80%,70% and 30%) is used for network testing/validation purposes.

With a training to validation ratio of 5%:95% the accuracy ranged from 33.57%, *N(4,1) at (200, 80)cm* to 94.25%, *N (1,3) at (50,140)cm*. The validation accuracy is low and requires more processing until 100% validation accuracy is reached.

As the aim is to locate the optimum cluster for data collection and to see the variation in the accuracy, therefore with a training to validation ratio of 10%:90% the accuracy ranged from 65.4%, *N(2,2) at (100, 110)cm* to 98.35%, *N (2,4) at (100, 170)cm* is unstable and needs further processing until this is reached.

With a training to validation ratio of 20%:80% the accuracy ranged from 85.87%, *N(4,2) at (200,110)cm* to 99.3%, *N (3,3) at (150,140)cm* more data set are required for training and the accuracy of the network is still low.

With a training to validation ratio of 30%:70% the accuracy ranged from 83.7%, *N(4,1) at (200,80)cm* to 99.5% , *N (1,4) at (50,170*)cm. As the training set rises to 30% the accuracy of the network decreases however it can still be improved as the desired accuracy is not yet attained.

Finally with a training to validation ratio of 70%:30% the accuracy ranged from 97.36 %, *N(2,1) at (100,80)cm* to 100%, *N(3,1*) at (150,80)cm, *N(4,1)* at (200,80)cm, *N(2,2)* at (100,110)cm, *N(1,3)* at (50,140)cm and grouped in *N(1,4)* at (50,170)cm, *N(2,4)* at (100,170)cm and *N(3,4)* at (150,170)cm. As the training set size rises to 70% the accuracy is increased to a higher validation accuracy. This proves that the cluster N(1,4), N(2,4) and N(3,4) is the best location for a good indication of sound propagation at a highest validation accuracy of 100%.

Table 8-10 Validation Accuracy Analysis

Height in cm / Distance in cm	Network	Validation Accuracy using 95% Dataset							
		N 1	80	*N 2*	110	*N 3*	140	*N 4*	170
50	*N 1*	*N(1,1)*	0.8224	*N(1,2)*	0.5648	*N(1,3)*	0.9425	*N(1,4)*	0.8733
100	*N 2*	*N(2,1)*	0.8823	*N(2,2)*	0.5857	*N(2,3)*	0.9126	*N(2,4)*	0.7016
150	*N 3*	*N(3,1)*	0.5494	*N(3,2)*	0.5453	*N(3,3)*	0.5982	*N(3,4)*	0.7016
200	*N 4*	*N(4,1)*	**0.3357**	*N(4,2)*	0.6069	*N(4,3)*	0.8858	*N(4,4)*	**0.4937**
Height in cm / Distance in cm	Network	Validation Accuracy using 90% Dataset							
		N 1	80	*N 2*	110	*N 3*	140	*N 4*	170
50	*N 1*	*N(1,1)*	0.8551	*N(1,2)*	**0.721**	*N(1,3)*	0.9684	*N(1,4)*	0.9132
100	*N 2*	*N(2,1)*	0.8945	*N(2,2)*	0.654	*N(2,3)*	0.875	*N(2,4)*	0.9835
150	*N 3*	*N(3,1)*	0.689	*N(3,2)*	0.6618	*N(3,3)*	0.9158	*N(3,4)*	0.8272
200	*N 4*	*N(4,1)*	0.8404	*N(4,2)*	0.7537	*N(4,3)*	0.8438	*N(4,4)*	0.9287
Height in cm / Distance in cm	Network	Validation Accuracy using 80% Dataset							
		N 1	80	*N 2*	110	*N 3*	140	*N 4*	170
50	*N 1*	*N(1,1)*	0.9331	*N(1,2)*	0.974	*N(1,3)*	0.9707	*N(1,4)*	0.9847
100	*N 2*	*N(2,1)*	0.9388	*N(2,2)*	0.8715	*N(2,3)*	0.9488	*N(2,4)*	0.9756
150	*N 3*	*N(3,1)*	0.988	*N(3,2)*	0.888	*N(3,3)*	0.993	*N(3,4)*	0.9802
200	*N 4*	*N(4,1)*	0.9723	*N(4,2)*	0.8587	*N(4,3)*	0.9136	*N(4,4)*	0.9595
Height in cm / Distance in cm	Network	Validation Accuracy using 70% Dataset							
		N 1	80	*N 2*	110	*N 3*	140	*N 4*	170
50	*N 1*	*N(1,1)*	0.9537	*N(1,2)*	0.9518	*N(1,3)*	0.9853	*N(1,4)*	0.9995
100	*N 2*	*N(2,1)*	0.9707	*N(2,2)*	0.9797	*N(2,3)*	0.9976	*N(2,4)*	0.9939
150	*N 3*	*N(3,1)*	0.991	*N(3,2)*	0.9263	*N(3,3)*	0.9887	*N(3,4)*	0.9939
200	*N 4*	*N(4,1)*	0.837	*N(4,2)*	0.8837	*N(4,3)*	0.9953	*N(4,4)*	0.9976
Height in cm / Distance in cm	Network	Validation Accuracy using 30% Dataset							
		N 1	80	*N 2*	110	*N 3*	140	*N 4*	170
50	*N 1*	*N(1,1)*	0.9934	*N(1,2)*	0.9978	*N(1,3)*	1	*N(1,4)*	1
100	*N 2*	*N(2,1)*	0.9736	*N(2,2)*	1	*N(2,3)*	0.9934	*N(2,4)*	1
150	*N 3*	*N(3,1)*	1	*N(3,2)*	0.9945	*N(3,3)*	0.9989	*N(3,4)*	1
200	*N 4*	*N(4,1)*	1	*N(4,2)*	0.9791	*N(4,3)*	0.9989	*N(4,4)*	0.9901

8.8 **Discussion**

This proves that the results show that a larger deeper convolutional neural network can achieve better accuracy based on the challenging acoustic dataset through supervised learning and it is evident that the smaller and narrower network results in a higher degradation of accuracy.

The accuracy in finding a suitable location for the acquisition of the acoustical data under the four operating discharge pressures has improved as the network was made larger and trained for longer. The CNN technique used for this classification and pattern recognition has proven to be effective.

It has been possible to validate which is the best location for a good indication of sound propagation at a training dataset size of 70% and validation accuracy using 30% dataset. Position (50, 170)cm, (100, 170)cm, (150, 170)cm, away from the compressor, manifest an ideal point to locate an optimal position for the collection of signals and has proven to be a good indication of sound propagation and for locating noise sources under the four operating discharge pressure conditions at different heights and distances.

The findings from this study prove that by training a smaller network, the accuracy worsens, whilst using more kernels and a bigger network, the higher the accuracy. However, a bigger network requires more time and it is important to find the right smaller structure that will reach higher accuracy and this was achieved through trial and error. Training the network can be a form of art rather than science as there are no set kernels.

Chapter 9. **Conclusions and Further Work**

This chapter concludes this thesis and is distributed into four sections; section one summarises the achievements of the research work described in this thesis and relates these achievements to the objectives which are defined in sub-chapter 9.1. This research has been undertaken in three Phases and examined under different advanced methods for the predictive maintenance/condition monitoring of rotating and fluid machines. Section 9.2 outlines the conclusion drawn from Phase I, Phase II and Phase III of this thesis. Contribution to knowledge is drawn from Section 9.3 and the final Section 9.4 discusses possible areas of future works which the author considers would further enhance this study and make a useful contribution to the advance monitoring of rotating and fluids machines.

9.1 Review of Research Objectives and Achievements

Several objectives were defined at the beginning of this thesis and they are documented in Section 1.3 Research Aims and Objectives. To ascertain if the specified conditions have been fulfilled, each of these objectives are to be visited in this chapter and the key findings summarised. Moreover, the contribution to knowledge and novelty is identified. The condition monitoring of the vacuum pump in the paper industry has received little consideration and the monitoring of the system is achieved fundamentally by the vibration analysis. To accomplish this research several objectives need to be met and the following shows a review of the progress:

Aim: This study aims to focus on the enhancement of the condition monitoring of a reciprocating compressor in a lab environment and a large industrial vacuum pump used in the paper industry by using a conventional and state of art monitoring system. To achieve this research, studies have been carried out in three separate successive phases. Phase I is the techniques evaluation, the objectives and achievements are as follows:

9.1.1 Phase I

Objective 1: Understand the current Condition Monitoring (CM) technology and find the gap in its application by reviewing the existing systems in the market and research community through intensive literature review.

Achievement: This has been made possible, the results are in Chapter 2 and the work is distributed in all three Phases.

Objective 2: To design a mathematical model and numerical analysis for the investigation of the behaviour of the dynamic responses of the Reciprocating Compressor (RC).

Achievement: This is accomplished in Chapter 3 of the mathematical modelling and numerical analysis in the dynamic responses of the RC.

Objective 3: To design and build a comprehensive reciprocating compressor test facility in the lab to simulate faults and obtain experimental data. These data samples will assist to analyse the effectiveness of the system with different monitoring strategies.

Achievement: Chapter 4 gives an explanation of the development, design and the test rigs with all the instruments used, together with the analysed report explaining the findings.

Objective 4: To familiarise and study the practical and theoretical aspects of all components of the compressor and study the function of the data acquisition so that samples of the raw data

signal from the machine can be captured, analysed and a report produced. Also to understand the signal processing methods and techniques used for analysis which is the Frequency and Time Domain, Root Mean Square (RMS), Instantaneous Angular Speed (IAS) spectrum and Current Waveform Spectrum.

Achievement: The results of this objective are in chapter four where different types of faults were seeded into the system then analysed and a report produced. Chapter four also shows the results of the various signal processing methods and techniques used for analysis, such as the Frequency and Time Domain, RMS, IAS spectrum and Current Waveform Spectrum.

Objective 5: To seed specific quantified faults into the machine so that experimental data can be gained on the subsequent system behaviour and its effect on the compressor performance so that data can be compared and analysed.

Achievement: This has been made possible, the results are in Chapter 4 in evaluating the condition monitoring techniques based on intrusive and non-intrusive in-cylinder pressure measurements

Objective 6: To implement various techniques relating to Surface Vibration (SV) and IAS into the system to analyse the effect and evaluate the possibility for field implementation in phase II. Examine the detection and diagnosis performances of the developed CM systems in line with potential issues for field implementation

Achievement: Chapter 4 explained the application of the SV and IAS techniques. In Phase I of the compressor work it has also been found that the dynamic pressure, IAS and motor current monitoring allows full detection of all induced faults including different leakages of discharge, inlet and intercooler, driving belt looseness and motor stator asymmetries with moderate signal conditioning and analysis.

9.1.2 Phase II

Objective 1: To study and evaluate the current CM technology which has the most potential to the paper industry by exploring the existing systems in the market and research community. To develop an analytic modelling of a vacuum pump and to implement a scheme based on a typical paper industry, built on actual demand.

Achievement: This has been made possible and the result of the analytic vacuum pump modelling is in Chapter 5 and the evaluation of the current CM technology, which has the most potential to the paper industry, is as shown in Chapter 6.

Objective 2: To assess the capability of the target system through its working history and planned maintenance schedule, for comparison in discussion and evaluation, by examining the suitability and performance during the full course of the CM process which includes the measurement system specification, data acquisition definition and implementation, data analysis method selection and evaluation, detection and diagnosis performance confirmation.

Achievement: A good understanding of data measured and how it has been interpreted has helped to gather several assumptions which have been documented in Chapter 6.

Objective 3: To conduct and investigate the feasibility of the scheme in terms of sensor installations and performances, data acquisition methods, system specification and fault diagnosis admissibility to enable sample data to be easily taken and analysed.

Achievement: Chapter 6 explains the feasibility of the scheme in terms of sensor installations.

Objective 4: To conduct a qualitative study and fault mode analysis of these pumps by examining the detection and diagnosis performance of the vacuum pumps by using the (vibration data statistic, airborne sound statistic, frequency spectra for vibration and envelope spectra) techniques to prove its effectiveness and IAS approaches.

Achievement: In Phase II of the Industrial CM work, Section 6.10 discussion, it has been found that there are discrete frequencies in the Envelope Spectra of the motors, pumps, and gearboxes which may be caused by some imbalance and wearing parts. However, it was not possible to install the shaft encoder for IAS acquisitions in Phase II of the vacuum pump as it was not practical to stop the machine due to high demand in production, but this is a possibility for future work.

9.1.3 Phase III

Objective 1: To apply Airborne sound acoustic learned from the Industrial Monitoring Machine from Phase II, into the Broom Wade compressor used in phase I.

Achievement: The results are in Chapter 7 Acoustic Monitoring of the Laboratory Compressor Based on Conventional Analysis.

Objective 2: To develop a movable rig for the collection of 16-point data away from the reciprocating compressor.

Achievement: This has been made possible through Section 7.2.1 measurement system layout and the Figure 7-4 General System Set up.

Objective 3: To study, identify, quantify and qualify the best location to capture the acoustic signal from the compressor.

Achievement: This has been made possible as shown in Section 7.3.5 Sound Localisation through Acoustic Imaging Technology

Objective 4: To study the Root Mean Square (RMS) range according to the sound localisation.

Achievement: This has been made possible as shown in Section 7.3.1 of the RMS Analysis in Time Domain.

Objective 5: To Study and apply the Convolutional Neural Networks (CNN) in determining and localising an optimal position away from the compressor for the collection of signals to find which signal proves to be a good indication of sound propagation and locating noise sources under the four operating discharge pressure conditions.

Achievement: The results are from Section 8.6 to 8.7 within which the CNN network has proven to be effective and confirming which is the best location for a good indication of sound propagation using 70% of the data set size for training and 30 % of the data set for the validation purposes/network testing. Position (50, 170) which is 50 cm away from the compressor at a height of 170 cm, *Network (N) (1,4), N (2,4)* at (100, 170)cm away and *N(3.4)* at *(150, 170)*cm away is the ideal point to locate an optimal position for the collection of signals and the detection of noise sources under the four operating discharge pressure conditions at different distances and heights.

9.2 Conclusions drawn from Experimental Results

The progress made in this thesis allows numerous conclusions and key findings to be reached in all three phases.

9.2.1 Phase I

From the mathematical modelling and numerical analysis of dynamics responses of the RC based from Chapter 3, it can be concluded that the in-cylinder pressure describes the RC operation and can be utilised for fault diagnosing in flow passages, however at a system level diagnosis it does not have the capability to indicate any surge from motor drives and mechanical transmission systems. IAS and motor current can both be used for system level diagnostics due to the significant changes between various fault cases however not at a

component level diagnostics. Acoustics from flow passages and structural vibration was found to be a better approach in respect to various faults comparison.

It can be concluded from the work in Section 4.7 that a time domain approach for the detection and diagnosis of faults in a Reciprocating Compressor (at various working pressures) is a relatively simple and straight forwards method, but it does not result in an accuracy that would ideally be sought. It is for this reason that a frequency domain equivalent approach is included within the recommendations for future work.

From the analysis in Section 4.9.1 it was found that vibration can provide both detection and diagnosis of these faults under the cost of high processing efforts.

The conclusion from the work in Section 4.11 proves that IAS is relatively easy to implement due to the simple sensor installation and low cost of the whole system and to compensate its diagnostic deficiency, a portable vibration monitoring system can be combined, however it will require more advanced signal analysis and diagnosis techniques.

The work in Section 4.10 and 4.11 concludes that the dynamic pressure, IAS and motor current monitoring allows good information regarding fault location and severity. It also gives a full detection of all induced faults including different leakages of discharge, inlet and intercooler, driving belt looseness and motor stator asymmetries.

9.2.2 Phase II

From the Analytical Modelling analysis work in Chapter 3 and the study from Chapter 4 it is concluded that LRVP share the same characteristic in the operation to that of the RC in relation of the internal pressure oscillations and as shown in Section 3.8.1, Figure 3-10 of the In-Cylinder Pressures under Different Discharge Pressures.

The conclusion drawn in Phase II is that the study from Phase I was beneficial in assisting the author and giving the knowledge and skill required to apply his learning in Phase II of an industrial working environment.

In can be concluded from the study in Phase II Section 6.6, 6.7 and 6.2.1 that the project is feasible and reliable as the consistency in the level of vibration on the Drive End (DE) of motor 3 as shown from the Figure 6-23, Figure 6-22, Figure 6-31 and Figure 6-36 indicates that the drive end of motor 3 has some concerns and needs addressing before it becomes a major problem.

It was found that Pump 3 also seems to be having an issue as shown from the Figure 6-29 and Figure 6-30 as these discrete frequencies could indicate the early start of bearing failure, worn or cracked blade, misalignment or unbalanced shaft rotation. The analysis of the techniques used has proven to be effective as there are some problematic internal system components concern on system 3, motor 3 and pump 3.

It has been proven that it is possible to use airborne sounds to indicate the health conditions for all of the machines as the frequency contents in low-frequency range exists which are correlated with vibration content based on the spectrum analysis of both sound and vibration signals from the vacuum pump system.

It has also been found that the proposed monitoring scheme, in terms of sensor installations, data acquisition procedures and signal processing methods in Chapter 6 are sufficiently acceptable. Especially, it needs only two microphones which are set up remotely, therefore the overall system can be relatively low cost and easily deployed in the field as detailed by the author [151].

9.2.3 Phase III

From Phase III, Section 7.3.1, Figure 7-7 it can be concluded that the RMS Analysis, acoustic signal at 1.1m height and 50 cm away from the compressor, shows a good indication of the sound propagation and in locating noise sources under all operating discharge pressure conditions. However, the RMS acoustic signal of the sound pressure declines when the microphones are further away from the compressor.

It can be concluded from Section 7.3.5 that the Spiral Array Figure 7-6 can locate sources of airborne sound at higher frequency as shown from Figure 7-13 as the second stage cylinder valve creates more noise when faulty. It is also proven that the distributed noise sources from Figure 7-13 radiate at a known frequency of 3000 to 3300Hz .

The conclusion from the work in Section 8.5 and 8.6 shows that there is no set principle for the CNN training procedure as it is done randomly and can be daunting to complete any effective training

From the study in Section 8.7 it was found that the CNN network was able to confirm which is the best location for a good indication of sound propagation. The final training achieved a higher validation of accuracy indicating the best location was whilst using 70% of the data set size for training and 30 % of the remaining dataset was used for validation purposes.

It can be concluded from Section 8.6 that when training a smaller network, the accuracy is lesser compared to a bigger network with more kernels where the accuracy is higher. However, a bigger network requires more time and it is important to find the right structure that will reach higher accuracy.

9.3 Contribution to Knowledge

The achievements of this research have led to a number of new contributions to knowledge in improving the monitoring of fluid machines.

First Contribution:

The mathematical modelling and numerical simulation of the RC and its results have successfully proven that direct numerical diagnostic between the signatures with baseline provides an easy and feasible approach to quantitatively assess various dynamic responses such as IAS/torsional vibration, motor current, structural vibration and airborne acoustics. It is the first time that accurate and reliable head to head comparisons have been attained numerically for these dynamic responses as detailed in Chapter 3.13.1. Due to the numerous amounts of uncertain errors in data acquisition and data processing, these are not easy to be accomplished. The numerical study has effectively demonstrated the ability to perform a larger volume of analysis tasks over different fault cases under a wide range of discharge pressures due to the modelling of vibroacoustic responses as multi-modal systems. This enables quantitative analysis of structural vibration and airborne acoustics from valve motions, gaining a detailed understanding of vibroacoustic providing sufficient knowledge for data acquisition and processing.

Second Contribution:

No previous work has investigated an RC in conjunction to a LRVP and as described in the qualitative results made from the RC works in Chapter 3 and Chapter 4 which can be referred to LRVP data analysis as LRVP share the same operation process to that of RC in relation to the internal pressure oscillations. From Section 3.8.1, Figure 3-10 it is also proven the that the force variation and dynamics of LRVP behave like an RC.

Third Contribution

So far no study has been found to investigate the detection and diagnosis of three sets of vacuum pump in a paper industry whilst in operation. The work presented in Chapter 6 is

believed to be unique in providing new combined CM approaches to detect anomalies based on the three sets of the vacuum pump.

Fourth Contribution: Combined Approach to CM

No previous research has used a spiral array to locate sources of airborne sound at a higher frequency and other combined conventional analysis techniques, at various distances and heights, away from an RC as detailed in Chapter 7.

Fifth Contribution:

No works have been found to investigate the finding of a suitable location for the acquisition of the acoustical data under the four operating discharge pressures from an RC through CNN. From this study it was found that training a smaller network worsens the training accuracy whilst using more kernels and a bigger network produced higher accuracy. However, a bigger network requires more time and it is important to find the right structure that will reach higher accuracy through trial and error.

9.4 Suggestion for Future Research

The study has shown that acoustic monitoring is a more economical and promising method for machine monitoring in processing industries. CNN can also be efficient however it is quite time consuming to train the networks. To find more cost effective approaches it is suggested that the future study will focus on:

First Suggestion: The investigation of more cost effective measurements techniques such as how CNN can be applied to thermal imaging, high-speed visions, micro acoustic arrays and Infrared Thermal (IRT) video recording to automatically track the condition of machines.

Improving this technology in diagnosing machine fault detection and prediction will allow the detection of many advanced fault conditions in machines at the highest accuracy.

Second Suggestion: The development of other fault detection techniques such as wireless encoders to monitor the IAS and motor current monitoring in fluid and rotating machine is recommended.

Third Suggestion: Implement and monitor the proposed RC fault detection techniques to other mechanical components such as bearings, pistons, pulleys, flywheels, connecting rods, leaking joints or gaskets, belt slipping, lack of lubrication and valves.

Fourth Suggestion: Recommend that the frequency domain is to be considered for further work in the investigation of in-cylinder fault comparison againgst the time domain.

Fifth Suggestion: Recommend further academic research to extract features for more efficient data processing such as high effective denoising algorithms.

Sixth Suggestion: Evaluate and develop other novel fault diagnosis AI methods such as fuzzy neural networks, fuzzy logic which will improve a better quality of vibration and acoustic monitoring depending on its application.

Seventh Suggestion: Recommend further academic research to extract features for more accurate and efficient data processing in the field, such as the Principal Component Analysis (PCA), Canonical Variate Analysis (CVA) and statistic methods for utilising existing control data.

Eighth Suggestion: Recommend that further academic research should be conducted into the effective use of envelope features to detect vibration faults in RCs.

Ninth Suggestion: Recommendation of further academic research in the combination of Six Sigma application to condition monitoring techniques such as vibration and acoustic to improve the Overall Effectiveness (OEE) of the Plant.

9.5 Publications Arising from this Work

Published

1. Performance Monitoring and Fault Diagnosis of Vacuum Pumps based on Airborne Sound, R. Appadoo, Prof. A. D. Ball & Dr F. Gu, School of Computing and Engineering, University of Huddersfield, Queensgate, Huddersfield HD1 3DH, UK. Proceedings of the 24th International Conference on Automation & Computing, Newcastle University, Newcastle upon Tyne, UK, 6-7 September 2018.
2. Condition Monitoring of Reciprocating Compressor on Acoustic Imaging, Miaoshuo Li, Robin Appadoo, Fengshou Gu and Andrew Ball, School of Computing and Engineering, University of Huddersfield, Queensgate, Huddersfield HD1 3DH, UK. The 32nd International Congress and Exhibition on Condition Monitoring and Diagnostic Engineering Management (COMADEM 2019).

Submitted

1. An Investigation into the Influence of Microphone Placements for the Condition Monitoring of Reciprocating Compressors; Robin Appadoo, Miaosho Li, Fengshou Gu, Andrew D. Ball, School of Computing and Engineering, University of Huddersfield, Queensgate, Huddersfield HD1 3DH, UK. Fifth Annual University of Huddersfield PGR Conference, 31st March 2020.

To be Submitted

1. An Investigation based into the CM of common Non-Intrusive Measurements based on a fluid machine.
2. A Combined Study of IAS based Condition Monitoring of a Reciprocating with Current Waveform based CM.

Appendix 1

Appendix 1 Damage Shaft, Impeller and Build-up of Scales Picture taken on 24/04/14

References

[1] Hand, A., *Electric motor maintenance and troubleshooting*. 2002: McGraw-Hill.

[2] Horning, G. *A method to monitor the thermal stress of power devices for direct stator flux controlled AC drives*. in *Power Electronics and Applications, 1993., Fifth European Conference on*. 1993. IET.

[3] Salisbury, R. *Thermal imaging and predictive maintenance: what the future has in store*. in *Cement Industry Technical Conference, 2000 IEEE-IAS/PCA*. 2000. IEEE.

[4] Wowk, V., *Machinery Vibration Measurement and Analysis,(1991)*. 1991, McGraw-Hill, New York.

[5] Agustiady, T.K. and E.A. Cudney, *Total Productive Maintenance: Strategies and Implementation Guide*. 2015: CRC Press.

[6] Institution, B.S., *Mechanical Vibration In Rotating And Reciprocating Machines*, B.S. Institution, Editor. 1976, British Standards Institution.

[7] McInerny, S.A. and Y. Dai, *Basic vibration signal processing for bearing fault detection.* IEEE Transactions on education, 2003. **46**(1): p. 149-156.

[8] Albarbar, A.S., *The acoustic condition monitoring of diesel engines*. 2006: The University of Manchester (United Kingdom).

[9] Zhu, J., et al., *Lubrication oil condition monitoring and remaining useful life prediction with particle filtering.* International Journal of Prognostics and Health Management, 2013. **4**: p. 124-138.

[10] Poley, J. *The metamorphosis of oil analysis*. in *Machinery Failure Prevention Technology (MFPT) Conference, Condition Based Maintenance Section 1, Conference Proceedings, Dayton, Ohio*. 2012.

[11] Sharma, B. and O. Gandhi, *Performance evaluation and analysis of lubricating oil using parameter profile approach.* Industrial Lubrication and Tribology, 2008. **60**(3): p. 131-137.

[12] Monitoring, T.C. *Thermal Imaging*. 2019 Available from: http://www.conditionmonitoring.ie/condition-monitoring-services.php.

[13] EBME, *EBME & Clinical Engineering Articles.*

[14] TIS. *Thermal Imaging Services UK ltd*. Available from: http://www.tisthermalimaging.co.uk/benefits.html.

[15] Todinov, M.T., *Risk-based reliability analysis and generic principles for risk reduction*. 2006: Elsevier.

[16] Al-Qattan, M.J., *Industrial Application of Speed and Power for Fault Detection and Diagnosis of a Large Compressor*. 2007, School Of Mechanical, Aerospace And Civil Engineering, Manchester University.

[17] Thomson, W.T. and R.J. Gilmore. *Motor Current Signature Analysis To Detect Faults In Induction Motor Drives-Fundamentals, Data Interpretation, And Industrial Case Histories*. in *Proceedings of the 32nd Turbomachinery Symposium*. 2003. Texas A&M University. Turbomachinery Laboratories.

[18] Davies, A., *Handbook of condition monitoring: techniques and methodology*. 2012: Springer Science & Business Media.

[19] Elhaj, M.A., *CONDITION MONITORING OF RECIPROCATING COMPRESSOR VALVES* 2005, University of Manchester.

[20] Plant, R. *Identifying Mechanical Faults with Motor Current Signature Analysis*. Available from: https://www.reliableplant.com/Read/29235/resolve-workplace-conflict.

[21] Penman, J., J. Hadwick, and A. Stronach, *Protection strategy against the occurrence of faults in electrical machines.* 1980.

[22] Saleh, A.F. 2005, School Of Mechanical, Aerospace And Civil Engineering, Manchester University.

[23] Dubravko, M. and Z. HEP, *BRIEF REVIEW OF MOTOR CURRENT SIGNATURE ANALYSIS.*

[24] Bandes, A. *Ultrasound Condition Monitoring*. Available from: http://www.uesystems.com/wp-content/uploads/2012/07/ultrasound-condition-monitoring-ue-v7.pdf.

[25] Smith, R., *Composite defects and their detection.* Materials science and engineering, 2009. **3**: p. 103-143.

[26] Rienstra, A., *Airborne Ultrasound: Predictive Maintenance for the Masses*, in *SDT North America*. 2005. p. 1-17.
[27] Buckley, J.M., *AN OVERVIEW OF THE PREDICTIVE MAINTENANCE APPLICATIONS OF AIRBORNE ULTRASOUND TESTING.*
[28] Charles, P., Sinha, Jyoti K., Gu, Fengshou, Lidstone, Liam and Ball, Andrew, *Detecting the crankshaft torsional vibration of diesel engines for combustion related diagnosis.* 2009.
[29] M. Desbazeille, R.B.R., F. Guillet, M. El Badaoui, C. Hoisnard, *Model-based diagnosis of large diesel engines based on angular speed variations of the crankshaft.* 2010.
[30] Leclere, Q. and N. Hamzaoui, *Using the moving synchronous average to analyze fuzzy cyclostationary signals.* 2014.
[31] Remond, D., *Practical performances of high-speed measurement of gear transmission error or torsional vibrations with optical encoders.* Measurement Science and Technology, 1998. **9**(3).
[32] Renaudin, L., et al., *Natural roller bearing fault detection by angular measurement of true instantaneous angular speed.* 2010. **24**(7).
[33] Zheng, Y. and A. Ball, *Numerical Simulation of a Multi-cylinder Reciprocating Compressor for Condition Monitoring*. 2005: University of Manchester.
[34] Yuhua Li, F.G., Georgina Harris, Andrew Ball, Nick Bennett, Ken Travis, *The Measurement Of Instantaneous Angular Speed.* Mechanical System And Signal Processing, 2005. **19**(4).
[35] Gu, F., Yesilyurt, I., Li, Yuhua, Harris, Georgina and Ball, Andrew *An investigation of the effects of measurement noise in the use of instantaneous angular speed for machine diagnosis.* 2006. **20**(6).
[36] Naid, A., et al., *Bispectrum Analysis of Motor Current Signals for Fault Diagnosis of Reciprocating Compressors.* 2009.
[37] Liang, B., F. Gu, and A.D. Ball, *A Preliminary Investigation of Valve Fault Diagnosis in Reciprocating Compressors.* Maintenance & Asset Management Journal, 1996.
[38] Elhaj. M, F.G., Shi Z, A.D Ball, Wright J, *Early detection of leakage in reciprocating compressor valves using vibration and acoustic continuous wavelet feature.* COMADEM, International Congress on Condition Monitoring and Diagnostic Engineering Management, 2001.
[39] Manepatil, S., Gs Yadava, B C Nakra *Modelling and computer simulation of reciprocating compressor with faults.* https://www.researchgate.net/journal/0020-3408_Journal_of_the_Institution_of_Engineers_India_Mechanical_Engineering_Division, 2000.
[40] N. I. I. Mansor, M.J.G., M. Z. Nuawi and S. E. M. Kamal, *MONITORING BEARING CONDITION USING AIRBORNE SOUND.* 2009.
[41] Collacott, R., *Mechanical fault diagnosis and condition monitoring*. 2012: Springer Science & Business Media.
[42] Tandon, N. and A. Choudhury, *A review of vibration and acoustic measurement methods for the detection of defects in rolling element bearings.* Tribology international, 1999. **32**(8): p. 469-480.
[43] Ramroop, G., et al. *Airborne Acoustic Condition Monitoring of a Gearbox System*. in *2001 5th Annual Maintenance and Reliability Conference (MARCON 2001)*. 2001.
[44] Kuttruff, H., *Acoustics: an introduction*. 2006: CRC Press.
[45] Mansor, N., et al., *Monitoring bearing condition using airborne sound.* International Journal of Mechanical and Materials Engineering, 2009. **4**(2): p. 152-155.
[46] The Physics Classroom. *Physics Tutorial*. [Pitch and Frequency]; Available from: https://www.physicsclassroom.com/class/sound/Lesson-2/Pitch-and-Frequency.
[47] Mr SK Singh, R.S. *Acoustics Based Condition Monitoring*. 7.
[48] Liang, B., *Condition Monitoring and Fault Diagnosis of Induction Motors*. 2000, PhD Thesis, Manchester School of Engineering, Department of Mechanical ….
[49] Erdelyi, E. and G. Horvay, *Vibration modes of stators of induction motors.* ASME Trans.,[E], 1957. **24**: p. 39-45.
[50] Mayes, I., A. Steer, and G. Thomas. *The application of vibration monitoring for fault diagnosis in large turbo-generators*. in *Proceedings of the Sixth Thermal Generation Specialists Meeting, Madrid.* 1981.
[51] Beranek, L.L. and T. Mellow, *Acoustics: sound fields and transducers*. 2012: Academic Press.
[52] Saruhan, H., et al., *Vibration analysis of rolling element bearings defects.* Journal of applied research and technology, 2014. **12**(3): p. 384-395.

[53] Al-Ghamd, A.M. and D. Mba, *A comparative experimental study on the use of acoustic emission and vibration analysis for bearing defect identification and estimation of defect size.* Mechanical systems and signal processing, 2006. **20**(7): p. 1537-1571.
[54] Pan, Y., *Heading toward artificial intelligence 2.0.* Engineering, 2016. **2**(4): p. 409-413.
[55] Holtel, S., *Artificial Intelligence Creates a Wicked Problem for the Enterprise.* Procedia Computer Science, 2016. **99**: p. 171-180.
[56] Ahmed, M., *The Use of Advanced Soft Computing for Machinery Condition Monitoring*. 2014.
[57] Priddy, K.L. and P.E. Keller, *Artificial neural networks: an introduction.* Vol. 68. 2005: SPIE press.
[58] Skymind. *A Beginner's Guide to Neural Networks and Deep Learning*. Available from: https://skymind.ai/wiki/neural-network.
[59] Thomas, A. *Neural Networks Tutorial – A Pathway to Deep Learning*. Available from: https://adventuresinmachinelearning.com/neural-networks-tutorial/.
[60] Shaikh, A. *Artificial Neural Network*. Available from: https://www.slideshare.net/MohdArrafatShaikh/artificial-neural-network-80825958.
[61] Chen, J.-R., *Theory and applications of artificial neural networks*. 1991, Durham University.
[62] *Artificial Neural Networks Applications and Algorithms*. Available from: https://www.xenonstack.com/blog/artificial-neural-network-applications/.
[63] Han, X. and Y. Li, *The application of convolution neural networks in handwritten numeral recognition.* Int. J. Database Theory Appl, 2015. **8**: p. 367-376.
[64] Saha, S. *A Comprehensive Guide to Convolutional Neural Networks — the ELI5 way*. Available from: https://towards datascience.com/a-comprehensive-guide-to-convolutional-neural-networks-the-eli5-way-3bd2b1164a53.
[65] Simard, P.Y., D. Steinkraus, and J.C. Platt. *Best practices for convolutional neural networks applied to visual document analysis*. in *Icdar*. 2003.
[66] Matlab. *Deep Learning in Matlab*. Available from: https://uk.mathworks.com/help/releases/R2019a/deeplearning/ug/deep-learning-in-matlab.html.
[67] Wiener, E., J.O. Pedersen, and A.S. Weigend. *A neural network approach to topic spotting*. in *Proceedings of SDAIR-95, 4th annual symposium on document analysis and information retrieval*. 1995. Las Vegas, NV.
[68] Tiwari, R. and S. Maiti, *Bayesian neural network modeling of tree-ring temperature variability record from the Western Himalayas.* 2011.
[69] Patel, J. and S. Upadhyay, *Comparison between artificial neural network and support vector method for a fault diagnostics in rolling element bearings.* Procedia engineering, 2016. **144**: p. 390-397.
[70] Ahmed, M., F. Gu, and A. Ball. *Feature selection and fault classification of reciprocating compressors using a genetic algorithm and a probabilistic neural network.* in *Journal of Physics: Conference Series*. 2011. IOP Publishing.
[71] Samanta, B., K. Al-Balushi, and S. Al-Araimi, *Artificial neural networks and support vector machines with genetic algorithm for bearing fault detection.* Engineering applications of artificial intelligence, 2003. **16**(7-8): p. 657-665.
[72] Samanta, B., *Gear fault detection using artificial neural networks and support vector machines with genetic algorithms.* Mechanical systems and signal processing, 2004. **18**(3): p. 625-644.
[73] The Economic Times Science. *New artificial intelligence system can predict earthquakes*. Available from: https://economicstimes.indiatimes.com/news/science/new-artificial-intelligence-system-can-predict-earthquakes/articleshow/61183410.cms?from=mdr.
[74] Aguiar, P.R., et al., *Digital Signal Processing for Acoustic Emission.* Data Acquisition Applications, 2012: p. 297.
[75] Kourousis D, A.A., Lenain J,Proust A. *Advances in Classification of Acoustic Emission Sources*. Available from: http://www.epandt.com/Biblio/EA2001-06A.pdf.
[76] Al-Balushi, K. and B. Samanta. *Gear fault diagnostics using wavelets and artificial neural network.* in *COMADEM 2000: 13 th International Congress on Condition Monitoring and Diagnostic Engineering Management*. 2000.
[77] Mahamad, A.K.B. *Diagnosis, Classification and Prognosis of Rotating Machine using Artificial Intelligence*. 2010; Available from: https://core.ac.uk/download/pdf/12007629.pdf.

[78] Menon, S., et al. *Wavelet-based acoustic emission detection method with adaptive thresholding*. in *Smart Structures and Materials 2000: Sensory Phenomena and Measurement Instrumentation for Smart Structures and Materials*. 2000. International Society for Optics and Photonics.
[79] Goebel, K. and P.K. Wright, *Monitoring and diagnosing manufacturing processes using a hybrid architecture with neural networks and fuzzy logic.* EUFIT, Proceedings, 1993. **2**.
[80] Ali, Y.H., *Artificial Intelligence Application in Machine Condition Monitoring and Fault Diagnosis.* Artificial Intelligence: Emerging Trends and Applications, 2018: p. 275.
[81] Ali, Y.H., et al. *Acoustic Emission and Artificial Intelligent Methods in Condition Monitoring of Rotating Machine–A Review*. in *National Conference For Postgraduate Research (NCON-PGR 2016)*. 2016.
[82] Lawson, D. and G. Marion, *An Introduction to Mathematical Modelling*. 2008: Bioinformatics and Statistics Scotland.
[83] Sasi, A.B., *The exploitation of instantaneous angular speed for condition monitoring of electric motors*, in *14th International Congress on Condition Monitoring and Diagnostic Engineering Management (COMADEM 2001)*. 2001: Manchester, UK.
[84] Elhaj, M., et al., *Numerical simulation and experimental study of a two-stage reciprocating compressor for condition monitoring.* Mechanical Systems and Signal Processing, 2008: p. pp.374-389

[85] Costagliola, M., *The theory of Spring Loaded valves for reciprocating Compressors Dynamics of a Reed Type Valve" D.Sc* in *Mech*. 1950. p. P.415.
[86] Wambsganss, M. and R. Cohen. *Dynamics of a Reciprocating Compressor with Automatic Reed Valves. II, Experiments and Evaluation*. in *Proceedings of the XII international congress of refrigeration*. 1967.
[87] MacLaren, J.F., *Review of Simple Mathematical Models of Valves in Reciprocating Compressors.* 1972.
[88] Borisoglebski, A.I. and R.W. Kuzmin, *Calculation of suction and compression processes in reciprocating compressors.* Khimisheskoe I Neftyonae Mashinostroenie nil, 1965: p. p.6.
[89] Traversari, A. and P. Lacitignola, *Use and calculation of ring type valves for reciprocatine compressors.* Quaderni Pignone, 1970(16).
[90] Li, W., Int. J. Refrig, 2012: p. pp. 1722–1733.
[91] Posch, S., et al., *Comparison and Validation of Semi-empirical Compressor Models for Cycle Simulation Application.* 2014.
[92] Singh, R., *MODELING OF MULTICYLINDER COMPRESSOR DISCHARGE SYSTEMS.* 1982.
[93] Elhaj, M.A., *Condition monitoring of reciprocating compressor valves*. 2005: The University of Manchester (United Kingdom).
[94] Dutra, T. and C.J. Deschamps, *A simulation approach for hermetic reciprocating compressors including electrical motor modeling.* International journal of refrigeration, 2015. **59**: p. 168-181.
[95] Liu, H., B. Lee, and Y. Tarng, *Monitoring of drill fracture from the current measurement of a three-phase induction motor.* International Journal of Machine Tools and Manufacture, 1996. **36**(6): p. 729-738.
[96] Mustafa, M.O., *Faults detection and diagnosis for three phase induction machines*. 2012, Luleå tekniska universitet.
[97] Krause, P.C., et al., *Analysis of electric machinery and drive systems*. Vol. 2. 2002: Wiley Online Library.
[98] Vas, P., *Electrical machines and drives: a space-vector theory approach*. Vol. 1. 1992: Clarendon press Oxford.
[99] Shahlari, A.J., et al., *Correlation of cylinder pressure–based engine noise metrics to measured microphone data.* International Journal of Engine Research, 2015. **16**(7): p. 829-850.
[100] McCarthy, D.J., *Vibration-based diagnostics of reciprocating machinery*. 1994, Massachusetts Institute of Technology.
[101] Fontana, P. and B. Huurdeman, *A new evaluation method for the thermodynamic behavior of air intake systems*. 2005, SAE Technical Paper.
[102] Chalet, D., et al., *A new modeling approach of pressure waves at the inlet of internal combustion engines.* Journal of Thermal Science, 2011. **20**(2): p. 181-188.

[103] Sasi, A.Y.B., *The exploitation of instantaneous angular speed for machinery condition monitoring*. 2005: The University of Manchester (United Kingdom).
[104] Price, G. and K. Botros, *Numerical and experimental analysis of the flow characteristics through a channel valve.* 1992.
[105] Heinz P. Bloch and J.J. Hoefner, *Reciprocating Compressors: Operation and Maintenance*. Compressor operation and maintenance. 1996, USA.
[106] Hanlon, P.C., *Compressor handbook*. 2001: McGraw-Hill.
[107] Bardou, O. and M. Sidahmed, *Early detection of leakages in the exhaust and discharge systems of reciprocating machines by vibration analysis.* Mechanical Systems and Signal Processing, 1994. **8**(5): p. 551-570.
[108] Mezher, H., et al., *Frequency based approach for simulating pressure waves at the inlet of internal combustion engines using a parameterized model.* Applied energy, 2013. **106**: p. 275-286.
[109] Karczub, D. and M. Norton, *Fundamentals of noise and vibration analysis for engineers*. 2003, Cambridge university press.
[110] Kim. Y, T.A., Yang B-S And Kosse.V, *Experimental Study on Condition Monitoring of Low Speed Bearings : Time Domain Analysis.* 5th Australasian Congress on Applied Mechanics, ACAM, 2007.
[111] G.DALPIAZA.RIVOLAR.RUBINI, *EFFECTIVENESS AND SENSITIVITY OF VIBRATION PROCESSING TECHNIQUES FOR LOCAL FAULT DETECTION IN GEARS.* 2000. **14**(3).
[112] Shreve, D.H., *Signal Processing For Effective Vibration Analysis.* IRD Mechanalysis, Inc 1995.
[113] Rao, S., *Mechanical Vibrations*. 5th Edition ed. 2004.
[114] A.K. S Jardine, D.L.A.D.B., *A review on machinery diagnostics and prognostics implementing condition-based maintenance.* 2006. **20**(7).
[115] J.R. Stack, R.G.H.A.T.G.H., *An amplitude Modulation detector for fault diagnosis in rolling element bearings.* IEEE 2004.
[116] Kahirdeh, A., *A Diagnosis Feature Space for Condition Monitoring and Fault Diagnosis of Ball Bearings*, in *Iran University of Science and Technology*. 2014. p. 52.
[117] Heng, R. and M.J.M. Nor, *Statistical analysis of sound and vibration signals for monitoring rolling element bearing condition.* Applied Acoustics, 1998. **53**(1-3): p. 211-226.
[118] Robert Williams Cox, I., *Minimally Intrusive Strategies for Fault Detection and Energy Monitoring*. 2006, MASSACHUSETTS INSTITUTE OF TECHNOLOGY. p. 215.
[119] Stiaccini, I., et al., *A hybrid time-frequency domain approach for numerical modeling of reciprocating compressors.* Energy Procedia, 2015. **81**: p. 1102-1112.
[120] Zhen, D., *A Study of Non-stationary Signal Processing for Machinery Condition Monitoring*. 2012, University of Huddersfield.
[121] Hoerbiger, *Compressor valves for better reliability, higher efficiency and safety*.
[122] He, D., Y. Pang, and G. Lodewijks, *Speed control of belt conveyors during transient operation.* Powder Technology, 2016. **301**: p. 622-631.
[123] Bloch, H.P. and A. Godse, *Compressors and modern process applications*. 2006: John Wiley & Sons.
[124] Rgeai, M.N., *Helical gearbox fault detection using motor current signature analysis*. 2007: The University of Manchester (United Kingdom).
[125] Limited, C.E.D., *CED Power1401*. 2003.
[126] Schmidhuber, J., *Deep learning in neural networks: An overview.* Neural networks, 2015. **61**: p. 85-117.
[127] Mobley, R.K., *An introduction to predictive maintenance*. 2002: Elsevier.
[128] Culbert, I. and W. Rhodes. *Using current signature analysis technology to reliably detect cage winding defects in squirrel cage induction motors*. in *Record of Conference Papers Industry Applications Society 52nd Annual Petroleum and Chemical Industry Conference*. 2005. IEEE.
[129] Zhang, Y., et al. *Condition monitoring and fault detection of a compressor using signal processing techniques*. in *American Control Conference, 2001. Proceedings of the 2001*. 2001. IEEE.
[130] John Aglitz, R.K.B., Donald E. Bolt, Thomas L. Butzbach, *INSTALLING LIQUID-RING VACUUM PUMPS*. p. 5.
[131] Zhang, Y., et al., *Application and research of new energy-efficiency technology for liquid ring vacuum pump based on turbulent drag reduction theory.* Vacuum, 2020. **172**: p. 109076.

[132] Huang, S., et al., *Theoretical model for the performance of liquid ring pump based on the actual operating cycle.* International Journal of Rotating Machinery, 2017. **2017**.
[133] Vertepov, Y.M., V. Matsenko, and V. Antonov, *Advances in water-ring vacuum pumps and compressors.* Chemical and petroleum engineering, 1997. **33**(5): p. 522-523.
[134] Pfleiderer, C., *Centrifugal pump for liquids and gases*. 1949, Springer, Berlin, Germany.
[135] Schulz, H., *The Pumps.* Springer-Verlag, Berlin Heidelberg, New York, 1977: p. 3O4-3.
[136] Segebrecht, U., *Liquid Ring Vacuum Pumps and Liquid Ring Compressors: Technical Details and Fields of Application*. 1994: Verlag Moderne Industrie.
[137] Prager, R. *Operational Conditions and Application Field of Liquid-Ring Machines*. in *Proceedings of the Third Conference on Fluid Mechanics and Fluid Machinery*. 1969.
[138] Powle, U.S. and S. Kar, *Investigations on pumping speed and compression work of liquid ring vacuum pumps.* Vacuum, 1983. **33**(5): p. 255-263.
[139] Bodik, I. and A. Tishchenko, *Effect of impeller circumferential velocity on the specific power demand of water-ring vacuum pumps.* Chemical and Petroleum Engineering, 1988. **24**(6): p. 289-290.
[140] Pandey, A., *Computational Analyses of the Unsteady, Three Dimensional Multiphase Flow in a Liquid Ring Vacuum Pump*. 2019, Purdue University Graduate School.
[141] Nash Elmo Uk Limited, *S11 Inst. Oper & Maint. Manual*, V.n.e.U. Limited, Editor., Nash Elmo Uk Limited.
[142] Box, E.T. *Positive-displacement-pumps*. [The Engineering Tool Box]; Available from: https://www.engineeringtoolbox.com/positive-displacement-pumps-d_414.html.
[143] Harris, N.S., *Vacuum Pumps.* Thermopedia.
[144] Solutions, S.G.T., *Pneumatic Engineering and General Ventilation Systems*. Schaeffler Global Technology.
[145] Edwards, *World Class Vacuum solutions*.
[146] Ebara Technology Inc, *EBARA CORPORATION PRECISION MACHINERY COMPANY*.
[147] Tsiafis, I., *CASE STUDY: SHAFT ALIGNMENT AND TOLERENCES VERIFICATION FOR EXPERIMENTAL DEVICE USING COORDINATE MEASURING MACHINE.* Center for Quality, 2015.
[148] Sung, D., et al., *study on vacuum pump monitoring using MPCA statistical method.* Journal of the Korean Vacuum Society, 2006. **15**(4): p. 338-346.
[149] Hsieh, F.-C., et al. *Monitoring on dry vacuum pump characteristics by mobile device*. in *Instrumentation and Measurement Technology Conference (I2MTC), 2012 IEEE International*. 2012. IEEE.
[150] Suguna Thanagasundram, Y.F.a.F.S.S., *A Labview based system for condition monitoring of a dry vacuum pump using AR Modelling Techniques*, in *Department of Engineering, University of Leicester*. 2007, Engineering.
[151] Appadoo, R., et al. *Performance Monitoring and Fault Diagnosis of Vacuum Pumps based on Airborne Sounds*. in *2018 24th International Conference on Automation and Computing (ICAC)*. 2018. IEEE.
[152] Automation, R., *Dynamix 2500 Data Collector*.
[153] Khorasani, A.M., G. Littlefair, and M. Goldberg, *Time domain vibration signal processing on milling process for chatter detection.* Journal of Machining and Forming Technologies, 2014. **6**(1/2): p. 45.
[154] Baydar, N. and A. Ball. *Detection of gear failures using wavelet transform and improving its capability by principal component analysis*. in *The 14 th International Congress on Condition Monitoring and Diagnostic Engineering Management, Andrew G. Starr and Raj BKN Rao, Eds. Manchester: Elsevier Science Ltd*. 2001.
[155] Filippenko, A., *Vibration analysis for predictive maintenance of rotating machines.* Acoustical Society of America Journal, 2002. **112**: p. 1237.
[156] Lebold, M., et al. *Review of vibration analysis methods for gearbox diagnostics and prognostics*. in *Proceedings of the 54th meeting of the society for machinery failure prevention technology*. 2000.
[157] Ummul Khair, H.F., Sarudin Al Hakim and Robbi Rahim, *Forecasting Error Calculation with Mean Absolute Deviation and Mean Absolute Percentage Error.* International Conference on Information and Communication Technology (IconICT) 2017.

[158] Kjaer, B., *Detecting faulty rolling-element bearings*
[159] Hutton, P., *Detecting acoustic emission in the presence of hydraulic noise.* non-destructive testing, 1969. **2**(2): p. 111-115.
[160] Li, W., et al., *A study of the noise from diesel engines using the independent component analysis.* Mechanical Systems and Signal Processing, 2001. **15**(6): p. 1165-1184.
[161] Zafar, T., et al., *A neural network based approach for background noise reduction in airborne acoustic emission of a machining process.* Journal of Mechanical Science and Technology, 2017. **31**(7): p. 3171-3182.
[162] Elasha, F., et al., *Application of acoustic emission in diagnostic of bearing faults within a helicopter gearbox.* Procedia CIRP, 2015. **38**: p. 30-36.
[163] Sharma, R.B. and A. Parey, *Condition monitoring of gearbox using experimental investigation of acoustic emission technique.* Procedia engineering, 2017. **173**: p. 1575-1579.
[164] Elamin, F., et al., *Diesel engine valve clearance detection using acoustic emission.* Advances in Mechanical Engineering, 2010. **2**: p. 495741.
[165] Wang, Y. and X. Peng. *Fault diagnosis of reciprocating compressor valve using acoustic emission*. in *ASME 2012 International Mechanical Engineering Congress and Exposition*. 2012. American Society of Mechanical Engineers.
[166] Nivesrangsan, P., J. Steel, and R. Reuben, *Acoustic emission mapping of diesel engines for spatially located time series—Part II: Spatial reconstitution.* Mechanical Systems and Signal Processing, 2007. **21**(2): p. 1084-1102.
[167] Sciences, I.o.C.A.o., *Popularization of scientific knowledge How Hearing Works?* 2007
[168] Mateo, C. and J.A. Talavera, *Short-time Fourier transform with the window size fixed in the frequency domain.* Digital Signal Processing, 2018. **77**: p. 13-21.
[169] Altaf, S. and S. Ahmad, *Machine Health Monitoring and Fault Diagnosis Techniques Review in Industrial Power-Line Network*, in *Modeling and Simulation in Engineering*. 2020, IntechOpen.
[170] Mehala, N. and R. Dahiya. *A comparative study of FFT, STFT and wavelet techniques for induction machine fault diagnostic analysis*. in *Proceedings of the 7th WSEAS international conference on computational intelligence, man-machine systems and cybernetics, Cairo, Egypt*. 2008.
[171] Krawczyk, M. and T. Gerkmann, *STFT phase reconstruction in voiced speech for an improved single-channel speech enhancement.* IEEE/ACM Transactions on Audio, Speech, and Language Processing, 2014. **22**(12): p. 1931-1940.
[172] *speechsignalprocessing/shorttimefourieranalysis/shorttimefourieranalysisnotes*. [cited libvolume2.xyz/biomedical/btech/semester7; Available from: http://libvolume2.xyz/biomedical/btech/semester7/speechsignalprocessing/shorttimefourieranalysis/shorttimefourieranalysisnotes2.pdf.
[173] Czerwinski, R.N. and D.L. Jones, *Adaptive short-time Fourier analysis.* IEEE Signal Processing Letters, 1997. **4**(2): p. 42-45.
[174] Behnam, H., et al. *Analyses of EEG background activity in Autism disorders with fast Fourier transform and short time Fourier measure*. in *2007 International Conference on Intelligent and Advanced Systems*. 2007. IEEE.
[175] Heaton, J., *Understanding the Kohonen Neural Network. Introduction to Neural Networks with Java. Heaton Research*. 2005, Inc.
[176] https://developer.nvidia.com/nvidia-developer-zone. *Convolutional Neural Network (CNN)*. Available from: https://developer.nvidia.com/discover/convolutional-neural-network.
[177] Glorot, X., A. Bordes, and Y. Bengio. *Deep sparse rectifier neural networks*. in *Proceedings of the fourteenth international conference on artificial intelligence and statistics*. 2011.
[178] Valenti, M., et al. *A convolutional neural network approach for acoustic scene classification*. in *2017 International Joint Conference on Neural Networks (IJCNN)*. 2017. IEEE.
[179] Zhao, R., et al., *Deep learning and its applications to machine health monitoring.* Mechanical Systems and Signal Processing, 2019. **115**: p. 213-237.